UC Berkeley
UC Berkeley Electronic Theses and Dissertations

Title

Inputs to midbrain dopamine neurons control nicotine aversion and motivated feeding

Permalink

https://escholarship.org/uc/item/7xk5n3hb

Author

Tose, Amanda Jeanne

Publication Date

2022

Peer reviewed|Thesis/dissertation

eScholarship.org Powered by the California Digital Library
University of California

Inputs to midbrain dopamine neurons control nicotine aversion and motivated feeding

By

Amanda Jeanne Tose

A dissertation submitted in partial satisfaction of the

requirements for the degree of

Doctor of Philosophy

in

Neuroscience

in the

Graduate Division

of the

University of California, Berkeley

Committee in charge:

Professor Stephan Lammel, Chair
Professor Linda Wilbrecht
Professor Helen Bateup
Professor Yang Dan

Summer 2022

Abstract

Inputs to midbrain dopamine neurons control nicotine aversion and motivated feeding

by

Amanda Jeanne Tose

Doctor of Philosophy in Neuroscience

University of California, Berkeley

Professor Stephan Lammel, Chair

The activity of ventral tegmental area dopamine neurons (VTA DA) in the midbrain is central to the generation of motivated behaviors, such as feeding. Drugs of abuse, such as nicotine, are capable of "hijacking" this system by artificially driving VTA DA activity to promote reinforcement, but high doses of nicotine are aversive. Many brain regions send inputs to the VTA to influence DA activity, including those independently sensitive to food or nicotine consumption, which can strongly modulate behavior. In Chapter 2, I describe how a high dose of nicotine can promote aversive behavior in mice by employing *in vivo* fiber photometry with nicotine and/or nicotinic acetylcholine receptor (nAChr) blockers, a computational model of nAChr activation and sensitization, and optogenetic behavior experiments. I reveal that a high dose of nicotine inhibits DA release in the canonical reward pathway, from VTA DA neurons that project to the lateral shell of the nucleus accumbens (NAcLat). Using a computational model as a guide, I show that the inhibition of NAcLat dopamine release arises from an alpha7 nAChr sensitive laterodorsal tegmentum (LDT) GABA projection to the VTA, which is activated by aversive nicotine. Finally, by suppressing activity of LDT GABA during delivery of an aversive dose of nicotine, I show diminished inhibition of NAcLat dopamine and that conditioned place aversion is prevented. In Chapter 3, I introduce the role of NAcLat inputs to the VTA which are sensitive to and can impose hedonic feeding behavior. Using *in vivo* and *ex vivo* electrophysiology, RNA sequencing, imaging with a novel peptide fluorescent sensor, and optogenetic behavior experiments, I reveal that NAcLat→VTA releases neurotensin and requires neurotensin receptor availability to drive hedonic feeding behavior. I find that in a high fat diet-induced obese mouse model, neurotensin release is diminished, which correlates with reduced hedonic feeding behavior and an inability to increase VTA DA firing and hedonic feeding behavior from optogenetic activation. Finally, by specifically overexpressing neurotensin in the NAcLat→VTA pathway in mice on high-fat diet (HFD), I will show that mice gain less weight and exhibit more locomotion and hedonic feeding behavior compared to control mice on HFD, partially ameliorating the negative impact of the obesogenic food environment. Together, these results highlight the power of inputs to VTA DA neurons to modify responses to nicotine and hedonic feeding, which can translate to targeted therapeutics for nicotine dependence and obesity in the future.

TABLE OF CONTENTS i
ACKNOWLEDGEMENTS iii
CHAPTER 1: INTRODUCTION 1
Mesolimbic dopamine signaling and nicotine 2
Nicotinic acetylcholine receptors (nAChRs) and endogenous cholinergic signaling in the brainstem 2
VTA DA is necessary for feeding behavior and is integrated into feeding circuits 3
Feeding neuropeptides in the nucleus accumbens 4
Striatal function changes in obesity 5
CHAPTER 2: AN INHIBITORY BRAINSTEM INPUT TO DOPAMINE NEURONS ENCODES NICOTINE AVERSION 7
INTRODUCTION 7
RESULTS 8
A computational model predicts divergent effects of rewarding versus aversive nicotine on dopamine cell activity 8
Aversive nicotine inhibits VTA dopamine cells when α4β2Rs are desensitized 11
Aversive nicotine reduces dopamine release in the lateral mesoaccumbal pathway through α7 receptors 14
LDT GABA inputs to VTA are excited by aversive nicotine through α7 receptors 18
Manipulation of LDT GABA cells alters the effects of aversive nicotine on dopamine release and behavior. 22
DISCUSSION 26
METHODS 28
SUPPLEMENTARY FIGURES 37
SUPPLEMENTARY DATA TABLE 51
CHAPTER 3: A NOVEL NEURAL PATHWAY FOR NEUROTENSIN MEDIATED REGULATION OF HEDONIC FEEDING BEHAVIOR AND OBESITY. 90
INTRODUCTION 90
RESULTS 90
NAcLat→VTA activity promotes motivated feeding behavior 90
NTS release from NAcLat→VTA pathway mediates hedonic feeding. 93
NAcLat→VTA is altered by food environment. 95
Reduced NAcLat→VTA NTS release in HFD can be countered to restore motivation and hedonic feeding 98
DISCUSSION 100
METHODS 101

SUPPLEMENTARY FIGURES 108
SUPPLEMENTARY DATA TABLE 123
REFERENCES 137

Acknowledgements

I am extremely grateful to my advisor, Stephan Lammel, for his energy and encouragement as well as the time he purposefully carved out for mentorship. His dedication to training catalyzed my love of science to grow.

Thanks also to the brilliant members of the Lammel lab and the excellent people I met in and through HWNI, for the inspiration and the fun.

I cannot express how deeply grateful I am to Nima Moini for his love and support.

And finally, I want to thank Rezz and electronic music, because graduate school wouldn't have been the same without you.

CHAPTER 1: INTRODUCTION

Midbrain dopamine neurons (DA) in the ventral tegmental area (VTA) that project to the nucleus accumbens (NAc) comprise the mesolimbic dopamine pathway. Mesolimbic dopamine signaling has been associated with reinforcement learning, motivated behavior, and reward processing (Berridge and Kringelbach, 2015; Berridge and Robinson, 1998; Schultz, 2016; Watabe-Uchida et al., 2017; Wise, 2004; Wise and Rompre, 1989) and dysfunctions in this system are associated with neuropsychiatric disorders and substance abuse (Björklund and Dunnett, 2007; Bromberg-Martin et al., 2010; Nestler and Carlezon, 2006; Robinson and Berridge, 2008; Schultz, 2007; Wise, 2004; Wise and Robble, 2020). Previously activity of mesolimbic VTA DA neurons were thought to solely encode positive reinforcement and reward prediction errors, where an increase in DA release in the NAc promotes reward and a reduction of DA release, as recorded during the omission of an expected reward, promotes aversion (Schultz, 2016). However, it is becoming increasingly clear that mesolimbic DA signaling is heterogeneous and a subset of VTA DA neurons specifically respond to negative outcomes and aversive stimuli (de Jong et al., 2019; Lammel et al., 2014). These two roles for DA neurons are anatomically distinct both within the VTA and based on projection targets. The canonical reward pathway is comprised of lateral VTA DA neurons that project to the lateral NAc, while medial VTA DA neurons that project to the ventromedial NAc and other targets signal aversion.

Importantly, this heterogeneous VTA DA system integrates inputs from many brain regions which are sensitive to a wide range of salient, appetitive, and aversive stimuli, in order to adjust motivation and impact behavior. Thus, to isolate the role of VTA DA in specific behaviors requires the study of afferent inputs and the specific circuits in which VTA DA is embedded. Retrograde anatomical tracing studies revealed that dozens of brain regions target VTA DA neurons, many of which are glutamatergic (Beier et al., 2015; Geisler et al., 2007; Lammel et al., 2012) and many studies focused on how glutamatergic inputs arising from these identified regions target VTA DA to affect behavior. For example, activation of glutamatergic inputs from the laterodorsal brainstem to VTA promote reward by activating VTA DA neurons in the lateral mesolimbic pathway, while glutamatergic neurons in the lateral habenula target medial VTA DA neurons in the mesocortical to drive aversion (Lammel et al., 2012). In addition, glutamatergic inputs from anterior cortex also project to VTA DA neurons that project to the lateral nucleus accumbens to support reinforcement of intracranial self-stimulation (Beier et al., 2015).

However much less work has explored the contribution of GABAergic inputs to VTA DA neurons and their potential impact on behavior, despite the discovery that GABAergic inputs arise from many of the same regions that send glutamatergic afferents to the VTA (Beier et al., 2015; Watabe-Uchida et al., 2012). GABAergic inputs arising from these structures could target VTA DA neurons themselves to suppress DA release in output regions or target local VTA GABA neurons to release DA neurons from tonic inhibition and increase DA release and thus GABAergic inputs have the potential to work in alignment or in opposition to glutamatergic inputs from the same region, if present.

Here, I will introduce and discuss two distinct GABAergic inputs to the VTA, from the laterodorsal tegmentum and from the lateral shell of the nucleus accumbens, to provide the

foundation for investigating their separate roles in nicotine aversion in Chapter 2 and motivated feeding behavior in Chapter 3.

Mesolimbic dopamine signaling and nicotine

All drugs of abuse are unified by their ability to impact VTA DA signaling, albeit by different mechanisms, to induce reward and promote behavioral reinforcement (Di Chiara and Imperato, 1988; Lüscher, 2013). Substances like heroin, cocaine, and nicotine "hijack" the mesolimbic reward system by directly or indirectly activating VTA DA neurons which drives synaptic plasticity and increases dopamine release in target regions. Nicotine is the psychoactive component found in tobacco, is highly reinforcing, and is the driver of the tobacco use epidemic, which affects an estimated 1.3 billion people worldwide and results in the deaths of over 8 million people a year (WHO, 2022). To address the public health burden of tobacco use, many studies have focused on understanding how nicotine promotes reward in the brain as a route to designing targeted therapeutic treatments to facilitate cessation of tobacco use. However, nicotine is unique among drugs of abuse in that high doses are acutely aversive and understanding how nicotine promotes aversion presents an additional avenue that can lead to future treatments.

Nicotine's aversive properties result in a few distinct features in substance users that differ from use of other highly addictive substances. For example, overdose and death from nicotine is relatively rare compared to other substances although nicotine's margin of exposure is similar to substances where overdose is quite common, as for heroin, cocaine, and alcohol (Henningfield et al., 1991; Lachenmeier and Rehm, 2015; Solarino et al., 2010). Animals can be trained to self-administer nicotine and will reliably increase responding when the dose of nicotine provided is too low but will take actions to stop receiving doses of nicotine that are too high (Ashton et al., 1979; Fowler and Kenny, 2011; Goldberg et al., 1983; St Helen et al., 2016). Although this type of responding occurs during administration of other drugs of abuse, only nicotine can produce a conditioned place aversion effect both when administered before or after the conditioning period (Fudala and Iwamoto, 1987). The aversive properties of nicotine may delay the onset of habit formation but are ultimately insufficient to prevent substance dependence because tolerance to high doses of nicotine develops over time, suggesting that the aversive effects diminish (Heishman and Henningfield, 2000). A more complete understanding of nicotine's aversive properties could be harnessed to support tobacco cessation therapies in the future.

Nicotinic acetylcholine receptors (nAChRs) and endogenous cholinergic signaling in the brainstem

Nicotine's effect on the brain is largely driven by its binding of nicotinic acetylcholine receptors (nAChRs). nAChRs are an integral part of the brain's cholinergic system which respond to synaptic release of endogenous acetylcholine. nAChRs are a large family of ligand-gated cation channels which bind either nicotine or acetylcholine to transfer ions across the neuronal membrane. These receptors are pentamers which are composed of five identical subunits or a combination of subunits α2-7 and β2-4, lending different receptor compositions and differing sensitivity to nicotine (Dineley et al., 2015; Wu, 2009). Experimental and modeling studies suggest that the activation of β2-containing nAChRs (β2*Rs) and α7-containing nAChRs (α7Rs)

mediate nicotine self-administration, with β2*Rs primarily expressed directly on VTA DA cells to increase firing rate and α7Rs on excitatory inputs that are responsible for burst firing and synaptic (Besson et al., 2012; Gao et al., 2010; Mameli-Engvall et al., 2006; Mansvelder and McGehee, 2000; Mansvelder et al., 2002; Markou and Paterson, 2001; Picciotto et al., 1998; Schilström et al., 2003). However, nicotine also desensitizes nAChRs, rendering them temporarily inactive, thus preventing further activation by endogenous acetylcholine or nicotine (Fenster et al., 1997; Picciotto et al., 2008; Wooltorton et al., 2003). Importantly, disruption of VTA α7Rs and β2*Rs can alter aversive and reward-related behavior in response to intra-VTA infusions of low concentrations of nicotine (Laviolette and van der Kooy, 2003).

The major source of endogenous cholinergic signaling in the VTA comes from laterodorsal tegmental nucleus (LDT)/pedunculopontine tegmental nucleus (PPT) which has been a focal point in nicotine research. The LDT contains cholinergic, GABAergic, and glutamatergic cells which send their projections to the VTA to impact behavior. Nicotine activates LDT cholinergic neurons and can promote reward (Ishibashi et al., 2009; Steidl et al., 2017). Activation of LDT glutamatergic projections to the VTA can also promote reward and result in burst firing of dopamine neurons (Lammel et al., 2012; Lodge and Grace, 2006). Although LDT GABAergic interneurons have been shown to modulate fear behaviors (Yang et al., 2016) and there is a major LDT GABAergic projection to the VTA (Soden et al., 2020), the role of LDT GABA projections to the VTA in behavior has been understudied. Due to the important role that LDT cell populations play in mediating the response to nicotine, the role of LDT GABA in response to aversive doses of nicotine merits further study and will be explored in Chapter 2.

VTA DA is necessary for feeding behavior and is integrated into feeding circuits

As much as an animal's behavior can become oriented to an unhealthy exogenous substance, like nicotine, VTA DA activity is also necessary for maintaining motivation for behaviors pertinent to survival, such as feeding. When the gene for tyrosine hydroxylase, the rate-limiting enzyme to synthesize dopamine, was deleted in mice, researchers found that mice became hypoactive and stopped feeding altogether. Unless mice were supplemented with L-DOPA, a precursor to dopamine, the animals starved to death (Zhou and Palmiter, 1995). While dopamine proved necessary for feeding in normal body weight mice, additional research probed whether dopamine is also necessary for feeding behavior in a mouse model of obesity. $Lep^{ob/ob}$ mice lack the receptor for leptin, a satiety hormone that increases circulating levels following food consumption, and rapidly experiences onset of severe obesity compared to control mice. When $Lep^{ob/ob}$ leptin mice were genetically crossed to additionally delete the gene for tyrosine hydroxylase, as with the previous mice, $Lep^{ob/ob}$ mice were also prevented from feeding unless supplemented with L-DOPA (Szczypka et al., 2000). Although these mice completely lacked a critical system for satiety, it suggests that dopamine signaling ultimately determines the maintenance of feeding behavior.

Feeding is critical for the survival of an animal and therefore many brain regions coordinate the decision to seek and consume food. VTA DA neurons themselves express receptors to respond to circulating feeding and metabolic signals like leptin, ghrelin, and insulin, and are part of a network of many other important brain regions that regulate feeding, including the paraventricular thalamic nucleus, hypothalamic regions such as lateral hypothalamus,

ventromedial hypothalamus, acuate nucleus, the dorsal and ventral striatum, and prefrontal cortex (Ferrario et al., 2016). Cell populations within all these regions influence VTA DA either directly or indirectly, and many via direct projections.

One of the largest anatomical connections to the VTA comes from the nucleus accumbens (NAc) (Beier et al., 2015; Watabe-Uchida et al., 2012) which provides important inhibitory feedback to the VTA. This NAc connection is comprised of medium spiny neurons (MSNs), which release the inhibitory neurotransmitter GABA and express dopamine receptor 1 (D1). The D1 receptor is a G-protein coupled receptor (GPCR) that upon binding dopamine initiates a G_s-coupled signaling cascade which activates adenylate cyclase which works to produce the secondary messenger cAMP. Although inhibitory, activation of the NAc input to the VTA preferentially targets VTA GABA neurons which drives increased DA neuron firing via disinhibition (Yang et al., 2018). However, previous work has shown conflicting findings on the role of NAc D1 neurons in feeding behavior. In one study activation of NAc D1 neurons drove an increase in licks of a sucrose solution (Tellez et al., 2016), another study found that activation of NAc D1+ inputs to the lateral hypothalamus specifically decreased consumption of sucrose solution (O'Connor et al., 2015). A major limitation of many studies on the role of NAc in feeding is that subregions of the NAc targeted are not taken into account or reported although there is emerging evidence that there are important opposing roles for medial vs lateral NAc in behavior (de Jong et al., 2019). Although the lateral shell NAc inputs to the VTA strongly impact DA neuron activity (Yang et al., 2018), their role in feeding behavior remained unexplored.

Feeding neuropeptides in the nucleus accumbens

Although MSNs in the NAc are GABAergic they also co-express many neuropeptides that can be released separately or co-released with GABA (Castro, et al., 2019). Neuropeptides are short amino acid sequences that can exert their effects in the central and peripheral nervous system. In general, many neuropeptides are packaged into specialized vesicles called dense core vesicles, which are larger and further away from the ready releasable pool small synaptic vesicles, which typically contain the fast-acting small molecule neurotransmitters like GABA and glutamate (Nurrish, 2014). Because of the distance of dense core vesicles from the synapse, neuropeptides are more likely to be released by a train of action potentials as opposed to a single action potential. Both synaptic and extrasynaptic neuropeptide release is possible and the reuptake and repackaging mechanisms for most neurotransmitters remains to be fully understood (Nusbaum et al., 2017).

In situ hybridization studies have found expression of many neuropeptides in the NAc that can modulate feeding behavior. Some of these include: dynorphin, cocaine- and amphetamine-related transcript (CART), neuropeptide y (NPY), and neurotensin (Nts) (Allen Institute, 2004). Neurotensin is particularly striking because of its apparent asymmetrical expression in the accumbens, with relatively greater expression localized in the lateral shell compared to the medial shell of the NAc. Neurotensin is a 13 amino acid peptide and mesolimbic VTA DA neurons express neurotensin receptor 1 (NtsR1) (Woodworth et al., 2017a). Early pharmacological studies found that intrabrain infusion of neurotensin into the VTA of food-deprived rats reduced chow consumption (Cador et al., 1986; Levine et al., 1983). These anorexic effects were thought to replicate the effect of endogenous release of neurotensin from

the lateral hypothalamus. In the lateral hypothalamus, the majority of neurons expressing the receptor for leptin, the circulating satiety hormone, also expressed neurotensin (Leinninger et al., 2011). Indeed, chemogenetic activation of lateral hypothalamus Nts neurons reduced chow consumption and promoted weight loss in mice (Woodworth et al., 2017b).

However, bath application of Nts on VTA DA neurons in slice can result in conflicting excitatory and inhibitory effects (Tschumi and Beckstead, 2019), which may suggest neurotensin can bidirectionally affect feeding behavior. For example, in response to ghrelin, a circulating hunger hormone, VTA DA neurons are activated and promote increased feeding behavior, and in response to leptin, VTA DA neuron firing is decreased and feeding is suppressed (Domingos et al., 2011; Hommel et al., 2006; Skibicka et al., 2011). Clearly, though neurotensin is capable of modulating feeding behavior, to understand its specific effect may require examining neurotensin release in a projection specific manner. It seems possible that the lateral shell of NAc releases Nts in the VTA to alter feeding in a manner opposed to the lateral hypothalamic system, which may underlie the seemingly opposing effects of Nts on VTA DA activity. However, whether the lateral shell releases Nts in the VTA or if Nts has circuit-specific effects has not been studied.

Striatal function changes in obesity

Obesity is an increasingly worsening public health epidemic, which results in one of the largest causes of preventable death worldwide (NCD-RisC, 2016). Although obesity can be the consequence of certain prescribed medication or genetic disorders, the vast majority of human obesity can be attributed to behavior, where an overconsumption of palatable food beyond homeostatic need promotes fat accumulation and weight gain. The mesolimbic DA system as described above is integrated in a network of feeding circuits which can respond to homeostatic signals, but its role in reward processing suggests this could be an important node that underlies obesity, where the rewarding properties of food drive intake beyond homeostatic need.

Studies in rodents and humans suggest that the striatum is altered in obesity. Dopamine D2 receptors are GPCRs that upon binding dopamine initiates a G_i-coupled signaling cascade that inhibits adenylate cyclase which reduces the production of cAMP. Expression of dopamine D2 receptors are reduced in the striatum in obese rats and virally knocking down striatal D2 receptors accelerates the onset of obesity (Johnson and Kenny, 2010). Studies in humans have also found less striatal D2 availability compared to normal weight individuals (Volkow et al., 2008). In addition, in functional imaging studies, obese subjects show decreased striatal activation in response to palatable food intake but increased activation in response to food cues compared to normal weight individuals (Stice et al., 2008) and the degree of this differential activation to food receipt and food cues correlates with future weight gain (Stice et al., 2010).

Although these seminal studies focused on dorsal striatum, others have found that the nucleus accumbens in the ventral striatum is also altered by high fat diet. Dopamine receptor 1 gene expression is reduced in the nucleus accumbens of obesity prone rats (Alsio et al., 2010). In addition, synaptic strength of different inputs onto nucleus accumbens neurons was altered in high fat diet compared to standard chow fed mice, with an increase in anterior paraventricular thalamus (aPVT) synaptic strength onto D1 MSNs and a reduction in prefrontal cortex (PFC) synaptic strength onto D2 MSNs (Christoffel, 2021).

Taken together, because D1 MSNs in the NAc lateral shell target VTA DA neurons to increase firing and promote reward behavior and neuropeptides that modulate feeding like neurotensin are expressed, this circuit seems a promising target to investigate peptide release and changes in feeding behavior driven by high fat diet-induced obesity. Experiments designed to shed light on these open questions are presented in Chapter 3.

CHAPTER 2: AN INHIBITORY BRAINSTEM INPUT TO DOPAMINE NEURONS ENCODES NICOTINE AVERSION

This chapter contains work from a manuscript accepted for publication in *Neuron:*

Liu, C.*, Tose, A.J.*, Verharen, J.P., Zhu, Y.,Tang, L.W., de Jong, J.W., Du, J.X., Lammel, S. (in press). An inhibitory brainstem input to dopamine neurons encodes nicotine aversion. *Neuron.*

*These authors contributed equally.

INTRODUCTION

A predominant hypothesis for nicotine addiction is that nicotine 'hijacks' natural reward processes in the brain (Dani and Harris, 2005; Laviolette and van der Kooy, 2004; Luscher and Malenka, 2011; Picciotto and Kenny, 2021). However, nicotine's behavioral responses are dose-dependent; nicotine is rewarding at low doses and acutely aversive at high doses (Fowler and Kenny, 2014; Fudala and Iwamoto, 1987; Fudala et al., 1985; Risinger and Oakes, 1995). Humans and animals maintain optimal blood nicotine levels by increasing consumption when nicotine levels are low and decreasing consumption when levels are too high (Ashton et al., 1979; Fowler and Kenny, 2011; St Helen et al., 2016). Notably, non-human primates will press a lever to stop additional infusions of nicotine (Goldberg et al., 1983). Although dose titration is common to other drugs of abuse like methamphetamine (Sambo et al., 2017), cocaine (Hnasko et al., 2007), and heroin (Loney et al., 2021), nicotine displays acutely aversive properties at high doses (Natarajan et al., 2011). While cocaine, methamphetamine, and ethanol can all generate an aversive phenotype in the conditioned place preference task, this effect is caused by delaying drug delivery until after animals have spent time in the conditioned chamber. When delivered before the conditioning period, the same doses of cocaine, methamphetamine, and ethanol induce conditioned place preference (Cunningham and Henderson, 2000; Ettenberg et al., 1999; Fudala and Iwamoto, 1990). To our knowledge, nicotine is the only drug observed to elicit an aversive phenotype in rodents both when the drug is delivered immediately before or after the conditioning period, suggesting its unique, acutely aversive effects (Fudala and Iwamoto, 1987). Nicotine's acutely aversive properties may explain the relative rarity of overdose compared to alcohol, heroin, and cocaine (Lachenmeier and Rehm, 2015). Furthermore, the aversive effects of nicotine can be experienced concurrently with the pleasurable effects (Sartor et al., 2010) and tolerance to high doses develops over time (Heishman and Henningfield, 2000), suggesting that nicotine aversion may be distinct from nicotine reward and tolerance to aversion may underlie the development of habitual nicotine consumption.

Recent research has pointed to a critical role of the habenulo-interpeduncular axis and its projections to the brainstem laterodorsal tegmentum (LDT) underlying the aversive actions of nicotine (Antolin-Fontes et al., 2015; Fowler et al., 2011; Frahm et al., 2011; Hsu et al., 2013; Tuesta et al., 2017; Wolfman et al., 2018). In contrast, the rewarding and reinforcing effects of nicotine and other drugs of abuse involve dopamine (DA) neurons in the ventral tegmental area (VTA) that release DA in the nucleus accumbens (NAc) (Di Chiara and Imperato, 1988; Luscher and Malenka, 2011). However, VTA_{DA} neurons are not a monolith; subpopulations defined by

anatomical location and projection target possess distinct properties and serve different functions (Lammel et al., 2012). The canonical reward prediction error encoding DA neurons are located in the lateral VTA and send projections to the lateral shell of the nucleus accumbens (NAcLat), while medial VTA_{DA} neurons send projections to the ventro-medial shell of the nucleus accumbens (NAcMed) and release DA in response to aversive stimuli and cues that predict them (de Jong et al., 2019). Whether distinct DA subcircuits that regulate reward and aversion underlie nicotine's dose-dependent effects remains uncertain.

Nicotine's effects on DA neurons are exerted through nicotinic acetylcholine receptors (nAChRs) (Graupner et al., 2013; Klink et al., 2001; Tapper et al., 2004). Experimental and modeling studies suggest that the activation of β2-containing nAChRs (β2*Rs) and α7-containing nAChRs (α7Rs) mediate nicotine self-administration, with β2*Rs primarily expressed directly on VTA_{DA} cells to increase firing rate and α7Rs on excitatory inputs that are responsible for burst firing and synaptic plasticity (Besson et al., 2012; Gao et al., 2010; Mameli-Engvall et al., 2006; Mansvelder and McGehee, 2000; Mansvelder et al., 2002; Markou and Paterson, 2001; Picciotto et al., 1998; Schilström et al., 2003). However, nicotine also desensitizes nAChRs, rendering them temporarily inactive, thus preventing further activation by endogenous acetylcholine or nicotine (Fenster et al., 1997; Picciotto et al., 2008; Wooltorton et al., 2003). Importantly, disruption of VTA α7Rs and β2*Rs can alter aversive and reward-related behavior in response to intra-VTA infusions of low concentrations of nicotine (Laviolette and van der Kooy, 2003). However, much of the work characterizing nAChRs and nicotine-related behaviors focused on lower doses that are reinforcing, therefore less is known about how high, aversive doses of systemic nicotine act on nAChRs to modulate DA cell activity and release.

RESULTS

A computational model predicts divergent effects of rewarding versus aversive nicotine on dopamine cell activity

In animal experiments, nicotine is often delivered via intraperitoneal (IP) or subcutaneous (SC) injections (Fudala and Iwamoto, 1987; Saal et al., 2003). However, the needle-poke from an injection is an aversive stimulus that may obscure the acute, aversive effects of nicotine on DA release. We therefore developed an intravenous (IV) infusion protocol that reliably induced dose-dependent conditioned place preference or aversion in response to infusions of low and high doses of nicotine, respectively. On Day 1, mice freely explored the behavior box for 10 minutes to obtain a pre-test baseline preference score for either chamber. On Days 2-4, each mouse received saline in the morning while confined to one chamber and nicotine in the afternoon while confined to the opposite chamber. Mice were randomly assigned to receive low or high nicotine doses. Infusions were delivered every 5 minutes through an implanted jugular vein catheter (JVC), for a total of 6 infusions over 30 minutes (**Figures 1A-1D**). The 5-minute interval between infusions allows the accumulation of nicotine to observe neural activity dynamics as brain nicotine concentration increases over time (Taylor et al., 2013; Tolu et al., 2013). On Day 5, animals again freely explored the behavior box for 10 minutes to obtain a post-test preference score. By assessing time spent in each chamber during the post-test compared to the pre-test, we found that mice receiving the low dose of nicotine spent more time in the nicotine-paired

chamber indicating a preference, whereas mice receiving the high dose spent less time in the nicotine-paired chamber indicating aversion.

To predict VTA_{DA} neuron activity in response to our IV nicotine protocol, we computationally modeled cell activation as a function of nicotine's effects on nAChRs containing α4 and β2 subunits (α4β2Rs), which are highly expressed on VTA_{DA} neurons and mediate nicotine's effects on DA release and behavioral reinforcement through direct activation and desensitization (Picciotto et al., 2008). For our model, we leveraged parameters established by Graupner, Maex, and Gutkin, who demonstrated a mechanism for nicotine-induced VTA_{DA} cell inhibition via α4β2R desensitization, disrupting activation of the receptor by endogenous acetylcholine (Graupner et al., 2013). To adapt their acute nicotine model to our nicotine infusion protocol, we modeled blood nicotine concentration from 6 nicotine infusions 5 minutes apart based on the half-life of nicotine in mice (Matta et al., 2007; Petersen et al., 1984). A single infusion of the aversive dose of nicotine is expected to activate and desensitize most of the α4β2Rs immediately, leaving them in an inactive state for subsequent infusions (**Figures 1E and 1F**). Consequently, the modeled VTA_{DA} cell response (expressing solely α4β2Rs) to the aversive dose of nicotine is a large increase in activity in response to the first infusion whereas subsequent nicotine infusions decrease VTA_{DA} activity relative to baseline (**Figures 1G and 1H**). Thus, VTA_{DA} cells are predicted to be inhibited by aversive nicotine due to the disruption of baseline activation by endogenous acetylcholine after α4β2Rs are desensitized. The rewarding dose, however, is modeled to desensitize α4β2Rs at a gradual rate which maintains VTA_{DA} cell activation, albeit with decreasing magnitude for each nicotine infusion. On average, the net effect of all nicotine infusions combined on VTA_{DA} cell activity is expected to be greater in response to a rewarding dose of nicotine (**Figure 1I**), which is consistent with the role that increased and decreased rates of DA transmission is thought to have on promoting reward and aversion, respectively (Bromberg-Martin et al., 2010; Schultz, 1997; Tsai et al., 2009).

Could nicotine's actions solely through α4β2Rs on VTA_{DA} neurons mediate its dose-dependent behavioral effects? A computational model of our IV infusion protocol suggests that the rewarding dose of nicotine activates α4β2Rs on VTA_{DA} cells while the aversive dose desensitizes α4β2Rs. Enhancing or disrupting the function of α4β2Rs on VTA_{DA} cells relative to baseline activity is modeled to give rise to dose-dependent VTA_{DA} cell activation and inhibition, respectively. This model suggests that a high, aversive dose of nicotine can reduce VTA_{DA} cell firing through α4β2Rs, providing a quantified hypothesis that can be tested experimentally.

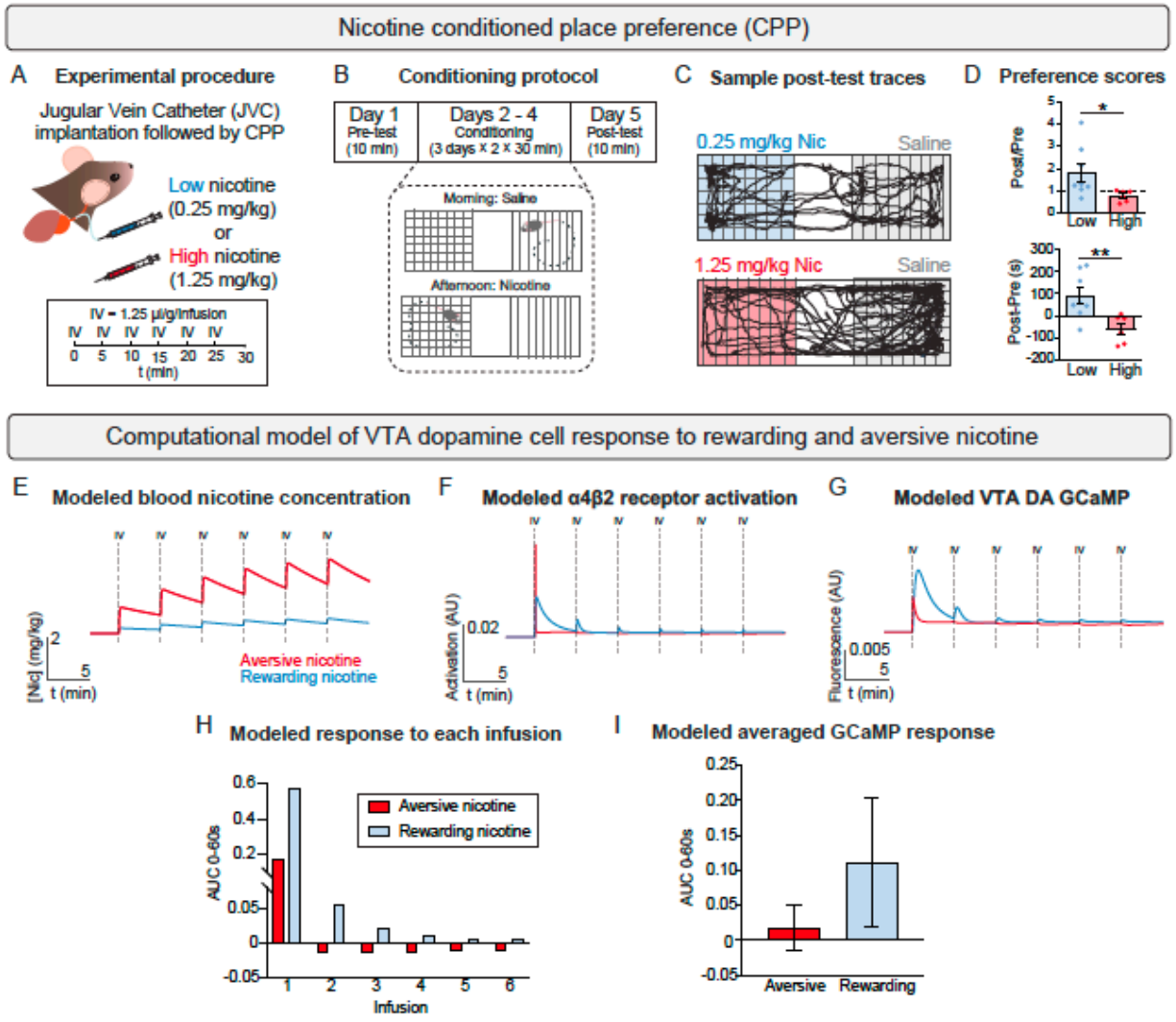

Figure 1. Dose-dependent effects of nicotine on behavior and modeled VTADA cell activity.
(A) Schematic of experimental design (CPP: conditioned place preference).
(B) Schematic of CPP procedure.
(C) Sample traces from representative animals during the post-test on day 5.
(D) Top: preference score as a ratio of time spent in the nicotine-paired chamber during the post-test relative to pre-test. Bottom: preference score as a difference between time spent in the nicotine-paired chamber during post-test relative to pre-test. (* $p < 0.05$, ** $p < 0.01$; data represent means ± SEM).
(E) Modeled blood nicotine concentration from aversive (red) and rewarding (blue) nicotine conditions during the 30-min infusion protocol.
(F) Modeled α4β2 receptor activation in response to aversive (red) and rewarding (blue) nicotine.
(G) Modeled GCaMP fluorescence in VTADA neurons expressing α4β2 receptors in response to aversive (red) and rewarding (blue) nicotine.
(H) Modeled area under the curve (AUC) for 60s post-infusion for each of 6 infusions during the 30-minute infusion protocol.

(I) Modeled average AUC across all 6 infusions (data represent modeled means ± SEM).

Aversive nicotine inhibits VTA dopamine cells when α4β2Rs are desensitized

To test the model predictions, we first examined the dose-dependent effects of nicotine on VTA_{DA} neurons by performing fiber photometry experiments in awake, head-fixed animals. DAT-Cre mice were injected with an adeno-associated virus (AAV) carrying Cre-dependent GCaMP6m into the VTA, and an optical fiber was implanted to allow for the recording of calcium transients from VTA_{DA} cell bodies in response to nicotine infusions. Calcium transients were recorded during the same 30-minute IV protocols we established to induce nicotine preference or aversion after an initial 10-minute baseline acclimation period (**Figures 2A, 2B and S1A**). We found that while saline infusions had very minor, if any, effects on VTA_{DA} activity, each infusion of the rewarding dose of nicotine consistently activated VTA_{DA} cells **(Figure 2C)**. As predicted by our computational model (**Figure 1H**), the first infusion of the high, aversive dose of nicotine activated VTA_{DA} cells and subsequent infusions suppressed cell activity **(Figures 2C and S1E)**. However, our model did not predict such prominent inhibition, nor did it predict an activation of VTA_{DA} cells beyond the first infusion that appears to wane with each infusion. By the final (i.e., sixth) infusion, VTA_{DA} activity was strongly inhibited by nicotine (**Figure 2C, inset**). Because the complete series of nicotine infusions was necessary to promote conditioned place preference or aversion (**Figure 1A-1D**), we calculated the average response of VTA_{DA} cell activity across infusions to reveal the net effect of rewarding or aversive nicotine. As a result, the rewarding dose of nicotine significantly activated VTA_{DA} cells, whereas infusions of an aversive dose caused a biphasic response with an inhibitory early component (EC) lasting 15s post-infusion and an excitatory late component (LC) from 15-60s (**Figures 2D, 2E and S1D-S1F**). Importantly, we counterbalanced the nicotine dose (rewarding or aversive) that animals received first to measure within-animal differences and there was no order effect of nicotine doses (**Figures S1B and S1C**).

Our model of nicotine's effects on VTA_{DA} cells through α4β2Rs captured the general trend of activation by low, rewarding nicotine and desensitization after the first infusion of high, aversive nicotine. However, the biphasic response was not predicted; the inhibition during the 0-15s EC was far greater in amplitude than expected and the increase in activity during the 15-60s LC was not predicted at all. Next, we followed-up on the most salient prediction of the model, that α4β2R desensitization explains the difference between the first and subsequent infusions, by generating a testable hypothesis for pharmacological antagonism of α4β2Rs with our computational model. Mimicking receptor desensitization can be achieved by blocking receptor activation with the competitive antagonist dihydro-beta-erythroidine (DHBE), which is selective for β2-containing nAChRs (Rice and Cragg, 2004). Because DHBE can become non-specific or fatal at high doses (Damaj et al., 1999), we modeled an 80% blockade of α4β2Rs to predict how DHBE treatment would affect VTA_{DA} cell activity during infusions of aversive nicotine (**Figures 2F and 2G**). DHBE treatment is predicted to disrupt the effects of aversive nicotine predominantly on the first infusion because both DHBE and aversive nicotine should desensitize a majority of α4β2Rs upon delivery, and infusions 2-6 of aversive nicotine are theorized to occur while α4β2Rs are already desensitized. To test this prediction, we combined fiber photometry of VTA_{DA} cells with DHBE pharmacology. To ensure that DHBE could take effect before the introduction of nicotine and that its effects would persist for the entire duration of the infusion

protocol, we pre-treated animals with IV DHBE 5 minutes into the initial baseline recording period then co-infused DHBE with aversive nicotine at the same dosage and intervals as in previous experiments (**Figures 2H and S1G**). Systemic delivery of antagonists is most comparable to systemic pharmaceutical treatment in humans, and co-infusion with nicotine allows constant availability of antagonists without additional stimuli mid-session like a needle-poke or intrabrain infusion, preventing stimulus-responses that may occlude the acute effects of nicotine infusion. Indeed, systemic DHBE reproduced the prediction from our computational model (**Figure 2G**); it reduced the response of VTA_{DA} cell activity to aversive nicotine, significantly reducing activation from the first infusion with minor effects during infusions 2-6 (**Figures 2I and 2J**). The replication of our model prediction supports the hypothesis that α4β2Rs play a role in activating VTA_{DA} cells but become desensitized by a high dose of nicotine. The persistent, desensitized state of α4β2Rs during nicotine exposure may be critical to the inhibition of VTA_{DA} cells in response to aversive nicotine. However, the effects of DHBE on the biphasic response of VTA_{DA} cells to aversive nicotine are inconclusive; the qualitative but not statistically significant difference between averaged EC and LC responses do not explain the role of α4β2Rs in mediating cell activity during either time component **(Figure 2K**). Further, the strength of inhibition in the EC and the observed increase in LC activity was not predicted by our model that assumed VTA_{DA} neurons are a homogenous population solely expressing α4β2Rs. This shortcoming necessitates the investigation of other receptors or cell populations in mediating VTA_{DA} cell activity in response to nicotine.

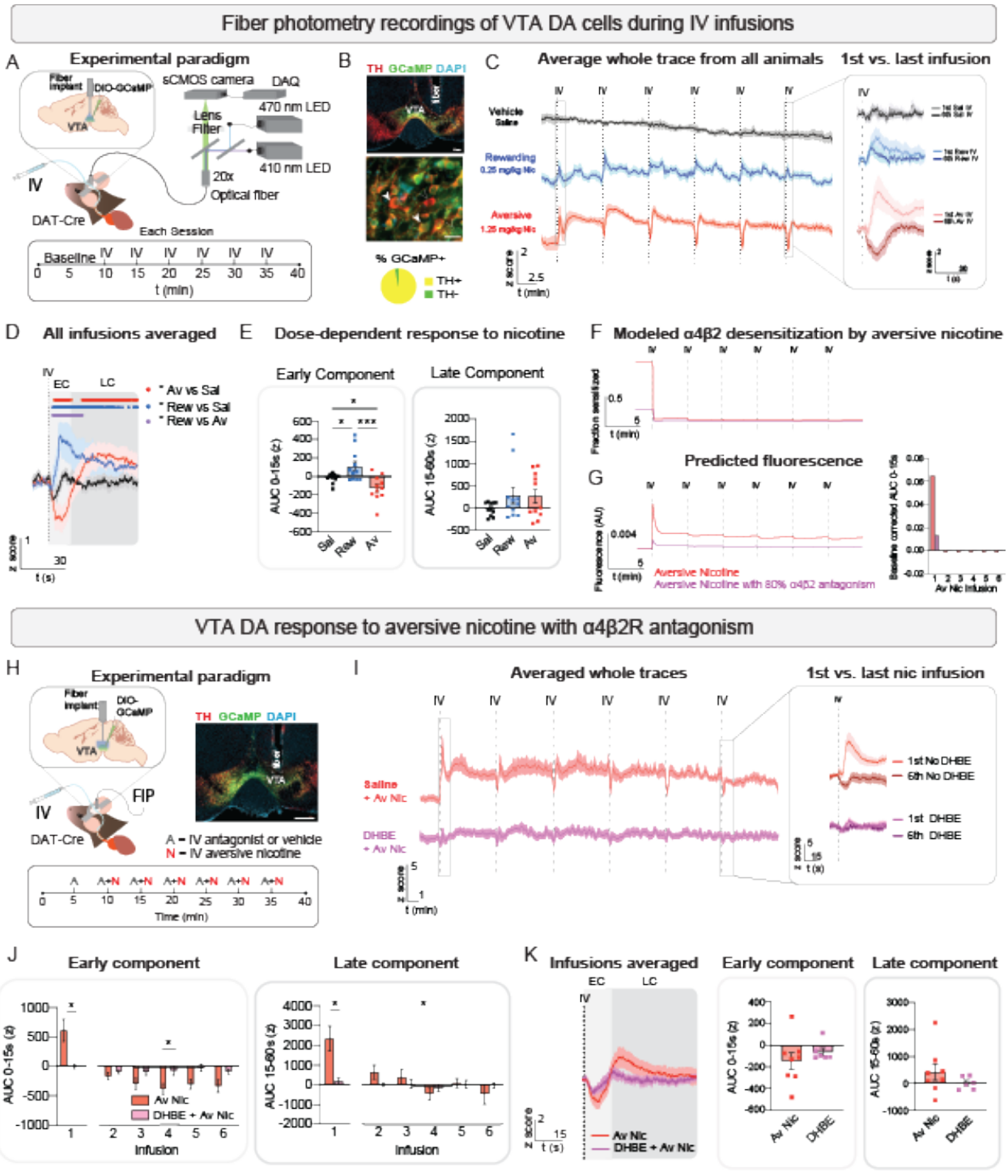

Figure 2. Aversive nicotine suppresses VTA$_{DA}$ cell activity through α4β2 receptor desensitization.

(A) Top: Schematic of a DAT-Cre mouse with AAV-DIO-GCaMP6m injected into VTA receiving IV infusions during fiber photometry recordings. Bottom: Schematic showing timeline for IV nicotine or saline infusions.

(B) Top: Optical fiber implant location in VTA (green - GCaMP; red - tyrosine hydroxylase (TH); blue - DAPI; scale bar 200 μm). Middle: Enlarged view (scale bar 25 μm). Bottom: 97% of GCaMP+ neurons are TH-immunopositive (yellow) and 3% are TH-immunonegative (green).
(C) Averaged GCaMP activity of VTA_{DA} neurons in response to saline (gray), rewarding (blue), and aversive nicotine (red). Inset: Overlays of averaged response to the first and sixth infusion for each condition. Light shading represents SEM.
(D) Averaged GCaMP activity of all six infusions showing 0-60s post-infusion in response to saline (gray), rewarding (blue), and aversive nicotine (red) (data represent means ± SEM). Dots above traces represent time points with significant differences between conditions from a multiple-comparisons test (red – aversive nicotine versus saline; blue – rewarding nicotine versus saline; purple – rewarding versus aversive nicotine). Gray backgrounds distinguish the approximate time windows during which the response to aversive nicotine and saline are significantly different (i.e., light gray: 0-15s (early component, EC); dark gray: 15-60s (late component, LC) (* $p < 0.05$; light shading represents SEM).
(E) Left: AUC for GCaMP response during EC (0-15s) is significantly lower in the aversive nicotine (Av, red) condition compared to saline (Sal, black) and rewarding nicotine (Rew, blue). Right: No significant differences between conditions during the LC (15-60s) (* $p < 0.05$, *** $p < 0.001$; data represent means ± SEM).
(F) Computational modeling of α4β2R desensitization by aversive nicotine predicts reduced sensitization in the presence of 80% antagonism of α4β2Rs (purple) compared to without α4β2R antagonist (red).
(G) Left: Predicted fluorescence in arbitrary units (AU) based on computational modeling of α4β2R activity as whole traces. Right: Baseline corrected AUCs during the EC (0-15s) predict reduced excitation in response to the first infusion and reduced inhibition during infusions 2-6.
(H) Left and bottom: Schematic showing AAV infusion and implantation of optical fibers in VTA of DAT-Cre mice. Fiber photometry recordings of VTA_{DA} neurons are performed during infusions of aversive nicotine (red) with antagonist pre-treatment and co-infusion (gray). Right: Anatomical verification of recording location in VTA (red – TH; green – GCaMP; blue – DAPI; scale bar 500 μm).
(I) Averaged whole traces of VTA_{DA} GCaMP activity in response to aversive nicotine (Av Nic) without DHBE (red) and with DHBE (purple). Inset: Comparison of response to the first and sixth infusions (area of light shading represents SEM).
(J) Averaged AUCs for each infusion during the EC (0-15s; left) and LC (15-60s; right) (gap denotes separate analyses for infusion 1 and infusions 2-6 due to non-normal distribution, * $p < 0.05$, data represent means ± SEM).
(K) Left: Averaged traces of all 6 infusions showing 0-60s post-infusion in response to aversive nicotine without DHBE (red) and in presence of DHBE (purple) (light shading represents SEM). Middle: Averaged AUC response across infusions during the EC (data represent means ± SEM). Right: Averaged AUC response across infusions during the LC (data represent means ± SEM).

Aversive nicotine reduces dopamine release in the lateral mesoaccumbal pathway through α7 receptors

The biphasic inhibitory and excitatory responses to aversive nicotine may arise from heterogenous VTA_{DA} cell populations with different projection targets (de Jong et al., 2019; Verharen et al., 2020). To explore this possibility, we injected the DA sensor dLight1.2 into the NAcMed and NAcLat and implanted optical fibers to measure DA release in both regions

simultaneously within animals. Each animal received IV infusions of saline and aversive nicotine on subsequent days while DA release was recorded (**Figures 3A and S2A**). Our results show that an inhibitory EC occurs in the NAcLat, whereas a significant increase of DA release can be observed during the LC in the NAcMed, confirming our hypothesis that the biphasic activity from the bulk VTA_{DA} cell body signal could be dissociated by projection target (**Figures 3B-3F**). Notably, the increase of DA release in NAcMed occurs primarily in response to the first infusion of aversive nicotine before α4β2Rs are desensitized and the decrease of DA release in NAcLat occurs after α4β2R desensitization by the first infusion (**Figures S2E and S2F**). In a separate experiment, we confirmed the behavioral relevance of reduced DA release in NAcLat; optogenetic silencing of VTA_{DA} terminals in NAcLat was sufficient to promote real-time place aversion, suggesting that inhibition of DA release in NAcLat is a crucial component of promoting aversion to high doses of nicotine (**Figures S2H-S2J**). We also recorded DA release in response to a rewarding dose of nicotine and found that there were no differences between NAcMed and NAcLat (**Figures S2B and S2C**), in accordance with previous research (Nguyen et al., 2021), nor was there an order effect of nicotine dose (**Figure S2D**). A comparison of dLight1.2 fluorescence and terminal GCaMP6m fluorescence in response to aversive nicotine showed no differences, further demonstrating the relationship between VTA_{DA} cell activity and DA release in NAc subregions (**Figures S2G**).

Next, we sought to understand which nAChRs may mediate these divergent effects of aversive nicotine on DA release in NAc subregions. While our model of α4β2R desensitization accurately predicted an inhibitory effect of aversive nicotine on VTA_{DA} cells through disruption of activation by endogenous acetylcholine, we did not anticipate that a distinct subpopulation of DA neurons would be activated. A possible driver of this activation may be the recruitment of α7Rs which require higher concentrations of nicotine to become activated and desensitized than α4β2Rs (Fenster et al., 1997; Wooltorton et al., 2003). To explore how antagonism of α4β2 and α7 receptors would alter DA release in the NAc, we carried out additional experiments in another cohort of animals with α4β2R antagonist DHBE, α7R antagonist methyllycaconitine (MLA), and the nonspecific nAChR antagonist mecamylamine (MEC) (**Figures 3G-3N and S2K-S2M**). We pre-treated animals with antagonist (or saline) 5 minutes into the initial baseline recording period then co-infused the antagonist with aversive nicotine at the same dosage and intervals as in previous experiments (**Figure 3H**). Consistent with our hypothesis that α4β2Rs drive activation specifically in response to the first infusion, EC DA release by the first infusion in both NAc subregions was decreased by DHBE (see infusion #1 in **Figures 3I, 3L and S2L-S2M)**. The absence of an effect on DA release in NAcLat by DHBE in subsequent infusions and when averaged across infusions is consistent with our recordings from VTA_{DA} cell bodies and the hypothesis that DHBE and aversive nicotine share a common function to desensitize α4β2Rs (**Figures 2K and 3N**). Furthermore, we found that LC activation was significantly reduced by MEC in both NAc subregions, but not by any other antagonists (**Figures 3J-K, 3M-3N and S2L-S2M**). Thus, receptors other than α4β2Rs and α7Rs are likely involved in increasing DA release in response to aversive nicotine during the LC. Lastly, both MEC and MLA prevented the behaviorally relevant decrease of EC DA release in the NAcLat by aversive nicotine, indicating that α7R-mediated inhibition was blocked (**Figure 3N**). Our former hypothesis that α7Rs contributed to the activation of VTA_{DA} cells through excitatory inputs to increase DA release in NAcMed was based on the known expression of α7Rs on glutamatergic inputs to VTA (Mansvelder and McGehee, 2000; Mansvelder et al., 2002). The surprising finding that α7Rs are

required for the inhibition of DA release during the EC by aversive nicotine suggests a role for α7R-mediated inhibitory input to VTA_{DA} neurons in nicotine aversion. These results suggest that a simple model of nicotine's dose-dependent actions on α4β2Rs on VTA_{DA} neurons alone is insufficient to explain the suppression of NAcLat DA release by aversive nicotine.

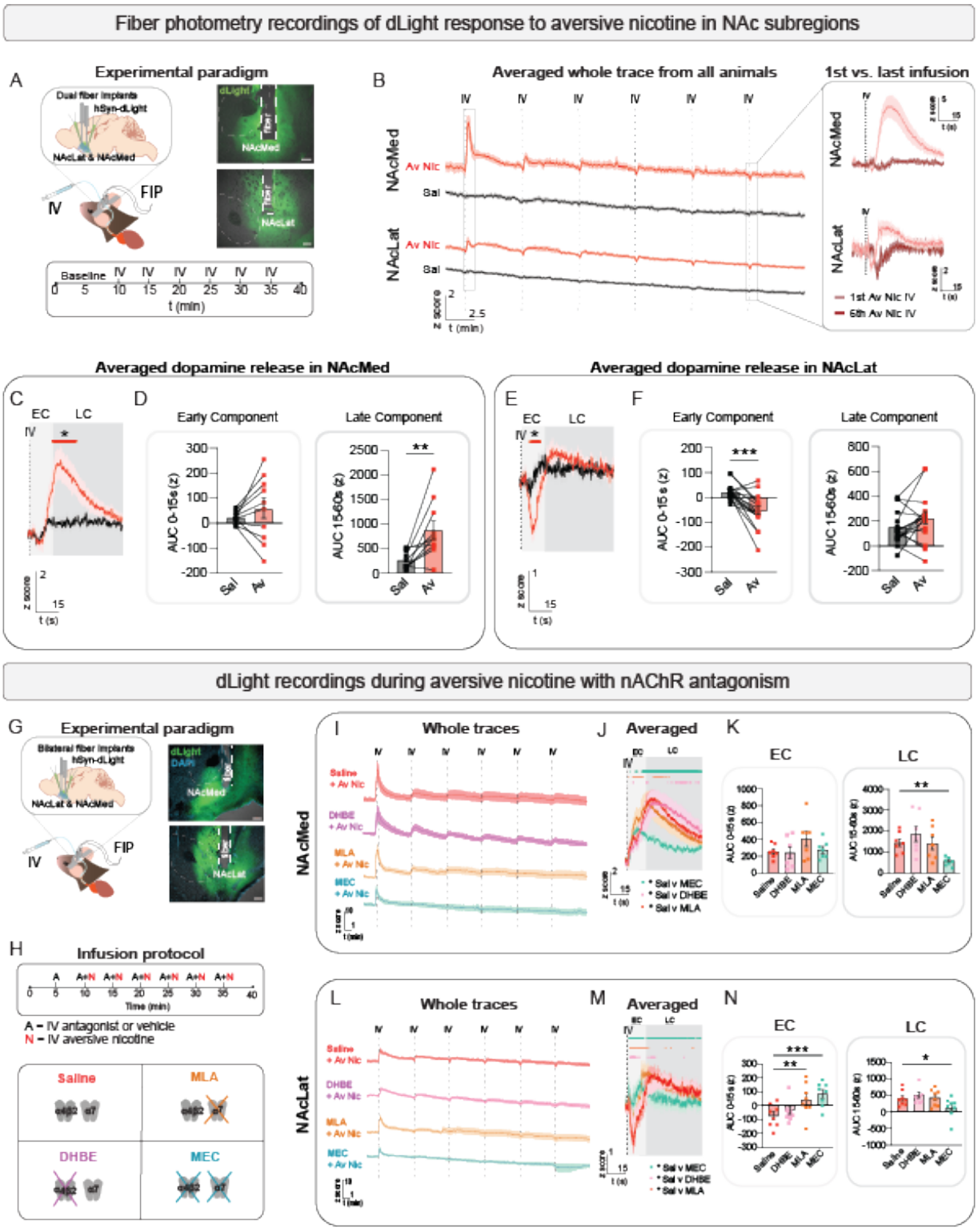

Figure 3. Aversive nicotine induces heterogenous DA release patterns in distinct NAc subregions which are modulated by nAChR antagonism.

(A) Left: Schematic of simultaneous dLight fiber photometry (FIP) recordings in NAc medial shell (NAcMed) and NAc lateral shell (NAcLat) during IV infusions of saline or aversive nicotine. Right: dLight expression (green) and fiber implant location in NAcMed (top) and NAcLat (bottom). Dotted lines delineate NAc core. (Scale bars 200 μm). Bottom: Schematic showing timeline for IV infusions.
(B) Averaged whole traces in response to aversive nicotine (Av Nic, red) and saline (Sal, black). Inset: Comparison between first (light red) and sixth (dark red) infusions in the Av Nic condition (light shading represents SEM).
(C) Averaged response to all infusions for Av Nic (red) and Sal (black) in NAcMed. Dots above traces represent time points with significant differences (* $p < 0.05$; light shading represents SEM).
(D) DA release in NAcMed significantly increased in response to Av Nic compared to Sal during the LC (right). No difference during the EC (left) (** $p < 0.01$; data represent means ± SEM).
(E) Averaged response to all infusions for Av Nic (red) and Sal (black) in NAcLat. Dots above traces represent time points with significant differences (* $p < 0.05$; light shading represents SEM).
(F) DA release in NAcLat significantly decreased in response to Av Nic compared to Sal during the EC (left). No difference during the LC (right, dark gray border) (*** $p < 0.001$; data represent means ± SEM).
(G) Left: Schematic of simultaneous dLight FIP recordings in NAcMed and NAcLat during IV infusions of aversive nicotine with nAChR antagonists. Right: dLight (green) expression and optical fiber locations in the NAcMed (top) and NAcLat (bottom). Dotted lines delineate NAc core (blue – DAPI; Scale bars 200 μm).
(H) Timeline and infusion protocol of aversive nicotine with nAChR antagonist pre-treatment and co-infusion of saline or nAChR antagonists (α7 (MLA), α4β2 (DHBE) or non-specific (MEC)).
(I) Averaged whole traces of dLight in NAcMed in response to Av Nic with saline (red), DHBE (purple), MLA (orange), and MEC (turquoise) (light shading represents SEM).
(J) Averaged dLight response in NAcMed across all six infusions of Av Nic with saline (red), DHBE (purple), MLA (orange), and MEC (turquoise). Dots above traces represent time points with significant differences between each antagonist and the saline condition (* $p < 0.05$; light shading represents SEM).
(K) Left: No significant differences in NAcMed dLight AUC during the EC. Right: During the LC, MEC significantly reduced NAcMed dLight AUC in response to Av Nic compared to no antagonist (saline) (** $p < 0.01$; data represent means ± SEM).
(L) Same as in (I), but for NAcLat.
(M) Same as in (J) but for NAcLat.
(N) Left: During the EC, MLA and MEC significantly attenuated the reduction of NAcLat dLight AUC to Av Nic. Right: During the LC, only MEC significantly reduced the NAcLat response to Av Nic (* $p < 0.05$, ** $p < 0.01$, *** $p < 0.001$; data represent means ± SEM).

LDT GABA inputs to VTA are excited by aversive nicotine through α7 receptors

While α4β2 and α7 receptors have both been implicated in nicotine reward and reinforcement, they possess distinct profiles in pharmacodynamics and anatomical expression (**Figure 4A**). Compared to α4β2Rs that are expressed on VTA_{DA} cells, α7Rs require higher concentrations of

nicotine to become activated and desensitized (**Figure 4B**) (Wooltorton et al., 2003). Thus, rewarding and aversive nicotine are expected to differentially affect α4β2 and α7 receptors and the cells that express them. A rewarding dose of nicotine is modeled to activate α4β2Rs with little effect on α7Rs, whereas aversive nicotine is predicted to activate α7Rs with each infusion and rapidly desensitize the majority of α4β2Rs in the first infusion, rendering the α4β2Rs unable to become activated by subsequent infusions of nicotine (**Figures 4C and 4D**). Thus, aversive nicotine should strongly activate a cell expressing α4β2Rs in the first infusion and cause inhibition relative to baseline during subsequent infusions while reliably activating cells expressing α7Rs (**Figure 4E**). Based on our finding that suppression of DA release in NAcLat during the EC is mediated by α7Rs, a logical hypothesis is the existence of an inhibitory input to VTA_{DA} cells that is activated by aversive nicotine through α7Rs (**Figure 4A**). Indeed, a previous study demonstrated that the inhibition of VTA_{DA} firing rate in response to high doses of nicotine was blocked by GABA receptor antagonists (Erhardt et al., 2002). In this updated model, the predicted net effect of aversive nicotine on a cell expressing α4β2Rs and receiving inhibitory input from a cell under the control of α7Rs is a slight reduction of activation from the first infusion and a stronger inhibition in response to subsequent infusions (**Figure 4F**).

Local VTA_{GABA} neurons are a major inhibitory regulator of VTA_{DA} neurons and are involved in nicotine reinforcement (Grieder et al., 2019; Tolu et al., 2013). Thus, VTA GABA cells are a candidate for reducing NAcLat DA release during the EC in response to aversive nicotine. We performed fiber photometry recordings from GAD2-Cre mice that were infused with an AAV carrying Cre-dependent GCaMP6m and implanted with an optical fiber in the VTA (**Figure S3A**). An aversive dose of nicotine, but not a rewarding dose, significantly activated VTA GABA neurons (**Figures S3B-S3E**). To determine which receptors contribute to the activation of local VTA GABA neurons by aversive nicotine, we performed recordings in the presence of nAChR antagonists (**Figure 4G**). VTA GABA neurons were excited by aversive nicotine during the EC, and only the nonspecific antagonist MEC significantly reduced this activation (**Figures 4H-4J and S3F-S3G**). Although there was a small, but not significant, reduction in response to aversive nicotine during MLA treatment, α7Rs are unlikely to be the primary mediator of aversive nicotine-induced activation of local VTA GABA neurons.

Next, we decided to explore a different source of α7R-mediated inhibitory input to VTA_{DA} cells. The brainstem laterodorsal tegmentum (LDT) is a major excitatory input to VTA_{DA} neurons, sending glutamatergic and cholinergic projections that mediate both general reward and nicotine reward (Dautan et al., 2016; Kohlmeier, 2013; Lammel et al., 2012; Omelchenko and Sesack, 2005; Steidl et al., 2017). The LDT also contains a separate, non-overlapping population of GABAergic (i.e., GAD2-expressing, LDT_{GABA}) neurons (**Figure S4A**) (Soden et al., 2020; Wang and Morales, 2009), which comprise ~30% of the cells that project to the VTA (**Figure S4B**). LDT_{GABA} neurons project more broadly to VTA and adjacent structures (e.g., interpeduncular nucleus, IPN) compared to glutamatergic LDT (i.e., VGLUT2-expressing, LDT_{VGLUT2}) neurons, which predominantly project to the lateral VTA (**Figures S4C and S4D**) (Lammel et al., 2012). Although VTA-projecting LDT_{GABA} neurons ($LDT_{GABA}\rightarrow VTA$) and VTA-projecting LDT_{VGLUT2} ($LDT_{VGLUT2}\rightarrow VTA$) neurons receive qualitatively similar inputs, significant differences in the proportion of inputs were detected in the deep mesencephalic nucleus, dorsal raphe nucleus, parabrachial nucleus and locus coeruleus (**Figures S4E-S4I**). Using fluorescent *in situ* hybridization, we found that the majority of LDT neurons expressing α7R mRNA co-express

GAD2 mRNA (**Figures S4J and S4K**). Importantly, brain-slice patch-clamp recordings revealed that LDT_{GABA} neurons make direct inhibitory synaptic connections onto NAcLat-projecting VTA_{DA} neurons (**Figures S5A-S5D**) and *in vivo* optogenetic stimulation of LDT_{GABA} neurons decreased DA release in the NAcLat (**Figures S5E-S5G**) and promoted real-time place aversion (**Figures S5H-S5K**) suggesting that LDT_{GABA} neurons are another candidate for α7R-mediated inhibitory input to VTA_{DA} neurons to encode nicotine aversion. Indeed, LDT_{GABA} terminals in the VTA are selectively activated by aversive, but not rewarding, nicotine (**Figures S6A-S6E**). To test whether $LDT_{GABA}\rightarrow VTA_{DA}$ neurons could be the α7R-mediated source of inhibition, we performed fiber photometry recordings from GAD2-Cre mice that have been infused with a 1:1 mix of AAV carrying Cre-dependent GCaMP6m and axon-targeted GCaMP6s into the LDT to improve fluorescent signal at axon terminals and implanted with an optical fiber in the VTA (**Figure S6F**). To determine which receptors contribute to the activation of $LDT_{GABA}\rightarrow$VTA neurons by aversive nicotine, we performed recordings with DHBE, MLA, and MEC treatment **(Figure 4K).** We found that both MEC and MLA reduce the EC activation in LDT_{GABA} inputs to the VTA by aversive nicotine (**Figures 4L-4N, S6G and S6H**).

Together, our results indicate that the activation of $LDT_{GABA}\rightarrow$VTA neurons by aversive nicotine is mediated by α7Rs, which makes this neural population a candidate for the inhibitory input in our model that drives the behaviorally relevant suppression of DA release in the NAcLat.

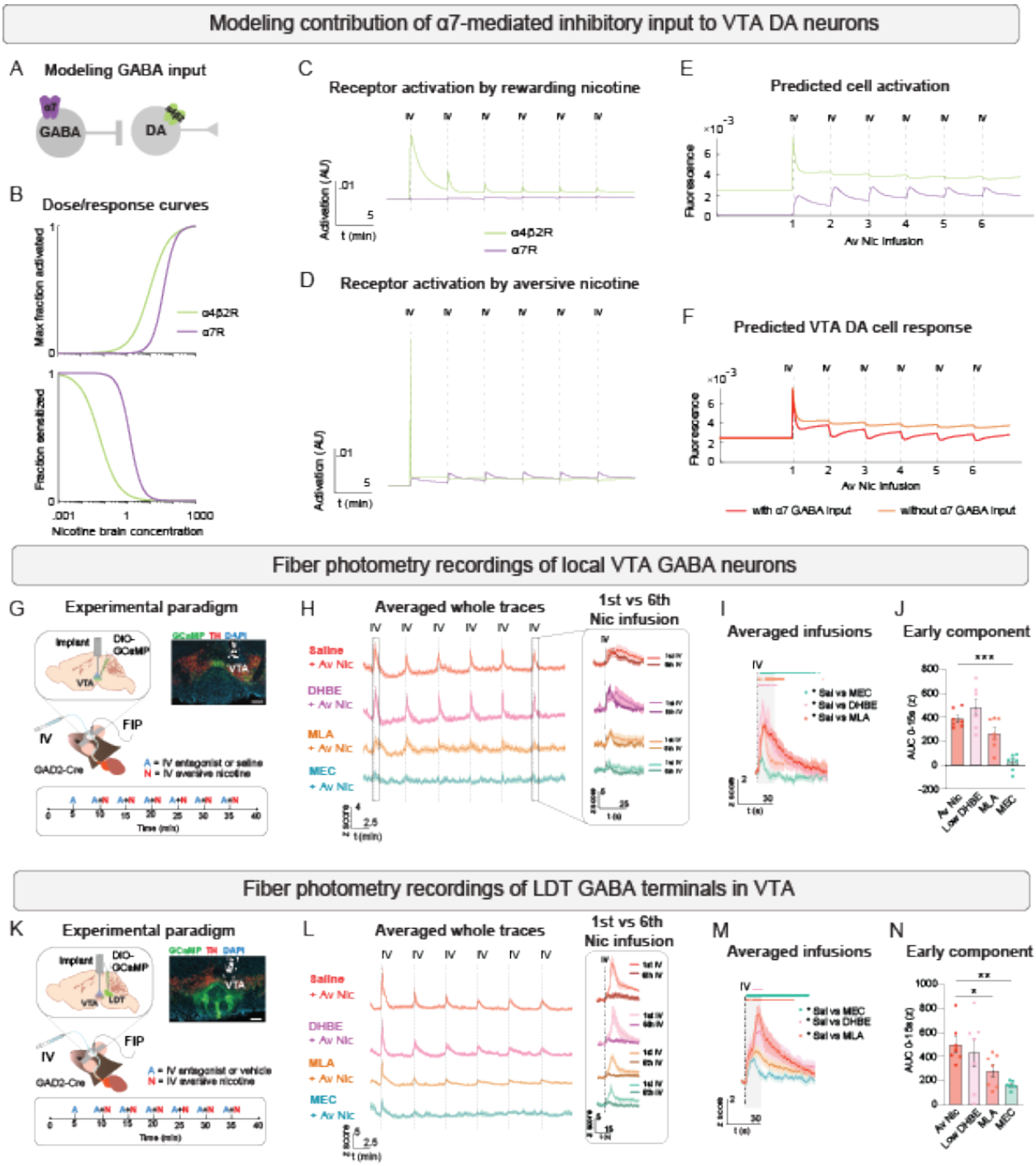

Figure 4. Computational modeling and FIP recordings suggest putative role for α7 nAChR modulation of LDT inhibitory inputs to VTADA neurons for aversive nicotine induced changes in DA release.

(A) Schematic of receptor expression and connectivity for predicting VTADA cell activity as a function of α4β2R (green) activity with inhibitory input under control of α7 (purple) nAChRs.

(B) Dose/response curves demonstrating that α4β2Rs (green) are activated and desensitized by lower concentrations of nicotine than α7 (purple) nAChRs.

(C) Modeling receptor activation by rewarding nicotine based on our infusion protocol (Figure 1) predicts higher activation of α4β2R (green) compared to α7Rs (purple) for each infusion, albeit with gradual desensitization.
(D) Modeling receptor activation by aversive nicotine predicts that the majority of α4β2Rs (green) are activated by the first infusion and exhibit decreased activation from infusions 2-6 due to receptor desensitization. Conversely, α7Rs (purple) are activated by each infusion of aversive nicotine.
(E) Predicted GCaMP fluorescence from a given cell expressing either α4β2Rs (green) or α7Rs (purple) in response to aversive nicotine.
(F) Modeled VTADA GCaMP activity in response to aversive nicotine with α4β2R expression and inhibitory input under control of α7Rs (red; as shown in schematic (A)) or without inhibitory input (orange).
(G) Top: Schematic showing FIP recordings from GCaMP-expressing VTA neurons in GAD2-Cre mice and IV infusions of saline, nicotine and/or nAChR antagonists. Bottom: Schematic showing timeline for IV administration of aversive nicotine and nAChR antagonists or saline. Right: Fiber implant in VTA with GCaMP (green) and TH (red) expression (blue – DAPI; scale bar 200 μM).
(H) Averaged whole traces of VTA GABA GCaMP activity in response to Av Nic with co-infusion of saline (red), DHBE (purple), MLA (orange), and MEC (turquoise). Inset: Comparisons between first and sixth infusion for each condition (light shading represents SEM).
(I) Averaged VTA GABA GCAMP activity for all 6 infusions in response to Av Nic with co-infusion of saline (red), MLA (orange), MEC (turquoise), and DHBE (purple). Dots above traces represent time points with significant differences from the saline condition (* $p < 0.05$; light shading represents SEM).
(J) MEC significantly reduced VTAGABA GCaMP activity in response to Av Nic during the EC (*** $p < 0.001$, data represent means ± SEM).
(K) Same experimental design as in (G), but for FIP recordings of LDTGABA terminals in the VTA.
(L) Same as in (H) but for LDTGABA→VTA.
(M) Same as in (I) but for LDTGABA→VTA.
(N) α7 (MLA) and non-specific (MEC) nAChR antagonists reduced LDTGABA→VTA activity response to Av Nic during the EC (* $p < 0.05$, ** $p < 0.01$, data represent means ± SEM).

Manipulation of LDT GABA cells alters the effects of aversive nicotine on dopamine release and behavior.

To understand the role of α7R-mediated inhibitory inputs on VTA_{DA} cells expressing α4β2Rs, we updated our computational model and predicted that the absence of inhibitory inputs would cause slightly higher activation in response to the first infusion of aversive nicotine and less inhibition by subsequent infusions (**Figures 5A-5C**). To directly test the model prediction, we genetically ablated LDT_{GABA} neurons and recorded DA release in response to aversive nicotine. Specifically, GAD2-Cre mice were injected in the LDT with an AAV carrying Cre-dependent mCherry (AAV-DIO-mCherry) as a control or a 1:1 mix of AAV-DIO-mCherry and AAV-flex-taCasp3 to induce apoptosis in infected neurons (Yang et al., 2013). dLight1.2 was injected into the NAcLat and NAcMed and optical fibers were implanted into these regions to allow simultaneous fiber photometry recordings of DA release during IV infusions (**Figures 5D, S7A**

and S7B). Adequate ablation of LDT_{GABA} cells by caspase was indicated by the absence of mCherry expression (**Figures 5E, S7A and S7B**). In accordance with our model prediction, we found a significant attenuation of the EC DA reduction in the NAcLat and a reduction of the LC DA release in response to the first infusion (**Figures 5F-H and S7C**). Surprisingly, animals injected with caspase in the LDT also showed a significant reduction in the LC of DA release in the NAcMed in response to aversive nicotine (**Figures 5I-5K and S7D**) indicating that LDT_{GABA} neurons may directly and/or indirectly influence NAcMed-projecting DA neurons.

After establishing that ablation of LDT_{GABA} neurons altered DA release in response to aversive nicotine, we sought to examine whether inhibition of the LDT_{GABA}→VTA pathway affects the behavioral response to aversive nicotine. We bilaterally targeted the LDT of GAD2-Cre mice with an AAV carrying the Cre-dependent inhibitory opsin halorhodopsin (AAV-DIO-eNpHR) or eYFP (AAV-DIO-eYFP) as a control and implanted angled optic fibers bilaterally towards the VTA (**Figure 5L)**. We found that control animals exhibited conditioned place aversion to high-dose nicotine, but nicotine aversion was not observed in the eNpHR group (**Figure 5M-5P**). Thus, inhibiting LDT_{GABA} terminals in the VTA successfully blocked the aversive effects of a high dose of nicotine. Additionally, optogenetic inhibition of LDT_{GABA} terminals in the VTA alone had no impact on non-nicotine dependent behavior such as real time place preference or open field locomotion (**Figure S7E-S7G**).

Collectively, these results establish that LDT_{GABA} neurons (i) contribute to the heterogeneous patterns of DA release in distinct NAc subregions induced by aversive nicotine and (ii) are necessary for nicotine-induced conditioned place aversion.

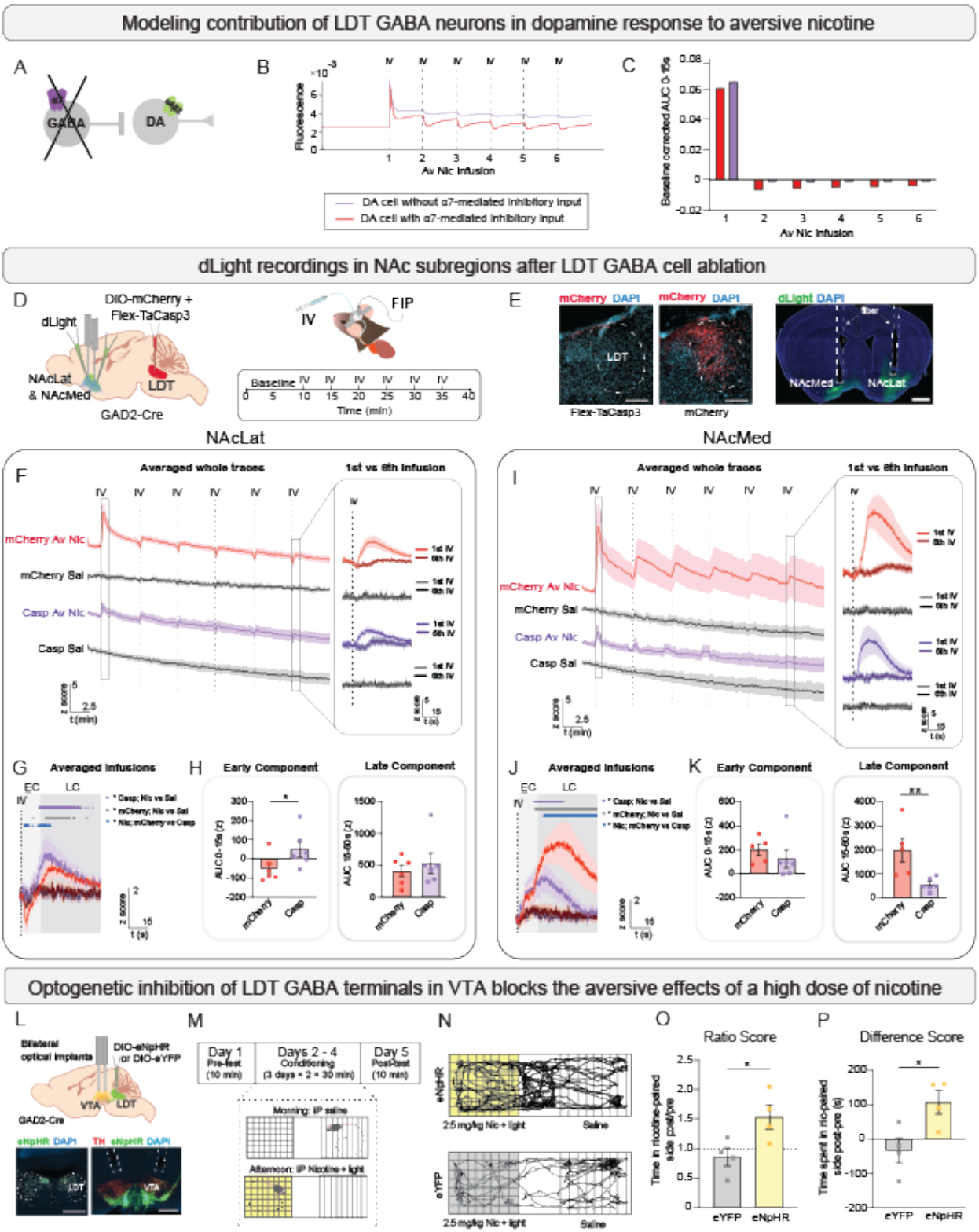

Figure 5. Manipulation of LDT GABA neurons reduces the effects of aversive nicotine on DA release in the NAc and prevents nicotine-induced aversion.

(A) Schematic representation of modeling VTADA cell activity with removal of α7R-mediated inhibitory inputs.
(B) Modeled GCaMP fluorescence of VTADA neurons expressing α4β2Rs with (red) and without (purple) α7R-mediated inhibitory input.
(C) Modeled baseline-corrected AUCs quantifying the EC of VTADA GCaMP fluorescence in response to aversive nicotine without α7R-mediated inhibitory input (purple) predicts a slightly higher activation in response to the first infusion of aversive nicotine and decreased suppression in response to infusions 2-6.
(D) Schematic showing simultaneous FIP recordings of NAcMed and NAcLat dLight and IV infusions of aversive nicotine or saline in mice with genetic ablation of LDT GABA neurons.
(E) Left: Histological verification of genetic ablation of LDT GABA neurons (Flex-TaCasp3, Caspase group) compared to control animals (mCherry, red) (scale bar 200 μm). Right: Optical fiber placement in NAcMed and NAcLat with dLight (green) expression (blue – DAPI; scale bar 1 mm).
(F) Averaged whole trace NAcLat dLight response to aversive nicotine Av Nic or saline in mice with genetic ablation of LDT GABA neurons or control animals (red - mCherry Av Nic; purple - Caspase Av Nic; black - mCherry Saline and Caspase Saline). Inset: Comparisons of first and last infusions (light shading represents SEM).
(G) dLight response in NAcLat averaged across all 6 infusions of saline or Av Nic in mice with genetic ablation of LDT GABA neurons or control animals. Dots above the traces denote significant differences in a multiple comparisons test (purple - Av Nic versus Saline in Caspase group; gray - Av Nic versus Saline in mCherry group; blue - Av Nic in mCherry versus Caspase groups) (* $p < 0.05$; light shading represents SEM).
(H) Left: Averaged NAcLat dLight AUC across infusions demonstrates more inhibition in mCherry compared to Caspase in response to Av Nic during the EC. Right: No significant difference between groups during the LC (* $p < 0.05$, data represent means ± SEM).
(I) Same as in (F) but for NAcMed.
(J) Same as in (G) but for NAcMed.
(K) Left: No significant difference between groups during the EC. Right: Averaged NAcMed dLight AUC across infusions reveals significant reduction in Caspase AUC during the LC compared to mCherry (** $p < 0.01$, data represent means ± SEM).
(L) Top: Schematic showing AAV infusions of Cre-dependent halorhodopsin (DIO-eNpHR) or eYFP into LDT of GAD2-Cre mice with bilateral optical fibers above VTA. Bottom: eNpHR (green) expression in LDT neurons (left) and in LDT terminals in the VTA (right) with location of optical fiber implants (red – TH, blue – DAPI; scale bars 500 μM).
(M) Schematic of conditioned place aversion assay and timeline.
(N) Trajectories of sample eNPHR and eYFP mice during post-test (day 5). Yellow (and gray) indicates chamber side paired with light delivery.
(O) Preference score as a ratio of time spent in the nicotine-paired chamber during the post-test relative to pre-test. (* $p < 0.05$; data represent means ± SEM).
(P) Preference score as a difference between time spent in the nicotine-paired chamber during post-test relative to pre-test. (* $p < 0.05$; data represent means ± SEM).

DISCUSSION

Effects of aversive nicotine in a heterogenous dopamine system

Our study supports the view that the reward-enhancing and reward-inhibiting properties (i.e., anxiety) of low doses of nicotine recruit discrete, concurrent DA circuits (Nguyen et al., 2021), and establishes a novel mechanism for how high doses of nicotine alter DA signaling in separate mesoaccumbal DA subsystems. In line with previous work, we found that a rewarding dose of nicotine increased VTA_{DA} activity (Imperato et al., 1986; Nguyen et al., 2021). However, a high aversive dose of nicotine bidirectionally altered DA signaling by inhibiting a canonical reward pathway (NAcLat) and activating a distinct mesoaccumbal DA pathway (NAcMed) previously shown to be activated by aversive stimuli and cues that predict them (de Jong et al., 2019; Verharen et al., 2020). These results support the idea that NAc subregions have specialized roles in dissociating nicotine motivational signaling (Sellings et al., 2008). Future studies are needed to understand whether LDT_{GABA} neurons directly or indirectly influence the medial mesoaccumbal DA pathway in response to aversive nicotine and whether other DA subsystems (e.g., mesoamygdaloid, mesoprefrontal) contribute to nicotine aversion.

Bridging the habenulo-interpeduncular axis with the mesolimbic dopamine system

Previous studies have shown that the habenulo-interpeduncular axis (i.e., projections from the medial habenula (mHb) to interpeduncular nucleus (IPN)) is involved in fear, anxiety, nicotine withdrawal, and nicotine aversion (Antolin-Fontes et al., 2015; Fowler and Kenny, 2014). mHb and IPN activity may signal the aversive effects of nicotine to downstream brain regions, such as the LDT (Wolfman et al., 2018). It is conceivable that a circuit mechanism for nicotine aversion may involve disinhibition of LDT_{GABA}→VTA neurons to reduce DA release in the NAcLat. Such disinhibition could arise from inhibition of local LDT interneurons (Yang et al., 2016) through IPN neurons (Wolfman et al., 2018), which are directly excited by mHb cells (Fowler et al., 2011; Frahm et al., 2011). Future studies are needed to elucidate local connectivity within the LDT and simultaneous *in vivo* recordings of multiple brain regions in the habenulo-interpeduncular-mesopontine-axis may further reveal how a response to aversive nicotine is coordinated.

Because our ablation of LDT_{GABA} cells targeted all GAD2-expressing LDT cells and terminal inhibition of LDT_{GABA}→VTA neurons can affect collateral projections via back-propagating action potentials, we cannot exclude LDT_{GABA} interneurons or those that project to regions other than the VTA in mediating the effects of aversive nicotine on DA release, including a direct inhibitory projection to the NAc (Coimbra et al., 2019). Although both nicotine and acetylcholine have the potential to directly and/or indirectly modulate striatal DA release (Cachope et al., 2012; Rice and Cragg, 2004; Threlfell et al., 2012), this mechanism seems unlikely in the case of LDT_{GABA}→NAc neurons, given that optogenetic stimulation of LDT_{GABA}→NAc inputs had no effect on place preference or aversion behavior (Coimbra et al., 2019), unlike the robust real-time place aversion we observed during LDT_{GABA}→VTA stimulation. On the other hand, it is likely that LDT_{GABA} neurons target additional cell populations beyond lateral VTA_{DA} neurons given that ablation of neurons also reduced the LC DA release in the NAcMed in response to aversive nicotine, and terminals from LDT_{GABA} neurons were detected in the IPN.

Our work also reveals that VTA_{GABA} neurons are strongly activated by aversive nicotine. Previous work has shown that stimulation of VTA_{GABA} cell bodies produces conditioned place aversion (Tan et al., 2012) and that projection-specific VTA_{GABA}→NAc stimulation impairs reward-seeking (Lowes et al., 2021). Although our pharmacological experiments indicate that VTA GABA neurons as a population are not strongly regulated by α7Rs, it remains unknown whether distinct subpopulations of VTA_{GABA} neurons could participate in the α7R-mediated suppression of NAcLat DA release by aversive nicotine. VTA_{GABA} neurons may therefore additionally contribute to nicotine aversion.

Despite the questions that remain regarding specific LDT_{GABA} and VTA_{GABA} neuronal subtypes in nicotine aversion, the neural circuit introduced here may explain how the habenulo-interpeduncular axis connects to the mesolimbic DA system via the brainstem mesopontine tegmentum.

A computational model for nicotine's dose-dependent effects

The dose-dependent effects of nicotine on behavior are likely the culmination of responses by many nAChRs, brain regions, cell-types, and other features that are difficult to integrate into one unifying theory. To avoid overcomplicating our model, we sought to fit as few parameters as possible that would account for the major dynamics observed to effectively simulate nicotine's dose-dependent effects on VTA_{DA} activity (Wilson and Collins, 2019). Further, isolating nicotine delivery to specific brain regions may have allowed a better understanding of each cell population's response, but systemic delivery is more relevant to human nicotine intake and pharmaceutical treatment.

Our methods balanced simplicity with specificity to model VTA_{DA} neurons as units under the control of direct receptor expression and the net effect of systemic nicotine on their inputs.
While rewarding nicotine activates α4β2Rs and increases VTA_{DA} cell activity, an aversive dose desensitizes the receptors and VTA_{DA} cells are no longer activated by nicotine, rendering them more susceptible to inhibition from afferent inputs. Indeed, when we systemically antagonized α4β2Rs with DHBE to mimic receptor desensitization, VTA_{DA} cell body activity was in alignment with our model.

The role of α7Rs in nicotine-related behaviors has been difficult to clarify, with contradictory findings about their role in nicotine reward, reinforcement, aversion, or lack thereof (Besson et al., 2012; Brunzell and McIntosh, 2012; Grottick et al., 2000; Laviolette and van der Kooy, 2003; Markou and Paterson, 2001). Nicotine conditioned place preference is blocked if α7R activity is enhanced during delivery of rewarding doses, by either pharmacological agonism or gain-of-function α7 mutant mice (Harenza et al., 2014). Additionally, intra-brain infusion of an α7R agonist decreased motivation to work for nicotine, whereas infusion of an α7R antagonist increased motivation (Brunzell and McIntosh, 2012). Our results show that α7 mRNA is expressed in LDT_{GABA} neurons, which are activated by a high, aversive dose of nicotine to inhibit VTA_{DA} neurons and decrease DA release in the NAcLat. Thus, nicotine's dual actions to recruit α7Rs and desensitize α4β2Rs may be important mechanisms in encoding nicotine reward and aversion.

The systemic, pharmacological antagonists used in our study can be non-specific at very high doses (Whiteaker et al., 2007). Therefore, cell-type specific gene deletion strategies of nAChRs and more specific antagonists (Brunzell and McIntosh, 2012) could be used in future studies to further delineate their roles in nicotine reward and aversion.

Relevance to treatments for nicotine addiction

Understanding the neurobiology of nicotine reward and aversion may inform the development of novel treatments to aid in nicotine cessation. Varenicline is currently the only available pharmaceutical designed specifically to support nicotine cessation. Prescribed to be taken daily, it partially agonizes α4β2Rs to provide relief from nicotine withdrawal and reduces nicotine-induced DA release (Coe et al., 2005; McCaul et al., 2019). Indeed, a recent study demonstrated that both VTA_{DA} cell activity and DA release in NAcLat in response to IP nicotine was reduced by varenicline (Goldstein et al., 2022). Because varenicline is also a full agonist at α7Rs and the binding of varenicline to α4β2Rs appears to favor the desensitized state (Mihalak et al., 2006), its effects may be explained by increasing nicotine aversion and decreasing nicotine reward through the mechanisms characterized in our study.

While we have established a role for α7R-mediated suppression of DA release in NAcLat via LDT_{GABA}→VTA activity following aversive nicotine, the mechanism underlying the increase of NAcMed DA release during the LC remains unclear; whether this increase is behaviorally relevant for nicotine aversion and which receptors mediate this effect are important topics for future studies.

With many unanswered questions about how to leverage nicotine's unique dose-dependent profile for nicotine addiction treatment in humans, our precise delineation of the neural circuitry and pharmacological mechanisms underlying nicotine aversion is a critical step towards defining novel therapeutic targets for smoking cessation pharmacotherapies.

AUTHOR CONTRIBUTIONS

Stereotactic injections: C.L, A.J.T. Fiber photometry: C.L., A.J.T., Y.Z., J.W.J. Electrophysiology: C.L. Behavior and optogenetics: C.L., L.W.T. Immunohistochemistry: C.L., Y.Z., J.X.D. Critical viral reagents: K.B.L. Computational modeling: C.L., J.P.H.V. Study design: C.L., A.J.T., S.L. Analysis & Interpretation: C.L., A.J.T., J.P.H.V., S.L. Manuscript writing: C.L., A.J.T., S.L.

METHODS

EXPERIMENTAL MODEL AND SUBJECT DETAILS

The following mouse lines (20-35g, 8–20 weeks old, males and females were counterbalanced across conditions with no significant effects of sex observed) were used for experiments: C57BL/6J mice (Jackson Laboratory, stock number: *000664*), DAT::IRES-Cre (Jackson Laboratory, stock number: *006660*, strain code: B6.SJL-Slc6a3tm1.1(cre)Bkmn/J), VGLUT2::IRES-Cre (Jackson Laboratory, stock number: *016963*, strain code: Slc17a6tm2(cre)Lowl/J), and GAD2::IRES-Cre (Jackson Laboratory, stock number: *010802*, strain code: Gad2tm2(cre)Zjh/J). All lines have been crossed onto the C57BL/6J background for

at least six generations. Mice were maintained on a 12:12 light cycle (lights on at 07:00). All procedures complied with the animal care standards set forth by the National Institutes of Health and were approved by University of California, Berkeley's Administrative Panel on Laboratory Animal Care.

METHOD DETAILS

STEREOTAXIC SURGERIES

As previously described (Lammel et al., 2012), all stereotaxic injections were performed under general ketamine–dexmedetomidine anesthesia and using a stereotaxic instrument (Kopf Instruments, Model 1900). For red fluorescent retrograde labeling, mice were injected unilaterally with fluorescent retrobeads (100 nl; LumaFluor Inc.) in the nucleus accumbens (NAc) lateral shell (NAcLat; bregma: 0.98 mm, lateral: 2 mm, ventral: −4.2 mm) or ventral tegmental area (VTA; bregma: -3.4 mm, lateral: 0.3 mm, ventral: -4.5 mm**)** using a 1 µl Hamilton syringe (Hamilton). The AAVs (adeno associated virus) used in this study were from the Deisseroth laboratory (AAV5-EF1α–DIO-hChR2(H134R)-eYFP; AAV5-EF1α-DIO-eYFP; AAV5-EF1α-DIO-mCherry; AAVDJ-DIO-GCaMP6m; AAV-EF1a-DIO-eNpHR3.0-eYFP ~10^{12} infectious units per ml, prepared by the University of North Carolina Vector Core Facility), from the Uchida lab (Harvard) (AAV5-flex-RG; AAV5-flex-TVA-mCherry; ~10^{12} infectious units per ml; prepared by the University of North Carolina Vector Core Facility), from the Tian Lab (UC Davis) (AAV5-hSyn-dLight1.2; AAV9-hSyn1-FLEX-axon-GCaMP6s; prepared by Addgene), from the MIT Vector Core (AAV8.2-hEF1a-DIO-synaptophysin-eYFP), or from the Shah lab (UCSF) (AAV5-flex-taCasp3-TEVp; ~10^{12} infectious units per ml; prepared by the University of North Carolina Vector Core Facility). RV-EnvA-ΔG-GFP was from Kevin Beier (UC Irvine), and 300 nl concentrated virus solution was injected into the VTA (same coordinates as above). For AAV viral injections, 100-500 nl of concentrated AAV solution was injected into the ventral NAc medial shell (NAcMed; bregma: 1.5 mm, lateral: 0.9 mm, ventral: -4.8 mm) and/or NAcLat (same coordinates as above), VTA (same coordinates as above), or laterodorsal tegmentum (LDT; bregma: -5 mm, lateral: 0.5 mm, ventral: -3.4 mm) using a syringe pump (Harvard Apparatus) at 150 nl/min. The injection needle was withdrawn 5 min after the end of the infusion. For behavioral experiments, animals injected with Cre-dependent Channelrhodopsin-2 (ChR2) or eYFP received unilateral implantation of a chronically implanted optical fiber (400 µm, NA = 0.48; Doric Lenses Inc.) dorsal to the VTA (bregma: −3.4 mm, lateral: 0.3 mm, ventral: −3.9 mm). For *in vivo* fiber photometry experiments, mice received unilateral implantation of a chronically implanted optical fiber (400 µm, NA = 0.48; Doric Lenses Inc.) in the VTA (same coordinates as above or angled at 15 degrees with bregma: -3.4 mm, lateral: 1.5 mm, ventral: -4.65 mm) or dual optical fibers in the NAcMed and NAcLat (same coordinates as above) of the same animal. One layer of adhesive cement (C&B Metabond; Parkell) followed by cranioplastic cement (Dental cement) was used to secure the fiber to the skull. The incision was closed with a suture and tissue adhesive (Vetbond; 3M). The animal was woken up with an I.P. injection of atipamezole and kept on a heating pad until it recovered from anesthesia. Experiments were performed 2–12 weeks (for AAVs) or 2–7 days (for retrobeads or rabies) after stereotactic injection. Injection sites and optical fiber placements were confirmed in all animals by preparing coronal sections (50–100 µm) of injection and implantation sites.

JUGULAR VEIN CATHETERIZATION

The protocol for surgical implantation of a catheter in the jugular vein was adapted from (Kmiotek et al., 2012). Briefly, animals were anesthetized with 1:1 ketamine-dexmedetomidine and their temperature maintained on a heating pad for the duration of the surgery. A 4 cm long polyurethane catheter (Silastic) with a silicone bulb 1 cm from the insertion end and a modified, blunted syringe tip on the infusion end was inserted into the jugular vein. After checking for patency, the catheter was secured to the jugular vein with knots made by sutures above and below the silicone bulb. The chest incision was closed with dissolvable sutures and tissue adhesive. The infusion end of the catheter was capped and cemented to the skull with adhesive cement (C&B Metabond; Parkell) followed by cranioplastic cement (dental cement). Mice were kept on a heating pad until recovered from anesthesia. Catheters were flushed daily with physiological saline, and heparin was infused to prevent clogging if necessary. Experiments were performed 2 days after jugular vein catheterization. Patency was verified after experiments were completed via infusion of sodium pentobarbital.

DRUG INFUSIONS

For nicotine infusion experiments, animals were infused with a total of 0.25 mg/kg or 1.25 mg/kg nicotine (free-base) dissolved in sterile, physiological 0.9% saline. Animals received infusions at a volume of 1.25 µl/g (41 µg/kg nicotine per infusion for 0.25 mg/kg total or 208 µg/kg/inf for 1.25 mg/kg total) six times over 30 minutes, every five minutes, through the jugular vein catheter. For fiber photometry experiments, animals were head-fixed on a running wheel and then underwent a 10-minute baseline recording session before the initiation of the same nicotine infusion protocol as shown in **Figure 1A**. In experiments involving nAChR antagonists, animals received a pre-treatment infusion of the antagonist or saline at minute 5 during the 10-minute baseline recording. nAChR antagonists were then co-infused with aversive nicotine according to the protocol described above starting at minute 10. Animals received aversive nicotine with MEC (1.1 mg/kg), MLA (4.5 mg/kg), DHBE (3 mg/kg, except GAD2-Cre animals, which received 1.7 mg/kg due to high fatality rates) or without antagonist on separate recording days with 48 hours between each session. Antagonist solutions were prepared in physiological saline to achieve free base doses at a volume of 1.25 µl/g/infusion whether delivered alone during the minute 5 pre-treatment or co-infused with 1.25 mg/kg free base nicotine

ELECTROPHYSIOLOGY

Mice were deeply anaesthetized with pentobarbital (200 mg/kg ip; Vortech). Coronal midbrain slices (200 µm) were prepared after intracardial perfusion with ice-cold artificial cerebrospinal fluid (ACSF) containing (in mM) 50 sucrose, 125 NaCl, 25 $NaHCO_3$, 2.5 KCl, 1.25 NaH_2PO_4, 0.1 $CaCl_2$, 4.9 $MgCl_2$, and 2.5 glucose (oxygenated with 95% O_2/5% CO_2). After 90 min of recovery, slices were transferred to a recording chamber and perfused continuously at 2–4 ml/min with oxygenated ACSF, containing (in mM) 125 NaCl, 25 $NaHCO_3$, 2.5 KCl, 1.25 NaH_2PO4, 11 glucose, 1.3 $MgCl_2$ and 2.5 $CaCl_2$ at ~30 °C. Cells were visualized with a 40x water-immersion objective on an upright fluorescent microscope (BX51WI; Olympus) equipped with infrared-differential interference contrast video microscopy and epifluorescence (Olympus). Patch pipettes (3.8–4.4 MΩ) were pulled from borosilicate glass (G150TF-4; Warner Instruments) and filled with internal solution, which consisted of (in mM) 130 CsCl, 1 EGTA, 10 HEPES, 1 MgATP, 0.2 NaGTP, 0.1% neurobiotin pH 7.35 (270–285 mOsm). Light-evoked IPSCs (**Figure S5A-S5D**) were recorded in the presence of 20 µM CNQX (6-cyano-7-nitroquinoxaline-2,3-dione, Bio-tech) and 50 µM D-AP5 (Tocris) to block AMPA and NMDA

receptors, respectively. We also added the voltage-gated sodium channel antagonist tetrodotoxin (TTX, 1 μM, Hello Bio) and the potassium channel antagonist 4-aminopyridine (4-AP, 1 mM, Sigma) to the bath solution in order to isolate monosynaptic inputs. Electrophysiological recordings were made at 32°C using a MultiClamp700B amplifier and acquired using a Digidata 1440A digitizer, sampled at 10 kHz, and filtered at 2 kHz. All data acquisition was performed using pCLAMP software (Molecular Devices). Channelrhodopsin-2 was stimulated by flashing 473 nm light through the light path of the microscope using an ultrahigh-powered light-emitting diode (LED) powered by an LED driver (Prizmatix) under computer control. A dual lamp house adaptor (Olympus) was used to switch between fluorescence lamp and LED light source. The light intensity of the LED was not changed during the experiments and the whole slice was illuminated (5 mW/mm2). Light-evoked IPSCs were obtained every 20 s with one pulse of 473 nm wavelength light (3 ms) with neurons voltage clamped at −70 mV. Series resistance (15–25 MΩ) and input resistance were monitored online. Data were analyzed offline using Clampfit (Molecular Devices) or IgorPro Software (Wavemetrics). Light-evoked IPSC amplitudes were calculated by averaging responses from 10 sweeps and then measuring the peak amplitude in a 50 ms window after the light pulse. Cells that did not show a peak in this window that exceeded the baseline noise were counted as non-responders. To determine the dopaminergic identity of retrobead-labeled VTA neurons (i.e., tyrosine hydroxylase (TH)-immunopositive or TH-immunonegative), cells were filled with neurobiotin (Vector) during patch clamp recordings, then fixed in 4% paraformaldehyde (PFA) and 24 h later immunostained for TH. All recorded retrobead-labeled cells were located in the lateral VTA and were TH-immunopositive.

FIBER PHOTOMETRY

Four to eight weeks after virus injection, animals were implanted with fiberoptic implants and/or jugular vein catheters and allowed to recover for 2-7 days before fiber photometry recordings. In experiments with dual fiberoptic implants (**Figures 3 and 5**), animals were implanted in one NAc subregion on one side, and the other region on the other side, sides counterbalanced between animals. For experiments involving IV infusions, a baseline of 10 minutes was recorded in head-fixed animals before initiating intravenous nicotine infusions (same protocol as shown in **Figure 1A**) with antagonist infusion at minute 5 for experiments involving antagonists (see '*DRUG INFUSIONS'* section above for dose and timing protocols). In experiment involving ChR2 stimulation of LDT_{GABA} neurons (**Figure S5E-S5G**), animals received 3-5mW 473 nm laser stimulation over 2 s (5 ms pulses at 20 Hz) every 10 s for a total of 20 trials per session. Calcium or DA transients were measured in head-fixed animals using a custom-built fiber photometry system as described previously (de Jong et al., 2019). Briefly, fluorescence signals were obtained by stimulating cells expressing GCaMP6m, GCaMP6s, or dLight1.2 with a 470 nm LED (20 μW at fiber tip) while calcium-independent signals were obtained by stimulating these cells with a 405 nm LED (20 μW at fiber tip). 470 nm and 405 nm LED light were alternated at 20 Hz and light emission was recorded using an sCMOS Camera (Hamamatsu Flash or Photometrics Prime), which acquired video frames containing the entire fiber bundle (2 fibers, 3 m in length, NA = 0.48, 400 μm core, Doric Lenses) at the same frequency. Video frames were analyzed online and fluorescent signals were acquired using custom acquisition code (de Jong et al., 2019). The fluorescent signal obtained after stimulation with 405 nm light was used to correct for movement artifacts as follows: first, the 405 nm signal was fitted to the 470 nm signal using the first and second coefficients of the polynomial that was the best fit (least squares) to the 470 nm signal. The fitted 405 nm signal was then subtracted from the 470 nm signal to obtain

the movement and bleaching-corrected signal. 405 nm stimulation was omitted from most dLight recordings to maximize light collection and a baseline tracking general photobleaching trend was subtracted instead. Although some movement may contribute to the signal detected, movement artifacts are minimized in a head-fixed setup and not expected to occlude the nicotine-related signal. Signals were normalized (Z score) based on the mean and standard deviation of signal during the pre-nicotine baseline period at 100-500 s (intact and caspase experiments) or 100-290 s (antagonist experiments) and peri-event plots for the nicotine infusions were generated. Baseline normalization was performed on the original ΔF/F signal using the time-window -2 to 0.5 sec prior to infusion. Thus, z scores accurately reflect the number of standard deviations from the mean during baseline and AUCs calculated are relative to signal immediately prior to infusion. If the AUCs of individual infusions were not normally distributed, assessed by a Kolmogorov-Smirnov test, analysis of the first infusion was performed separately from analysis of infusions 2-6.

BEHAVIORAL ASSAYS

All behavioral tests were performed during the light phase in a temperature (68-74°F) and humidity (40-60%) controlled room that is illuminated by eight 32 W fluorescent lights each producing 2925 lumens. Behavioral equipment was cleaned with 70% EtOH and an odor remover (Nature's Miracle) between individual animals.

Conditioned Place Preference or Aversion (CPP or CPA): For experiments involving IV infusions of nicotine (**Figure 1)**, animals recovered from jugular vein catheterization for 2 days before beginning the CPP protocol. On the first pre-test day, mice were placed in the center compartment of a custom-made three-compartment chamber and allowed to explore the full chamber freely for 10 min while their movement in the chamber was recorded via a video tracking system (Biobserve). During the next 3 days, mice were placed in one side of the chamber, for 30 min, blocked from exploring the other regions, and infused with sterile, physiological 0.9% saline (volume: 1.25 µl/g) six times over 30 minutes, every five minutes, through the jugular vein catheter. In the afternoon, mice were placed in the opposite chamber for 30 min and infused with nicotine (total dose: 0.25 mg/kg or 1.25 mg/kg free base; each infusion: 41 µg/kg or 208 µg/kg) dissolved in saline every 5 minutes. Conditioning chambers were assigned according to a biased method to pair the hypothesized rewarding dose of nicotine (0.25 mg/kg) with the less-preferred side on the initial pre-test and the hypothesized aversive dose of nicotine (1.25 mg/kg) was paired with the initially preferred chamber. On the final post-test day, mice were again allowed to explore the full chamber freely for 10 min while movement was recorded. The time spent in each compartment (nicotine-conditioned, neutral, and saline-conditioned) was calculated and compared on post-test to pre-test scores to generate place preference (or avoidance) scores. For experiments involving optogenetic inhibition (**Figure 5L-5P**), animals recovered from fiberoptic implantation for at least 7 days before CPP. The behavioral paradigm was identical except mice were injected intraperitoneally (IP) with 10 µl/g saline immediately before the morning conditioning session and in the afternoon session, animals received 2.5 mg/kg nicotine IP (dissolved in 10 µl/g saline) and continuous 3-5 mW 589 nm light. Nicotine reliably induces conditioned place aversion at high doses, whether delivered IP or IV. We chose to deliver aversive nicotine via intraperitoneal injection in this experiment to replicate the methods used by Wolfman et al., 2018 to establish the habenulo-interpeduncular axis as a regulator of nicotine aversion.

Real-time Place Preference and Aversion (**Figures S2H-S2I**, **S5H-S5J and S7F**): Six weeks after virus injection, mice with optogenetic implants were connected to a fiberoptic cable and placed in a custom-made three-compartment chamber (same as above). For optogenetic stimulation, the cable was connected to a 473 nm or 589 nm DPSS laser diode (Laserglow) through an FC/PC adaptor, and laser output was controlled using a Master-8 pulse stimulator (A.M.P.I.). Power output was tested using a digital power meter (Thorlabs) and was checked before and after each experimental animal; output during light stimulation was estimated to be 3-5 mW/mm^2 at the targeted tissue 200 μm from the fiber tip (www.optogenetics.org/calc). The left side of the chamber was designated as the initial stimulation side (Phase 1) and after 10 min the stimulation side was switched to the other previously non-stimulated side of the chamber (Phase 2). The middle of the chamber was a neutral area that was never paired with stimulation. At the start of each session, the mouse was placed in the middle of the chamber, and every time the mouse crossed to the stimulation side, constant laser stimulation (473 nm: 20 Hz, 5 ms pulses; 589 nm: continuous light) was delivered until the mouse exited the stimulation area. There was no interruption between Phase 1 and Phase 2. The movement of the mice was recorded via a video tracking system (Biobserve) and the time the mice spent in each area (stimulated, non-stimulated, neutral) was calculated.

Open Field Test: For optogenetics (**Figures S2J, S5K and S7G**), mice were placed in the open field chamber and their movement was recorded and analyzed for 15 min using video-tracking (Biobserve). The 15-min session was divided into three 5-min epochs; during the first epoch, there was no light stimulation (off), during the second epoch the animal received light stimulation (on), and during the third epoch there was no light stimulation (off). Light output and frequency were the same as described in the real-time place preference section.

COMPUTATIONAL MODELING

We calculated blood-nicotine concentrations in our infusion experiment using nicotine's estimated half-life in C57BL/6J mice of 9.2 minutes (Siu and Tyndale, 2007) nicotine reaching the blood immediately upon intravenous infusion.

$$[Nic]_1 = [Nic]_0 e^{\frac{-ln\,(2)}{9.2}}$$

Blood nicotine concentrations (mg/kg) were converted into brain nicotine concentrations (μM) without a multiplication factor since no empirical data was available on the relationship between blood and brain nicotine concentrations in mice and our simulated data recruited α7 receptors at the high, but not low dose of nicotine similar to observations made in mice (Fenster et al., 1997; Wooltorton et al., 2003). For nicotine to reach the brain from the blood, we applied a temporal delay, given that the brain nicotine concentration peaks ~11 s after it peaks in the blood (Berridge et al., 2010); we implemented this delay by letting the brain nicotine concentration follow the blood concentration at a rate of 25% of the concentration difference per second. Then, for both the α4β2 and α7 receptors, we calculated (de)sensitization and net activation of each of the receptors based on equations modified from Graupner et al., 2013 with a constant baseline acetylcholine (ACh) concentration of 0.1 μM. The time course of activation and desensitization for each receptor is given by

$$\frac{dy}{dt} = \frac{(y_\infty(Nic, ACh) - y)}{\tau_y(Nic, ACh)}$$

where $\tau_y(Nic, ACh)$ is the time constant where a steady state for $y_\infty(Nic, ACh)$ is achieved. The maximal activation (a_∞) or sensitization (s_∞) for a given Nic/ACh concentration are determined by the half-maximal concentrations of nAChR activation (EC_{50}) and sensitization (IC_{50}) according to the following Hill equations

$$a_\infty(Nic, ACh) = \frac{(ACh + \alpha Nic)^{n_a}}{EC_{50}^{n_a} + (ACh + \alpha Nic)^{n_a}}$$

$$s_\infty(Nic, ACh) = \frac{IC_{50}^{n_s}}{IC_{50}^{n_s} + (Nic + \eta ACh)^{n_s}}$$

where α accounts for the affinity for α4β2 (α = 3) and α7 (α = 2) receptors for Nic relative to ACh, η is a fraction that determines how much ACh drives receptor desensitization, and n_a and n_s represent the Hill coefficients of activation and sensitization respectively.

The time constant for receptor desensitization (τ_d) for a given Nic/ACh concentration is determined by the fastest time constant at which the receptor is desensitized (τ_0), the desensitization recovery time constant (τ_{max}), the concentration at which the desensitization time constant is half-minimum (K_τ), and the fraction of ACh concentration that influences the desensitization time constant (η) according to the following equation:

$$\tau_d(Nic, ACh) = \tau_0 + \tau_{max} \frac{K_\tau^{n_\tau}}{K_\tau^{n_\tau} + (Nic + \eta ACh)^{n_\tau}}$$

Rise and decay filters were applied to each receptor activation curve to depict bulk photometry signals more accurately from the experimental data, given the relatively slow response kinetics of fluorophores (Akerboom et al., 2012) the fluorophore signal was set to follow the true receptor activation curve at a rate of 5% of the difference between the two signals per second. For the antagonist simulation (**Figures 2F and 2G**), sensitization was set at 20% of its baseline value (mimicking an 80% receptor desensitization by α4β2R antagonist DHBE due to its fatality at high doses). For predicting the response of DA neurons (expressing α4β2Rs) that receives an α7 receptor-expressing GABAergic input (**Figures 4E, 4F and 5A-5C**), we subtracted the activation of an α7 receptor-activated unit from the activation of an α4β2R-expressing unit at 50% strength.

HISTOLOGY AND MICROSCOPY

Immunohistochemistry and Microscopy: Were performed as described previously in (Lammel et al., 2012). Briefly, after intracardial perfusion with 4% paraformaldehyde in PBS, pH 7.4, the brains were post-fixed overnight and coronal brain sections (50 or 100 μm) were prepared. Sections were stained overnight in a primary antibody solution (rabbit anti-TH, mouse anti-TH

(all Millipore), all 1:1000). Twenty-four hours later, sections were stained for 4 hours in secondary antibody solution (goat anti-mouse Alexa Fluor 488, goat anti-rabbit Alexa Fluor 488 (all Thermo Fisher Scientific), all 1:750). Image acquisition was performed with Zeiss LSM 710 laser scanning confocal microscope using 20x or 40x objectives and on a Zeiss AxioImager M2 upright widefield fluorescence/differential interference contrast microscope with charge-coupled device camera using 5x, 10x and 20x objectives. Images were analyzed using ImageJ. Sections were labeled relative to bregma using landmarks and neuroanatomical nomenclature as described in "*The Mouse Brain in Stereotaxic Coordinates*" (Franklin and Paxinos, 2013). All images presented with multiple colors represent a composite of images collected with different excitation wavelengths.

In situ Hybridization: To determine the extent of co-expression of VGLUT2 and GAD2 in LDT neurons (**Figure S4A**), we combined Cre-dependent viral fluorophore expression with *in situ* hybridization. Probe sequence for the *Vglut2* and *Gad1* and *Gad2* DIG RNA probes as well as the free floating *in situ* protocol were adapted from (Weissbourd et al., 2014). GAD2-Cre (n = 2 mice) and VGLUT2-Cre (n = 2 mice) mice were injected with 500 nl AAV5-EF1α-DIO-eYFP into the LDT. Two weeks later, the animals were euthanized and 100 µm sections of the LDT were sliced and washed in diethyl pyrocarbonate (DEPC)-treated PBS and treated with a 7 µg/ml proteinase K solution for 10 min at 37°C. Proteinase K was inactivated using 4% PFA in PBS, which was followed by washing in PBS and acetylation in 0.25% acetic anhydride in 0.1 M triethanolamine in DEPC-treated water. Tissue sections were incubated overnight in hybridization solution (50% deionized formamide, 1x Denhardt's, 10% Dextran sulphate and 5x Saline-Sodium Citrate (SSC)) with 100 ng/ml probe at 55°C. Stringency washes were in 2x SSC with 50% formamide for 1 hour, and in 2x SSC and 0.2x SSC for 20 min, each at 65°C. This was followed by blocking for 1 hour in DIG blocking buffer (Roche) and overnight incubation at 25°C in 1:1000 Anti-Digoxigenin-AP FAB fragments (Roche). Slices from the VGLUT2-Cre animals were incubated with probes for *Gad1/2* RNA and slices from GAD2-Cre animals were incubated with probes for *Vglut2* mRNA. Because the *in situ* hybridization procedure attenuates fluorescence, tissue sections were co-stained with a chicken anti-GFP (1:1000, Abcam). Primary antibody incubation was for 2 hours and was followed by washing steps in DIG wash buffer (Roche) and incubation with secondary antibodies (Alexa Fluor 546 goat anti-rabbit, Alexa Fluor 647 goat anti-mouse (all 1:750, Thermo Fisher Scientific) and Alexa Fluor 477 goat anti-chicken (1:750, Abcam) as well as the alkaline phosphatase substrate reacting with NBT/BCIP in detection buffer (Roche). Slides were imaged on a Zeiss AxioImager M2 microscope using a 20x objective. Quantification of co-expression was manually counted using ImageJ.

Whole Brain Input Mapping: To map inputs to LDT_{GABA}→VTA and $LDT_{Glutamate}$→VTA neurons (**Figures S4E-S4I**), we used a rabies virus-based genetic mapping strategy to label presynaptic inputs onto designated starter cell populations, and quantified input cell data using a customized, semi-automated whole-brain mapping Matlab script. Specifically, VGLUT2-Cre (n = 4 mice) and GAD2-Cre (n = 3 mice) mice were injected with AAV-FLEX-TVA-mCherry (i.e., a cellular receptor for subgroup A avian leukosis viruses) and AAV-FLEX-RG (i.e., rabies virus glycoprotein; 250 nl, 1:1) into the LDT and four weeks later, 300 nl RV-EnvA-ΔG-GFP (i.e., pseudotyped, glycoprotein-deficient, GFP-expressing rabies virus) was injected into the VTA (see "*Stereotaxic Injections*" for coordinates). Seven days after injection, mice were perfused with 4% PFA in PBS. For input mapping, 50 µm sections of the whole brain, excluding the

olfactory bulb and cerebellum, were prepared, and scanned using a Zeiss Axio Scan Z1 microscope. Individual slices were aligned using customized Matlab scripts. GFP-positive pixels were identified on the basis of a pixel-intensity threshold in the green channel. False-positive pixels (artifacts) were manually identified and removed. Positive pixels were assigned to different brain areas based on "*The Mouse Brain in Stereotaxic Coordinates*" (Franklin and Paxinos, 2013). Pixels per brain area were then represented as a percentage of total input pixels. 31 slices were randomly selected to validate this semi-automated quantification method and a human observer counted GFP-positive cells in these regions. These results demonstrated a high correlation between manual scoring of input neurons by an independent observer and our automated segmentation procedure ($R2 = 0.9$, $n = 31$ slices).

Fluorescent in situ hybridization: The fluorescent *in situ* hybridization experiments (**Figures S4J-S4K**) were conducted using a commercially available RNAscope® Multiplex Fluorescent Reagent Kit V2 (ACD Bio, USA). Brains were extracted and snapfrozen by submerging them into frozen isopentane (-70 to -50°C). They were stored in an airtight container in a -80°C freezer. 16 μm coronal LDT brain slices were prepared using a cryostat, placed on Superfrost Plus microscope slides (Fisher Scientific, USA) and stored in a -80°C freezer. On the next day, brain slices were fixed in 4% paraformaldehyde (PFA) in PBS (30 min) followed by an ethanol dehydration procedure (20 min). Slices were then bathed in hydrogen peroxide (10 min), followed by protease IV from the RNAscope® kit (15 min). Next, probe mixes were made containing α7R (Mm-Chrna7), GAD2 (Mm-Gad2). Probe mixes were applied to the brain slices for hybridization (2 hours at 40°C). After amplification of the signal (using AMP1, AMP2 and AMP3 from the RNAscope® kit), channel C1 was developed using green Opal 520 (Akoya Biosciences, USA) and channel C2 was developed using orange Opal 570 (Akoya Biosciences, USA). Lastly, nuclei were stained using DAPI (from the RNAscope® kit) and brain slices were sealed with ProLong Gold Antifade mountant (Thermo Fisher Scientific, USA) and a glass coverslip. Images were taken using a confocal microscope (LSM710, Carl Zeiss Inc.) at 5 different z depths (spanning 4.4 μm), and images were flattened by taking the maximum projection across the z direction. Regions of interest (ROIs) were identified using a machine learning-based segmentation algorithm NucleAIzer37 based on the DAPI channel. The amount of visible mRNA across the DAPI-identified region was used as a proxy for total mRNA in the cell. All identified regions of interest were manually sorted by an investigator who was blind to brain region and probe mix. ROIs were removed if they (i) showed overlap with other regions of interest or (ii) were segmentated inadequately by the algorithm. Using a custom-made MATLAB algorithm, the remaining cells were analyzed based on the percentage of DAPI-positive pixels that were also positive for targeted mRNA. To adjust for potential differences in staining and/or image quality, we compared pixels in all regions of interest to background fluorescence levels in each image. To do this, we first established a 'null distribution' that quantifies the distribution in pixel intensity values for cells putatively negative for targeted mRNA. Each cell's distribution of pixel intensities was compared to the null distribution for the targeted mRNA and a correlation coefficient R was calculated. If R of a cell's distribution compared to the null distribution was less than 0.85, then a cell was labeled as positive for the targeted mRNA.

QUANTIFICATION AND STATISTICAL ANALYSIS

Student's t tests (paired and unpaired), one-way or two-way ANOVA tests, and mixed effects analyses were used to determine statistical differences using GraphPad Prism 9 (Graphpad

Software). Kolmogorov-Smirnov tests were performed on AUCs of individual infusions to check for a normal distribution. Holm-Sidak's post hoc analysis was applied when a one-way ANOVA or mixed effects analysis showed a significant main effect, or a two-way ANOVA or mixed effects analysis showed a significant interaction. Statistical significance was * $p < 0.05$, ** $p < 0.01$, *** $p < 0.001$. All data are presented as means ± SEM. All details of the statistical analysis including means, SEMs, and number of animals used are summarized in **Supplementary Table S1**.

SUPPLEMENTARY FIGURES

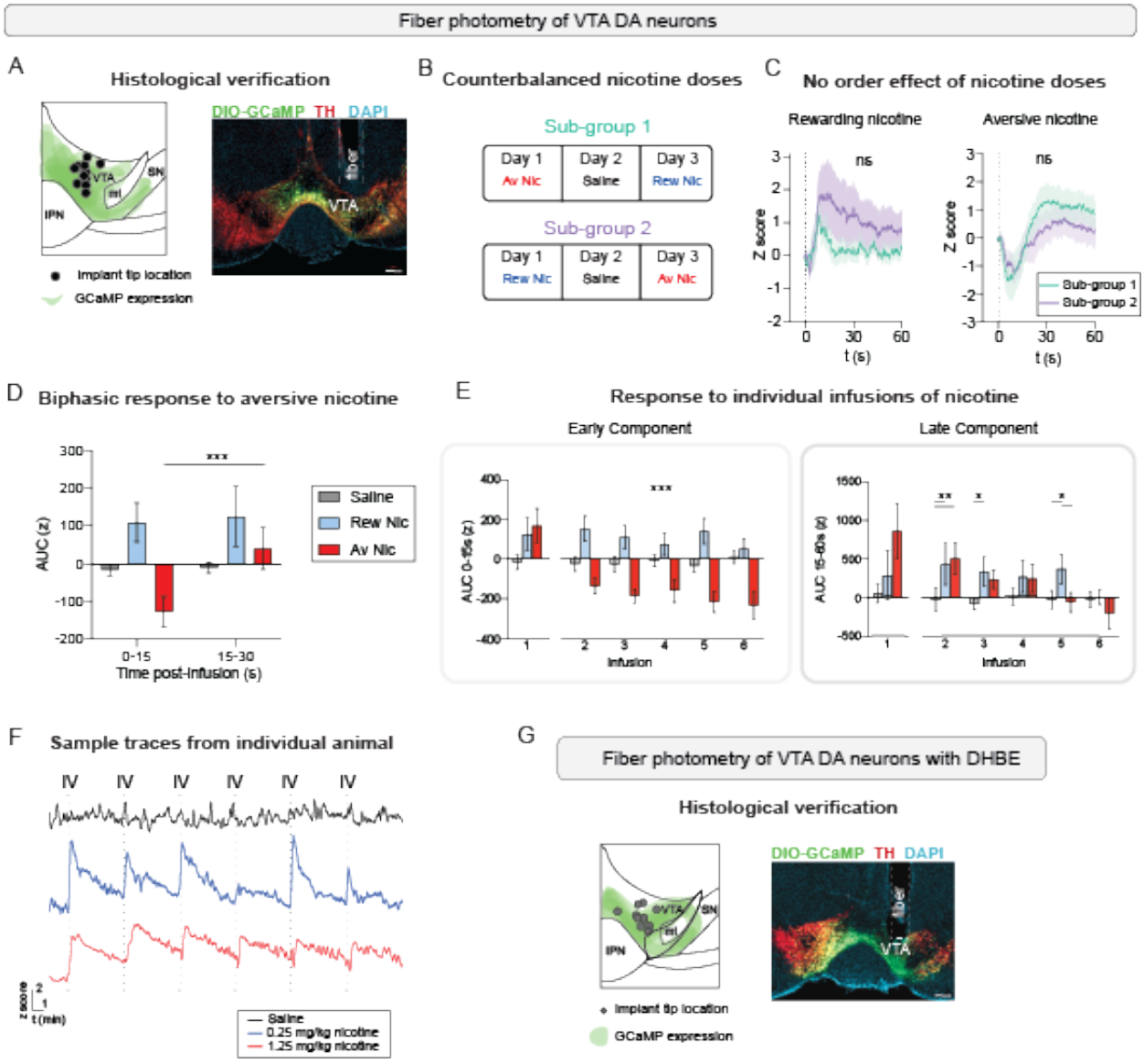

Figure S1. Fiber photometry of VTA DA cell bodies, Related to Figure 2.
(A) Histological verification (left) and sample fluorescent image (right) of GCaMP6m (green) expression and optical fiber placements in VTA of DAT-Cre mice (n = 11 mice) used for

experiments shown in **Figures 2A-2E** (red - tyrosine hydroxylase (TH), blue – DAPI; IPN: interpeduncular nucleus, VTA: ventral tegmental area, SN: substantia nigra, ml: medial lemniscus, DAT: dopamine transporter) (scale bar 200 μm).
(B) Animals were randomly divided into two groups and the initial nicotine dose was counter-balanced across days.
(C) No significant (ns) difference in VTA DA GCaMP6m activity between sub-group 1 (turquoise, n = 5 mice) or sub-group 2 (purple, n = 6 mice) in response to rewarding (left) or aversive (right) nicotine (area of light shading represents SEM).
(D) AUCs of averaged VTA DA GCaMP6m response to saline (grey), rewarding nicotine (blue), and aversive nicotine (red) (within-animal, n = 11 mice) of equivalent time bins (15 s) demonstrates a significantly different response across time only in the aversive nicotine condition (*** $p < 0.001$; data represent means ± SEM).
(E) Left: Averaged VTA DA GCaMP6m responses for individual infusions during the early component (0-15s) reveal consistent activation of VTA DA cells by rewarding nicotine, but a gradual suppression of activity by aversive nicotine after the first infusion. Right: The inhibitory effects of aversive nicotine are less pronounced during the remainder of the 60s post-infusion response and the activation by rewarding nicotine gradually decreases with each infusion (gap denotes separate analyses for infusion 1 and infusions 2-6 due to non-normal distribution, * $p < 0.05$, ** $p < 0.01$, *** $p < 0.001$; data represent means ± SEM).
(F) Sample whole traces from a representative animal receiving saline (grey), rewarding nicotine (blue) or aversive nicotine (red).
(G) Histological verification (left) and sample fluorescent image (right) of GCaMP6m expression and optical fiber placements in VTA of DAT-Cre mice (n = 11 mice) used in experiments shown in **Figures 2H-2K** (scale bar 200 μm).

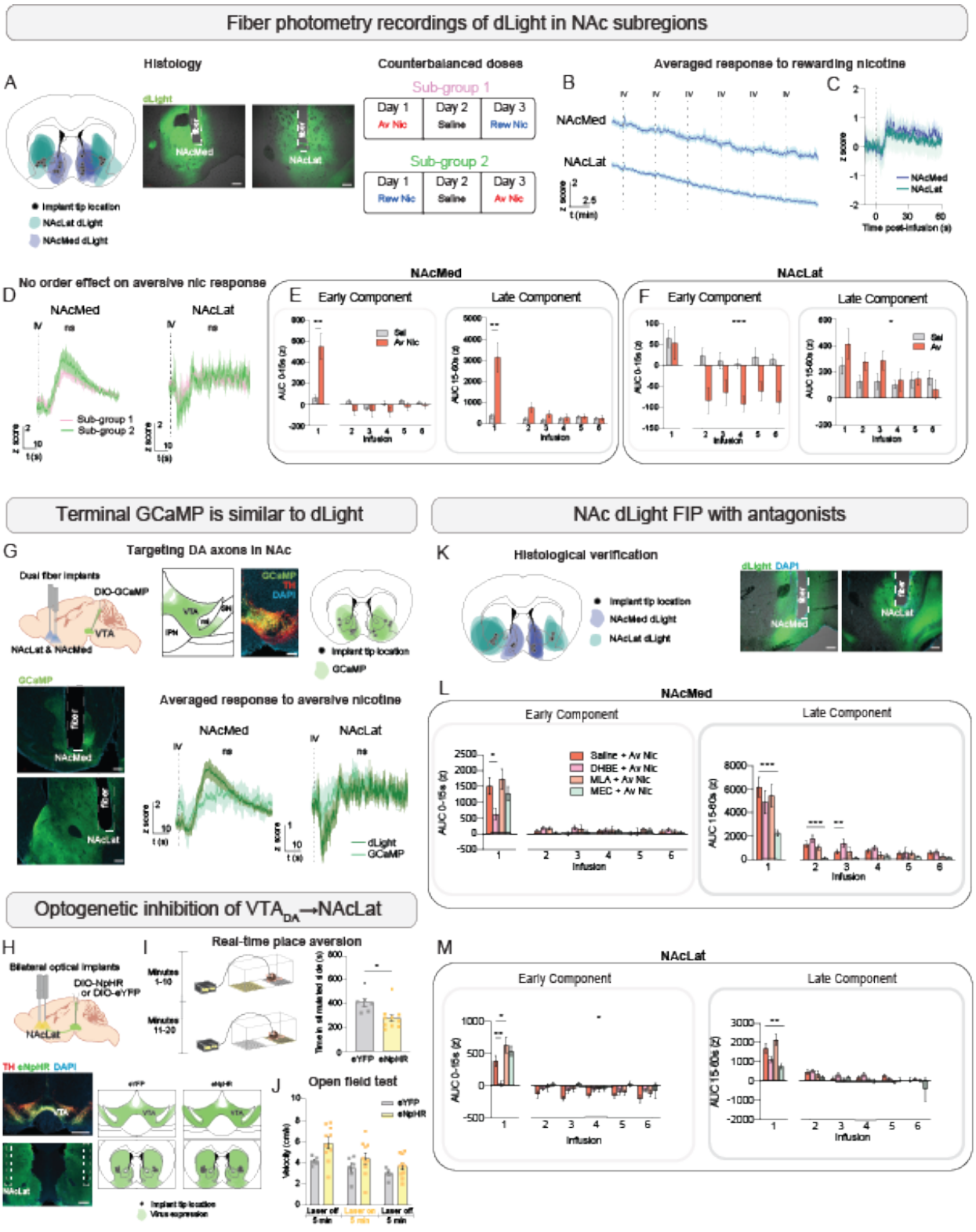

Figure S2. Fiber photometry recordings of dLight and GCaMP in separate NAc subregions, Related to Figure 3.

(A) Left: Histological verification of dLight1.2 expression and optical fiber placements in NAc medial shell (NAcMed) and NAc lateral shell (NAcLat) for experiments shown in **Figures 3A-3F**. Middle: Sample fluorescent images of the respective brain structures (green – dLight1.2; scale bars 200 μm). Right: To facilitate within-animal comparisons of nicotine dose, the order of nicotine dose was counterbalanced between two randomly assigned sub-groups.
(B) Averaged whole traces of dLight response to the rewarding dose of nicotine in NAcMed and NAcLat (area of light shading represents SEM).
(C) Peri-infusion plots of dLight fluorescence averaged across infusions for NAcMed (indigo) compared to NAcLat (turquoise). A 2-way ANOVA with multiple comparisons test for each time point from 1 s pre-infusion to 60 s post-infusion (10 Hz sample rate, n = 611 data points) revealed no significant (ns) differences between NAc subregions (area of light shading represents SEM).
(D) No order effect was observed between animals that received the aversive dose first (sub-group 1, pink) or the rewarding dose first (sub-group 2, green) in the NAcMed or NAcLat when performing a 2-way ANOVA with multiple comparisons test for each time point (n = 611 data points; area of light shading represents SEM).
(E) AUCs for dLight response to individual infusions of aversive nicotine (Av Nic, red) or saline (Sal, grey) in the NAcMed reveal that the increase of DA release during the early and late components occur primarily in response to the first infusion (gap denotes separate analyses for infusion 1 and infusions 2-6 due to non-normal distribution, ** $p < 0.01$, data represent means ± SEM).
(F) AUCs for dLight response to individual infusions during the early (left) and late (right) component in NAcLat (gap denotes separate analyses for infusion 1 and infusions 2-6 due to non-normal distribution, * $p < 0.05$, *** $p < 0.001$, data represent means ± SEM).
(G) Top left: Schematic of experimental design of targeting GCaMP6m to VTA DA neurons in DAT-Cre mice and implantation of optical fibers in NAcMed and NAcLat. Fiber photometry (FIP) recordings are performed during IV infusions of aversive nicotine. Top right: Histological verification of GCaMP6m expression in VTA and optical fiber placements in NAcMed and NAcLat. Bottom: Sample fluorescent images of GCaMP6m (green) expression in VTA (red – TH, blue – DAPI; scale bar 200 μm) (left) and optical fiber placements in NAcMed and NAcLat (right) (scale bars 200 μm). No significant differences between dLight and GCaMP signals in either NAcMed or NAcLat when performing a 2-way ANOVA with multiple comparisons test for each time point (n = 611 points; area of light shading represents SEM).
(H) Top: Schematic of experimental design. Bottom: Sample fluorescent image and schematics showing histological verification of eYFP or eNpHR (green) expression in the VTA of DAT-Cre mice (red - TH); blue - DAPI) as well as verification of optical fiber locations in the NAcLat (scale bars 500 μm).
(I) Left: Schematic of real-time place preference/aversion assay. Animals received 589 nm light on different sides of the chamber. Right: Bar graph showing that eNpHR mice (n = 10) spent significantly less time in the light-paired side of the chamber compared to eYFP control mice (n = 6 mice) (* $p < 0.05$, data represent means ± SEM).
(J) Bar graph showing no significant differences in general locomotor behavior (with or without 589 nm light) in the open field test between eNpHR (n = 10 mice) and eYFP (n = 6 mice) mice.
(K) Left: Histological verification of dLight1.2 expression and optical fiber placements in NAcMed and NAcLat for experiments shown in **Figures 3G-3N**. Right: Sample fluorescent images of the respective brain structures (green – dLight, blue – DAPI) (scale bars 200 μm).

(L) AUCs of dLight response to individual infusions of aversive nicotine with pretreatment and co-infusion of antagonists in NAcMed during the early and late component (gap denotes separate analyses for infusion 1 and infusions 2-6 due to non-normal distribution, * $p < 0.5$, ** $p < 0.01$, *** $p < 0.001$; data represent means ± SEM).
(M) Same as in (L) but for NAcLat (gap denotes separate analyses for infusion 1 and infusions 2-6 due to non-normal distribution, * $p < 0.5$, ** $p < 0.01$, data represent means ± SEM).

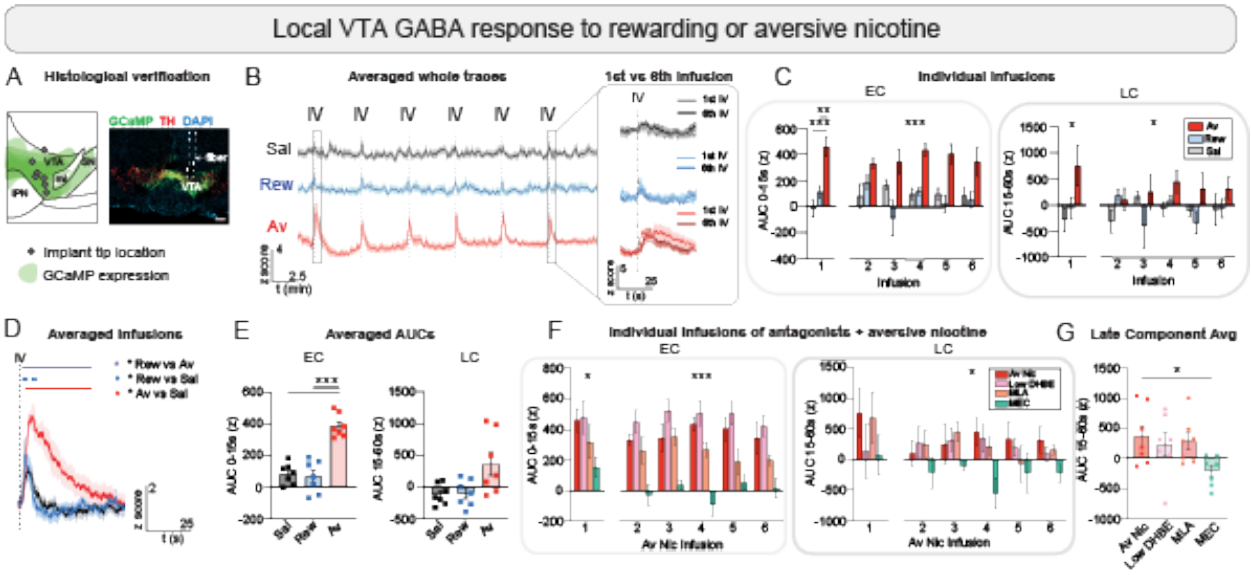

Figure S3. VTA GABA response to rewarding or aversive nicotine, Related to Figure 4.
(A) Left: Histological verification of GCaMP6m expression and optical fiber placements in VTA of GAD2-Cre mice (n = 7 mice) for experiments shown in **Figures 4G-4J**. Right: Sample fluorescent image of the VTA showing TH-immunohistochemistry (red) and GCaMP6m (green) expression. Note, that TH-immunopositive cells do not co-express GCaMP6m (blue – DAPI, scale bar 200 µm).
(B) Averaged whole traces for saline (Sal, grey), rewarding nicotine (Rew, blue), and aversive nicotine (Av, red) infusions recorded in VTA GABA neurons. Inset: Comparison between first and last infusions (area of light shading represents SEM).
(C) AUCs for GCaMP response in VTA GABA neurons to individual infusions during the early (left) and late (right) components (gap denotes separate analyses for infusion 1 and infusions 2-6 due to non-normal distribution; EC: early component; LC: late component; * $p < 0.5$, ** $p < 0.01$, *** $p < 0.001$; data represent means ± SEM).
(D) Peri-infusion plot of averaged GCaMP response in VTA GABA neurons across infusions for saline (black), rewarding nicotine (blue), and aversive nicotine (red) (area of light shading represents SEM). Dots above traces denote significant differences from a multiple comparisons test after 2-way ANOVA (purple – rewarding versus aversive nicotine, blue – rewarding nicotine versus saline, red – aversive nicotine versus saline; * $p < 0.05$).
(E) AUCs for the early (left) and late (right) components averaged across infusions recorded in VTA GABA neurons. The aversive dose of nicotine elicits a significantly higher response compared to rewarding nicotine and saline conditions during the early component (*** $p < 0.001$, data represent means ± SEM).

(F) AUCs of GCaMP response in VTA GABA neurons to individual infusions of aversive nicotine with pretreatment and co-infusion of antagonists during the early (left) and late (right) components (gap denotes separate analyses for infusion 1 and infusions 2-6 due to non-normal distribution, * $p < 0.5$, *** $p < 0.001$; data represent means ± SEM).
(G) Averaged AUC GCaMP response in VTA GABA neurons to aversive nicotine with antagonists during the late component. Only MEC significantly reduced GCaMP activity in VTA GABA neurons in response to aversive nicotine (* $p < 0.05$, data represent means ± SEM).

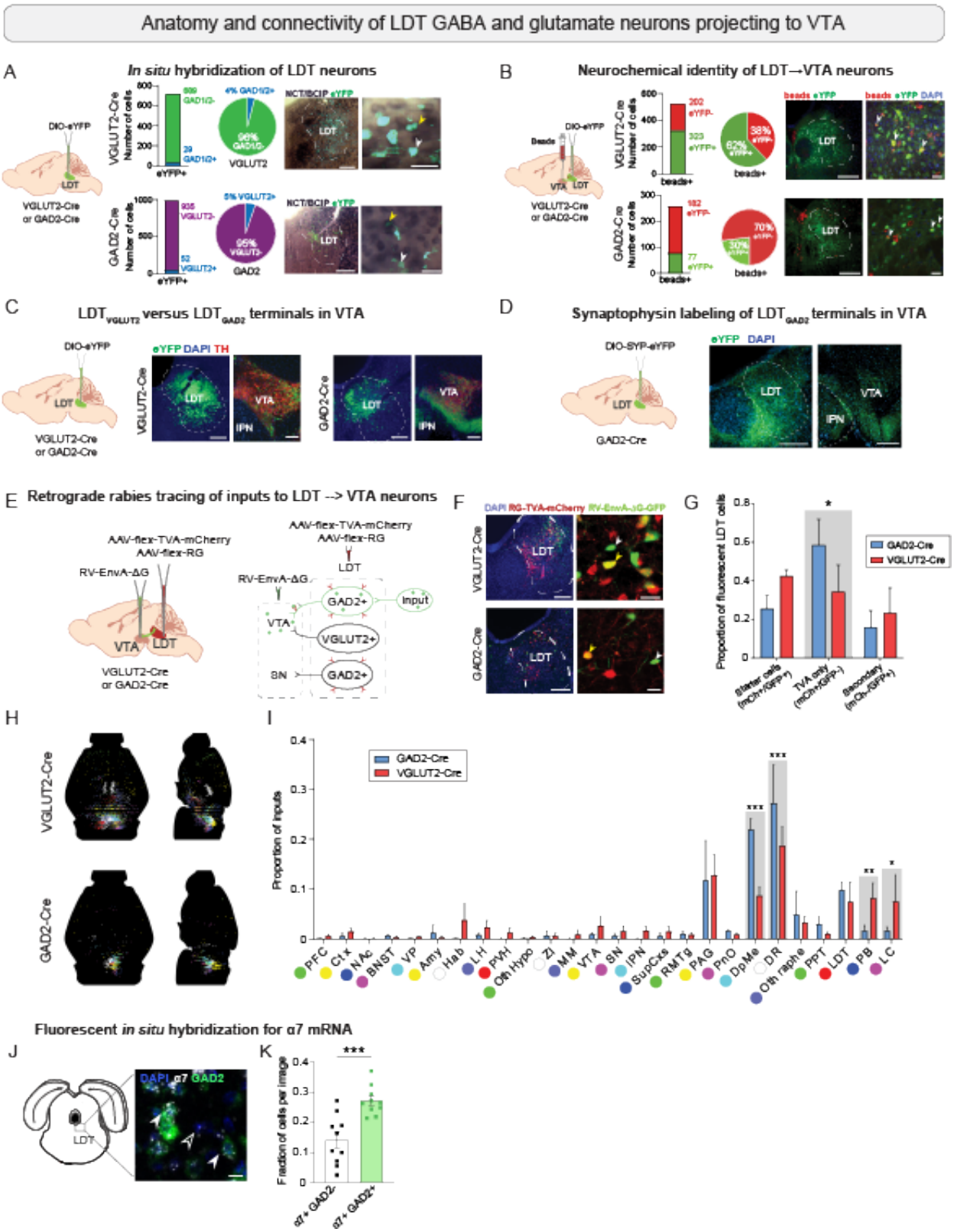

Figure S4. Anatomy and connectivity of LDT GABA and glutamate neurons, Related to Figure 4.

(A) Left: VGLUT2-Cre (n = 3 mice) or GAD2-Cre (n = 3 mice) mice were injected with AAV-DIO-eYFP into the LDT to label glutamatergic (i.e., VGLUT2-expressing) or GABAergic (i.e., GAD2-expressing) cells, respectively. Middle: *in situ* hybridization was performed for *GAD1* and *GAD2* mRNA in VGLUT2-Cre animals and *VGLUT2* mRNA in GAD2-Cre animals to quantify co-expression of these genes. Only 4% of eYFP-positive cells in the LDT of VGLUT2-Cre animals were also positive for *GAD1/GAD2* mRNA (n = 29/718 cells). Similarly, only 5% of eYFP-positive cells in the LDT of GAD2-Cre animals were also positive for *VGLUT2* mRNA (n = 52/987 cells). Right: Sample images showing eYFP-positive (green) cells in the LDT and express of *GAD1/GAD2* (top) or *VGLUT2* (bottom) mRNA. Yellow arrows indicate cells co-expressing *GAD1/GAD2* or *VGLUT2* mRNA and eYFP, whereas white arrows indicate cells that express eYFP but lack expression *GAD1/GAD2* or *VGLUT2* (scales bars 250 µm (left), 20 µm (right)).
(B) Left: VGLUT2-Cre (n = 4 mice) or GAD2-Cre (n = 3 mice) mice were injected with AAV-DIO-eYFP into the LDT. In the same animals, red fluorescent retrobeads were injected into the VTA to retrogradely label VTA-projecting LDT neurons. Middle: Co-labeling of beads-containing and eYFP-expressing LDT cells was quantified. In VGLUT2-Cre mice, 62% of beads-containing (i.e., VTA-projecting) LDT cells were also positive for eYFP (n = 323/525 cells). In GAD2-Cre mice, 30% of beads-containing (i.e., VTA-projecting) LDT cells were also positive of eYFP (n = 77/259 cells). Right: Sample images showing beads-labeled cells and eYFP-positive cells in the LDT of VGLUT2-Cre (top) and GAD2-Cre (bottom) mice. White arrows indicate eYFP-positive cells that contain retrobeads (scales bars 125 µm (left), 50 µm (right)).
(C) Left: VGLUT2-Cre (n = 8 mice) or GAD2-Cre (n = 5 mice) were injected with AAV-DIO-eYFP into the LDT and distribution of eYFP-positive terminals in the VTA and adjacent structures was analyzed. Right: Sample images demonstrating the qualitative difference between the distribution of eYFP-positive (green) terminals in the VTA from VGLUT2-Cre and GAD2-Cre animals (red – TH, blue - DAPI) (scales bars 250 µm (left), 125 µm (right)).
(D) Left: GAD2-Cre (n = 10 mice) were injected with AAV-DIO-synaptophysin-eYFP into the LDT and distribution of eYFP-positive terminals in the VTA was analyzed. Right: Sample fluorescent images showing synaptophysin-labeled (green) terminals in the VTA and IPN (blue – DAPI) (scales bars 250 µm (left), 125 µm (right)).
(E) Left: VGLUT2-Cre (n = 4 mice) and GAD2-Cre (n = 3 mice) mice were injected with AAV-flex-TVA-mCherry and AAV-flex-RG in the LDT to enable cell-type specific tracing of input neurons. Subsequent injection of RV-EnvA-ΔG-GFP into the VTA of the same VGLUT2-Cre and GAD2-Cre mice resulted in GFP-expression in cells that make direct monosynaptic input onto VTA-projecting $LDT_{Glutamate}$ or VTA-projecting LDT_{GABA} neurons, respectively. Right: Schematic showing experimental design for mapping whole-brain inputs to VTA-projecting LDT_{GABA} neurons in a GAD2-Cre animal.
(F) Sample confocal images showing starter cells (mCherry-positive (red) and GFP-positive (green); yellow arrows), TVA-expressing (mCherry-positive, GFP-negative), and secondary/input cells (mCherry-negative, GFP-positive; white arrows) in the LDT of VGLUT2-Cre (top) and GAD2-Cre (bottom) mice (blue – DAPI) (scales bars 250 µm (left), 20 µm (right)).
(G) Bar graph showing quantification of starter cells, TVA-expressing and secondary cells in the LDT of GAD2-Cre (blue) and VGLUT2-Cre (red) mice (* $p < 0.05$, data represent means ± SEM).
(H) Horizontal and sagittal views of processed whole brains displaying brain-wide inputs to

VTA-projecting $LDT_{Glutamate}$ (top) or VTA-projecting LDT_{GABA} neurons (bottom). Color code indicates different brain structures.
(I) Quantification of inputs to VTA-projecting LDT_{GABA} neurons (blue) and VTA-projecting $LDT_{Glutamate}$ (red) neurons. Data are presented as proportion of inputs counted in each individual brain structure. Color code corresponds to brain structures shown in (H) (Abbreviations: PFC – prefrontal cortex; green, Ctx – cortex; yellow, NAc – nucleus accumbens; blue, BNST – bed nucleus of the stria terminalis; magenta, VP – ventral pallidum; cyan, Amy – amygdala; yellow, Hab – habenula; white, LH – lateral hypothalamus; purple, PVH – paraventricular hypothalamus; red, Oth Hypo – other hypothalamic regions; green, ZI – zona incerta; white, MM – medial mammillary nuclei; purple, VTA – ventral tegmental area; yellow, SN – substantia nigra; magenta, IPN – interpeduncular nucleus; cyan, SupCxs – superior colliculus; blue, RMTg – rostromedial tegmental nucleus; green, PAG – periaqueductal gray; yellow, PnO – pontine nucleus oralis; magenta, DpMe – deep mesencephalic nucleus, cyan; DR – dorsal raphe; cyan, Oth raphe – other raphe nuclei; purple, PPT – pedunculopontine tegmentum; green, LDT – laterodorsal tegmentum; red, PB – parabrachial nucleus; blue, LC – locus coeruleus, magenta) (* $p < 0.05$, ** $p < 0.01$, *** $p < 0.001$; data represent means ± SEM).
(J) Sample image of fluorescent *in situ* hybridization in the LDT targeting mRNA for GAD2 (green) and α7 (white) (scale bar 10 μm).
(K) Bar graph showing significant larger number of LDT cells co-express α7 and GAD2 mRNA compared to LDT cells expressing α7 but lacking GAD2 mRNA (n = 3 mice; *** $p < 0.001$, data represent means ± SEM).

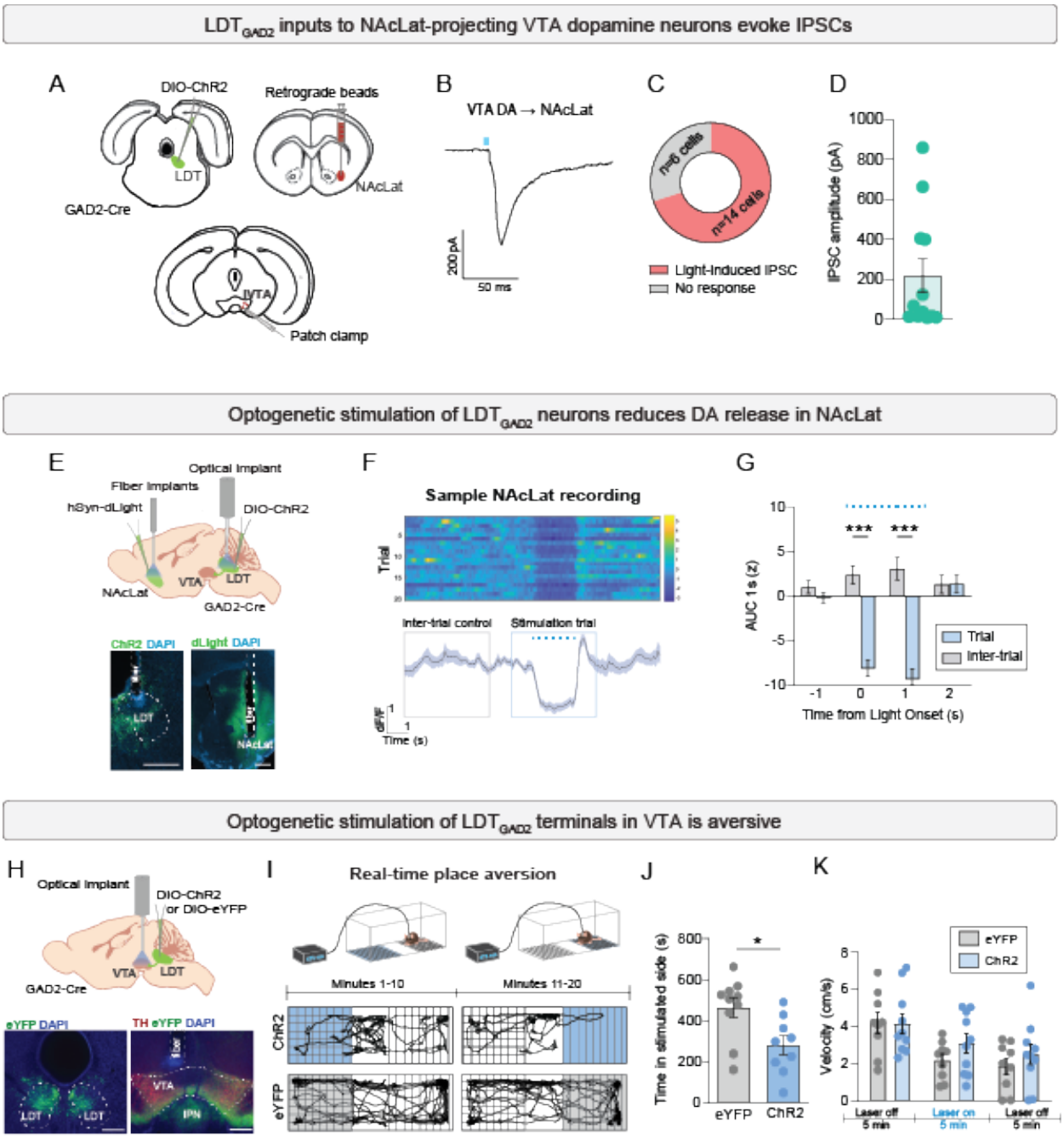

Figure S5. Functional connectivity of LDT GABA neurons, Related to Figure 4.
(A) Schematics showing that GAD2-Cre animals (n = 8 mice) were injected with AAV-DIO-ChR2 into the LDT and fluorescent retrobeads into the NAcLat. Brain-slice, patch-clamp recordings were performed from retrogradely-labeled DA neurons that were located in the lateral VTA (lVTA).
(B) Representative light-induced IPSC from a bead-labeled VTA DA neuron.
(C) Proportions of recorded NAcLat-projecting DA cells that responded (n = 14 cells, red) or did not respond (n = 6 cells, grey) to light stimulation of LDT terminals in the VTA.

(D) Bar graph showing mean amplitude of light-induced IPSCs recorded from NAcLat-projecting DA cells (n = 14 cells; data represent mean ± SEM).
(E) Top: Schematic showing that GAD2-Cre mice (n = 3 mice) were injected with AAV-DIO-ChR2 into the LDT and an optical fiber was implanted above the LDT. The same mice were injected with AAV-hSyn-dLight1.2 into the NAcLat and an optical fiber was implanted above the NAcLat. Bottom: Sample images showing histological verification of ChR2 (green) expression and optical fiber location in the LDT (left) and dLight (green) expression and optical fiber location in the NAcLat (right) (blue - DAPI; scale bars 500 μm).
(F) Sample recording session with 20 trials. A 2 s pulse-train of 20 Hz 5 ms pulses of 3-5 mW 488 nm light was delivered to the LDT while dLight was simultaneously recorded in the NAcLat.
(G) Bar graph showing significant reduction in dLight signals during the light stimulation period when compared to dLight signals that were recorded between trials (*** $p < 0.001$, data represent mean ± SEM).
(H) Top: Schematic showing that GAD2-Cre animals received bilateral injection of AAV-DIO-ChR2 (n = 9 mice) or AAV-DIO-eYFP (n =10 mice) into the LDT and an optical fiber was implanted over the VTA to optogenetically stimulate LDT_{GABA} terminals in the VTA. Bottom: Sample fluorescent images showing eYFP (green) expression in the LDT (left) and VTA (right). Note, that the optical fiber was place above the VTA (blue – DAPI, red – TH; scale bars 400 μm (left), 250 μm (right)).
(I) Top: Schematic of experimental design showing real-time place preference/avoidance paradigm. Bottom: Sample traces showing movement of GAD2-Cre mice expressing ChR2 (top) or eYFP (bottom) in the LDT and received 20 Hz light stimulation in the VTA when they entered the left (Minutes 1-10) or right (Minutes 11-20) side of the behavioral chamber.
(J) Bar graph showing that animals expressing ChR2 in the LDT spent significantly less time in the light-paired side of the behavioral chamber compared to eYFP-expressing mice (* $p < 0.05$; data represent means ± SEM).
(K) Bar graph showing that no significant difference in locomotor activity was observed in the open field test between ChR2 (blue, n= 9 mice) and eYFP-expressing (grey, n = 10 mice) GAD2-Cre mice before, during or after 20 Hz light stimulation (data represent means ± SEM).

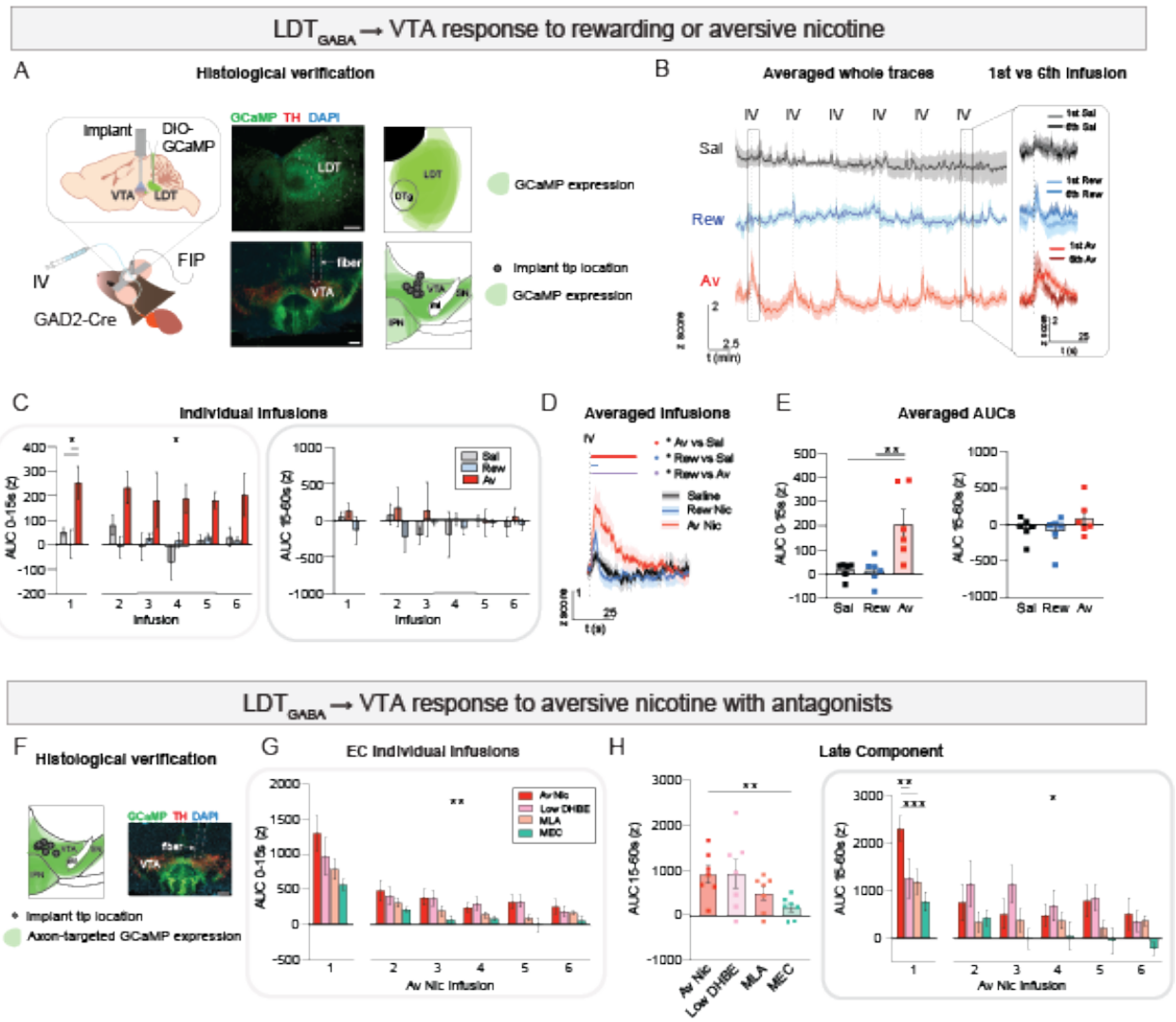

Figure S6. Fiber photometry of LDT$_{GABA}$→VTA neurons, Related to Figure 4.

(A) Left: Schematic showing experimental design for injection of GAD2-Cre animals (n = 6 mice) with AAV-DIO-GCaMP6m into the LDT and an optical fiber implanted in the VTA. During fiber photometry recordings, mice received IV infusions of saline, rewarding nicotine or aversive nicotine. Middle: Sample fluorescent images showing GCaMP (green) expression in the LDT (top, scale bar 200 µm) and optical fiber placement in the VTA (bottom, scale bar 200 µm) (red – TH, blue - DAPI). Right: Histological verification of GCaMP expression in LDT (top) and optical fiber placements in the VTA (bottom) (DTg - dorsal tegmental nucleus).

(B) Averaged whole traces of LDT$_{GABA}$→VTA GCaMP activity in response to saline (Sal, grey), rewarding nicotine (Rew, blue), and aversive nicotine (Av, red). Inset: Comparison between first and last infusion (area of light shading represents SEM).

(C) AUCs of GCaMP response in the LDT$_{GABA}$→VTA pathway to saline, rewarding nicotine, and aversive nicotine during the early (left) and late (right) components (gap denotes separate analyses for infusion 1 and infusions 2-6 due to non-normal distribution, * $p < 0.5$, data represent means ± SEM).

(D) Peri-infusion plot of averaged GCaMP response in the LDT$_{GABA}$→VTA pathway to saline (black), rewarding nicotine (blue), and aversive nicotine (red) (area of light shading represents

SEM). Dots above traces denote time points where significant differences between conditions were observed from a multiple comparisons test following a 2-way ANOVA analysis (red – aversive nicotine versus saline, blue – rewarding nicotine versus saline, purple – rewarding nicotine versus aversive nicotine).
(E) Averaged AUCs of GCaMP signals in the LDT_{GABA}→VTA pathway across infusions during the early (left) and late (right) components (** $p < 0.01$; data represent means ± SEM).
(F) Left: Histological verification of GAD2-Cre animals (n = 7 mice) showing GCaMP expression and optical fiber placements in the VTA for experiments shown in **Figures 4K-4N**. Right: Sample fluorescent image of the VTA (green – GcaMP, red – TH, blue – DAPI; scale bar 200 μm).
(G) AUCs of GCaMP signals in the LDT_{GABA}→VTA pathway for individual infusions during the early component in response to IV administration of aversive nicotine (Av nic) and antagonists (gap denotes separate analyses for infusion 1 and infusions 2-6 due to non-normal distribution, ** $p < 0.01$, data represent means ± SEM).
(H) AUCs of GCaMP signals in the LDT_{GABA}→VTA pathway for response to aversive nicotine and antagonists during the late component averaged across infusions (left) and for each infusion (right) (gap denotes separate analyses for infusion 1 and infusions 2-6 due to non-normal distribution; * $p < 0.05$, ** $p < 0.01$, *** $p < 0.001$; data represent means ± SEM).

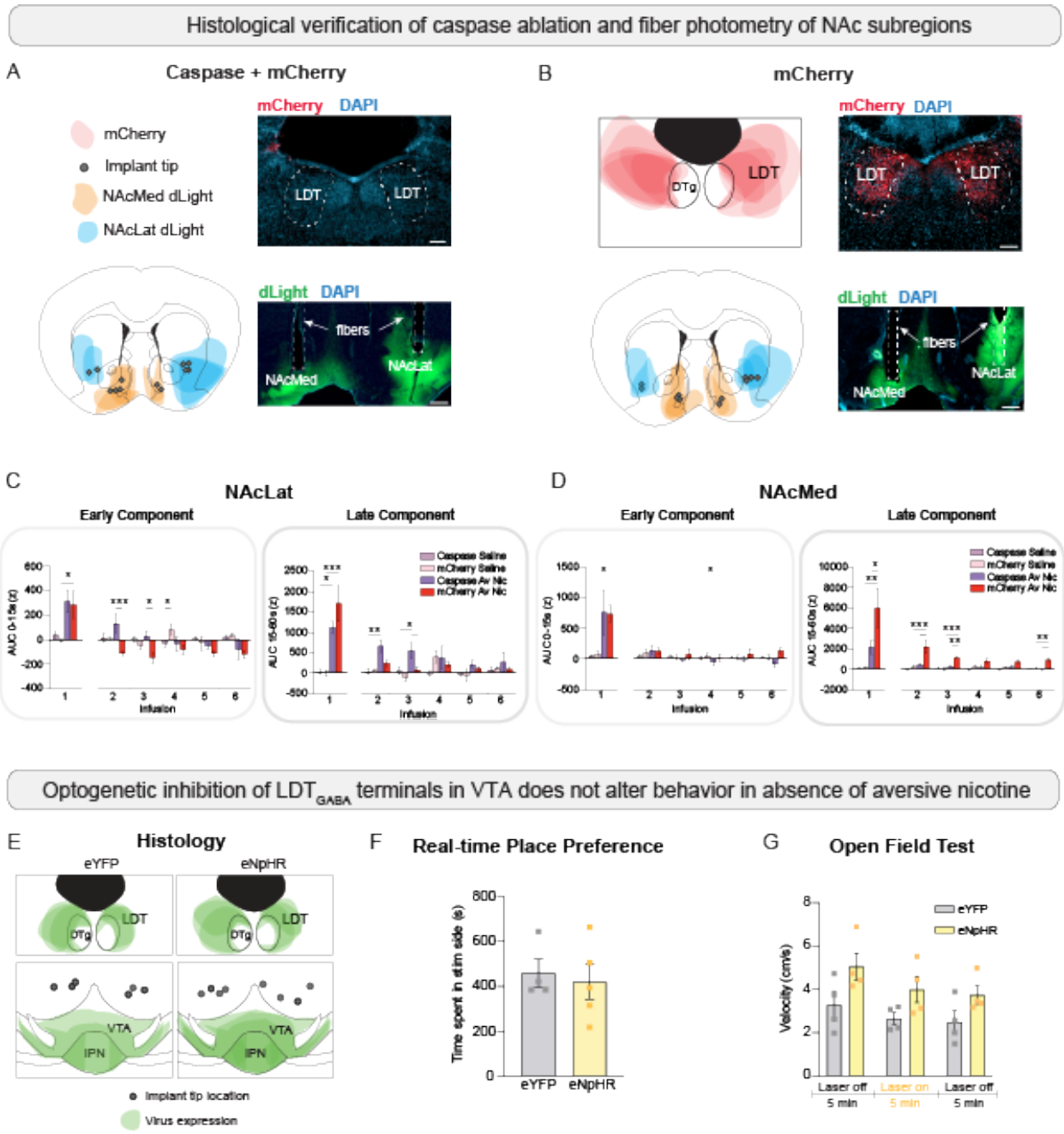

Figure S7. Histological verification of caspase ablation, fiber photometry of NAc subregions and optogenetic inhibition of LDT$_{GABA}$→VTA pathway, Related to Figure 5.

(A) Histological verification of viral expression and optical fiber placements of GAD2-Cre animals (n = 6 mice) that were bilaterally injected with AAV-flex-TaCasp3 and AAV-DIO-mCherry into the LDT as well as dLight1.2 (green) into the NAcMed and NAcLat. The absence of mCherry-positive (red) cells in the LDT indicates successful ablation of LDT$_{GABA}$ neurons (blue – DAPI; scale bars 200 µm (top) and 500 µm (bottom)).

(B) Histological verification of viral expression and optical fiber placements of GAD2-Cre control animals (n = 5 mice) that were injected bilaterally with AAV-DIO-mCherry into the LDT. dLight1.2 was infused into the NAcMed and NAcLat. Note the presence of mCherry-positive (red) cells in the LDT (blue – DAPI; scale bars 200 µm (top) and 500 µm (bottom)).
(C) Left: dLight1.2 AUCs during the early component for mCherry and Caspase groups in response to saline and aversive nicotine. Right: Same, but for the late component (gap denotes separate analyses for infusion 1 and infusions 2-6 due to non-normal distribution, * $p < 0.05$, ** $p < 0.01$, *** $p < 0.001$, data represent means ± SEM).
(D) Same as in (C) but for dLight1.2 recordings in NAcMed (gap denotes separate analyses for infusion 1 and infusions 2-6 due to non-normal distribution, * $p < 0.05$, ** $p < 0.01$, *** $p < 0.001$, data represent means ± SEM).
(E) Schematics showing histological verification of eNpHR and eYFP expression (green) in the LDT (top) and VTA (bottom). Grey dots indicate location of the optical fibers above the VTA.
(F) Bar graph showing no significant difference in time spent in the light-paired chamber between eNpHR mice (n = 5 mice) and eYFP mice (n = 4 mice) during the real-time place preference/aversion task (data represent means ± SEM).
(G) Bar graph showing no significant difference in general locomotor behavior between eNpHR (n = 4 mice) and eYFP (n = 4 mice) mice in the open field test with or without 589 nm light delivery (data represent means ± SEM).

SUPPLEMENTARY DATA TABLE

Table S1. TABLE OF STATISTICAL TEST OUTCOMES

Data	Mean ± SEM	Statistical Test	N	Outcome measure	p value
Fig 1D (Above) Post/Pre Pref Score	**0.25 mg/kg:** 1.82 ± 0.4 **1.25 mg/kg:** 0.79 ± 0.1	Unpaired t-test	**0.25 mg/kg:** 8 mice **1.25 mg/kg:** 6 mice	Post/Pre Ratio Preference Score	p = 0.0495, two-tailed, t = 2.185, df = 12
Fig 1D (Above) Post/Pre Pref Score	**0.25 mg/kg:** 1.82 ± 0.4 **Theoretical median:** 1 ± 0	One sample t-test to test low dose against neutral preference score	**0.25 mg/kg:** 8 mice **Theoretical median:** 8 values	Post/Pre Ratio Preference Score	p = 0.03, one-tailed, t = 2.041, df = 14
Fig 1D (Above) Post/Pre Pref Score	**1.25 mg/kg:** 0.78 ± 0.1 **Theoretical median:** 1 ± 0	One sample t-test to test high dose against neutral preference score	**1.25 mg/kg:** 8 mice **Theoretical median:** 6 values	Post/Pre Ratio Preference Score	p = 0.03, one-tailed, t = 2.191, df = 10
Fig 1D (Below) Difference Score	**0.25 mg/kg:** 88.4 ± 36.8 **1.25 mg/kg:** -59.9 ± 26.3	Unpaired t-test	**0.25 mg/kg:** 8 mice **1.25 mg/kg:** 6 mice	Post-Pre Difference Score	p = 0.01, two-tailed, t = 3.064, df = 12

Data	Mean ± SEM	Statistical Test	N	Outcome measure	p value
Fig 1D (Below) Difference Score	**0.25 mg/kg:** 88.4 ± 36.8 **Theoretical median:** 0 ± 0	One sample t-test to test low dose against neutral difference score	**0.25 mg/kg:** 8 mice **Theoretical median:** 8 values	Post-Pre Difference Score	p = 0.02, one-tailed, t = 2.404, df = 14
Fig 1D (Below) Difference Score	**1.25 mg/kg:** -59.9 ± 26.29 **Theoretical median:** 0 ± 0	One sample t-test to test high dose against neutral difference score	**1.25 mg/kg:** 6 mice **Theoretical median:** 6 values	Post-Pre Difference Score	p = 0.02, one-tailed, t = 2.280, df = 10
Fig 2D DAT Avg Inf Traces	Column means: **Rew Nic:** 0.65 ± 0.014 **Av Nic:** 0.23 ± 0.028 **Saline:** -0.05 ± 0.006	Two-way Repeated Measures ANOVA with Holm-Šídák's multiple comparisons test	n = 11 mice (611 data points)	z-score of GCaMP fluorescence	Effect of Time p < 0.001 Effect of Dose p = 0.15 Interaction Time x Dose p < 0.001 Multiple comparisons: Time points with p values ≤ 0.05 denoted by dot on bar graph
Fig 2E DAT Early Component	**Rew:** 109.9 ± 51.92 **Av:** -127.2 ± 40.47 **Sal:** -16.28 ± 15.07	One-Way Repeated Measures ANOVA with Holm-Šídák's multiple comparisons test	n = 11 mice	Area Under the Curve (AUC) 0-15 seconds post-infusion	Effect of dose: p < 0.001, F (2, 20) = 15.72 Multiple comparisons: Rew vs. Av: p < 0.001 Rew vs. Sal: p = 0.01 Av vs. Sal: p = 0.02
Fig 2E DAT Late Component	**Rew:** 285.1 ± 185.2 **Av:** 264.6 ± 151.9 **Sal:** -16.46 ± 44.8	One-Way Repeated Measures ANOVA with Holm-Šídák's multiple comparisons test	n = 11 mice	Area Under the Curve (AUC) 15-60 seconds post-infusion	Effect of dose: p = 0.19, F (2, 20) = 1.805 No effect, post-hoc is not justified
Fig 2J DAT DHBE Early Component Infusions 1-6	**Saline:** 613.02 ± 187.83 -166.57 ± 64.14 -296.36 ± 97.06 -385.68 ± 91.99 -299.52 ± 84.33 -333.77 ± 105.86 **DHBE:** -2.61 ± 35.42 -90.09 ± 28.52 -96.06 ± 57.05 -74.09 ± 75.00 -23.42 ± 66.89 -86.18 ± 40.36	Kolmogorov-Smirnov normality test	**Saline:** 8 mice **DHBE:** 6 mice	Area Under the Curve (AUC) 0-15 seconds post-infusion	Saline: p = 0.0007 DHBE: p > 0.1000

Data	Mean ± SEM	Statistical Test	N	Outcome measure	p value
Fig 2J DAT DHBE Late Component Infusions 1-6	**Saline:** 2339.56 ± 636.96 653.22 ± 352.01 393.98 ± 399.88 -448.02 ± 343.43 81.63 ± 231.06 -467.23 ± 513.63 **DHBE:** 197.23 ± 149.05 29.15 ± 76.42 64.31 ± 233.05 -152.94 ± 172.93 26.97 ± 195.16 -32.37 ± 152.8	Kolmogorov-Smirnov normality test	**Saline:** 8 mice **DHBE:** 6 mice	Area Under the Curve (AUC) 15-60 seconds post-infusion	Saline: p = 0.009 DHBE: p > 0.100
Fig 2J DAT DHBE EC 1st Infusion	**Saline:** 613.02 ± 187.83 **DHBE:** -2.61 ± 35.42	Unpaired t-test	**Saline:** 8 mice **DHBE:** 6 mice	Area Under the Curve (AUC) 0-15 seconds post-infusion	p = 0.017, two-tailed, t = 2.783, df = 12
Fig 2J DAT DHBE EC Infusions 2-6	**Saline:** -166.57 ± 64.14 -296.36 ± 97.06 -385.68 ± 91.99 -299.52 ± 84.33 -333.77 ± 105.86 **DHBE:** -90.09 ± 28.52 -96.06 ± 57.05 -74.09 ± 75.00 -23.42 ± 66.89 -86.18 ± 40.36	Two-way Repeated Measures ANOVA with Holm-Šídák's multiple comparisons test	**Saline:** 8 mice **DHBE:** 6 mice	Area Under the Curve (AUC) 0-15 seconds post-infusion	Effect of Infusion: p = 0.105, F (4, 48) = 2.033 Effect of Dose: p = 0.053, F (1, 12) = 4.619 Interaction: p = 0.048, F (4, 48) = 2.589 <u>Multiple Comparisons:</u> **2nd infusion:** p = 0.509 **3rd infusion:** p = 0.167 **4th infusion:** p = 0.043 **5th infusion:** p = 0.077 **6th infusion:** p = 0.103
Fig 2J DAT DHBE LC 1st Infusion	**Saline:** 2339.56 ± 636.96 **DHBE:** 197.23 ± 149.05	Unpaired t-test	**Saline:** 8 mice **DHBE:** 6 mice	Area Under the Curve (AUC) 15-60 seconds post-infusion	p = 0.015, two-tailed, t = 2.841, df = 12
Fig 2J DAT DHBE LC Infusions 2-6	**Saline:** 653.22 ± 352.01 393.98 ± 399.88 -448.02 ± 343.43 81.63 ± 231.06 -467.23 ± 513.63 **DHBE:** 29.15 ± 76.42 64.31 ± 233.05 -152.94 ± 172.93 26.97 ± 195.16 -32.37 ± 152.8	Two-way Repeated Measures ANOVA with Holm-Šídák's multiple comparisons test	**Saline:** 8 mice **DHBE:** 6 mice	Area Under the Curve (AUC) 15-60 seconds post-infusion	Effect of Infusion: p = 0.023, F (4, 48) = 3.114 Effect of Dose: p = 0.882, F (1, 12) = 0.023 Interaction: p = 0.138, F (4, 48) = 1.833 No interaction, post-hoc is not justified
Fig 2K DAT DHBE Avg Trace	<u>Column means:</u> **Saline:** 0.460 ± 0.043 **DHBE:** -0.065 ± 0.016	Mixed-effects analysis	**Saline:** 8 mice **DHBE:** 6 mice	z-score of GCaMP fluorescence	Effect of Time: p < 0.001, F (610,6100) = 13.34 Effect of Drug: p = 0.50, F (1,10) = 0.500 Interaction: p < 0.001, F (610, 1212) = 4.547 <u>Multiple comparisons:</u> No significant differences

Data	Mean ± SEM	Statistical Test	N	Outcome measure	p value
Fig 2K DAT DHBE Early component	**Saline:** -144.8 ± 77.02 **DHBE:** -62.08 ± 36.21	Unpaired t-test	**Saline:** 8 mice **DHBE:** 6 mice	Area Under the Curve (AUC) 0-15 seconds post-infusion	p = 0.40, two-tailed, t = 0.871, df = 12
Fig 2K DAT DHBE Late component	**Saline:** 425.5 ± 304.3 **DHBE:** 22 .06 ± 95.51	Unpaired t-test	**Saline:** 8 mice **DHBE:** 6 mice	Area Under the Curve (AUC) 15-60 seconds post-infusion	p = 0.29, two-tailed, t = 1.107, df = 12
Fig 3C NAcMed Avg Traces	Column means: **Av Nic:** 0.499 ± 0.045 **Saline:** 0.058 ± 0.012	Two-way Repeated Measures ANOVA with Holm-Šídák's multiple comparisons test	n = 10 mice (611 time points)	z-score of dLight fluorescence	Effect of Time: p < 0.001, F (610, 5490) = 19.80 Effect of Drug: p = 0.007, F (1, 9) = 12.06 Interaction: p < 0.001, F (610, 5490) = 9.86 Multiple comparisons: Time points with p values ≤ 0.05 denoted by dot on bar graph
Fig 3D NAcMed EC	**Saline:** 20.96 ± 8.051 **Av Nic:** 55.88 ± 41.63	Paired t-test	n = 10 mice	Area Under the Curve (AUC) 0-15 seconds post-infusion	p = 0.36, two-tailed, t = 0.9694, df = 9
Fig 3D NAcMed LC	**Saline:** 267.4 ± 55.97 **Av Nic:** 882.6 ± 187.4	Paired t-test	n = 10 mice	Area Under the Curve (AUC) 15-60 seconds post-infusion	p = 0.007, two-tailed, t = 3.453, df = 9
Fig 3E NAcLat Avg Trace	Column means: **Saline:** 0.284 ± 0.007 **Av Nic:** 0.274 ± 0.019	Two-way Repeated Measures ANOVA with Holm-Šídák's multiple comparisons test	n = 16 mice (611 time points)	z-score of dLight fluorescence	Effect of Time: p < 0.001, F (610, 9150) = 10.53 Effect of Drug: p = 0.89, F (1, 15) = 0.01876 Interaction: p < 0.001, F (610, 9150) = 6.064 Multiple comparisons: Time points with p values ≤ 0.05 denoted by dot on bar graph
Fig 3F NAcLat EC	**Saline:** 22.54 ± 8.411 **Av Nic:** -56.00 ± 17.32	Paired t-test	n = 16 mice	Area Under the Curve (AUC) 0-15 seconds post-infusion	p < 0.001, two-tailed, t = 4.765, df = 15
Fig 3F NAcLat LC	**Saline:** 151.0 ± 34.56 **Av Nic:** 223.4 ± 49.42	Paired t-test	n = 16 mice	Area Under the Curve (AUC) 15-60 seconds post-infusion	p = 0.12, two-tailed, t = 1.662, df = 15
Fig 3J NAcMed pharm Avg traces	Column means: **DHBE:** 3.447 ± 0.061 **MLA:** 3.000 ± 0.054 **MEC:** 1.402 ± 0.028 **Saline:** 3.263 ± 0.059	Two-way Repeated Measures ANOVA with Holm-Šídák's multiple comparisons test	n = 7 mice	z-score of dLight fluorescence	Effect of Time: p < 0.001, F (610, 3660) = 20.05 Effect of Drug: p < 0.001, F (3, 18) = 10.43 Interaction: p < 0.001, F (1830, 10980) = 7.188 Multiple comparisons: Time points with p values ≤ 0.05 denoted by dot on bar graph

Data	Mean ± SEM	Statistical Test	N	Outcome measure	p value
Fig 3K NAcMed pharm EC	**DHBE:** 242.2 ± 66.90 **MLA:** 407.7 ± 89.69 **MEC:** 277.3 ± 40.45 **Saline:** 257.6 ± 31.3	One-Way Repeated Measures ANOVA with Holm-Šídák's multiple comparisons test	n = 7 mice	Area Under the Curve (AUC) 0-15 seconds post-infusion	Effect of Drug: $p = 0.04$, $F (3, 18) = 3.281$ Multiple comparisons: Saline vs DHBE: $p = 0.93$ Saline vs MLA: $p = 0.06$ Saline vs MEC: $p = 0.93$
Fig 3K NAcMed pharm LC	**DHBE:** 1863 ± 366.5 **MLA:** 1423 ± 298.6 **MEC:** 578.9 ± 66.57 **Saline:** 1450 ±186.7	One-Way Repeated Measures ANOVA with Holm-Šídák's multiple comparisons test	n = 7 mice	Area Under the Curve (AUC) 15-60 seconds post-infusion	Effect of Drug: $p < 0.001$, $F (3, 18) = 12.11$ Multiple comparisons: Saline vs DHBE: $p = 0.15$ Saline vs MLA: $p = 0.90$ Saline vs MEC: $p = 0.003$
Fig 3M NAcLat pharm Avg traces	Column means: **DHBE:** -1.134 ± 0.026 **MLA:** 0.779 ± 0.025 **MEC:** 0.364 ± 0.012 **Av Nic:** 0.631 ± 0.033	Two-way Repeated Measures ANOVA with Holm-Šídák's multiple comparisons test	N = 8 mice	z-score of dLight fluorescence	Effect of Time: $p < 0.001$, $F (610, 4270) = 19.59$ Effect of Drug: $p = 0.16$, $F (3, 21) = 1.875$ Interaction: $p < 0.001$, $F (1830, 12810) = 6.196$ Multiple comparisons: Time points with p values ≤ 0.05 denoted by dot on bar graph
Fig 3N NAcLat pharm EC	**DHBE:** -46.89 ± 27.29 **MLA:** 42.96 ± 41.78 **MEC:** 85.38 ± 30.62 **Saline:** -72.81 ± 28.94	One-Way Repeated Measures ANOVA with Holm-Šídák's multiple comparisons test	n = 8 mice	Area Under the Curve (AUC) 0-15 seconds post-infusion	Effect of Drug: $p < 0.001$, $F (3, 21) = 10.80$ Multiple comparisons: Saline vs DHBE: $p = 0.43$ Saline vs MLA: $p = 0.003$ Saline vs MEC: $p < 0.001$
Fig 3N NAcLat pharm LC	**DHBE:** 463.3 ± 78.94 **MLA:** 432.6 ± 89.08 **MEC:** 136.2 ± 107.9 **Saline:** 404.7 ± 80.57	One-Way Repeated Measures ANOVA with Holm-Šídák's multiple comparisons test	n = 8 mice	Area Under the Curve (AUC) 15-60 seconds post-infusion	Effect of Drug: $p = 0.004$, $F (3, 21) = 5.955$ Multiple comparisons: Saline vs DHBE: $p = 0.76$ Saline vs MLA: $p = 0.76$ Saline vs MEC: $p = 0.02$
Fig 4I VTA GABA pharm Avg Traces	Column means: **Av Nic:** 1.236 ± 0.046 **DHBE:** 1.161 ± 0.060 **MLA:** 0.897 ± 0.030	Two-way Repeated Measures ANOVA with Holm-Šídák's multiple comparisons test	n = 7 mice	z-score of GCaMP fluorescence	Effect of Time: $p < 0.001$, $F (610, 3660) = 23.50$ Effect of Drug: $p = 0.006$, $F (3, 18) = 5.843$ Interaction: $p < 0.001$, $F (1830, 10980) = 6.600$ Multiple comparisons: Time points with p values ≤ 0.05 denoted by dot on bar graph

Data	Mean ± SEM	Statistical Test	N	Outcome measure	p value
Fig 4J VTA GABA pharm EC	**Av Nic:** 387 ± 28.03 **MLA:** 265.7 ± 48.38 **MEC:** 23.37 ± 25.16 **DHBE:** 481.8 ± 65.51	One-Way Repeated Measures ANOVA with Holm-Šídák's multiple comparisons test	n = 7 mice	Area Under the Curve (AUC) 0-15 seconds post-infusion	Effect of Drug: $p < 0.001$, $F (3, 18) = 18.73$ Multiple comparisons: Av Nic vs MLA: $p = 0.15$ Av Nic vs MEC: $p < 0.001$ Av Nic vs Low DHBE: $p = 0.16$
Fig 4M LDT GABA pharm Avg Traces	Column means: **MLA:** 1.265 ± 0.025 **MEC:** 0.545 ± 0.018 **Av Nic:** 2.298 ± 0.055 **DHBE:** 2.214 ± 0.040	Two-way Repeated Measures ANOVA with Holm-Šídák's multiple comparisons test	n = 7 mice	z-score of GCaMP fluorescence	Effect of Time: $p < 0.001$, $F (610, 3660) = 18.12$ Effect of Drug: $p = 0.005$, $F (3, 18) = 6.129$ Interaction: $p < 0.001$, $F (1830, 10980) = 5.088$ Multiple comparisons: Time points with p values ≤ 0.05 denoted by dot on bar graph
Fig 4N LDT GABA pharm EC	**MLA:** 281.1 ± 51.72 **MEC:** 161.1 ± 12.51 **Av Nic:** 498.9 ± 62.41 **DHBE:** 430.2 ± 114.6	One-Way Repeated Measures ANOVA with Holm-Šídák's multiple comparisons test	n = 7 mice	Area Under the Curve (AUC) 0-15 seconds post-infusion	Effect of Drug: $p = 0.004$, $F (3, 18) = 6.431$ Multiple comparisons: Saline vs DHBE: $p = 0.43$ Saline vs MLA: $p = 0.04$ Saline vs MEC: $p = 0.003$
Fig 5J NAcMed Caspase Avg traces	Column means: **mCh Nic:** 3.590 ± 0.066 **Casp Nic:** 1.519 ± 0.037 **mCh Sal:** 0.341 ± 0.010 **Casp Sal:** 0.200 ± 0.007	Two-way Repeated Measures ANOVA with Holm-Šídák's multiple comparisons test	**Casp:** n = 6 mice, **mCh:** n = 5 mice	z-score of dLight fluorescence	Effect of Condition: $p < 0.001$, $F (3, 19) = 14.20$ Effect of Time: $p < 0.001$, $F (610, 11590) = 8.613$ Interaction: $p < 0.001$, $F (1830, 11590) = 4.786$ Multiple comparisons: Time points with p values ≤ 0.05 denoted by dot on bar graph
Fig 5K NAcMed Casp EC	**mCh:** 200.2 ± 47.41 **Casp:** 124.6 ± 73.46	Unpaired t-test	**Casp:** n = 6 mice, **mCh:** n = 5 mice	Area Under the Curve (AUC) 0-15 seconds post-infusion	$p = 0.22$, one-tailed, $t = 0.8239$, $df = 9$
Fig 5K NAcMed Casp LC	**mCh:** 1990 ± 495.6 **Casp:** 559.9 ± 108.2	Unpaired t-test	**Casp:** n = 6 mice, **mCh:** n = 5 mice	Area Under the Curve (AUC) 15-60 seconds post-infusion	$p = 0.006$, one-tailed, $t = 3.089$, $df = 9$
Fig 5G NAcLat Casp Avg Traces	Column means: **mCh Nic:** 0.593 ± 0.026 **Casp Nic:** 0.964 ± 0.025 **mCh Sal:** 0.135 ± 0.009 **Casp Sal:** 0.065 ± 0.006	Two-way Repeated Measures ANOVA with Holm-Šídák's multiple comparisons test	**Casp:** n = 6 mice **mCh:** n = 6 mice	z-score of dLight fluorescence	Effect of Condition: $p = 0.008$, $F (3, 20) = 5.288$ Effect of Time: $p < 0.001$, $F (610, 12200) = 13.84$ Interaction: $p < 0.001$, $F (1830, 12200) = 3.834$ Multiple comparisons: Time points with p values ≤ 0.05 denoted by dot on bar graph

Data	Mean ± SEM	Statistical Test	N	Outcome measure	p value
Fig 5H NAcLat Casp EC	**mCh:** -50.85 ± 28.85 **Casp:** 50.94 ± 39.55	Unpaired t-test	**Casp:** n = 6 mice **mCh:** n = 6 mice	Area Under the Curve (AUC) 0-15 seconds post-infusion	p = 0.03, one-tailed, t = 2.079, df = 10
Fig 5H NAcLat Casp LC	**mCh:** 413.0 ± 88.54 **Casp:** 537.7 ± 155.1	Unpaired t-test	**Casp:** n = 6 mice **mCh:** n = 6 mice	Area Under the Curve (AUC) 15-60 seconds post-infusion	p = 0.25, one-tailed, t = 0.6983, df = 10
Fig 5O CPP Post/Pre Pref Score	**eYFP:** 0.853 ± 0.151 **eNpHR:** 1.540 ± 0.207	Unpaired t-test	**eYFP:** n = 4 mice **eNpHR:** n = 4 mice	Post/Pre Ratio Preference Score	p = 0.04, two-tailed, t=2.677, df=6
Fig 5P CPP Diff Score	**eYFP:** -33.35 ± 35.54 **eNpHR:** 106.2 ± 33.14	Unpaired t-test	**eYFP:** n = 4 mice **eNpHR:** n = 4 mice	Post-Pre Difference Score	p = 0.03, two-tailed, t=2.872, df=6
Fig S1C DAT Order Effect Rew Nic	Column means: **Sub-group 1:** 0.210 ± 0.011 **Sub-group 2:** 1.010 ± 0.020	Two-way Repeated Measures ANOVA with Holm-Šídák's multiple comparisons test	**Sub-group 1:** n = 5 mice **Sub-group 2:** n = 6 mice	z-score of GCaMP fluorescence	Effect of First Dose: p = 0.33, F (1, 9) = 1.071 Effect of Time: p < 0.001, F (610, 5490) = 4.440 Interaction: p < 0.001, F (610, 5490) = 1.519 Multiple comparisons: No significant differences
Fig S1C DAT Order Effect Av Nic	Column means: **Sub-group 1:** 0.461 ± 0.038 **Sub-group 2:** 0.028 ± 0.022	Two-way Repeated Measures ANOVA with Holm-Šídák's multiple comparisons test	**Sub-group 1:** n = 5 mice **Sub-group 2:** n = 6 mice	z-score of GCaMP fluorescence	Effect of First Dose: p = 0.50, F (1, 9) = 0.5018 Effect of Time: p < 0.001, F (610, 5490) = 15.73 Interaction: p < 0.001, F (610, 5490) = 1.515 Multiple comparisons: No significant differences
Fig S1D DAT Biphasic	**Rew 0-15s:** 109.9 ± 51.9 **Rew 15-30s:** 124.9 ± 78.7 **Av 0-15s:** -127.2 ± 40.5 **Av 15-30s:** 40.2 ± 55.5 **Sal 0-15s:** -16.3 ± 15.1 **Sal 15-30s:** -10.1 ± 14.4	Two-way Repeated Measures ANOVA with Holm-Šídák's multiple comparisons test	n = 11 mice	z-score of GCaMP fluorescence	Effect of Dose: p = 0.0133, F (2, 20) = 5.408 Effect of Time Period: p = 0.0097, F (1, 10) = 10.15 Interaction: p = 0.0029, F (2, 20) = 7.942 Multiple comparisons: **0-15s vs 15-30s:** Rew: p = 0.8742 Av: p = 0.0001 Sal: p = 0.8742

Data	Mean ± SEM	Statistical Test	N	Outcome measure	p value
Fig S1E DAT FIP EC Infusions 1-6	**Rew Nic:** 126.04 ± 80.97 152.57 ± 63.84 110.88 ± 57.80 75.7 ± 56.92 141.34 ± 63.89 52.58 ± 50.25 **Av Nic:** 169.07 ± 85.62 -137.21 ± 39.45 -185.89 ± 35.04 -159.98 ± 57.38 -215.97 ± 51.4 -233.13 ± 66.63 **Saline:** -14.7 ± 35.38 -24.33 ± 35.73 -25.26 ± 41.49 -9.63 ± 29.77 -33.08 ± 33.48 9.28 ± 29.68	Kolmogorov-Smirnov normality test	n = 11 mice, 66 values, 3 conditions	Area Under the Curve (AUC) 0-15 seconds post-infusion	Rew Nic: p = 0.0923 Av Nic: p = 0.0005 Saline: p > 0.1000
Fig S1E DAT FIP LC Infusions 1-6	**Rew Nic:** 290.15 ± 315.6 431.13 ± 269.34 339.17 ± 190.43 272.16 ± 211.96 372.39 ± 195.75 5.71 ± 92.66 **Av Nic:** 863.75 ± 359.75 508.99 ± 198.51 238.2 ± 124.05 246.8 ± 182.46 -64.64 ± 125.43 -205.63 ± 204.56 **Saline:** 57.07 ± 117.93 -28.02 ± 153.35 -85.99 ± 70.2 13.48 ± 109.32 -31.1 ± 118.62 -24.18 ± 93.13	Kolmogorov-Smirnov normality test	n = 11 mice, 66 values, 3 conditions	Area Under the Curve (AUC) 15-60 seconds post-infusion	Rew Nic: p < 0.0001 Av Nic: p = 0.0330 Saline: p > 0.1000
Fig S1E DAT FIP EC 1st infusion	**Rew Nic:** 126.0 ± 80.97 **Av Nic:** 169.1 ± 85.62 **Saline:** -14.70 ± 35.38	One-Way Repeated Measures ANOVA with Holm-Šídák's multiple comparisons test	n = 11 mice	Area Under the Curve (AUC) 15-60 seconds post-infusion	Effect of Dose: p < 0.074, F (2, 20) = 2.984 No effect, post-hoc test not justified.

Data	Mean ± SEM	Statistical Test	N	Outcome measure	p value
Fig S1E DAT FIP EC Infusions 2-6	**Rew Nic:** 152.57 ± 63.84 110.88 ± 57.80 75.7 ± 56.92 141.34 ± 63.89 52.58 ± 50.25 **Av Nic:** -137.21 ± 39.45 -185.89 ± 35.04 -159.98 ± 57.38 -215.97 ± 51.4 -233.13 ± 66.63 **Saline:** -24.33 ± 35.73 -25.26 ± 41.49 -9.63 ± 29.77 -33.08 ± 33.48 9.28 ± 29.68	Two-way Repeated Measures ANOVA with Holm-Šídák's multiple comparisons test	n = 11 mice	Area Under the Curve (AUC) 0-15 seconds post-infusion	Effect of Infusion: p = 0.62, F (4, 40) = 0.6612 Effect of Dose: p < 0.001, F (2, 20) = 21.59 Interaction: p = 0.21, F (8, 80) = 1.387 No interaction; post-hoc test not justified.
Fig S1E DAT FIP LC 1st infusion	**Rew Nic:** 290.15 ± 315.6 **Av Nic:** 863.75 ± 359.75 **Saline:** 57.07 ± 117.93	One-Way Repeated Measures ANOVA with Holm-Šídák's multiple comparisons test	n = 11 mice	Area Under the Curve (AUC) 15-60 seconds post-infusion	Effect of Dose: p < 0.089, F (2, 20) = 2.741 No effect, post-hoc test not justified.
Fig S1E DAT FIP LC Infusions 2-6	**Rew Nic:** 431.13 ± 269.34 339.17 ± 190.43 272.16 ± 211.96 372.39 ± 195.75 5.71 ± 92.66 **Av Nic:** 508.99 ± 198.51 238.2 ± 124.05 246.8 ± 182.46 -64.64 ± 125.43 -205.63 ± 204.56 **Saline:** -28.02 ± 153.35 -85.99 ± 70.2 13.48 ± 109.32 -31.1 ± 118.62 -24.18 ± 93.13	Two-way Repeated Measures ANOVA with Holm-Šídák's multiple comparisons test	n = 11 mice	Area Under the Curve (AUC) 15-60 seconds post-infusion	Effect of Infusion: p = 0.016, F (4, 40) = 3.464 Effect of Dose: p = 0.215, F (2, 20) = 1.663 Interaction: p = 0.034, F (8, 80) = 2.219 <u>Multiple comparisons:</u> **2nd infusion:** Rew vs Av: p = 0.608 Rew vs Sal: p = 0.006 Av vs Sal: p = 0.002 **3rd infusion:** Rew vs Av: p = 0.506 Rew vs Sal: p = 0.018 Av vs Sal: p = 0.069 **4th infusion:** Rew vs Av: p = 0.867 Rew vs Sal: p = 0.248 Av vs Sal: p = 0.248 **5th infusion:** Rew vs Av: p = 0.015 Rew vs Sal: p = 0.018 Av vs Sal: p = 0.825 **6th infusion:** Rew vs Av: p = 0.420 Rew vs Sal: p = 0.844 Av vs Sal: p = 0.419

Data	Mean ± SEM	Statistical Test	N	Outcome measure	p value
Fig S2C NAcMed vs NAcLat Rew Dose	Column means: **NAcMed:** 0.335 ± 0.007 **NAcLat:** 0.202 ± 0.005	Two-way Repeated Measures ANOVA with Holm-Šídák's multiple comparisons test	**NAcLat:** n = 16 **NAcMed:** n = 9	z-score of dLight fluorescence	Effect of Subregion: p = 0.321, F (1, 23) = 1.028 Effect of Time: p < 0.0001, F (1200, 27600) = 5.047 Interaction: p = 0.881, F (1200, 27600) = 0.9512 No interaction, post-hoc test not justified.
Fig S2D NAcMed Order Effect	Column means: **Rew first:** 0.144 ± 0.034 **Av first:** 0.090 ± 0.021	Two-way Repeated Measures ANOVA with Holm-Šídák's multiple comparisons test	**Rew first:** n = 5 mice **Av first:** n = 5 mice	z-score of dLight fluorescence	Effect of Time: p < 0.001, F (1200, 9600) = 14.45 Effect of Order: p = 0.52, F (1, 8) = 0.4559 Interaction: p < 0.001, F (1200, 9600) = 1.218 Multiple comparisons: No significant differences
Fig S2D NAcLat Order Effect	Column means: **Rew first:** -0.028 ± 0.035 **Av first:** 0.038 ± 0.021	Two-way Repeated Measures ANOVA with Holm-Šídák's multiple comparisons test	**Rew first:** n = 7 **Av first:** n = 9	z-score of dLight fluorescence	Effect of First Dose: p = 0.49, F (1, 14) = 0.5013 Effect of Time: p < 0.001, F (610, 8540) = 4.764 Interaction: p = 0.02, F (610, 8540) = 1.122 Multiple comparisons: No significant differences
Fig S2E NAcMed EC Infusions 1-6	**Saline:** 62.97 ± 28 33.11 ± 23.49 -40.73 ± 13.66 12.14 ± 28.58 39.19 ± 19.69 19.11 ± 19.09 **Av Nic:** 552.88 ± 126.8 -58.37 ± 44.49 -61.14 ± 60.73 -66.54 ± 46.97 -22.35 ± 36.56 -9.21 ± 27.04	Kolmogorov-Smirnov normality test	n = 10 mice	Area Under the Curve (AUC) 0-15 seconds post-infusion	Saline: p > 0.1000 Av Nic: p < 0.0001
Fig S2E NAcMed EC 1st Infusion	**Saline:** 62.97 ± 28 **Av Nic:** 552.88 ± 126.	Paired t-test	n = 10 mice	Area Under the Curve (AUC) 0-15 seconds post-infusion	p = 0.0016, two-tailed, t = 4.440, df = 9
Fig S2E NAcMed EC Infusions 2-6	**Saline:** 33.11 ± 23.49 -40.73 ± 13.66 12.14 ± 28.58 39.19 ± 19.69 19.11 ± 19.09 **Av Nic:** -58.37 ± 44.49 -61.14 ± 60.73 -66.54 ± 46.97 -22.35 ± 36.56 -9.21 ± 27.04	Two-way Repeated Measures ANOVA with Holm-Šídák's multiple comparisons test	n = 10 mice	Area Under the Curve (AUC) 0-15 seconds post-infusion	Effect of Infusions: p = 0.253, F (4, 36) = 1.403 Effect of Drug: p = 0.096, F (1, 9) = 3.450 Interaction: p = 0.680, F (4, 36) = 0.578 No interaction, post-hoc test not justified

Data	Mean ± SEM	Statistical Test	N	Outcome measure	p value
Fig S2E NAcMed LC Infusions 1-6	**Saline:** 366.19 ± 113.99 226.48 ± 89.5 163.29 ± 105.21 241.23 ± 104.01 344.45 ± 80.22 262.71 ± 75.19 **Av Nic:** 3147.03 ± 691.76 765.07 ± 215.31 452.77 ± 167.98 302.87 ± 152.66 351.53 ± 87.24 276.47 ± 118.84	Kolmogorov-Smirnov normality test	n = 10 mice	Area Under the Curve (AUC) 15-60 seconds post-infusion	Saline: p > 0.1000 Av Nic: p < 0.0001
Fig S2E NAcMed LC 1st Infusion	**Saline:** 366.19 ± 113.99 **Av Nic:** 3147.03 ± 691.76	Paired t-test	n = 10 mice	Area Under the Curve (AUC) 15-60 seconds post-infusion	P = 0.002, two-tailed, t = 4.389, df = 9
Fig S2E NAcMed LC Infusions 2-6	**Saline:** 226.48 ± 89.5 163.29 ± 105.21 241.23 ± 104.01 344.45 ± 80.22 262.71 ± 75.19 **Av Nic:** 765.07 ± 215.31 452.77 ± 167.98 302.87 ± 152.66 351.53 ± 87.24 276.47 ± 118.84	Two-way Repeated Measures ANOVA with Holm-Šídák's multiple comparisons test	n = 10 mice	Area Under the Curve (AUC) 15-60 seconds post-infusion	Effect of Infusions: p = 0.155, F (4, 36) = 1.779 Effect of Drug: p = 0.202, F (1, 9) = 1.891 Interaction: p = 0.064, F (4, 36) = 2.443 No interaction, post-hoc test not justified.
Fig S2F NAcLat EC Infusions 1-6	**Saline:** 63.35 ± 19.92 22.77 ± 17.88 10.8 ± 20.48 3.56 ± 11.77 20.95 ± 19.92 13.8 ± 12.31 **Av Nic:** 53.62 ± 39.15 -83.71 ± 29.76 -64.44 ± 29.54 -91.84 ± 18.08 -61.75 ± 21.64 -87.91 ± 26.74	Kolmogorov-Smirnov normality test	n = 16 mice	Area Under the Curve (AUC) 0-15 seconds post-infusion	Saline: p > 0.100 Av Nic: p = 0.002
Fig S2F NAcLat EC 1st infusion	**Saline:** 63.35 ± 19.92 **Av Nic:** 53.62 ± 39.15	Paired t-test	n = 16 mice	Area Under the Curve (AUC) 0-15 seconds post-infusion	p = 0.807, two-tailed, t = 0.2486, df = 15

Data	Mean ± SEM	Statistical Test	N	Outcome measure	p value
Fig S2F NAcLat EC Infusions 2-6	**Saline:** 22.77 ± 17.88 10.8 ± 20.48 3.56 ± 11.77 20.95 ± 19.92 13.8 ± 12.31 **Av Nic:** -83.71 ± 29.76 -64.44 ± 29.54 -91.84 ± 18.08 -61.75 ± 21.64 -87.91 ± 26.74	Two-way Repeated Measures ANOVA with Holm-Šídák's multiple comparisons test	n = 16 mice	Area Under the Curve (AUC) 0-15 seconds post-infusion	Effect of Drug: p = 0.0002, F (1, 15) = 24.43 Effect of Infusions: p = 0.6546, F (4, 60) = 0.6134 Interaction: p = 0.8975, F (4, 60) = 0.2679 No interaction, post-hoc test not justified.
Fig S2F NAcLat Indiv Inf LC	**Saline:** 246.19 ± 58.99 129.44 ± 48.89 129.94 ± 58.57 103.73 ± 29.77 139.98 ± 63.47 156.73 ± 56.87 **Av Nic:** 413.64 ± 118.26 281.33 ± 68.71 288.85 ± 70.94 139.39 ± 84.23 148.86 ± 52.00 68.26 ± 73.02	Kolmogorov-Smirnov normality test	n = 16 mice	Area Under the Curve (AUC) 15-60 seconds post-infusion	Saline: p > 0.1000 Av Nic: p = 0.0993
Fig S2F NAcLat Indiv Inf LC	**Saline:** 246.19 ± 58.99 129.44 ± 48.89 129.94 ± 58.57 103.73 ± 29.77 139.98 ± 63.47 156.73 ± 56.87 **Av Nic:** 413.64 ± 118.26 281.33 ± 68.71 288.85 ± 70.94 139.39 ± 84.23 148.86 ± 52.00 68.26 ± 73.02	Two-way Repeated Measures ANOVA with Holm-Šídák's multiple comparisons test	n = 16 mice	Area Under the Curve (AUC) 15-60 seconds post-infusion	Effect of Drug: p = 0.12, F (1, 15) = 2.763 Effect of Infusions: p = 0.002, F (5, 75) = 4.105 Interaction: p = 0.21, F (5, 75) = 1.465 No interaction, post-hoc test not justified.
Fig S2G NAcMed Terminal GCaMP	<u>Column means:</u> **dLight:** 0.499 ± 0.045 **GCaMP:** 0.951 ± 0.022	Two-way Repeated Measures ANOVA with Holm-Šídák's multiple comparisons test	**dLight:** n = 10 mice **GCaMP:** n = 5 mice	z-score of fluorescence	Effect of Fluorescent Sensor: p = 0.25, F (1, 13) = 1.464 Effect of Time: p < 0.001, F (610, 7930) = 9.837 Interaction: p < 0.001, F (610, 7930) = 2.655 <u>Multiple comparisons:</u> No significant differences

Data	Mean ± SEM	Statistical Test	N	Outcome measure	p value
Fig S2G NAcLat Terminal GCaMP	**dLight:** 0.009 ± 0.025 **GCaMP:**0.297 ± 0.015	Two-way Repeated Measures ANOVA with Holm-Šídák's multiple comparisons test	**dLight:** n = 16 mice **GCaMP:** n = 5 mice	z-score of fluorescence	Effect of Fluorescent Sensor: p = 0.02, F (1, 19) = 6.003 Effect of Time: p < 0.001, F (610, 11590) = 2.656 Interaction: p > 0.99, F (610, 11590) = 0.6247 No interaction, post-hoc test not justified.
Fig S2I Real-time Place Preference	**eYFP:** 278.3 ± 30.38 **eNpHR:** 411.9 ± 36.60	Unpaired t-test	**eYFP:** n = 6 mice **eNpHR:** n = 10 mice	Time spent in light-paired chamber (s)	p = 0.02, two-tailed, t=2.658, df=14
Fig S2J Velocity in Open Field Test	**Laser Off 1:** eYFP: 4.153 ± 0.147 **eNpHR**: 5.834 ± 0.520 **Laser On:** eYFP: 3.526 ± 0.428 **eNpHR**: 4.428 ± 0.516 **Laser Off 2:** eYFP: 2.960 ± 0.194 **eNpHR**: 3.678 ± 0.336	Two-way Repeated Measures ANOVA with Holm-Šídák's multiple comparisons test	**eYFP:** n = 6 mice **eNpHR:** n = 10 mice	Velocity (cm/s)	Effect of Time: p <0.001, F (2,28) = 19.15 Effect of Virus: p = 0.07, F (1,14) = 3.801 Interaction: p = 0.19, F (2,28) = 1.755 No interaction, post-hoc test not justified.
Fig S2L NAcMed pharm EC Infusions 1-6	**DHBE:** 628.6 ± 176.3 191.5 ± 51.65 197.41 ± 68.57 131.68 ± 52.67 68.63 ± 112.92 136.27 ± 59.81 **MLA:** 1732.47 ± 318.21 175.2 ± 40.87 168.18 ± 113.7 131.93 ± 99.27 157.75 ± 52.06 80.71 ± 55.03 **MEC:** 1268.24 ± 222.5 37.19 ± 26.15 52.04 ± 63.46 108.98 ± 48.9 128.28 ± 49.87 69.2 ± 21.71 **Saline:** 1514.35 ± 265.02 90.43 ± 66.49 -2.56 ± 67.71 106.05 ± 49.67 17.65 ± 48.3 77.46 ± 69.62	Kolmogorov-Smirnov normality test	n = 7 mice	Area Under the Curve (AUC) 0-15 seconds post-infusion	DHBE: p = 0.0005 MLA: p < 0.0001 MEC: p < 0.0001 Saline: p < 0.0001

Data	Mean ± SEM	Statistical Test	N	Outcome measure	p value
Fig S2L NAcMed pharm EC 1st Infusion	**DHBE:** 628.6 ± 176.3 **MLA:** 1732.47 ± 318.21 **MEC:** 1268.24 ± 222.5 **Saline:** 1514.35 ± 265.02	One-Way Repeated Measures ANOVA with Holm-Šídák's multiple comparisons test	n = 7 mice	Area Under the Curve (AUC) 0-15 seconds post-infusion	Effect of Antagonist: p = 0.0008, F (3,18) = 8.967 <u>Multiple comparisons:</u> Saline vs DHBE: p = 0.0049 Saline vs MLA: p = 0.4952 Saline vs MEC: p = 0.4952
Fig S2L NAcMed pharm EC Infusions 2-6	**DHBE:** 191.5 ± 51.65 197.41 ± 68.57 131.68 ± 52.67 68.63 ± 112.92 136.27 ± 59.81 **MLA:** 175.2 ± 40.87 168.18 ± 113.7 131.93 ± 99.27 157.75 ± 52.06 80.71 ± 55.03 **MEC:** 37.19 ± 26.15 52.04 ± 63.46 108.98 ± 48.9 128.28 ± 49.87 69.2 ± 21.71 **Saline:** 90.43 ± 66.49 -2.56 ± 67.71 106.05 ± 49.67 17.65 ± 48.3 77.46 ± 69.62	Mixed-effects Model with Holm-Šídák's multiple comparisons test	n = 7 mice	Area Under the Curve (AUC) 0-15 seconds post-infusion	Fixed Effect of Infusions: p = 0.899, F (4, 24) = 0.263 Fixed Effect of Antagonist: p = 0.205, F (3, 18) = 1.690 Interaction: p = 0.377, F (12, 70) = 1.096 No interaction, post-hoc test not justified.

Data	Mean ± SEM	Statistical Test	N	Outcome measure	p value
Fig S2L NAcMed pharm LC Infusions 1-6	**DHBE:** 4906.56 ± 985.54 1805.28 ± 290.5 1421.87 ± 323.24 1042.16 ± 209.78 609.74 ± 414.39 671.53 ± 199.23 **MLA:** 5466.84 ± 963.17 1058.18 ± 208.87 693.81 ± 382.72 446.15 ± 249.7 533.49 ± 190.3 340.89 ± 178.25 **MEC:** 2265.15 ± 259.16 173.87 ± 88.77 193.59 ± 99.91 367.78 ± 130.3 266.05 ± 55.01 206.89 ± 67.6 **Saline:** 6186.95 ± 855.08 1302.82 ± 265.89 682.02 ± 189.58 779.52 ± 172.55 568.48 ± 153.4 629.3 ± 155.76	Kolmogorov-Smirnov normality test	n = 7 mice	Area Under the Curve (AUC) 15-60 seconds post-infusion	DHBE: p = 0.004 MLA: p < 0.0001 MEC: p < 0.0001 Saline: p < 0.0001
Fig S2L NAcMed pharm LC 1st Infusion	**DHBE:** 4906.56 ± 985.54 **MLA:** 5466.84 ± 963.17 **MEC:** 2265.15 ± 259.16 **Saline:** 6186.95 ± 855.08	One-Way Repeated Measures ANOVA with Holm-Šídák's multiple comparisons test	n = 7 mice	Area Under the Curve (AUC) 15-60 seconds post-infusion	Effect of Antagonist: p < 0.0001, F (3,18) = 13.96 <u>Multiple comparisons:</u> Saline vs DHBE: p = 0.1783 Saline vs MLA: p = 0.4822 Saline vs MEC: p < 0.0001

Data	Mean ± SEM	Statistical Test	N	Outcome measure	p value
Fig S2L NAcMed pharm LC Infusions 2-6	**DHBE:** 1805.28 ± 290.5 1421.87 ± 323.24 1042.16 ± 209.78 609.74 ± 414.39 671.53 ± 199.23 **MLA:** 1058.18 ± 208.87 693.81 ± 382.72 446.15 ± 249.7 533.49 ± 190.3 340.89 ± 178.25 **MEC:** 173.87 ± 88.77 193.59 ± 99.91 367.78 ± 130.3 266.05 ± 55.01 206.89 ± 67.6 **Saline:** 1302.82 ± 265.89 682.02 ± 189.58 779.52 ± 172.55 568.48 ± 153.4 629.3 ± 155.76	Mixed-effects Model with Holm-Šídák's multiple comparisons test	n = 7 mice	Area Under the Curve (AUC) 15-60 seconds post-infusion	Fixed Effect of Infusions: p = 0.0002, F (4, 24) = 8.759 Fixed Effect of Antagonist: p < 0.001, F (3, 18) = 15.05 Interaction: p = 0.0087, F (12, 70) = 2.498 <u>Multiple comparisons:</u> **2nd infusion:** Saline vs DHBE: p = 0.059 Saline vs MLA: p = 0.286 Saline vs MEC: p < 0.0001 **3rd infusion:** Saline vs DHBE: p = 0.008 Saline vs MLA: p = 0.959 Saline vs MEC: p = 0.089 **4th infusion:** Saline vs DHBE: p = 0.441 Saline vs MLA: p = 0.380 Saline vs MEC: p = 0.265 **5th infusion:** Saline vs DHBE: p = 0.926 Saline vs MLA: p = 0.926 Saline vs MEC: p = 0.647 **6th infusion:** Saline vs DHBE: p = 0.805 Saline vs MLA: p = 0.505 Saline vs MEC: p = 0.293
Fig S2M NAcLat pharm EC Infusions 1-6	**DHBE:** 31.8 ± 43.15 -55.24 ± 25.1 -76.25 ± 42.6 -67.39 ± 29.23 -98.51 ± 43.36 -69.4 ± 27.66 **MLA:** 637.66 ± 126.37 -32.8 ± 60.22 -54.46 ± 34.8 -57.07 ± 38.92 -111.68 ± 34.87 -123.88 ± 47.92 **MEC:** 542.34 ± 74.74 24.1 ± 35.36 42.74 ± 9.44 -44.81 ± 41.37 26.96 ± 42.99 -79.04 ± 119.73 **Av Nic:** 386.2 ± 82.16 -136.68 ± 52.61 -200.07 ± 34.52 -157.96 ± 28.99 -159.7 ± 36.01 -209.17 ± 57.65	Kolmogorov-Smirnov normality test	n = 8 mice	Area Under the Curve (AUC) 0-15 seconds post-infusion	DHBE: p = 0.0051 MLA: p < 0.0001 MEC: p < 0.0001 Saline: p < 0.0001

Data	Mean ± SEM	Statistical Test	N	Outcome measure	p value
Fig S2M NAcLat pharm EC 1st Infusion	**DHBE:** 31.8 ± 43.15 **MLA:** 637.66 ± 126.37 **MEC:** 542.34 ± 74.74 **Saline:** 386.2 ± 82.16	One-Way Repeated Measures ANOVA with Holm-Šídák's multiple comparisons test	n = 8 mice	Area Under the Curve (AUC) 0-15 seconds post-infusion	Effect of Antagonist: $p < 0.0001$, $F(3, 21) = 21.49$ Multiple comparisons: Saline vs DHBE: $p = 0.001$ Saline vs MLA: $p = 0.016$ Saline vs MEC: $p = 0.132$
Fig S2M NAcLat pharm EC Infusions 2-6	**DHBE:** -55.24 ± 25.1 -76.25 ± 42.6 -67.39 ± 29.23 -98.51 ± 43.36 -69.4 ± 27.66 **MLA:** -32.8 ± 60.22 -54.46 ± 34.8 -57.07 ± 38.92 -111.68 ± 34.87 -123.88 ± 47.92 **MEC:** 24.1 ± 35.36 42.74 ± 9.44 -44.81 ± 41.37 26.96 ± 42.99 -79.04 ± 119.73 **Saline:** -136.68 ± 52.61 -200.07 ± 34.52 -157.96 ± 28.99 -159.7 ± 36.01 -209.17 ± 57.65	Mixed-effects Model with Holm-Šídák's multiple comparisons test	n = 8 mice	Area Under the Curve (AUC) 0-15 seconds post-infusion	Fixed Effect of Infusions: $p = 0.3931$, $F(4, 28) = 1.063$ Fixed Effect of Antagonist: $p = 0.0002$, $F(3, 21) = 10.99$ Interaction: $p = 0.7793$, $F(12, 82) = 0.6654$ No interaction, post-hoc test not justified.

Data	Mean ± SEM	Statistical Test	N	Outcome measure	p value
Fig S2M NAcLat pharm LC Infusions 1-6	**DHBE:** 1129.5 ± 155.61 540.07 ± 88.76 328.01 ± 112.23 338.51 ± 110.11 121.68 ± 98.04 109.9 ± 60.61 **MLA:** 2162.32 ± 286.33 340.56 ± 183.59 74.99 ± 94.53 78.72 ± 66.73 -78.76 ± 96.65 17.86 ± 102.91 **MEC:** 782.56 ± 129.01 212.79 ± 82.72 198.81 ± 48.58 -15.73 ± 98.43 71.02 ± 111.2 -432.01 ± 627.85 **Av Nic:** 1706.26 ± 270.8 466.73 ± 121.71 128.76 ± 100.71 192.52 ± 82.94 284.09 ± 76.52 47.35 ± 140.01	Kolmogorov-Smirnov normality test	n = 8 mice	Area Under the Curve (AUC) 15-60 seconds post-infusion	DHBE: p = 0.0021 MLA: p < 0.0001 MEC: p < 0.0001 Saline: p < 0.0001
Fig S2M NAcLat pharm LC 1st Infusion	**DHBE:** 1129.5 ± 155.61 **MLA:** 2162.32 ± 286.33 **MEC:** 782.56 ± 129.01 **Saline:** 1706.26 ± 270.8	One-Way Repeated Measures ANOVA with Holm-Šídák's multiple comparisons test	n = 8 mice	Area Under the Curve (AUC) 15-60 seconds post-infusion	Effect of Antagonist: p < 0.0001, F (3, 21) = 13.31 <u>Multiple comparisons:</u> Saline vs DHBE: p = 0.070 Saline vs MLA: p = 0.131 Saline vs MEC: p = 0.003

Data	Mean ± SEM	Statistical Test	N	Outcome measure	p value
Fig S2M NAcLat pharm LC Infusions 2-6	**DHBE:** 540.07 ± 88.76 328.01 ± 112.23 338.51 ± 110.11 121.68 ± 98.04 109.9 ± 60.61 **MLA:** 340.56 ± 183.59 74.99 ± 94.53 78.72 ± 66.73 -78.76 ± 96.65 17.86 ± 102.91 **MEC:** 212.79 ± 82.72 198.81 ± 48.58 -15.73 ± 98.43 71.02 ± 111.2 -432.01 ± 627.85 **Saline:** 466.73 ± 121.71 128.76 ± 100.71 192.52 ± 82.94 284.09 ± 76.52 47.35 ± 140.01	Mixed-effects Model with Holm-Šídák's multiple comparisons test	n = 8 mice	Area Under the Curve (AUC) 15-60 seconds post-infusion	Fixed Effect of Infusions: p = 0.037, F (4, 28) = 2.966 Fixed Effect of Antagonist: p = 0.038, F (3, 21) = 3.373 Interaction: p = 0.874, F (12, 82) = 0.552 No interaction, post-hoc test not justified.
Fig S3C VTA GABA EC Infusions 1-6	**Rew Nic:** 113.19 ± 44.29 187.35 ± 53.87 -89.52 ± 135.95 114.8 ± 26.91 21.72 ± 65.38 53.06 ± 58.6 **Av Nic:** 459.63 ± 76.13 331.68 ± 40.68 345.09 ± 94.06 435.95 ± 45.87 404.23 ± 75.22 345.66 ± 107.81 **Saline:** -16.47 ± 64.79 81.08 ± 92.08 166.36 ± 36.9 95.99 ± 41.35 96.12 ± 43.57 81.47 ± 62.79	Kolmogorov-Smirnov normality test	n = 7 mice	Area Under the Curve (AUC) 0-15 seconds post-infusion	Rew Nic: p = 0.0008 Av Nic: p = 0.0034 Saline: p = 0.0455
Fig S3C VTA GABA EC 1st Infusion	**Rew Nic:** 113.19 ± 44.29 **Av Nic:** 459.63 ± 76.13 **Saline:** -16.47 ± 64.79	One-Way Repeated Measures ANOVA with Holm-Šídák's multiple comparisons test	n = 7 mice	Area Under the Curve (AUC) 0-15 seconds post-infusion	Effect of Dose: p = 0.0004, F (2, 12) = 16.01 <u>Multiple comparisons:</u> Rew vs Av: p = 0.0036 Rew vs Sal: p = 0.1620 Sal vs Av: p = 0.0004

Data	Mean ± SEM	Statistical Test	N	Outcome measure	p value
Fig S3C VTA GABA EC Infusions 2-6	**Rew Nic:** 187.35 ± 53.87 -89.52 ± 135.95 114.8 ± 26.91 21.72 ± 65.38 53.06 ± 58.6 **Av Nic:** 331.68 ± 40.68 345.09 ± 94.06 435.95 ± 45.87 404.23 ± 75.22 345.66 ± 107.81 **Saline:** 81.08 ± 92.08 166.36 ± 36.9 95.99 ± 41.35 96.12 ± 43.57 81.47 ± 62.79	Two-way Repeated Measures ANOVA with Holm-Šídák's multiple comparisons test	n = 7 mice	Area Under the Curve (AUC) 0-15 seconds post-infusion	Effect of Infusion: p = 0.5121, F (4, 24) = 0.842 Effect of Drug: p < 0.0001, F (2, 12) = 38.41 Interaction: p = 0.3301, F (10, 60) = 1.386 No interaction, post-hoc test not justified.
Fig S3C VTA GABA LC Infusions 1-6	**Rew Nic:** -53.88 ± 203.37 195.34 ± 115 -400.63 ± 420.36 92.81 ± 95.81 -337.31 ± 219.21 -60.36 ± 182.79 **Av Nic:** 758.82 ± 388.37 100.76 ± 216.18 250.73 ± 333.85 451.35 ± 224.03 326.65 ± 286.37 324.51 ± 215.54 **Saline:** -279.25 ± 227.73 -309.98 ± 219.65 172.18 ± 94.27 -73.28 ± 138.48 -108.58 ± 106.17 -91.06 ± 305.32	Kolmogorov-Smirnov normality test	n = 7 mice	Area Under the Curve (AUC) 15-60 seconds post-infusion	Rew Nic: p < 0.0001 Av Nic: p > 0.1000 Saline: p = 0.0927
Fig S3C VTA GABA LC 1st Infusion	**Rew Nic:** -53.88 ± 203.37 **Av Nic:** 758.82 ± 388.37 **Saline:** -279.25 ± 227.73	One-Way Repeated Measures ANOVA with Holm-Šídák's multiple comparisons test	n = 7 mice	Area Under the Curve (AUC) 15-60 seconds post-infusion	Effect of Dose: p = 0.0434, F (2, 12) = 4.120 <u>Multiple comparisons:</u> Rew vs Av: p = 0.105 Rew vs Sal: p = 0.565 Sal vs Av: p = 0.054

Data	Mean ± SEM	Statistical Test	N	Outcome measure	p value
Fig S3C VTA GABA LC Infusions 2-6	**Rew Nic:** 195.34 ± 115 -400.63 ± 420.36 92.81 ± 95.81 -337.31 ± 219.21 -60.36 ± 182.79 **Av Nic:** 100.76 ± 216.18 250.73 ± 333.85 451.35 ± 224.03 326.65 ± 286.37 324.51 ± 215.54 **Saline:** -309.98 ± 219.65 172.18 ± 94.27 -73.28 ± 138.48 -108.58 ± 106.17 -91.06 ± 305.32	Two-way Repeated Measures ANOVA with Holm-Šídák's multiple comparisons test	n = 7 mice	Area Under the Curve (AUC) 15-60 seconds post-infusion	Effect of Infusion: $p = 0.855$, $F(4, 24) = 0.331$ Effect of Dose: $p = 0.029$, $F(2, 12) = 4.838$ Interaction: $p = 0.350$, $F(8, 48) = 1.147$ No interaction, post-hoc test not justified.
Fig S3D VTA GABA Avg traces	<u>Column means:</u> **Rew Nic:** -0.046 ± 0.021 **Av Nic:** 1.236 ± 0.046 **Saline:** -0.050 ± 0.018	Two-way Repeated Measures ANOVA with Holm-Šídák's multiple comparisons test	n = 7 mice	z-score of GCaMP fluorescence	Effect of Time: $p < 0.001$, $F(610, 3660) = 18.52$ Effect of Drug: $p < 0.001$, $F(2, 12) = 15.61$ Interaction: $p < 0.001$, $F(1220, 7320) = 9.068$ <u>Multiple comparisons</u>: Time points with p values ≤ 0.05 denoted by dot on bar graph
Fig S3E VTA GABA EC	**Rew Nic:** 66.77 ± 39.02 **Av Nic:** 387.0 ± 28.03 **Saline:** 84.09 ± 24.79	One-Way Repeated Measures ANOVA with Holm-Šídák's multiple comparisons test	n = 7 mice	Area Under the Curve (AUC) 0-15 seconds post-infusion	Effect of Drug: $p < 0.001$, $F(2, 12) = 68.43$ <u>Multiple comparisons:</u> Rew vs Av: $p < 0.001$ Rew vs Sal: $p = 0.58$ Av vs Sal: $p < 0.001$
Fig S3E VTA GABA LC	**Rew Nic:** -94.01 ± 80.31 **Av Nic:** 368.8 ± 182.1 **Saline:** -115.0 ± 62.42	One-Way Repeated Measures ANOVA with Holm-Šídák's multiple comparisons test	n = 7 mice	Area Under the Curve (AUC) 15-60 seconds post-infusion	Effect of Drug: $p = 0.008$, $F(2, 12) = 7.355$ No effect, post-hoc test not justified.

Data	Mean ± SEM	Statistical Test	N	Outcome measure	p value
Fig S3F VTA GABA EC pharm Infusions 1-6	**Saline:** 459.63 ± 76.13 331.68 ± 40.68 345.09 ± 94.06 435.95 ± 45.87 404.23 ± 75.22 345.66 ± 107.81 **MLA:** 320.12 ± 109.4 262.23 ± 89.06 353.1 ± 58.17 269.54 ± 48.49 189.15 ± 81.12 199.95 ± 32.52 **MEC:** 155.11 ± 66.51 -28.88 ± 71.66 37.28 ± 31.56 -94 ± 72.63 53.88 ± 45.55 16.26 ± 64.69 **DHBE:** 479.49 ± 107.09 450.98 ± 74.89 525.6 ± 70.87 506.5 ± 81.19 505.64 ± 73.73 422.48 ± 69.7	Kolmogorov-Smirnov normality test	n = 7 mice	Area Under the Curve (AUC) 0-15 seconds post-infusion	Saline: p = 0.0034 MLA: p > 0.1000 MEC: p > 0.1000 DHBE: p > 0.1000
Fig S3F VTA GABA pharm EC 1st Infusion	**Saline:** 459.63 ± 76.13 **MLA:** 320.12 ± 109.4 **MEC:** 155.11 ± 66.51 **DHBE:** 479.49 ± 107.09	One-Way Repeated Measures ANOVA with Holm-Šídák's multiple comparisons test	n = 7 mice	Area Under the Curve (AUC) 0-15 seconds post-infusion	Effect of Antagonist: p = 0.025, F (3, 18) = 3.975 <u>Multiple comparisons:</u> Saline vs MLA: p = 0.450 Saline vs MEC: p = 0.051 Saline vs DHBE: p = 0.854

Data	Mean ± SEM	Statistical Test	N	Outcome measure	p value
Fig S3F VTA GABA pharm EC Infusions 2-6	**Saline:** 331.68 ± 40.68 345.09 ± 94.06 435.95 ± 45.87 404.23 ± 75.22 345.66 ± 107.81 **MLA:** 262.23 ± 89.06 353.1 ± 58.17 269.54 ± 48.49 189.15 ± 81.12 199.95 ± 32.52 **MEC:** -28.88 ± 71.66 37.28 ± 31.56 -94 ± 72.63 53.88 ± 45.55 16.26 ± 64.69 **DHBE:** 450.98 ± 74.89 525.6 ± 70.87 506.5 ± 81.19 505.64 ± 73.73 422.48 ± 69.7	Two-way Repeated Measures ANOVA with Holm-Šídák's multiple comparisons test	n = 7 mice	Area Under the Curve (AUC) 0-15 seconds post-infusion	Effect of Infusion: $p = 0.577$, $F (4, 24) = 0.735$ Effect of Antagonist: $p < 0.001$, $F (3, 18) = 22.88$ Interaction: $p = 0.477$, $F (12, 72) = 0.979$ No interaction, post-hoc test not justified
Fig S3F VTA GABA pharm LC Infusions 1-6	**Saline:** 758.82 ± 388.37 100.76 ± 216.18 250.73 ± 333.85 451.35 ± 224.03 326.65 ± 286.37 324.51 ± 215.54 **MLA:** 681.9 ± 419.32 248.56 ± 224.8 453.54 ± 155.64 219.27 ± 141.82 -69.8 ± 294.1 160.82 ± 80.05 **MEC:** 71.36 ± 321.35 -212.34 ± 256.55 -111.38 ± 66.74 -548.45 ± 251.03 -216.68 ± 317.51 -222.3 ± 148.88 **DHBE:** 137.31 ± 442.78 274.29 ± 260.75 323.41 ± 184.23 345.03 ± 217.33 195.46 ± 144.85 93.14 ± 121.86	Kolmogorov-Smirnov normality test	n = 7 mice	Area Under the Curve (AUC) 15-60 seconds post-infusion	Saline: $p > 0.100$ MLA: $p = 0.086$ MEC: $p = 0.014$ DHBE: $p > 0.100$

Data	Mean ± SEM	Statistical Test	N	Outcome measure	p value
Fig S3F VTA GABA pharm LC 1st Infusion	**Saline:** 758.82 ± 388.37 **MLA:** 681.9 ± 419.32 **MEC:** 71.36 ± 321.35 **DHBE:** 137.31 ± 442.78	One-Way Repeated Measures ANOVA with Holm-Šídák's multiple comparisons test	n = 7 mice	Area Under the Curve (AUC) 15-60 seconds post-infusion	Effect of Antagonist: p = 0.216, F (3, 18) = 1.637 No effect, post-hoc test not justified.
Fig S3F VTA GABA pharm LC Infusions 2-6	**Av Nic:** 100.76 ± 216.18 250.73 ± 333.85 451.35 ± 224.03 326.65 ± 286.37 324.51 ± 215.54 **MLA:** 248.56 ± 224.8 453.54 ± 155.64 219.27 ± 141.82 -69.8 ± 294.1 160.82 ± 80.05 **MEC:** -212.34 ± 256.55 -111.38 ± 66.74 -548.45 ± 251.03 -216.68 ± 317.51 -222.3 ± 148.88 **DHBE:** 274.29 ± 260.75 323.41 ± 184.23 345.03 ± 217.33 195.46 ± 144.85 93.14 ± 121.86	Two-way Repeated Measures ANOVA with Holm-Šídák's multiple comparisons test	n = 7 mice	Area Under the Curve (AUC) 15-60 seconds post-infusion	Effect of Infusion: p = 0.801, F (4, 24) = 0.408 Effect of Antagonist: p = 0.031, F (3, 18) = 3.713 Interaction: p = 0.723, F (12, 72) = 0.724 No interaction, post-hoc test not justified.
Fig S3G VTA GABA pharm LC	**Av Nic:** 368.8 ± 182.1 **MLA:** 282.4 ± 144.1 **MEC:** -206.6 ± 93.76 **DHBE:** 228.1 ± 194.2	One-Way Repeated Measures ANOVA with Holm-Šídák's multiple comparisons test	n = 7 mice	Area Under the Curve (AUC) 15-60 seconds post-infusion	Effect of Antagonist: p = 0.06, F (3, 18) = 3.019 No effect, post-hoc test not justified.
Fig S4G Rabies starter cells	<u>GAD2-Cre:</u> **mCh+/GFP+:** 0.255 ± 0.039 **mCh+/GFP-:** 0.585 ± 0.077 **mCh-/GFP+:** 0.160 ± 0.050 <u>VGLUT2-Cre:</u> **mCh+/GFP+:** 0.424 ± 0.017 **mCh+/GFP-:** 0.342 ± 0.070 **mCh-/GFP+:** 0.231 ± 0.065	Two-Way Repeated Measures ANOVA with Holm-Šídák's multiple comparisons test	**GAD2-Cre:** n = 3 mice **VGLUT2-Cre:** n = 4 mice	Proportion of fluorescent cells	Effect of Cell type: p = 0.0122, F (2, 10) = 7.065 Effect of Genotype: p = 0.2108, F (1, 5) = 2.059 Interaction: p = 0.0383, F (2, 10) = 4.603 <u>Multiple comparisons:</u> **GAD2 vs VGLUT2:** mCh+/GFP+: p = 0.1112 mCh+/GFP-: p = 0.0290 mCh-/GFP+: p = 0.3825

Data	Mean ± SEM	Statistical Test	N	Outcome measure	p value
Fig S4I Rabies inputs	GAD2-Cre: **PFC:** 0.001 ± 0.001 **Cortex:** 0.006 ± 0.004 **NAcc:** 0.001 ± 0 **BNST:** 0.007 ± 0.001 **VP:** 0.001 ± 0.001 **Amy:** 0.012 ± 0.009 **Hab:** 0.002 ± 0.001 **LH:** 0.008 ± 0.002 **PH:** 0.001 ± 0 **Other hypoth:** 0.002 ± 0.001 **ZI:** 0.007 ± 0.005 **MM:** 0.001 ± 0 **VTA:** 0.009 ± 0.002 **SN:** 0.006 ± 0.003" **IPN:** 0 ± 0 **SupCxs:** 0.005 ± 0.004 **RMTg:** 0.01 ± 0.003 **PAG:** 0.117 ± 0.046 **PnO:** 0.016 ± 0.001 **DpMe:** 0.219 ± 0.013 **DR:** 0.272 ± 0.044 **Other raphe:** 0.048 ± 0.027 **PPT:** 0.03 ± 0.008 **LDT:** 0.098 ± 0.009 **PB:** 0.016 ± 0.006 **LC:** 0.016 ± 0.005 VGLUT2-Cre: **PFC:** 0.006 ± 0.002 **Cortex:** 0.015 ± 0.003 **NAcc:** 0.001 ± 0 **BNST:** 0.004 ± 0.002 **VP:** 0.005 ± 0.001 **Amy:** 0.003 ± 0.002 **Hab:** 0.038 ± 0.016 **LH:** 0.024 ± 0.007 **PH:** 0.013 ± 0.005 **Other hypoth:** 0.004 ± 0.001 **ZI:** 0.006 ± 0.003 **MM:** 0.009 ± 0.004 **VTA:** 0.027 ± 0.009 **SN:** 0.015 ± 0.005 **IPN:** 0.017 ± 0.004 **SupCxs:** 0.015 ± 0.005 **RMTg:** 0.008 ± 0.002 **PAG:** 0.128 ± 0.02 **PnO:** 0.009 ± 0.001 **DpMe:** 0.086 ± 0.009 **DR:** 0.187 ± 0.019 **Other raphe:** 0.033 ± 0.006 **PPT:** 0.011 ± 0.002 **LDT:** 0.074 ± 0.02 **PB:** 0.081 ± 0.015 **LC:** 0.075 ± 0.027	Two-Way ANOVA with Holm-Šídák's multiple comparisons test	**GAD2-Cre:** n = 3 mice **VGLUT2-Cre:** n = 4 mice	Proportion of input cells	Effect of Brain Region: $p < 0.0001$, $F(25, 130) = 41.29$ Effect of Genotype: $p = 0.8348$, $F(1, 130) = 0.044$ Interaction: $p < 0.0001$, $F(25, 130) = 5.017$ Multiple comparisons: **GAD2-Cre vs VGLUT2-Cre:** PFC: p > 0.9999 Cortex: p > 0.9999 NAcc: p > 0.9999 BNST: p > 0.9999 VP: p > 0.9999 Amy: p > 0.9999 Hab: p = 0.5497 LH: p = 0.9995 PH: p > 0.9999 Other hypoth: p > 0.9999 ZI: p > 0.9999 MM: p > 0.9999 VTA: p = 0.9990 SN: p > 0.9999 IPN: p = 0.9991 SupCxs: p > 0.9999 RMTg: p > 0.9999 PAG: p > 0.9999 PnO: p > 0.9999 DpMe: p < 0.0001 DR: p < 0.0001 Other raphe: p = 0.9995 PPT: p = 0.9978 LDT: p = 0.9769 PB: p = 0.0048 LC: p = 0.0173

Data	Mean ± SEM	Statistical Test	N	Outcome measure	p value
Fig S4K Co-expression of GAD2 in α7+ cells	**LDT α7+:** GAD-: 0.1408 ± 0.02599 GAD+: 0.2721 ± 0.01526	Paired t-test	n = 10 images (n = 3 mice)	Fraction of cells per image	p < 0.001, two-tailed, t=6.626, df=9
Fig S5D IPSC Amplitude	**IPSC Amplitude:** 189.8 ± 74.89	No statistical test performed	n = 14 cells	IPSC Amplitude (pA)	N/A, no statistical test performed
Fig S5G NAcLat dLight Response to LDT GABA stim	**-1s from Light Onset:** Trial: -0.192 ± 0.574 Inter-Trial: 1.014 ± 0.706 **0s from Light Onset:** Trial: -8.135 ± 0.909 Inter-Trial: 2.373 ± 1.052 **1s from Light Onset:** Trial: -9.348 ± 1.142 Inter-Trial: 3.086 ± 1.237 **2s from Light Onset:** Trial: 1.379 ± 0.944 Inter-Trial: 1.330 ± 1.015	Two-Way Repeated Measures ANOVA with Holm-Šídák's multiple comparisons test	n = 3 mice Inter-trial samples: 60 Trial samples: 60	Area under the curve (AUC) over 1s	Effect of Light: p < 0.001, F (1,59) = 26.19 Effect of Time: p < 0.001, F (3,177) = 20.94 Interaction: p < 0.001, F (3,177) = 38.31 **Multiple Comparisons:** -1s from Light Onset: p = 0.43 0s from Light Onset: p < 0.001 1s from Light Onset: p < 0.001 2s from Light Onset: p = 0.96
Fig S5J LDT GAD opto Real-time Place Aversion	**eYFP:** 463 ± 48.08 **ChR2:** 280.1 ± 46.28	Unpaired t-test	**eYFP:** 10 mice **ChR2:** 9 mice	Time spent in light-paired chamber (s)	p = 0.014, t = 2.738, df = 17
Fig S5K LDT GAD opto Open Field Test	eYFP: **Off 1:** 1259.134 ± 168.372 **On:** 652.810 ± 101.515 **Off 2:** 556.601 ± 128.643 ChR2: **Off 1:** 1251.831 ± 163.599 **On:** 928.520 ± 155.968 **Off 2:** 749.889 ± 169.680	Two-Way Repeated Measures ANOVA with Holm-Šídák's multiple comparisons test	**eYFP:** 10 mice **ChR2:** 9 mice	Distance traveled (cm)	Effect of Light: p < 0.0001, F (2, 34) = 15.49 Effect of Virus: p = 0.3793, F (1, 17) = 0.815 Interaction: p = 0.4473, F (2, 34) = 0.824 No interaction, multiple comparisons test not justified.
Fig S6C LDT GABA EC 1st Infusion	**Saline:** 54.13 ± 15.94 **Av Nic:** 254.64 ± 65.13 **Rew Nic:** 47.7 ± 68.21	Mixed-effects analysis with Holm-Šídák's multiple comparisons test	n = 6 mice	Area Under the Curve (AUC) 0-15 seconds post-infusion	Fixed effect of Drug: p = 0.015, F (2, 10) = 6.540 Multiple comparisons: Sal vs Av: p = 0.03 Sal vs Rew: p = 0.75 Av vs Rew: p = 0.02

Data	Mean ± SEM	Statistical Test	N	Outcome measure	p value
Fig S6C LDT GABA EC Infusions 2-6	**Saline:** 80.69 ± 40.74 -9.17 ± 55.74 -73.27 ± 70.1 19.51 ± 19.29 31.09 ± 38.34 **Aversive:** 234.32 ± 65.8 182.03 ± 113.78 188.97 ± 57.86 182.01 ± 32.83 204.6 ± 87.28 **Reward:** 40.34 ± 62.31 53.57 ± 27.09 29.13 ± 27.16 31.24 ± 14.55 16.99 ± 14.06	Mixed-effects analysis with Holm-Šídák's multiple comparisons test	n = 6 mice	Area Under the Curve (AUC) 0-15 seconds post-infusion	Fixed Effect of Infusion: p = 0.318, F (4, 24) = 1.246 Fixed Effect of Drug: p = 0.018, F (2, 12) = 5.708 Interaction: p = 0.650, F (8, 33) = 0.748 No interaction, post-hoc test not justified.
Fig S6C LDT GABA LC Infusions 1-6	**Saline:** 51.44 ± 63.34 80.62 ± 141.9 -208.2 ± 114.22 -192.01 ± 311.25 -6.91 ± 73.87 -90.19 ± 134.35 **Av Nic:** 136.44 ± 97.39 180.83 ± 266.66 148.84 ± 372.87 13.57 ± 82.45 -32.06 ± 185.89 61.8 ± 108.38 **Rew Nic:** -135.69 ± 189.87 -227.42 ± 200.18 -29.02 ± 37.95 -104.54 ± 97.63 -37.22 ± 45.73 -59.44 ± 76.44	Kolmogorov-Smirnov normality test	n = 6 mice	Area Under the Curve (AUC) 15-60 seconds post-infusion	Saline: p = 0.001 Av Nic: p = 0.014 Rew Nic: p < 0.0001
Fig S6C LDT GABA LC 1st Infusion	**Saline:** 51.44 ± 63.34 **Av Nic:** 136.44 ± 97.39 **Rew Nic:** -135.69 ± 189.87	One-Way Repeated Measures ANOVA with Holm-Šídák's multiple comparisons test	n = 6 mice	Area Under the Curve (AUC) 15-60 seconds post-infusion	Main effect of Drug: p = 0.188, F (2, 10) = 1.988 No effect, post-hoc test not justified

Data	Mean ± SEM	Statistical Test	N	Outcome measure	p value
Fig S6C LDT GABA LC Infusions 2-6	**Saline:** 80.62 ± 141.9 -208.2 ± 114.22 -192.01 ± 311.25 -6.91 ± 73.87 -90.19 ± 134.35 **Av Nic:** 180.83 ± 266.66 148.84 ± 372.87 13.57 ± 82.45 -32.06 ± 185.89 61.8 ± 108.38 **Rew Nic:** -227.42 ± 200.18 -29.02 ± 37.95 -104.54 ± 97.63 -37.22 ± 45.73 -59.44 ± 76.44	Mixed-effects analysis with Holm-Šídák's multiple comparisons test	n = 6 mice	Area Under the Curve (AUC) 15-60 seconds post-infusion	Fixed Effect of Infusion: p = 0.967, F (4, 20) = 0.136 Effect of Drug: p = 0.412, F (2, 10) = 0.971 Interaction: p = 0.810, F (8, 37) = 0.551 No interaction, post-hoc test not justified.
Fig S6D LDT GABA avg traces	<u>Column Means:</u> **Saline:** -0.062 ± 0.008 **Av Nic:** 0.478 ± 0.025 **Rew Nic:** -0.138 ± 0.210	Two-way Repeated Measures ANOVA with Holm-Šídák's multiple comparisons test	n = 6 mice	z-score of GCaMP fluorescence	Effect of Time: p < 0.001, F (610, 3050) = 9.271 Effect of Drug: p = 0.07, F (2, 10) = 3.514 Interaction: p < 0.001, F (1220, 6100) = 4.126 <u>Multiple comparisons</u>: Time points with p values ≤ 0.05 denoted by dot on bar graph
Fig S6E LDT GABA EC	**Saline:** 17.83 ± 13.21 **Av Nic:** 207.8 ± 60.13 **Rew Nic:** 14.65 ± 1.22	One-Way Repeated Measures ANOVA with Holm-Šídák's multiple comparisons test	n = 6 mice	Area Under the Curve (AUC) 0-15 seconds post-infusion	Effect of Drug: p = 0.005, F (2, 10) = 9.633 <u>Multiple comparisons:</u> Sal vs Av Nic: p = 0.010 Sal vs Rew Nic: p = 0.95 Av Nic vs Rew Nic: p = 0.010
Fig S6E LDT GABA LC	**Saline:** -55.39 ± 63.62 **Av Nic:** 84.90 ± 98.70 **Rew Nic:** -98.89 ± 96.14	One-Way Repeated Measures ANOVA with Holm-Šídák's multiple comparisons test	n = 6 mice	Area Under the Curve (AUC) 15-60 seconds post-infusion	Effect of Drug: p = 0.32, F (2, 10) = 1.299 No effect, post-hoc test not justified.

Data	Mean ± SEM	Statistical Test	N	Outcome measure	p value
Fig S6G LDT GABA pharm EC Infusions 1-6	**Saline:** 1301.16 ± 249.93 485.3 ± 143.98 387.21 ± 115.03 243.25 ± 66.03 324.67 ± 98.57 251.75 ± 107.37 **DHBE:** 973.31 ± 268.86 408.32 ± 129.41 377.23 ± 107.68 300.88 ± 87.71 330.44 ± 87.25 191.09 ± 68.25 **MLA:** 789.31 ± 138.74 306.12 ± 62.82 196.1 ± 74.42 141.85 ± 42.79 88.1 ± 43.24 165.36 ± 24.88 **MEC:** 566.84 ± 75.63 213.85 ± 32.01 64.93 ± 58.85 84.89 ± 34.42 -16.9 ± 97.66 53.37 ± 57.89	Kolmogorov-Smirnov normality test	n = 7 mice	Area Under the Curve (AUC) 0-15 seconds post-infusion	Saline: p = 0.0008 DHBE: p = 0.0091 MLA: p = 0.0001 MEC: p = 0.0151
Fig S6G LDT GABA pharm EC 1st Infusion	**Saline:** 1301.16 ± 249.93 **DHBE:** 973.31 ± 268.86 **MLA:** 789.31 ± 138.74 **MEC:** 566.84 ± 75.63	One-Way Repeated Measures ANOVA with Holm-Šídák's multiple comparisons test	n = 7 mice	Area Under the Curve (AUC) 0-15 seconds post-infusion	Main effect of Antagonist: p = 0.107, F (3, 18) = 2.345 No effect, post-hoc test not justified

Data	Mean ± SEM	Statistical Test	N	Outcome measure	p value
Fig S6G LDT GABA pharm EC Infusions 2-6	**Saline:** 485.3 ± 143.98 387.21 ± 115.03 243.25 ± 66.03 324.67 ± 98.57 251.75 ± 107.37 **DHBE:** 408.32 ± 129.41 377.23 ± 107.68 300.88 ± 87.71 330.44 ± 87.25 191.09 ± 68.25 **MLA:** 306.12 ± 62.82 196.1 ± 74.42 141.85 ± 42.79 88.1 ± 43.24 165.36 ± 24.88 **MEC:** 213.85 ± 32.01 64.93 ± 58.85 84.89 ± 34.42 -16.9 ± 97.66 53.37 ± 57.89	Two-way Repeated Measures ANOVA with Holm-Šídák's multiple comparisons test	n = 7 mice	Area Under the Curve (AUC) 0-15 seconds post-infusion	Effect of Infusion: p = 0.003, F (4, 24) = 5.323 Effect of Antagonist: p = 0.003, F (3, 18) = 6.526 Interaction: p = 0.890, F (12, 72) = 0.528 No interaction, post-hoc test not justified.
Fig S6H LDT GABA pharm LC	**Saline:** 904.5 ± 191.7 **MLA:** 490.9 ± 149.3 **MEC:** 171.9 ± 90.63 **DHBE:** 921.6 ± 312.5	One-Way Repeated Measures ANOVA with Holm-Šídák's multiple comparisons test	n = 7 mice	Area Under the Curve (AUC) 15-60 seconds post-infusion	Effect of Antagonist: p = 0.007, F (3, 18) = 5.524 <u>Multiple comparisons:</u> Av Nic vs MLA: p = 0.14 Av Nic vs MEC: p = 0.010 Av Nic vs DHBE: p = 0.94

Data	Mean ± SEM	Statistical Test	N	Outcome measure	p value
Fig S6H LDT GABA pharm LC Infusions 1-6	**Saline:** 2311.96 ± 259.38 764.42 ± 383.81 23.64 ± 316.91 499.4 ± 227.73 795.64 ± 330.09 531.83 ± 331.75 **DHBE:** 1271.25 ± 420.93 1161.51 ± 476.91 1154.01 ± 384.98 702.17 ± 326.44 867.61 ± 261.79 373.28 ± 218.57 **MLA:** 1202.86 ± 252.57 358.27 ± 212.97 390.81 ± 233.89 381.28 ± 167.35 228.5 ± 162.59 383.87 ± 110.26 **MEC:** 786.47 ± 206.42 443.69 ± 160.57 -3.06 ± 215.33 66.52 ± 296.3 -48.35 ± 276.29 -213.68 ± 137.94	Kolmogorov-Smirnov normality test	n = 7 mice	Area Under the Curve (AUC) 15-60 seconds post-infusion	Saline: p = 0.031 DHBE: p > 0.100 MLA: p = 0.003 MEC: p > 0.100
Fig S6H LDT GABA pharm LC 1st Infusion	**Saline:** 2311.96 ± 259.38 **MLA:** 1202.86 ± 252.57 **MEC:** 786.47 ± 206.42 **DHBE:** 1271.25 ± 420.93	One-Way Repeated Measures ANOVA with Holm-Šídák's multiple comparisons test	n = 7 mice	Area Under the Curve (AUC) 15-60 seconds post-infusion	Main effect of Antagonist: p = 0.0002, F (3, 18) = 11.53 <u>Multiple comparisons:</u> Sal vs MEC: p = 0.0001 Sal vs MLA: p = 0.0033 Sal vs DHBE: p = 0.0047

Data	Mean ± SEM	Statistical Test	N	Outcome measure	p value
Fig S6H LDT GABA pharm LC Infusions 2-6	**Saline:** 764.42 ± 383.81 23.64 ± 316.91 499.4 ± 227.73 795.64 ± 330.09 531.83 ± 331.75 **DHBE:** 1161.51 ± 476.91 1154.01 ± 384.98 702.17 ± 326.44 867.61 ± 261.79 373.28 ± 218.57 **MLA:** 358.27 ± 212.97 390.81 ± 233.89 381.28 ± 167.35 228.5 ± 162.59 383.87 ± 110.26 **MEC:** 443.69 ± 160.57 -3.06 ± 215.33 66.52 ± 296.3 -48.35 ± 276.29 -213.68 ± 137.94	Two-way Repeated Measures ANOVA with Holm-Šídák's multiple comparisons test	n = 7 mice	Area Under the Curve (AUC) 15-60 seconds post-infusion	Effect of Infusion: p = 0.265, F (4, 24) = 1.394 Effect of Antagonist: p = 0.016, F (3, 18) = 4.475 Interaction: p = 0.520, F (12, 72) = 0.933 No interaction, post-hoc test not justified.
Fig S7C NAcLat Casp EC Infusions 1-6	**Casp Sal:** 36.21 ± 24.25 15.96 ± 34.9 3.61 ± 24.97 -33.59 ± 29.69 6.98 ± 20.31 19.81 ± 14.91 **mCh Sal:** -9.11 ± 18.32 4.79 ± 17.6 -51.91 ± 29.88 82.44 ± 40.36 -30.26 ± 57.55 33.88 ± 15.22 **Casp Av Nic:** 312.53 ± 86.71 132.74 ± 77.43 32.29 ± 34.78 -35.22 ± 63.42 -54.75 ± 26.9 -81.97 ± 84.23 **mCh Av Nic:** 284.07 ± 110.03 -116.11 ± 24.96 -149.82 ± 44.05 -83.42 ± 36.6 -118.27 ± 23.89 -121.53 ± 34.59	Kolmogorov-Smirnov normality test	**Caspase:** n = 6 mice **mCherry:** n = 6 mice	Area Under the Curve (AUC) 0-15 seconds post-infusion	Casp Sal: p > 0.1000 mCh Sal: p = 0.0313 Casp Av Nic: p = 0.0109 mCh Av Nic: p < 0.0001

Data	Mean ± SEM	Statistical Test	N	Outcome measure	p value
Fig S7C NAcLat Casp EC 1st Infusion	**Casp Sal:** 36.21 ± 24.25 **mCh Sal:** -9.11 ± 18.32 **Casp Av:** 312.53 ± 86.71 **mCh Av:** 284.07 ± 110.03	Ordinary One-Way ANOVA with Holm-Šídák's multiple comparisons test	**Caspase:** n = 6 mice **mCherry:** n = 6 mice	Area Under the Curve (AUC) 0-15 seconds post-infusion	Main effect of Condition: p = 0.007, F (3, 20) = 5.354 Multiple comparisons: Casp Saline vs. mCh Sal: p = 0.884 Casp Sal vs. Casp Av Nic: p = 0.051 mCh Sal vs. mCh Av Nic: p = 0.044 Casp Av Nic vs. mCh Av Nic: p = 0.884
Fig S7C NAcLat Casp EC Infusions 2-6	**Casp Sal:** 15.96 ± 34.9 3.61 ± 24.97 -33.59 ± 29.69 6.98 ± 20.31 19.81 ± 14.91 **mCh Sal:** 4.79 ± 17.6 -51.91 ± 29.88 82.44 ± 40.36 -30.26 ± 57.55 33.88 ± 15.22 **Casp Av Nic:** 132.74 ± 77.43 32.29 ± 34.78 -35.22 ± 63.42 -54.75 ± 26.9 -81.97 ± 84.23 **mCh Av Nic:** -116.11 ± 24.96 -149.82 ± 44.05 -83.42 ± 36.6 -118.27 ± 23.89 -121.53 ± 34.59	Two-way Repeated Measures ANOVA with Holm-Šídák's multiple comparisons test	**Caspase:** n = 6 mice **mCherry:** n = 6 mice	Area Under the Curve (AUC) 0-15 seconds post-infusion	Effect of Infusion: p < 0.091, F (4, 80) = 2.078 Effect of Condition: p = 0.018, F (3, 20) = 4.218 Interaction: p = 0.003, F (12, 80) = 2.814 Multiple comparisons: **2nd infusion:** Casp Sal vs. mCh Sal: p = 0.850 Casp Sal vs. Casp Av Nic: p = 0.126 mCh Sal vs. mCh Av Nic: p = 0.126 Casp Av Nic vs. mCh Av Nic: p = 0.0003 **3rd infusion:** Casp Sal vs. mCh Sal: p = 0.573 Casp Sal vs. Casp Av Nic: p = .626 mCh Sal vs. mCh Av Nic: p = 0.339 Casp Av Nic vs. mCh Av Nic: p = 0.015 **4th infusion:** Casp Sal vs. mCh Sal: p = 0.217 Casp Sal vs. Casp Av Nic: p = 0.978 mCh Sal vs. mCh Av Nic: p = 0.034 Casp Av Nic vs. mCh Av Nic: p = 0.782 **5th infusion:** Casp Sal vs. mCh Sal: p = 0.777 Casp Sal vs. Casp Av Nic: p = 0.734 mCh Sal vs. mCh Av Nic: p = 0.521 Casp Av Nic vs. mCh Av Nic: p = 0.734 **6th infusion:** Casp Sal vs. mCh Sal: p = 0.811 Casp Sal vs. Casp Av Nic: p = 0.236 mCh Sal vs. mCh Av Nic: p = 0.055 Casp Av Nic vs. mCh Av Nic: p = 0.752

Data	Mean ± SEM	Statistical Test	N	Outcome measure	p value
Fig S7C NAcLat Casp LC Infusions 1-6	**Casp Sal:** 37.57 ± 60.82 42.56 ± 67.88 57.41 ± 94.88 -11.5 ± 61.84 -30.07 ± 48.94 92.85 ± 61.21 **mCh Sal:** 6.75 ± 74.31 71.46 ± 20.08 -105.07 ± 91.21 403.1 ± 143.19 -50.32 ± 150.81 139.11 ± 35.72 **Casp Av Nic:** 1124.03 ± 144.85 664.87 ± 149.43 557.48 ± 194.68 384.71 ± 279.8 224.75 ± 102.62 270.29 ± 251.04 **mCh Av Nic:** 1708.71 ± 434.05 247.86 ± 77.16 91.64 ± 77.47 216.63 ± 69.48 117.99 ± 52.04 95.1 ± 53.75	Kolmogorov-Smirnov normality test	**Casp:** n = 6 mice **mCh:** n = 6 mice	Area Under the Curve (AUC) 15-60 seconds post-infusion	Casp Sal: p > 0.1000 mCh Sal: p = 0.0078 Casp Av Nic: p > 0.1000 mCh Av Nic: p < 0.0001
Fig S7C NAcLat Casp LC 1st Infusion	**Casp Sal:** 37.57 ± 60.82 **mCh Sal:** 6.75 ± 74.31 **Casp Av:** 1124.03 ± 144.85 **mCh Av:** 1708.71 ± 434.05	Ordinary One-Way ANOVA with Holm-Šídák's multiple comparisons test	**Casp:** n = 6 mice **mCh:** n = 6 mice	Area Under the Curve (AUC) 15-60 seconds post-infusion	Main effect of Condition: p < 0.0001, F (3, 20) = 12.90 <u>Multiple comparisons:</u> Casp Saline vs. mCh Sal: p = 0.927 Casp Sal vs. Casp Av Nic: p = 0.012 mCh Sal vs. mCh Av Nic: p = 0.0003 Casp Av Nic vs. mCh Av Nic: p = 0.176

Data	Mean ± SEM	Statistical Test	N	Outcome measure	p value
Fig S7C NAcLat Casp LC Infusions 2-6	**Casp Sal:** 42.56 ± 67.88 57.41 ± 94.88 -11.5 ± 61.84 -30.07 ± 48.94 92.85 ± 61.21 **mCh Sal:** 71.46 ± 20.08 -105.07 ± 91.21 403.1 ± 143.19 -50.32 ± 150.81 139.11 ± 35.72 **Casp Av Nic:** 664.87 ± 149.43 557.48 ± 194.68 384.71 ± 279.8 224.75 ± 102.62 270.29 ± 251.04 **mCh Av Nic:** 247.86 ± 77.16 91.64 ± 77.47 216.63 ± 69.48 117.99 ± 52.04 95.1 ± 53.75	Two-way Repeated Measures ANOVA with Holm-Šídák's multiple comparisons test	**Casp:** n = 6 mice **mCh:** n = 6 mice	Area Under the Curve (AUC) 15-60 seconds post-infusion	Effect of Infusion: p = 0.030, F (4, 80) = 2.830 Effect of Condition: p = 0.034, F (3, 20) = 3.507 Interaction: p = 0.023, F (12, 80) = 2.143 <u>Multiple comparisons:</u> **2nd infusion:** Casp Sal vs. mCh Sal: p = 0.870 Casp Sal vs. Casp Av Nic: p = 0.004 mCh Sal vs. mCh Av Nic: p = 0.574 Casp Av Nic vs. mCh Av Nic: p = 0.077 **3rd infusion:** Casp Sal vs. mCh Sal: p = 0.607 Casp Sal vs. Casp Av Nic: p = 0.028 mCh Sal vs. mCh Av Nic: p = 0.607 Casp Av Nic vs. mCh Av Nic: p = 0.038 **4th infusion:** Casp Sal vs. mCh Sal: p = 0.118 Casp Sal vs. Casp Av Nic: p = 0.128 mCh Sal vs. mCh Av Nic: p = 0.647 Casp Av Nic vs. mCh Av Nic: p = 0.647 **5th infusion:** Casp Sal vs. mCh Sal: p = 0.909 Casp Sal vs. Casp Av Nic: p = 0.561 mCh Sal vs. mCh Av Nic: p = 0.813 Casp Av Nic vs. mCh Av Nic: p = 0.813 **6th infusion:** Casp Sal vs. mCh Sal: p = 0.991 Casp Sal vs. Casp Av Nic: p = 0.899 mCh Sal vs. mCh Av Nic: p = 0.991 Casp Av Nic vs. mCh Av Nic: p = 0.899

Data	Mean ± SEM	Statistical Test	N	Outcome measure	p value
Fig S7D NAcMed Casp EC Infusions 1-6	**Casp Sal:** 50.43 ± 14.15 48.33 ± 30.58 36.17 ± 25.16 14.46 ± 38.04 24.94 ± 22.12 34.77 ± 18.2 **mCh Sal:** 78.75 ± 50.08 103.55 ± 53.87 33.26 ± 37.39 49.95 ± 39.57 25.01 ± 40.54 26.43 ± 48.6 **Casp Av Nic:** 764.63 ± 369.41 148.17 ± 71.77 -16.98 ± 34.76 -57.96 ± 53.05 -1.74 ± 52.91 -88.43 ± 52.57 **mCh Av Nic:** 738.41 ± 141.02 133.31 ± 46.56 80.32 ± 92.01 21.8 ± 63.18 90.32 ± 78.73 137.32 ± 52.09	Kolmogorov-Smirnov normality test	**Caspase:** n = 6 mice, **mCherry:** n = 5 mice	Area Under the Curve (AUC) 0-15 seconds post-infusion	Casp Sal: p > 0.1000 mCh Sal: p > 0.1000 Casp Av Nic: p < 0.0001 mCh Av Nic: p < 0.0001
Fig S7D NAcMed Casp EC 1st Infusion	**Casp Sal:** 50.43 ± 14.15 **mCh Sal:** 78.75 ± 50.08 **Casp Av:** 764.63 ± 369.41 **mCh Av:** 738.41 ± 141.02	Ordinary One-Way ANOVA with Holm-Šídák's multiple comparisons test	**Caspase:** n = 6 mice, **mCherry:** n = 5 mice	Area Under the Curve (AUC) 0-15 seconds post-infusion	Main effect of Condition: p = 0.039, F (3, 18) = 3.454 <u>Multiple comparisons:</u> Casp Saline vs. mCh Sal: p = 0.995 Casp Sal vs. Casp Av Nic: p = 0.137 mCh Sal vs. mCh Av Nic: p = 0.169 Casp Av Nic vs. mCh Av Nic: p = 0.995

Data	Mean ± SEM	Statistical Test	N	Outcome measure	p value
Fig S7D NAcMed Casp EC Infusions 2-6	**Casp Sal:** 48.33 ± 30.58 36.17 ± 25.16 14.46 ± 38.04 24.94 ± 22.12 34.77 ± 18.2 **mCh Sal:** 103.55 ± 53.87 33.26 ± 37.39 49.95 ± 39.57 25.01 ± 40.54 26.43 ± 48.6 **Casp Av Nic:** 148.17 ± 71.77 -16.98 ± 34.76 -57.96 ± 53.05 -1.74 ± 52.91 -88.43 ± 52.57 **mCh Av Nic:** 133.31 ± 46.56 80.32 ± 92.01 21.8 ± 63.18 90.32 ± 78.73 137.32 ± 52.09	Two-way Repeated Measures ANOVA with Holm-Šídák's multiple comparisons test	**Caspase:** n = 6 mice, **mCherry:** n = 5 mice	Area Under the Curve (AUC) 0-15 seconds post-infusion	Effect of Infusion: p = 0.014, F (4, 72) = 1.136 Effect of Condition: p = 0.256, F (3, 18) = 1.471 Interaction: p = 0.346, F (12, 72) = 1.136 No interaction, post-hoc test not justified.
Fig S7D NAcMed Casp LC Infusions 1-6	**Casp Sal:** 93.58 ± 65.34 25.45 ± 95.35 114.19 ± 80.61 -46.72 ± 78.96 34.65 ± 90.31 87.6 ± 28.64 **mCh Sal:** 172.98 ± 44.34 236.22 ± 158.74 -0.56 ± 153.91 252.58 ± 197.19 203.29 ± 73.19 68.75 ± 105.46 **Casp Av Nic:** 2171.6 ± 695.85 463.3 ± 72.31 287.23 ± 41.2 205.74 ± 136.91 223.6 ± 197.81 7.86 ± 119.37 **mCh Av Nic:** 6021.43 ± 1893.59 2234.56 ± 652.6 1147.31 ± 90 831 ± 228.64 760.38 ± 239.88 947.98 ± 184.82	Kolmogorov-Smirnov normality test	**Caspase:** n = 6 mice, **mCherry:** n = 5 mice	Area Under the Curve (AUC) 15-60 seconds post-infusion	Casp Sal: p > 0.1000 mCh Sal: p > 0.1000 Casp Av Nic: p < 0.0001 mCh Av Nic: p < 0.0001

Data	Mean ± SEM	Statistical Test	N	Outcome measure	p value
Fig S7D NAcMed Casp LC 1st Infusion	**Casp Sal:** 93.58 ± 65.34 **mCh Sal:** 172.98 ± 44.34 **Casp Av:** 2171.6 ± 695.85 **mCh Av:** 6021.43 ± 1893.59	Ordinary One-Way ANOVA with Holm-Šídák's multiple comparisons test	**Caspase:** n = 6 mice, **mCherry:** n = 5 mice	Area Under the Curve (AUC) 15-60 seconds post-infusion	Main effect of Condition: p = 0.0011, F (3, 18) = 8.299 Multiple comparisons: Casp Saline vs. mCh Sal: p = 0.953 Casp Sal vs. Casp Av Nic: p = 0.313 mCh Sal vs. mCh Av Nic: p = 0.003 Casp Av Nic vs. mCh Av Nic: p = 0.038
Fig S7D NAcMed Casp LC Infusions 2-6	**Casp Sal:** 25.45 ± 95.35 114.19 ± 80.61 -46.72 ± 78.96 34.65 ± 90.31 87.6 ± 28.64 **mCh Sal:** 236.22 ± 158.74 -0.56 ± 153.91 252.58 ± 197.19 203.29 ± 73.19 68.75 ± 105.46 **Casp Av Nic:** 463.3 ± 72.31 287.23 ± 41.2 205.74 ± 136.91 223.6 ± 197.81 7.86 ± 119.37 **mCh Av Nic:** 2234.56 ± 652.6 1147.31 ± 90 831 ± 228.64 760.38 ± 239.88 947.98 ± 184.82	Two-way Repeated Measures ANOVA with Holm-Šídák's multiple comparisons test	**Caspase:** n = 6 mice, **mCherry:** n = 5 mice	Area Under the Curve (AUC) 15-60 seconds post-infusion	Effect of Infusion: p = 0.0005, F (4, 72) = 5.641 Effect of Condition: p < 0.0001, F (3, 18) = 19.30 Interaction: p = 0.001, F (12, 72) = 3.179 Multiple comparisons: **2nd infusion:** Casp Sal vs. mCh Sal: p = 0.626 Casp Sal vs. Casp Av Nic: p = 0.231 mCh Sal vs. mCh Av Nic: p < 0.0001 Casp Av Nic vs. mCh Av Nic: p < 0.0001 **3rd infusion:** Casp Sal vs. mCh Sal: p = 0.741 Casp Sal vs. Casp Av Nic: p = 0.741 mCh Sal vs. mCh Av Nic: p = 0.0004 Casp Av Nic vs. mCh Av Nic: p = 0.006 **4th infusion:** Casp Sal vs. mCh Sal: p = 0.591 Casp Sal vs. Casp Av Nic: p = 0.591 mCh Sal vs. mCh Av Nic: p = 0.143 Casp Av Nic vs. mCh Av Nic: p = 0.093 **5th infusion:** Casp Sal vs. mCh Sal: p = 0.836 Casp Sal vs. Casp Av Nic: p = 0.836 mCh Sal vs. mCh Av Nic: p = 0.201 Casp Av Nic vs. mCh Av Nic: p = 0.201 **6th infusion:** Casp Sal vs. mCh Sal: p = 0.985 Casp Sal vs. Casp Av Nic: p = 0.985 mCh Sal vs. mCh Av Nic: p = 0.008 Casp Av Nic vs. mCh Av Nic: p = 0.003
Fig S7F LDT GABA inhibition Real-time Place Preference	**eYFP:** 459.4 ± 62.59 **eNpHR:** 420.1 ± 77.64	Unpaired t-test	**eYFP:** n = 4 mice **eNpHR:** n = 5 mice	Time spent in light-paired chamber (s)	p = 0.72, two-tailed, t=0.3785, df=7

Data	Mean ± SEM	Statistical Test	N	Outcome measure	p value
Fig S7G LDT GABA inhibition Open Field Test	**Laser off 1:** eYFP: 3.264 ± 0.613 **eNpHR**: 5.5052 ± 0.625 **Laser on:** eYFP: 2.650 ± 0.274 **eNpHR**: 3.993 ± 0.609 **Laser off 2:** eYFP: 2.484 ± 0.517 **eNpHR**: 3.732 ± 0.421	Two-way Repeated Measures ANOVA with Holm-Šídák's multiple comparisons test	**eYFP:** n = 4 mice **eNpHR:** n = 4 mice	Velocity (cm/s)	Effect of Time: p = 0.007, F (2,12) = 7.567 Effect of Virus: p = 0.07, F (1,6) = 4.800 Interaction: p = 0.61, F (2,12) = 0.5098 No interaction, post-hoc test not justified.

CHAPTER 3: A NOVEL NEURAL PATHWAY FOR NEUROTENSIN MEDIATED REGULATION OF HEDONIC FEEDING BEHAVIOR AND OBESITY.

This chapter is a manuscript in preparation for submission and summarizes a joint project I conducted with Neta Gazit Shimoni. Many others contributed to this work, including: Charlotte Seng, Yihan Jin, Ignas Cerniauskus, Tamas Lukacsovich, Hongbin Yang, Jeroen P H Verharen, Christine Liu, Eric Hu, Lilly W Tang, Jonathan Read, Byungkook Lim, Lin Tian, Csaba Földy, and Stephan Lammel.

INTRODUCTION

Ventral tegmental area dopamine neurons (VTA DA) and their inputs are critical for generating motivated behavior, including feeding (Ferrario, et al., 2016; Wise, 2004). The lateral shell of the nucleus accumbens (NAcLat) is one of the largest inputs to the VTA and a key circuit node of the brain's reward system (Beier et al., 2015; Watabe-Uchida et al., 2012), yet few studies have investigated the contribution of this region to motivated behavior. Intriguingly, the NAc expresses many feeding-related neuropeptides, including neurotensin (NTS), that can co-release with neurotransmitters to influence downstream activity in VTA DA neurons, where NTS receptors are expressed (Tschumi and Beckstead, 2019; Woodworth et al., 2017a, 2018). While known changes to motivated feeding behavior occur in diet-induced obesity in humans and rodents (Davis et al., 2008; Donofry et al., 2020; Finger et al., 2012; Harb & Almeida, 2014; la Fleur et al., 2007), the extent to which this alters brain circuits that promote motivation is unknown.

Here, we employ a novel neurotensin sensor, patch-seq, and combined optogenetic behavior and electrophysiology to demonstrate that activity in NAcLat→VTA releases NTS to drive motivated feeding behavior but is altered in high fat diet-induced (HFD) obese mice. Using a custom viral strategy to target NAcLat→VTA we find that overexpressing NTS in this pathway partially restores motivated behavior and attenuates weight gain on HFD. Our work demonstrates a novel role for NAcLat→VTA to promote motivated feeding behavior as well as a surprising orexigenic effect of NTS release in the VTA, highlighting that circuit-specific manipulations of NTS are critical in order to understand and harness the translational potential of NTS in the treatment of obesity.

RESULTS

NAcLat→VTA activity promotes motivated feeding behavior

To assess baseline motivation to consume different food types, we recorded the amount of food consumed by mice given 15 minutes access to a chamber containing a cup of a single food type. On separate days, mice were presented with different foods. Mice consume greater amounts of calorically dense, palatable food, such as butter, chocolate, peanut butter, and jelly, compared to regular chow (Fig. 1a,b). Because ventral tegmental area dopamine neurons (VTA DA) are critical for generating motivated behavior such as feeding and previous work has defined a large anatomical projection from nucleus accumbens lateral shell (NAcLat) to the VTA (Beier et al., 2015; Watabe-Uchida et al., 2012), we confirmed that fluorescence from D1+ neurons in

NAcLat were located in the VTA and retrograde tracers injected into the VTA labelled cell bodies in the NAcLat and overlap with D1+ cells (Supplementary Fig.1a-d) and next, sought to determine if activating this pathway can modulate feeding behavior. To test this, we injected AAV-hSyn-ChR2 (ChR2) or AAV-hSyn-eYFP (eYFP) in the NAcLat and implanted an optic fiber above the VTA (Fig. 1c, Supplementary Fig. 2a). Six weeks later, mice were placed in a chamber with access to a cup of a single food type for 1 hour, divided into four 15 minute trials. During each trial, mice were provided a new cup of the same food type, and the previous cup was removed. During Trial 3, we delivered blue light stimulation through the implanted optic fiber. We found that ChR2 stimulation of NAcLat→VTA specifically increased consumption of palatable foods (i.e., jelly, butter, peanut butter, and chocolate), but not less palatable foods such as standard chow or quinine-adulterated butter (Fig. 1d,e). A 24hr fast elevated standard chow consumption compared to the same mice when sated, but light stimulation in Trial 3 did not alter chow consumption compared to control mice (Fig. 1f). In separate experiments, light stimulation increased Trial 1 hedonic feeding and low frequency light stimulation was not able to alter Trial 3 feeding behavior (Supplementary Fig. 2b,c). Weights of ChR2 and eYFP mice did not differ before or after the series of feeding experiments (Supplementary Fig. 2d). Additionally, we found light stimulation in ChR2 mice implanted with an optic fiber above NAcLat did not increase palatable food consumption in Trial 3 (Supplementary Fig. 2e), suggesting that projection-specific stimulation is necessary to increase hedonic feeding. Collectively, these results show that optogenetic stimulation of NAcLat→VTA specifically increases motivation to consume palatable food.

Optogenetic stimulation artificially alters neural activity and therefore does not demonstrate whether naturally occurring neural activity in NAcLat→VTA neurons correlates with hedonic food consumption. To address this limitation, we performed *in vivo* electrophysiological recordings from optogenetically-identified VTA-projecting NAcLat cells in mice that were given free access to different food types. To do this, we injected mice with a retrograde-transported virus expressing Cre-recombinase (EIAV-CAG-Cre) into the VTA and Cre-dependent ChR2 (AAV-DIO-ChR2) into the NAcLat. Six weeks later, we implanted a custom-made drivable optoelectrode (optrode) above the NAcLat and monitored the activity of units in mice during time spent in a chamber with food cups fitted with a piezo-touch sensor to record feeding times (Fig. 1g, Supplementary Fig. 3a,b). Mice were allowed 15 minutes free access to chow, followed by 15 minutes free access to jelly. At the end of the recording session in the absence of food, we delivered low frequency light stimulation to identify ChR2 expressing units (Supplementary Fig. 3c). We analyzed well-isolated units and calculated light response probability and latency for each unit to identify projection-defined NAcLat cells (i.e., opto-tagged cells) (Fig. 1h,i and Supplementary Fig. 3d-h). Opto-tagged unit firing rate strongly correlated with jelly sensor rate, but not chow sensor rate (Fig. 1j,k). During bouts of food consumption, unit average firing rate was higher during jelly consumption compared to before or after bout, but no change was observed during bouts of chow consumption (Fig. 1l). K-means clustering of all tagged and non-tagged unit firing rate and pulse width revealed three main clusters with varying responsiveness to chow and jelly consumption. Most tagged units were found in cluster B, which grouped units that only increase firing to jelly consumption. Clusters that primarily contain non-tagged units, additionally increase firing during chow consumption (Supplementary Fig. 4). These results together suggest that activity of NAcLat→VTA cells correlates with and drives hedonic feeding and is unrelated to non-hedonic food consumption.

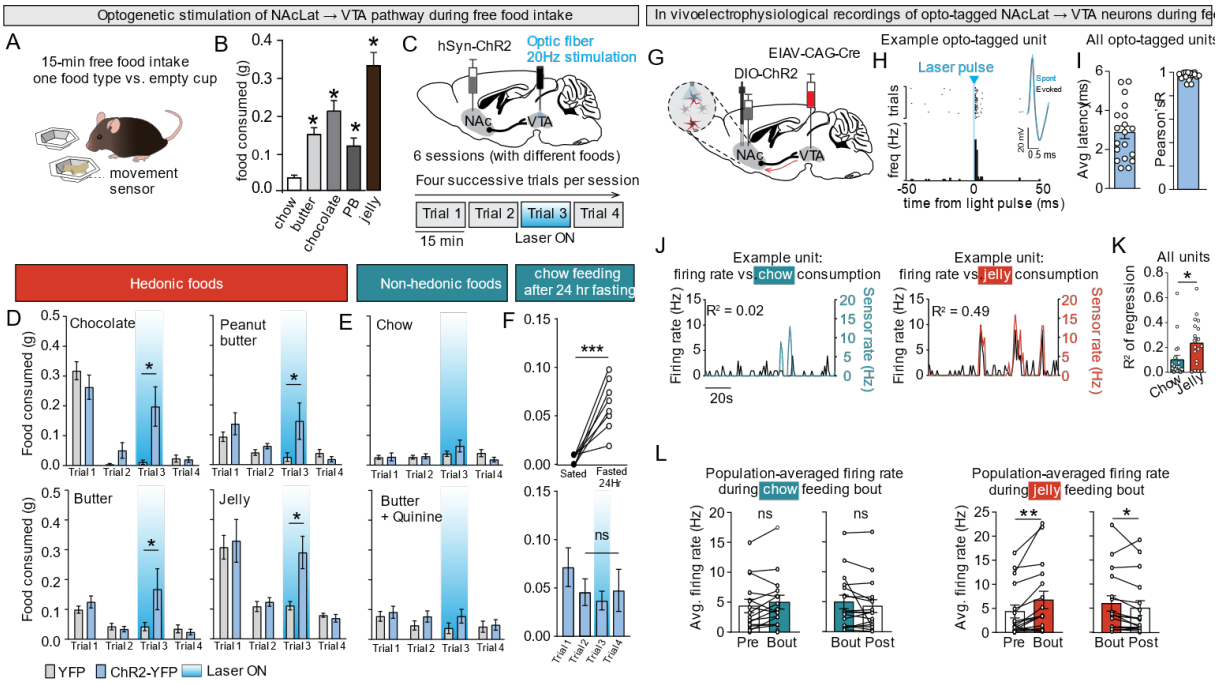

Figure 1. Activity of NAcLat→VTA pathway promotes hedonic feeding.

(A) Mice were exposed to different food types for 15 min.

(B) Mice consumed large amounts of palatable foods (butter, chocolate, peanut butter (PB), jelly) but not chow (1way RM ANOVA, n=9 mice, $p<0.05$).

(C) Experimental design. Mice were presented with a specific food type over 4 consecutive 15 min trials. Light stimulation (20Hz, 5ms) during trial #3.

(D) Light stimulation of NAcLat→VTA evokes consumption of hedonic foods (chocolate, peanut butter, butter and jelly ($n_{ChR2}=9$, $n_{eYFP}=9$)).

(E) Top: No effect of NAcLat→VTA pathway stimulation on chow consumption ($n_{ChR2}=10$, $n_{eYFP}=9$) Bottom: same but for butter with quinine added ($n_{ChR2}=7$, $n_{eYFP}=7$ mice).

(F) Top: Baseline chow levels were higher after 24hrs food restriction ($n_{control}=7$, $n_{FR}=5$ mice). Bottom: Light stimulation of NAcLat→VTA does not increase consumption of chow despite food restriction (n=6 mice).

(G) Experimental design for *in-vivo* electrophysiology.

(H) Raster plot and corresponding histogram showing the latency of light-evoked spikes relative to light pulses (5 ms). Inset: Spontaneous (black) and evoked (turquoise) mean action potential waveforms for NAcLat→VTA neurons.

(I) Left: Mean response latency to laser stimulation. Right: correlation between evoked and spontaneous spike waveforms.

(J) Left: Correlation between firing rate and food sensor activation rate during a 15 min trial with chow (turquoise) or jelly (red) in one example unit.

(K) Average unit activity correlates with jelly but not chow consumption (*$p<0.05$, unpaired t-test).

(L) Activity of NAcLat→VTA cells increased during feeding bout onset and decreased after feeding bout termination during jelly (red) but not chow (turquoise) consumption (paired t-tests, *$p<0.05$, **$p<0.01$) (n=19 tagged units analyzed in all graphs). Statistical analysis: [D, E] 2way

RM ANOVA with multiple comparisons. [B,F_{Bottom}] 1way RM ANOVA with multiple comparisons [$F_{Top,}$ L]. paired t-test. [K] unpaired t-test.

NTS release from NAcLat→VTA pathway mediates hedonic feeding.

Prior work in our lab has shown that NAcLat neurons are GABAergic and form synapses onto VTA GABA neurons to disinhibit VTA DA neurons and promote reward-related behavior. However, beyond action via fast neurotransmitters, many studies report that feeding can be regulated by peripherally and centrally active peptide release in the VTA (Ferrario et al., 2016) and the NAc is known to express many feeding-related peptides (Castro and Bruchas, 2019). Therefore, we explored whether NAcLat→VTA is capable of driving feeding behavior via parallel peptide release. To do this, we implemented single-cell patch-sequencing where mice were injected with fluorescent retrobeads in the VTA to label VTA-projecting neurons in NAcLat. We recorded from beads-labelled NAcLat cells and collected intrinsic membrane properties and responses to current injection to confirm cell health before extracting cell cytosol for RNA sequencing (Supplementary Fig. 5a). Analysis of RNA expression confirmed known high expression of dynorphin but revealed that the neuropeptide neurotensin (NTS) is highly expressed in the NAcLat→VTA pathway compared to other feeding-related peptides, and was detected in 95% of collected NAcLat→VTA cells (Fig. 2a). Additional anatomical studies verified clear overlap between NTS and NAcLat→VTA labelled cells in NAcLat (Supplementary Fig. 5b). We found greater co-localization of NTS with dopamine receptor 1 expressing cells in NAcLat compared to NAcMed (Supplementary Fig. 5c,d). NAcLat NTS cells expressing YFP target the VTA where NTS receptor 1 (NTSR1) is expressed on the majority of tyrosine hydroxylase (TH+) cells in the VTA (Supplementary Fig. 5e,f). Together, these findings led us to hypothesize that NTS is released by the NAcLat→VTA pathway and influences VTA DA cell firing and hedonic feeding behavior.

To probe whether NAcLat terminals in the VTA can release NTS, we employed ntsLight1.1, a novel GPCR fluorescent sensor that robustly increases fluorescence in the presence of NTS in cultured cells in a concentration-dependent manner (Supplementary Fig 6a). Mice were injected with ntsLight1.1 into the VTA and AAV-hSyn-Chrimson-tdTomato (Chrimson) into the NAcLat and a separate group of mice were infused with only ntsLight1.1 into the VTA (Sensor only). Six weeks later, we recorded ntsLight1.1 fluorescence from VTA brain slices during light stimulation (Supplementary Fig. 6b-d). Red light stimulation increased NtsLight fluorescence in VTA slices of Chrimson mice, but not in Sensor only mice (Fig. 2b). Chrimson induced ntsLight fluorescence was greater in lateral VTA compared to medial VTA and not detected in regions dorsal to VTA where NAcLat terminals are not found in anatomical tracing studies (Supplementary Fig. 6e). Control experiments verified that delivering blue light or red light stimulation in isolation is insufficient to increase NtsLight fluorescence (Supplementary Fig. 6f). Finally, to rule out the potential confounding contribution of tdTomato fluorescence on recorded NtsLight fluorescence, we found that stimulating VTA slices with green light, which excites tdTomato more and Chrimson less compared to red light, reduced the NtsLight fluorescence in the VTA as expected (Supplementary Fig. 6g). Together, these experiments provide the first evidence that NTS originating from NAcLat can be released in the VTA.

To assess the function of NTS in the VTA, we found that bath application of NTS increased action potential firing of VTA DA neurons that project to NAcLat (VTA DA→NAcLat: VTA DA neurons that project to NAcLat also reciprocally receive inputs from NAcLat (Yang et al., 2018)), but not VTA GABA neurons (Supplementary Fig. 7a,b). This finding corresponds to previous work that NTS receptors are mainly expressed on DA neurons in the VTA (Opland et al., 2013; Woodworth et al., 2017b, 2017c). Next, in whole-cell patch clamp recordings of VTA DA neurons we found that ChR2 stimulation of NAcLat terminals in the VTA increased firing of VTA DA→NAcLat , but not in VTA slices that were bathed in solution containing an NTS receptor antagonist (SR142948) (Fig. 2c). Finally, in mice placed in a chamber with free access to jelly (same assay as in Fig. 2) we found that intra-VTA infusion of SR142948 prevented an increase in jelly consumption from optogenetically stimulating NAcLat→VTA compared to mice that received an intra-VTA infusion of saline (Fig. 2d and Supplementary Fig. 7c). Importantly, SR142948 alone did not alter firing of VTA DA neurons in slice or baseline feeding behavior compared to saline infusion. Our results indicate that NTS receptor availability is necessary for NAcLat stimulation to drive firing of VTA DA neurons and increase hedonic feeding.

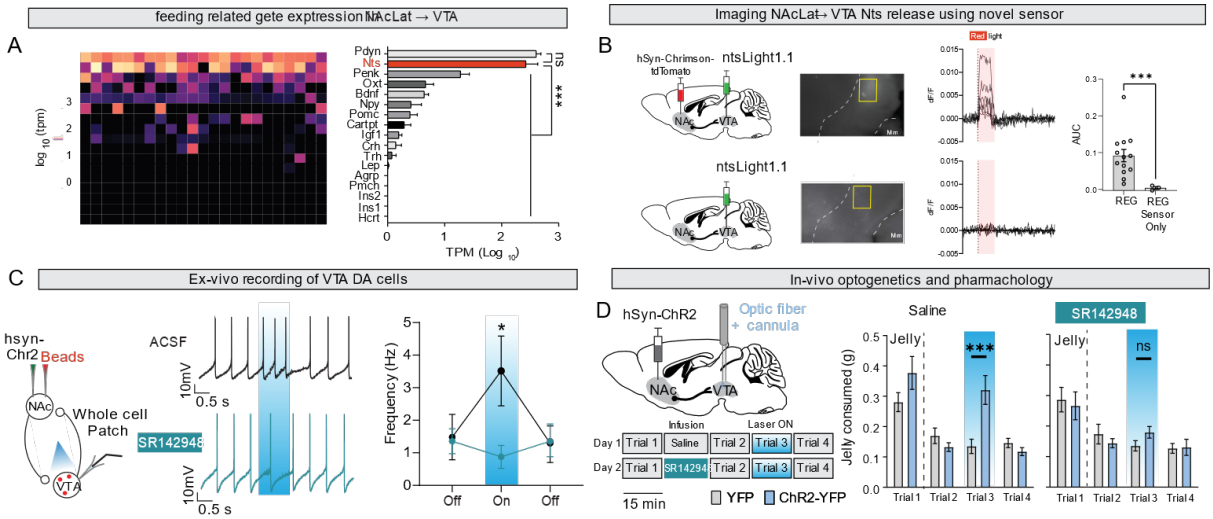

Figure 2. Neurotensin release in NAcLat→VTA drives activation of VTA DA and drives hedonic feeding.

(A) Single cell patch sequencing of NAcLat→VTA neurons. Left: Each column displays relative expression of feeding-related genes for an individual cell. Right: Neurotensin (Nts, red) is strongly expressed compared to other feeding related genes, at a similar level to dynorphin (Pdyn), a marker for direct pathway neurons (1way ANOVA with multiple comparisons, n = 21 NAcLat→VTA cells, ***p<0.001).

(B) Left: ntsLight was expressed in VTA with (top) or without (bottom) Chrimson expression in NAcLat. Middle: Traces from sample lateral VTA ROIs (left) reveal that light stimulation of NAcLat→VTA produces an increase in ntsLight fluorescence from Chrimson-expressing mice compared to mice without Chrimson (N=5 mice, $n_{Chrimson+}$=13 slices; N=1 mouse, $n_{Chrimson-}$=3 slices; unpaired t-test, ***p<0.001).

(C) Left: Experimental design for whole cell patch clamp experiment. Middle: Example recordings of spontaneous firing from retrobead-labeled VTA DA cells in normal ACSF (black) or with added NTS receptor antagonist (SR142948, 1μM, turquoise). Right: Optogenetic

stimulation of NAcLat terminals in VTA increases firing of NAcLat-projecting DA neurons in ACSF but not in the presence of SR142948 (n_{ACSF} =16 cells, $n_{SR142948}$=21 cells; *p<0.05, 2way RM ANOVA with multiple comparisons).
(D) Left: Experimental design for *in vivo* pharmacology / optogenetics experiment. Right: Optogenetic stimulation increases jelly consumption during laser stimulation in trial #3 after saline infusion, but not after SR142948 infusion (500nl, 6mM, n_{ChR2}=7, n_{eYFP}=10 mice, ***p<0.001, ns: not significant; 2way RM ANOVA with multiple comparisons).

NAcLat→VTA is altered by food environment.

Hedonic food consumption is complexly related to motivation, weight, and obesity. While overconsumption of hedonic food leads to weight gain and promotes obesity (Hariri and Thibault, 2010; Sampey et al., 2011), continuous access to hedonic foods results in a state of reduced motivation characterized by lower mobility (Sharma et al., 2012), decreased drive to consume hedonic food in an acute timeframe (Altherr et al., 2021; Arcego et al., 2020; Beutler et al., 2020; Espinosa-Carrasco et al., 2018; Johnson and Kenny, 2010), and reduced motivation to work for food reward (Cagniard et al., 2006; Hanlon et al., 2004; Salamone et al., 2009; Taylor and Robbins, 1986; Wise et al., 1978). It is therefore conceivable that brain circuits that regulate feeding and motivation, like NAcLat→VTA are sensitive to changes in the food environment. To test this possibility, mice were placed on a high fat choice diet (HFD) where both regular (4% fat) and hedonic high-fat chow (60% fat) were available in the home cage (Fig. 3a). REG diet mice reliably consume high amounts of HFD in an acute setting, and optogenetic activation of NAcLat→VTA increased consumption of HFD (Supplementary Fig. 8a). Mice placed on HFD rapidly gained weight compared to mice on regular diet (REG) (Fig. 3b). When provided 15 min free access to different types of food, HFD mice consumed less hedonic food compared to REG mice (Fig. 3c). In a separate group of mice fed an obesogenic cafeteria-style diet, we observed the same reduction in hedonic food consumption compared to REG (Supplementary Fig. 9) which has been shown in prior studies (Espinosa-Carrasco et al., 2018; Johnson and Kenny, 2010) (Fig. 3c) Notably, food environment, rather than body weight alone, drives changes in acute hedonic feeding behavior, since obese mice taken off HFD return to REG mice levels of hedonic feeding despite significantly greater body weight (Supplementary Fig. 8b).

Next, we examined if the reduced motivation to consume hedonic foods on HFD is reflected by changes in NAcLat→VTA activity. We performed patch clamp recordings in beads-labelled NAcLat neurons that project to VTA from REG and HFD mice and found that HFD cells were less excitable at high current injections but did not differ in intrinsic membrane properties (Supplementary Fig. 10). To assess whether NAcLat→VTA activity during food consumption is altered by HFD, we collected *in vivo* electrophysiological recordings of opto-tagged units from HFD mice allowed free access to different types of food (Fig. 3d,e and Supplementary Fig. 11). We found that opto-tagged HFD unit firing displayed low correlation with chow or jelly sensor rate, and this correlation was significantly less compared to REG units (Fig. 3f-h). HFD unit activity did not change at onset or conclusion of feeding bouts of chow or jelly (Fig. i). Notably, K-means clustering of all HFD units produced three clusters, and most tagged units belonged to cluster B (76%) (Supplementary Fig. 12), similarly to the case of REG units (Supplementary 4). However, the activity of the units in all three clusters from HFD mice, was no longer correlated with feeding of either jelly or chow.

Although we found that activity of NAcLat→VTA uncoupled from hedonic food consumption, we wanted to test whether manipulation of NAcLat→VTA in HFD could influence downstream activity in the VTA and feeding behavior as on REG diet. Surprisingly, in brain slices, optogenetic activation of NAcLat→VTA no longer increased firing in VTA DA→NAcLat neurons and no change in intrinsic excitability or membrane properties was measured (Fig. 3j and Supplementary Fig. 14). Similarly during behavior, optogenetic activation no longer increased hedonic feeding in HFD mice when sated or when starved for 24 hours (Fig. 3k and Supplementary Fig. 13a-c), even though light stimulation induced real time place preference (Supplementary Fig. 13e). Once again, food environment was more influential than body weight on hedonic feeding, since (i) when HFD mice were placed on REG diet for several weeks, optogenetic stimulation increased hedonic feeding and (ii) the optogenetic-driven feeding in REG mice was lost after just one week of HFD, prior to significant weight gain (Fig. 3k and Supplementary Fig. 13d,f).

Our findings reveal that the relationship of NAcLat→VTA activity on hedonic feeding is sensitive to food environment, but whether this is specific to NAcLat→VTA or mirrored by other feeding related VTA-projecting brain circuits was unknown. The hypothalamus senses metabolic signals of hunger, satiety, and fat accumulation to reciprocally modulate food consumption and sends inputs to the VTA (Fulton et al., 2006; Lam et al., 2005; Morton et al., 2006; Schwartz et al., 2000). Replicating prior research (Jennings et al., 2015; Nieh et al., 2015, 2016), we found that optogenetically stimulating lateral hypothalamus (LH) inputs to the VTA, increased both jelly and chow intake in REG mice (Supplementary Fig. 15a-d). However, although innate motivation to consume jelly was reduced on HFD (see Trial 1), activation of LH→VTA continued to stimulate consumption of jelly on HFD as well as when mice returned to REG diet. (Supplementary Fig. 15e,f). Thus, we find that the specificity of NAcLat→VTA activity to hedonic food consumption and sensitivity to food environment is a distinctive feature compared to LH→VTA.

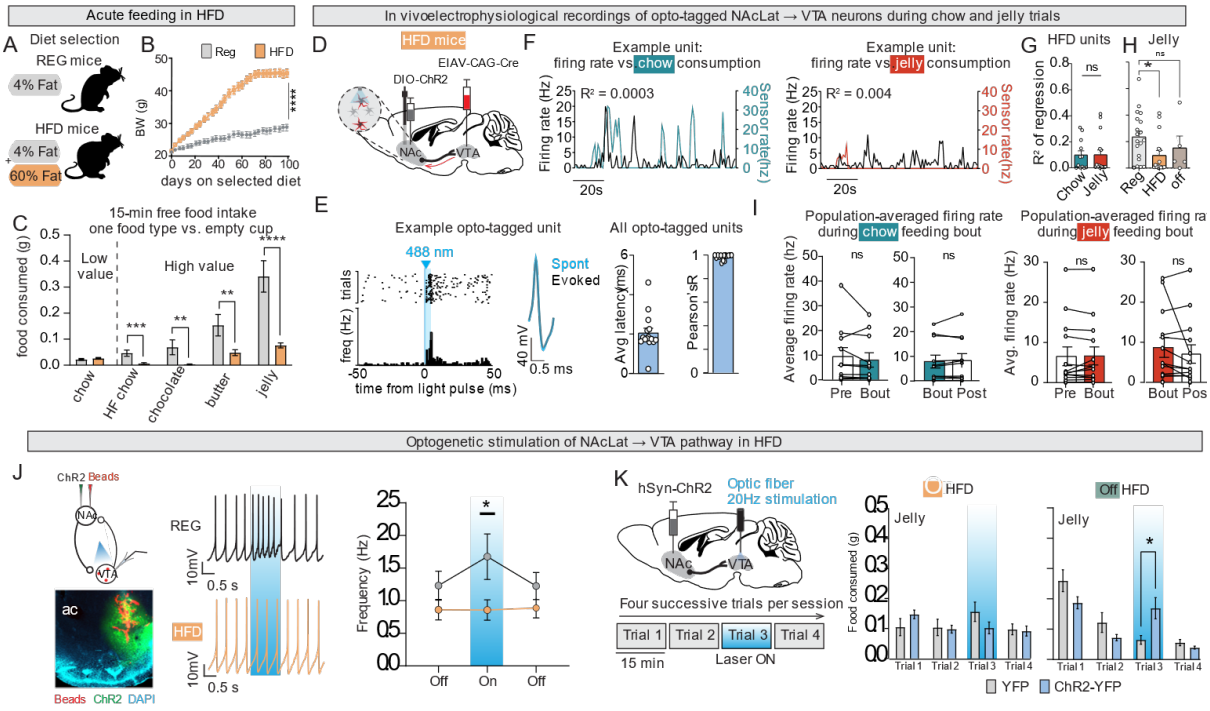

Figure 3. High fat diet (HFD) unlinks NAcLat→VTA activity from hedonic feeding.

(A) Mice were placed on standard chow (4% fat, REG) or on a high-fat choice diet (60% fat and 4% fat, HFD) for > 4 weeks.

(B) HFD mice gain more weight compared to REG mice (2way RM ANOVA, n_{REG}=9, n_{HFD}=19 mice).

(C) HFD mice consumed similar amounts of chow, but less hedonic foods compared to REG mice during 15 minutes of free access (n_{REG}=11, n_{HFD}=19, **p<0.01, ***p<0.001, ****p<0.0001, unpaired t-test for each food type).

(D) Experimental design for in-vivo electrophysiology recorded in HFD mice.

(E) Left: Raster plot and histogram showing the latency of light-evoked spikes relative to light pulses (5 ms). Middle: Spontaneous (black) and evoked (turquoise) mean action potential waveforms for NAcLat→VTA neurons. Right: Mean response latency to laser stimulation (left) and correlation between evoked and spontaneous spike waveforms (right).

(F) Correlation between example opto-tagged unit firing rate and food sensor activation rate during a 15 min trial with chow (turquoise) or jelly (red).

(G) Unit activity weakly correlates with food consumption and does not differ between jelly (red) or chow (turquoise) on HFD (unpaired t-test, n_{Jelly}=16, n_{Chow}=12, ns).

(H) Correlation between unit activity and jelly feeding is higher in REG then HFD (n_{REG}=19, n_{HFD}=16, unpaired t-test, *p<0.05).

(I) Unit average firing rate did not differ between onset or offset of feeding bouts compared to during feeding bout for jelly (red) and chow (turquoise). (paired t-test for each food type, n_{Jelly}=16, n_{Chow}=12, ns).

(J) Left: Experimental design for whole-cell patch clamp recording. Middle: Example recordings of spontaneous firing from retrobead-labeled VTA DA cells from REG (black) and HFD (orange) mice. Right: Optogenetic stimulation of NAcLat terminals in VTA increase firing of NAcLat-projecting DA neurons in REG but not HFD mice (REG: n=16 cells, HFD: n=21 cells; *p<0.05, 2way RM ANOVA with multiple comparisons).

(K) Left: Experiment design. Optogenetic stimulation of NAcLat→VTA during trial #3 does not increase hedonic feeding in HFD mice (middle), but does increase hedonic feeding in same mice taken off HFD for 3 weeks (right) (n_{eYFP} = 9 mice, n_{ChR2} = 6 mice; ns – not significant, *p<0.05, 2way RM ANOVA with multiple comparisons).

Reduced NAcLat→VTA NTS release in HFD can be countered to restore motivation and hedonic feeding.

Because optogenetic stimulation in HFD failed to reinstate an increase in VTA DA firing and hedonic feeding, which in REG mice is dependent on NTS receptor availability (Fig. 2), we next pursued whether NTS signaling in NAcLat→VTA is altered in HFD. To test this, we recorded ntsLight in *ex vivo* VTA brain slices from HFD mice and found that optogenetic stimulation of NAcLat terminals resulted in significantly less ntsLight fluorescence in HFD mice compared to REG mice (Fig. 4a-d and Supplementary Fig. 17a). Although measures of RNA expression imperfectly report amount of translation, we did not detect differences in NTS RNA expression between REG and HFD mice using fluorescent *in situ* hybridization and projection-specific patch-sequencing, which may suggest NTS release probability is reduced in HFD rather than amount of NTS (Supplementary Fig. 18). In addition, we found no differences between REG and HFD mice in NTSR1 expression on TH+ neurons in the VTA and action potential firing of VTA DA →NAcLat neurons in response to bath application of NTS (Supplementary Fig. 16), which led us to hypothesize that restoring NTS in NAcLat→VTA may reverse changes in HFD.

To test this, we used a custom virus to selectively overexpress NTS (NTS-OE) only in NAcLat cells that project to the VTA in mice on HFD (Fig. 4e and Supplementary Fig. 19a). NTS-OE restored hedonic feeding during free access to jelly and when induced by optogenetic stimulation in HFD mice (Fig. 4f,h). Moreover, HFD NTS-OE mice showed improved open field locomotion compared to HFD mice, without differences in body temperature (Fig. 4i and Supplementary Fig. 19b). Finally, we observed a significant attenuation in weight gain in NTS-OE HFD mice compared to control HFD mice (Fig. 4j and Supplementary Fig. 19c). Together, we demonstrate that reduced NAcLat→VTA NTS release in HFD correlates to reduced motivation characterized in diet induced obese mice. Selective overexpression of NTS in NAcLat→VTA increases motivation in HFD which partially restores normal locomotion, and ultimately limits weight gain on HFD.

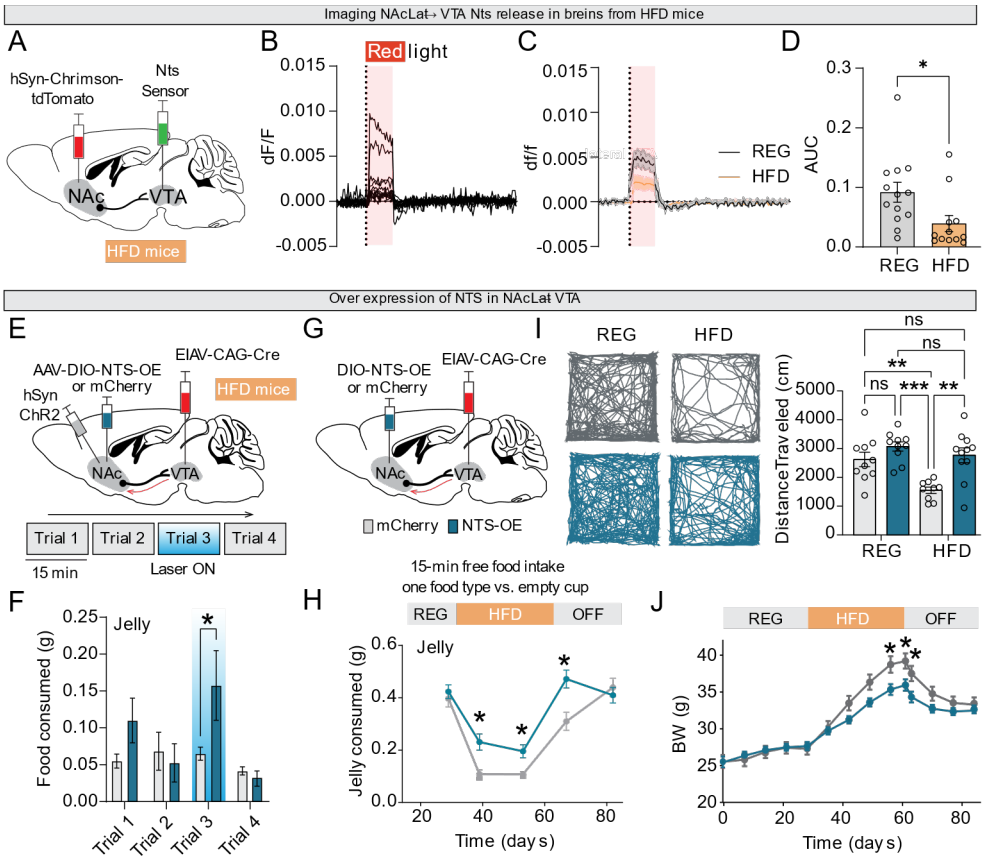

Figure 4. Upregulation of NTS in NAcLat→VTA pathway attenuates HFD induced reduction in motivation and weight gain. (A) Experimental design for ntsLight experiment.
(B) Left: lateral VTA ntsLight fluorescence during light stimulation of NAcLat→VTA in HFD mice (N=3 mice, n= 12).
(C) Average traces of lateral VTA ntsLight fluorescence during light stimulation of NAcLat→VTA in REG and HFD mice.
(D) Area under the curve during chrimson stimulation reveals that HFD have significantly reduced ntsLight fluorescence compared to REG mice.
(D) (n_{REG}= 14 slices from n=5 mice, n_{HFD} = 12 slices from n = 3 mice, unpaired t-test, *p<0.05).
(E) Experimental design and behavioral assay for optogenetic stimulation in HFD mice with (NTSOE) and without (mCherry) upregulation of neurotensin in NAcLat→VTA.
(F) Optogenetic stimulation of NAcLat→VTA induces hedonic feeding in NTS-OE, HFD mice (blue) compared with HFD mice expressing a control vector (gray) in NAcLat→VTA cells (2-way RM ANOVA with multiple comparisons, n_{NTS-OE}=4, $n_{mCherry}$=6 mice).
(G) Experimental design for measures of feeding, weight, and locomotion in HFD mice with (NTSOE; blue) and without (mCherrry;gray) upregulation of neurotensin in NAcLat→VTA.
(H) NTSOE (blue) and control (gray) mice experienced a series of diet changes (above: REG, HFD, and OFF HFD) during which jelly consumption during 15-min of free access was measured. NTS-OE mice show increased jelly consumption on HFD and one week OFF HFD compared to control mice (2-way RM ANOVA with multiple comparisons, *p<0.05), n_{NTS-OE}=14, $n_{mCherry}$=10 mice).

(I) Left: Example tracks of NTS-OE mice (blue) and control (gray) mice during exploration in an open field when on REG or HFD. Right: NTSOE mice (blue) traveled more distance in an open field compared to control mice (gray) when on HFD but not on REG (2-way ANOVA with multiple comparisons, **p<0.01,***p<0.001, $n_{REG\ mCherry}$ =10 , $n_{REG\ NTS\text{-}OE}$=10, $n_{HFD\ mCherry}$ =9 mice, $n_{HFD\ NTS\text{-}OE}$=11).
(J) Weight measured in NTSOE (blue) and control (gray) mice during a series of diet changes. NTS-OE mice show attenuated weight gain during HFD and one week OFF HFD compared to control mice, but not during REG (2-way RM ANOVA with multiple comparisons, $n_{NTS\text{-}OE}$=14, $n_{mCherry}$=10).

DISCUSSION

Many brain regions coordinate the motivation to eat which necessitates cell-type and projection-specific studies to dissect unique circuit-specific contributions to feeding behavior. Using this approach, we find that activation of NAcLat→VTA specifically increases hedonic feeding which stands in contrast to NAcMed inputs to the VTA and LH that suppress feeding (Bond et al., 2020; O'Connor et al., 2015). Similarly, several studies have reported that systemic or intra-VTA infusions of NTS decrease food consumption (Cador et al., 1986; Cooke et al., 2009; Hawkins, 1986). These results mimic the effects of LH NTS activation, which releases NTS in the VTA and suppresses feeding (Patterson et al., 2015; Woodworth et al., 2017b). Conversely, we find that activation of NAcLat→VTA releases NTS and increases hedonic feeding behavior, which is dependent on NTSR availability in the VTA, providing to our knowledge, the first evidence of NTS signaling in the VTA driving an increase in feeding behavior.

Diet-induced obesity is a strong modifier of motivated feeding behavior, where HFD mice work less to obtain food rewards in Pavlovian and operant tasks. These occur in parallel to a complex cascade of additional brain and body changes that culminate in altered metabolism such as leptin and insulin resistance, dysregulation of circadian-entrained feeding, and decreased locomotion. While overconsumption of calories beyond homeostatic need necessarily promotes weight gain and fat storage, we and others find this is an oversimplification of the cause and maintenance of obesity and propose several additional domains for obesity treatment outside of calorie restriction, such as restoring normal motivation, locomotion, and circadian-entrained eating. Here, we find that motivation to consume hedonic foods is reduced in HFD and reflects a reduction in NTS release in NAcLat→VTA. By overexpressing NTS in this pathway, we find increased motivation for hedonic feeding, decreased home cage consumption of HFD, increased locomotion, and decreased body weight relative to HFD control mice which may arise directly or indirectly due to changes in motivation. Although heightened motivation promoted greater consumption of palatable foods acutely, which alone could exacerbate obesity outcomes, this same increased motivation may drive the observed increase in locomotion and bias behavior in the homecage away from eating, resulting in attenuated weight gain. Given the pervasive body- and brain wide expression of NTS receptors and the many additional known functions mediated by NTS, our work demonstrates that circuit-specific manipulations are necessary in order to harness the therapeutic potential of NTS in obesity

EXPERIMENTAL MODEL AND SUBJECT DETAILS

The following mouse lines were used for experiments: C57BL/6J mice (Jackson Laboratory, stock number: 000664), Nts-Cre (Jackson Laboratory, stock number: 017525, strain code: B6;129-Ntstm1(cre)Mgmj/J), Ai9 (Jackson Laboratory, stock number: 007905, B6;129S6-Gt(ROSA)26Sortm9(CAG-tdTomato)Hze/J), Drd1-Cre (MMRRC, stock number: 017264-UCD, strain code: STOCK Tg(Drd1-cre)EY262Gsat/Mmucd). All lines have been crossed onto the C57BL/6J background for at least six generations. Mice were maintained on a 12:12 light cycle (lights on at 07:00). Male and female mice were used for electrophysiology and histology. Behavior experiments were in male mice. All procedures complied with the animal care standards set forth by the National Institutes of Health and were approved by University of California, Berkeley's Administrative Panel on Laboratory Animal Care.

METHODS

DIET PROTOCOLS

Regular diet (REG) mice were provided ad libidum access to standard chow (5053 PicoLab Rodent Diet 20, Lab Diet) in their home cage. High fat diet (HFD) mice were provided ad libidum access to both standard chow and 60% fat chow (Research Diets #D12492) for a minimum of 4 weeks prior to experiments. Off HFD (OFF) are HFD mice that had the 60% fat chow removed and were returned to ad libidum standard chow only in their home cage. Cafeteria-diet mice (CAF) mice were provided ad libidum access to standard chow supplemented with cafeteria style foods. Mice were given two types of high fat foods (cookies, chocolate, bacon, ham, waffles, biscuits, sausages), for a minimum of 4 weeks prior to experiments. in addition, Mice weights were recorded at least one time per week.

STEREOTAXIC SURGERIES

All stereotaxic injections were performed under general ketamine–dexmedetomidine anesthesia and using a stereotaxic instrument (Kopf Instruments, Model 1900). For red fluorescent retrograde labeling, mice were injected unilaterally with fluorescent retrobeads (100 nl; LumaFluor Inc.) in the nucleus accumbens (NAc) lateral shell (NAcLat; bregma: 1.1 mm, lateral: 1.8 mm, ventral: −5mm) or ventral tegmental area (VTA; bregma: -3.3 mm, lateral: 0.4 mm, ventral: -4.5 mm) using a 1 µl Hamilton syringe (Hamilton). The AAVs (adeno associated virus) used in this study were from the Deisseroth Lab (AAV5-EF1α–DIO-hChR2(H134R)-eYFP; AAV5-EF1α-DIO-eYFP; AAV5-EF1α-DIO-mCherry; AAV5-hSyn-hChR2(H134R)-EYFP; AAV5-hSyn-EYFP; AAV5-EF1a-DIO-eNpHR3.0-eYFP; ~1012 infectious units per ml, prepared by the University of North Carolina Vector Core Facility); from the Boyden Lab (AAV5-Syn-ChrimsonR-tdTomato); from the MIT Vector Core (AAV8.2-hEF1a-DIO-synaptophysin-eYFP;~1013 infectious units per ml); from the Tian Lab (UC Davis) (AAV5-hSyn-ntsLight1.1), or from the Lim Lab (UCSD) (RG-EIAV-CAG-Cre). For AAV viral injections, 300-500 nl of concentrated AAV solution was injected into the NAcLat (same coordinates as above), VTA (same coordinates as above), and/or LH (bregma: -.9mm, lateral: 1mm, ventral: 5mm) using a syringe pump (Harvard Apparatus) at 150 nl/min. The injection needle was withdrawn 5 min after the end of the infusion. For behavioral experiments, animals injected with Channelrhodopsin-2 (ChR2) or eYFP received unilateral implantation of a chronically implanted optical fiber (200 µm, NA = 0.37; Newdoon) dorsal to the VTA (bregma: −3.3 mm, lateral: 0.4 mm, ventral: −3.9 mm) or dorsal to the NAcLat (bregma: 1.1 mm, lateral:

1.8 mm, ventral: −4.5mm). One layer of adhesive cement (C&B Metabond; Parkell) followed by cranioplastic cement (Dental cement) was used to secure the fiber to the skull. The incision was closed with a suture and tissue adhesive (Vetbond; 3M). The animal was woken up with an I.P. injection of atipamezole and kept on a heating pad until it recovered from anesthesia. Experiments were performed 6–12 weeks (for AAVs) or 2–7 days (for retrobeads) after stereotactic injection. Injection sites and optical fiber placements were confirmed in all animals by preparing coronal sections (50–100 μm) of targeted brain regions.

ELECTROPHYSIOLOGY

Ex vivo electrophysiology

Mice were deeply anaesthetized with pentobarbital (200 mg/kg ip; Vortech). Coronal brain slices containing NAcLat or VTA (200 μm) were prepared after intracardial perfusion with ice-cold artificial cerebrospinal fluid (ACSF) containing (in mM) 50 sucrose, 125 NaCl, 25 NaHCO3, 2.5 KCl, 1.25 NaH2PO4, 0.1 CaCl2, 6.174 MgCl2, 2.96 kynurenic acid (NAcLat slices only) and 2.5 glucose (oxygenated with 95% O2/5% CO2). After 60-90 min of recovery, slices were transferred to a recording chamber and perfused continuously at 2–4 ml/min with oxygenated ACSF, containing (in mM) 125 NaCl, 25 NaHCO3, 2.5 KCl, 1.25 NaH2PO4, 2.5 glucose, 22.5 sucrose, 2.058 MgCl2 and 2 CaCl2 at ~30 °C. Cells were visualized with a 40x water-immersion objective on an upright fluorescent microscope (BX51WI; Olympus) equipped with infrared-differential interference contrast video microscopy and epifluorescence (Olympus). For whole-cell current clamp recordings, patch pipettes (3.8–4.4 MΩ) were pulled from borosilicate glass (G150TF-4; Warner Instruments) and filled with internal solution, which consisted of (in mM) 135 K-gluconate, 5 KCl, 10 HEPES, 0.1 EGTA, 2 MgCl2, 2 MgATP, 0.2 NaGTP, pH 7.35 (290-300 mOsm). For perforated patch recordings, patch pipettes were first filled with internal solution as above and then were back filled with internal solution containing 100μg/mL gramicidin. Electrophysiological recordings were made at 32°C using a MultiClamp700B amplifier and acquired using a Digidata 1440A digitizer, sampled at 10 kHz, and filtered at 2 kHz. All data acquisition was performed using pCLAMP software (Molecular Devices). Channelrhodopsin-2 was stimulated by flashing 473 nm light through the light path of the microscope using an ultrahigh-powered light-emitting diode (LED) powered by an LED driver (Prizmatix) under computer control. A dual lamp house adaptor (Olympus) was used to switch between fluorescence lamp and LED light source. The light intensity of the LED was not changed during the experiments and the whole slice was illuminated (5 mW/mm2). For recording the effect of neurotensin on cell firing, a stable recording was first made in normal ACSF (baseline), then ACSF containing 1μM neurotensin (Sigma Aldrich, PubChem SID: 329818664) was perfused into the recording chamber for 2-5min before recording again, finally normal ACSF was perfused into the recording chamber for an additional 2-5 minutes before recording firing (washout). For recording the effect of neurotensin receptor antagonist on cell firing, half of slices were incubated and recorded in ACSF containing 1μM SR142948 (Tocris, PubChem SID: 5311451). Series resistance (15–25 MΩ) and input resistance were monitored online. Data were analyzed offline using Clampfit (Molecular Devices) or custom MATLAB scripts.

In vivo electrophysiology

Animals were implanted with a custom-built optrode unilaterally above the NacLat (NAcLat; bregma: 1.1 mm, lateral: 1.8 mm, ventral: −4mm), which consisted of eight tetrodes (12-μm

polyimide-coated nickel-chrome wire protected by silica tubing) glued to a 200-μm optical fiber using epoxy. The tetrodes protruded from the tip of the optical fiber by ~0.5 mm. Wire tips were cut flat, and gold plated to reduce impedance to ~200 kΩ at 1 kHz. A small screw fixed to the skull served as a ground electrode. Data collection began <1 week after the optrode implantation. Neural signals were recorded using a Digital Lynx 4SX system with an HS-18-MM headstage pre-amplifier (Neuralynx). Recorded signals were filtered between 0.6 and 6 kHz and sampled at 32 kHz. Spikes were sorted offline using SpikeSort3D 2.5.4 (Neuralynx) software. At the end of each recording session, the optrode was moved ventrally for ~40 μm until active units were detected. The final recording location was verified using histology after the electrolytic lesions (12 μA, 30 s). K- means clustering of tagged and non-tagged units was performed on all the units (REG and HFD) using the mean firing frequency (collected without food) and spike width.
ChR2-tagged neurons were identified by delivering 473 nm (0.8 mW/mm2, 1-5-ms pulses) of light at 2-Hz frequency for 2–3 min. A 2-ms bin with the highest number of spikes in the interval (0, +100 ms) around the laser pulse was identified. To test if the identified strongest response to light was higher than chance, we shuffled all the spike times in the same (0, +100 ms) interval 10,000 times and counted the highest number of spikes in a 2-ms bin for each iteration. If the number of spikes in the 2-ms bin from the real data exceeded the 99.9th percentile value of the distribution of number of spikes in the most active 2-ms bin for the shuffled data, we classified the cell as light responsive. Response latency was defined as the average response time in the most active 2-ms bin, and only units with response latency<8ms were classified as tagged.
For detection of feeding events, a piezo-based sensor was placed under the food plate. Activation of the sensor was transmitted as a TTL signal to the Neuralynx recording system via an Arduino uno board, to obtain precise time locked events. A camera was placed over the chamber and used to later verify feeding bouts with sensor activation.

BEHAVIORAL ASSAYS
All behavioral tests were performed during the light phase (unless otherwise specified) in a temperature (68-74°F) and humidity (40-60%) controlled room that is illuminated by eight 32 W fluorescent lights each producing 2925 lumens. Behavioral equipment was cleaned with 70% EtOH between individual animals.

Acute feeding: Mice were placed in a chamber (25 cm L x 25 cm W x 25 cm H) with two small empty weigh boats fixed to the floor on opposite corners. Following a 10-minute habituation period, one empty weigh boat was replaced with a boat containing a pre-measured amount of a specific food type (standard chow, 60% fat chow, chocolate, peanut butter, strawberry jelly, or butter) while the other weigh boat remained empty. After 15 minutes, the weigh boat was measured and subtracted from the initial weight to determine amount consumed.
In experiments with optogenetic stimulation, mice with optogenetic implants were attached to a fiberoptic cable which was connected to a 473 nm DPSS laser diode (Laserglow) through an FC/PC adaptor, and laser output was controlled using a Master-8 pulse stimulator (A.M.P.I.). Power output was tested using a digital power meter (Thorlabs) and was checked before and after each experimental animal; output during light stimulation was estimated to be 3-5 mW/mm2 at the targeted tissue 200 μm from the fiber tip (www.optogenetics.org/calc). optogenetic experiments consisted of 4 trials (15 minutes each, 60 minutes total). Mice were provided a new pre-measured weigh boat of food every Trial. During Trial #3, 20Hz 5ms blue light was delivered through the fiberoptic cable. At the end of the test, all weigh boats containing

food were measured and subtracted from initial weight to determine total food consumed during each Trial. In the experiments in Fig. 1f, mice were starved prior to acute feeding assay by removing all food from home cage food hopper for 24hr prior to experiment. In experiments with optogenetic stimulation and intrabrain cannula infusions (Fig. 2d), mice were implanted with a hollow cannula (PlasticsOne, 33G 4.6 MM) over the VTA (bregma: -3.3 mm, lateral: 0.5 mm, ventral: -4.5 mm). Opto-infusion experiments were done >1 week after cannula surgery. Mice were placed in a chamber for habituation, and trial #1 as described above. Between Trial #1 and Trial #2 the mice were taken to a separate box where they were infused with Saline or 100 μM SR142948 (500nl via infusion pump at a rate of 300 nL/min), an additional 10 minutes were given for absorption of the infused solution before placing the mice back for the remaining trials #2-4. On trial #3, light stimulation was given via the internal cannula using a custom-made optic fiber.

Homecage feeding: Mice in homecage feeding experiments received a pre-measured amount of standard chow and 60% fat chow which was then removed from the food hopper and measured every 24 hours for each cage.

Open Field Test: Mice were placed in a custom open field chamber (50 cm L x 50 cm W x 50 cm H) and their movement was recorded and analyzed for 15 min using video-tracking (Biobserve).

Real-time Place Preference (RtPP): At least six weeks after virus injection, mice with optogenetic implants were connected to a fiberoptic cable and placed in a custom-made three-compartment chamber. For optogenetic stimulation, the cable was connected to a 473 nm DPSS laser diode (Laserglow) through an FC/PC adaptor, and laser output was controlled using a Master-8 pulse stimulator (A.M.P.I.). Power output was tested using a digital power meter (Thorlabs) and was checked before and after each experimental animal; output during light stimulation was estimated to be 3-5 mW/mm2 at the targeted tissue 200 μm from the fiber tip (www.optogenetics.org/calc). One side of the chamber was designated as the initial stimulation side (Phase 1) and after 10 min the stimulation side was switched to the other previously non-stimulated side of the chamber (Phase 2). The middle of the chamber was a neutral area that was never paired with stimulation. At the start of each session, the mouse was placed in the middle of the chamber, and every time the mouse crossed to the stimulation side, constant laser stimulation (473 nm: 20 Hz, 5 ms pulses) was delivered until the mouse exited the stimulation area. There was no interruption between Phase 1 and Phase 2. The first stimulation side was counterbalanced across mice. The movement of the mice was recorded via a video tracking system (Biobserve) and the time the mice spent in each area (stimulated, non-stimulated, neutral) was calculated.

CHARACTERIZING NTSLIGHT1.1 AND IMAGING EX VIVO NEUROTENSIN RELEASE

ntsLight1.1 was first expressed in cultured hippocampal neurons with different concentrations of neurotensin applied. ntsLight1.1 reliably increased fluorescence in the presence of neurotensin in a concentration dependent manner. Next, mice were injected with virus containing AAV5-syn-ntsLight1.1 in the VTA and AAV5-Syn-ChrimsonR-tdTomato into NAcLat or LH. At least 4 weeks after virus injection, acute coronal midbrain slices were prepared as for ex vivo electrophysiology and were transferred to a recording chamber and perfused continuously at 2–4

ml/min with oxygenated ACSF. Slices were visualized under a custom-built open-source macroscope (github.com/Llamero/DIY_Epifluorescence_Macroscope) fitted with high power LEDs and a Teledyne Kinetix sCMOS camera. Specifically, custom drawn regions of interest were imaged at a rate of 20Hz during 10ms simultaneous 474nm LED stimulation and camera exposure for a total of 20 seconds. In the middle of the recording, 1 second of 20Hz 5ms 635nm LED stimulation was delivered to the slice outside of camera exposure time, so that specifically no light from stimulating Chrimson was recorded. Green light stimulation experiments were performed as with red light stimulation, with 1 second of 20Hz 5ms 554nm LED stimulation delivered. To determine dF/F for different VTA subregions, the fluorescence from an ROI drawn away from sensor and Chrimson-expressing regions was divided from the fluorescence in VTA subregions. Because photobleaching curves were not identical between different regions of the tissue, an additional baseline subtraction was performed. To do this, a window of dF/F signal around Chrimson stimulation time was removed, the remaining dF/F data was smoothed, and a estimated polynomial fit trendline was drawn through the smooth data and across the removed stimulation time window. This trendline was subtracted from the complete dF/F signal. Area under the curve was calculated as an approximate trapezoidal integral during stimulation time.

SINGLE-CELL PATCH RNA SEQUENCING

Sample collection: Procedure was described previously in Földy et al. (2016). To minimize interference with subsequent molecular experiments, only a small amount of intracellular solution (~1 µl; not autoclaved or treated with RNase inhibitor) was used in the glass pipette during electrophysiological recordings. Before and during recording, all surface areas - including manipulators, microscope knobs, computer keyboard, etc. - that the experimenter needed to contact during the experiment were cleaned with RNaseZAP solution (Sigma). After whole-cell patch-clamp recordings, the cell's cytosol was aspirated via the glass pipette used during the recording. Although the aspirated cytosol may have contained genomic DNA, our choice of cDNA preparation, which involved poly-A based mRNA selection, virtually eliminated the possibility of genomic contamination in the RNAseq data. For sample collection, we quickly removed the pipette holder from the amplifier head stage and used positive pressure to expel samples into microtubes containing cell collection buffer while gently breaking the glass pipette tip. Cell collection microtubes were stored on ice until they were used.

cDNA library preparation: Described previously in Földy et al. (2016). Briefly, single-cell mRNA was processed using Clontech's SMART-Seq Single Cell kit. As a first step, cells were collected via pipette aspiration into 1 µL of 10x collection buffer, and were spun briefly and snap frozen on dry ice. Samples were stored at −80°C until further processing, which was performed according to manufacturer's protocol. Resulting cDNA was harvested and analyzed on a Fragment Analyzer (Advanced Analytical). Library preparation was performed using Nextera XT DNA Sample Preparation Kit (Illumina) as described in the protocol. Following library preparation, cells were pooled and sequenced using NextSeq 150 high-output kit in an Illumina NextSeq 500 System with 2x75 paired-end reads.

Processing of RNA sequencing data: After sequencing, raw reads were de-multiplexed and pre-processed using Trimmomatic and Flexbar. Then, raw sequencing reads were aligned to the Ensembl GRCm38 reference transcriptome (Version-2015-06-25), using the STAR aligner with the following parameters: trimLeft = 10, minTailQuality = 15, minAverageQuality = 20 and

minReadLength = 30. 'Single-end/paired-end' and 'sense/antisense/both' options. Gene counts were calculated using featureCounts. For convenience, Ensembl gene IDs were converted to gene symbols using the mouse GRCm38 gtf file (ftp://ftp.ensembl.org/pub/release-86/gtf/mus_musculus/Mus_musculus.GRCm38.86.gtf.gz) as a reference. In the few cases where different Ensembl gene IDs identified the same gene symbol, average gene counts were used.

Gene categories: Altogether, expression of N = 22,800 genes were analyzed ('All'). This list was generated using Ensemble Biomart, with the following specifications "Database=Ensembl Genes 85, Dataset=Mus Musculus genes (GRCm38.p4), Attributes=Ensemble Gene ID and Associated Gene Name." 'CAM' (N = 396) and 'ion channel' (N = 207): these categories included genes as described previously (Földy et al., 2016).

Quality control: All data analysis was performed using Python. First, for each cell, we calculated the number of unique genes and the fraction of aligned reads. Second, we calculated the mean and standard deviation of these two values across all cells. Cells that had both values less than 1 standard deviation below the mean, or had one value above the mean and the other less than 1.5 standard deviations below the mean were considered to pass quality control. For the rest, we calculated their correlation (minimum of Pearson and Spearman) against the average of all cells within their respective cell type that passed quality control. Cells with correlation > 0.4 were considered to pass quality control, otherwise they failed quality control.

Normalization of gene expression: After quality control, cells (represented by raw gene count vectors) were pooled together and normalized using scran (Lun et al., 2016), with sizes 20, 40, 60, 80, 100. Cells that had negative or zero size were removed. For further analysis, gene counts were converted into log-space by the transformation, where was the normalized gene count of the i-th gene.

HISTOLOGY AND MICROSCOPY

Immunohistochemistry and Microscopy: Were performed as described previously in 1 Briefly, after intracardial perfusion with 4% paraformaldehyde in PBS, pH 7.4, the brains were post-fixed overnight and coronal brain sections (50 or 100 μm) were prepared. Sections were stained overnight in a primary antibody solution (rabbit anti-TH, mouse anti-TH (all Millipore), chicken anti-GFP (Abcam), all 1:1000). Twenty-four hours later, sections were stained for 2 hours in secondary antibody solution (goat anti-mouse Alexa Fluor 488, goat anti-rabbit Alexa Fluor 488, goat anti-mouse Alexa Fluor 546, goat anti-rabbit Alexa Fluor 546, (all Thermo Fisher Scientific), goat anti-chicken Alexa Fluor 488 (Abcam), all 1:750). Image acquisition was performed with Zeiss LSM 710 laser scanning confocal microscope using 20x or 40x objectives and on a Zeiss AxioImager M2 upright widefield fluorescence/differential interference contrast microscope with charge-coupled device camera using 5x, 10x and 20x objectives. Images were analyzed using ImageJ. Sections were labeled relative to bregma using landmarks and neuroanatomical nomenclature as described in "The Mouse Brain in Stereotaxic Coordinates" (Franklin and Paxinos, 2013). All images presented with multiple colors represent a composite of images collected with different excitation wavelengths.

Fluorescent in situ hybridization: The fluorescent in situ hybridization experiments were conducted using a commercially available RNAscope® Multiplex Fluorescent Reagent Kit V2

(ACD Bio, USA). Brains were extracted and snapfrozen by submerging them into frozen isopentane (-70 to -50°C). They were stored in an airtight container in a -80°C freezer. 16 μm coronal LDT brain slices were prepared using a cryostat, placed on Superfrost Plus microscope slides (Fisher Scientific, USA) and stored in a -80°C freezer. On the next day, brain slices were fixed in 4% paraformaldehyde (PFA) in PBS (30 min) followed by an ethanol dehydration procedure (20 min). Slices were then bathed in hydrogen peroxide (10 min), followed by protease IV from the RNAscope® kit (15 min). Next, probe mixes were made for neurotensin (Mm-Nts-C2), dopamine receptor1 (Mm-Drd1), neurotensin receptor 1 (Mm-Ntsr1-C2), tyrosine hydroxylase (Mm-Th) . Probe mixes were applied to the brain slices for hybridization (2 hours at 40°C). After amplification of the signal (using AMP1, AMP2 and AMP3 from the RNAscope® kit), channel C1 was developed using green Opal 520 (Akoya Biosciences, USA) and channel C2 was developed using orange Opal 570 (Akoya Biosciences, USA). Lastly, nuclei were stained using DAPI (from the RNAscope® kit) and brain slices were sealed with ProLong Gold Antifade mountant (Thermo Fisher Scientific, USA) and a glass coverslip. Images were taken using a confocal microscope (LSM710, Carl Zeiss Inc.) at 5 different z depths (spanning 4.4 μm), and images were flattened by taking the maximum projection across the z direction. Regions of interest (ROIs) were identified using a machine learning-based segmentation algorithm NucleAIzer37 based on the DAPI channel. The amount of visible mRNA across the DAPI-identified region was used as a proxy for total mRNA in the cell. All identified regions of interest were manually sorted by an investigator who was blind to brain region and probe mix. ROIs were removed if they (i) showed overlap with other regions of interest or (ii) were segmentated inadequately by the algorithm. Using a custom-made MATLAB algorithm, the remaining cells were analyzed based on the percentage of DAPI-positive pixels that were also positive for targeted mRNA. To adjust for potential differences in staining and/or image quality, we compared pixels in all regions of interest to background fluorescence levels in each image. To do this, we first established a 'null distribution' that quantifies the distribution in pixel intensity values for cells putatively negative for targeted mRNA. Each cell's distribution of pixel intensities was compared to the null distribution for the targeted mRNA and a correlation coefficient R was calculated. If R of a cell's distribution compared to the null distribution was less than 0.85, then a cell was labeled as positive for the targeted mRNA.

QUANTIFICATION AND STATISTICAL ANALYSIS

Student's t tests (paired and unpaired), one-way or two-way ANOVA tests, and mixed effects analyses were used to determine statistical differences using GraphPad Prism 9 (Graphpad Software). Holm-Sidak's post hoc analysis was applied when a one-way ANOVA or mixed effects analysis showed a significant main effect, or a two-way ANOVA or mixed effects analysis showed a significant interaction. Statistical significance was * $p < 0.05$, ** $p < 0.01$, *** $p < 0.001$. All data are presented as means ± SEM. All details of the statistical analysis including means, SEMs, and number of animals used are summarized in Supplementary Table S1.

SUPPLEMENTARY FIGURES

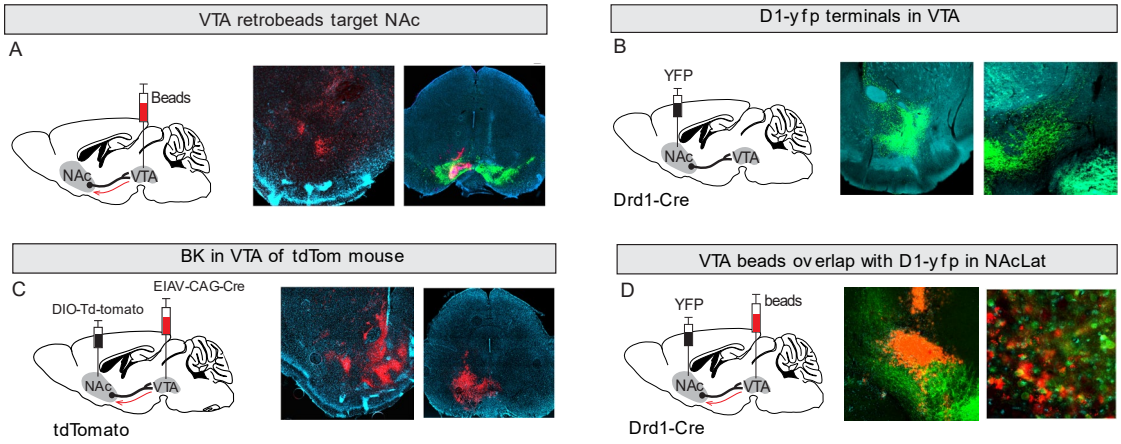

Supplementary Figure 1. Anatomical tracing of NAcLat→VTA, Related to Figure 1.
(A) Fluorescent retrobeads (red) injected into VTA are found in NAcLat of WT mice.
(B) AAV-DIO-eYFP injected into NAcLat (middle) of Drd1-Cre mouse reveals eYFP terminals in VTA (right).
(C) Injection of a virus that retrogradely transports Cre (EIAV-CAG-Cre) into the VTA (right) of a tdTomato reporter mouse (Ai9) reveals tdTomato positive cells in NAcLat (middle).
(D) Fluorescent retrobeads injected into VTA of Drd1-Cre mouse with AAV-DIO-eYFP injected into NAcLat show overlap of beads and eYFP in both VTA (middle) and NAcLAt (right).

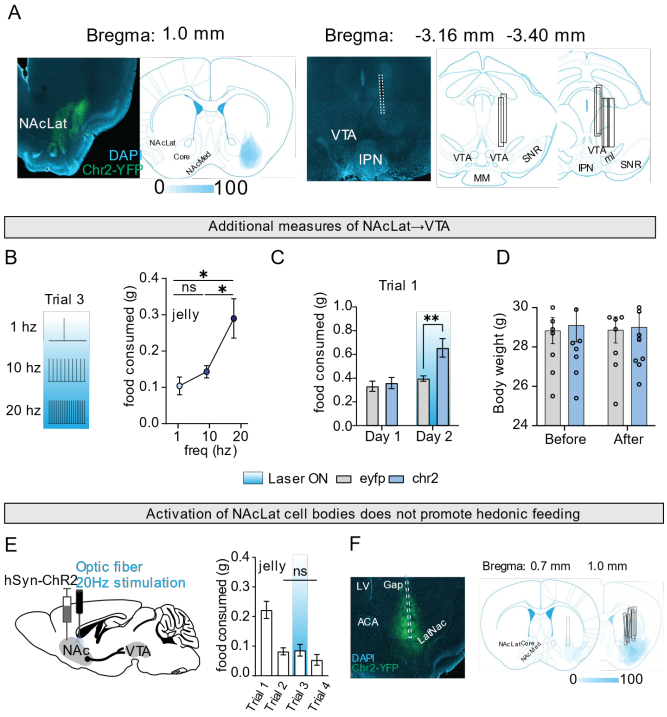

Supplementary Figure 2. Histology and additional optogenetic behavior experiments in NAcLat projections to VTA and cell bodies, Related to Figure 1.

(A) Histological verification of ChR2 injection site in NAcLat (left) and optic fiber implant above VTA (right) showing example image and group analysis summary.
(B) Frequency dependence of induced hedonic feeding by optogenetic stimulation of NAcLat→VTA during Trial #3. Light stimulation increased jelly feeding in high (20 Hz) but not low frequency (1,10 Hz) stimulation (n=10, 1-way RM ANOVA).
(C) Optogenetic activation of NAcLat→VTA increases jelly consumption during Trial #1 when natural drive to consume jelly is high (eYFP=8, nCHR2=9, 2-way RM ANOVA).
(D) There was no difference in average body weight between ChR2 and eYFP mice. Body weight for both groups did not differ before and after the series of optogenetic feeding experiments. (eYFP=9, nCHR2=10, 2-way RM ANOVA).
(E) Virus expressing ChR2 (AAV-hSyn-ChR2) was injected into NAcLat and an optic fiber was implanted above NAcLat cell bodies. Optogenetic stimulation of NAcLat cell bodies during Trial #3 did not change jelly feeding (n=8, 1-way RM ANOVA).
(F) Histological verification of ChR2 expression and implant location in NAcLat.

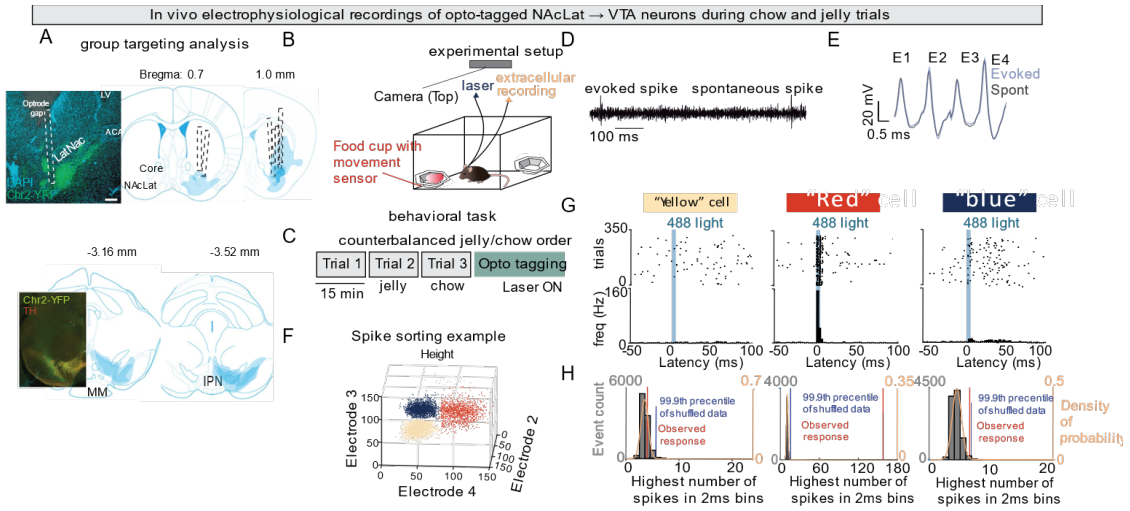

Supplementary Figure 3. Histology, spike sorting, and opto-tagging analysis for *in vivo* electrophysiology recordings during feeding behavior in REG mice, Related to Figure 1.
(A) Histological verification of ChR2 expression and optrode location in NAcLat (above) and VTA (below) showing example images and group analysis summary.
(B) Mice were placed in a chamber with two cups. One cup contained a single food type fitted with a touch sensor to record feeding times, which was confirmed by video recording.
(C) Schedule of consecutive 15 min trials of no food (Trial #1) followed by free access to different food types (Chow or Jelly) during recording of opto-tagged NAcLat→VTA units. Free access to jelly or chow was counterbalanced between Trials #2 and 3. At the end of Trial #3, laser stimulation (1-5 ms, 2Hz) was used to identify light responses in recorded units.
(D) Example recording with light evoked and spontaneous spike.
(E) Example of a single unit's spontaneous (gray) and evoked (blue) spike waveform as recorded on the four separate channels (E1-E4) of the optrode.
(F) Example of spike sorting. 3D plot of three simultaneously-recorded units according to action potential height. Colors indicate action potentials that belong to separate units.

(G) Raster plots showing example units from (F) firing 50 ms before and 100 ms after a 5 ms 488nm laser pulse. Each row represents a single trial containing one blue light pulse. Blue bar indicates time of blue laser stimulation. Cell labeling corresponds to the color scheme in (F) (data represent means ± SEM).
(H) Spike histograms corresponding to raster plot in (G).

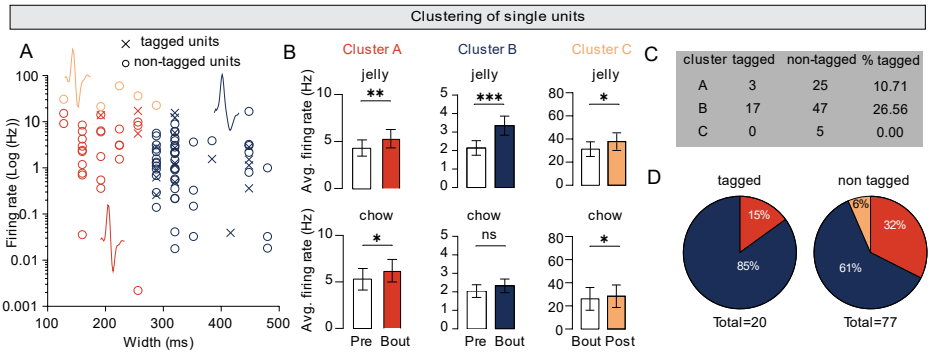

Supplementary Figure 4. Clustering of grouped optotagged and non-optotagged units during feeding behavior, Related to Figure 1.
(A) K-means clustering of all units recorded in NAcLat of REG mice based on firing rate and action potential width (clustering of REG units was combined with HFD, see Fig. 3 and Supplementary Fig. 12). Separate clusters and corresponding example spike are indicated by color.
(B) (Top) Average firing rate of the units in each cluster before (Pre) and during feeding bout (Bout) for jelly. (Bottom) as above but for chow. Colors correspond to cluster plotted in (A). (n_A =28, n_B =57, n_C=5, unpaired t-test, *p<0.05, **p<0.01, ***p<0.001).
(C) Table summary of tagged and non-tagged REG units in each cluster.
(D) Relative proportions of each cluster assigned to tagged (left) and non-tagged (right) REG units.

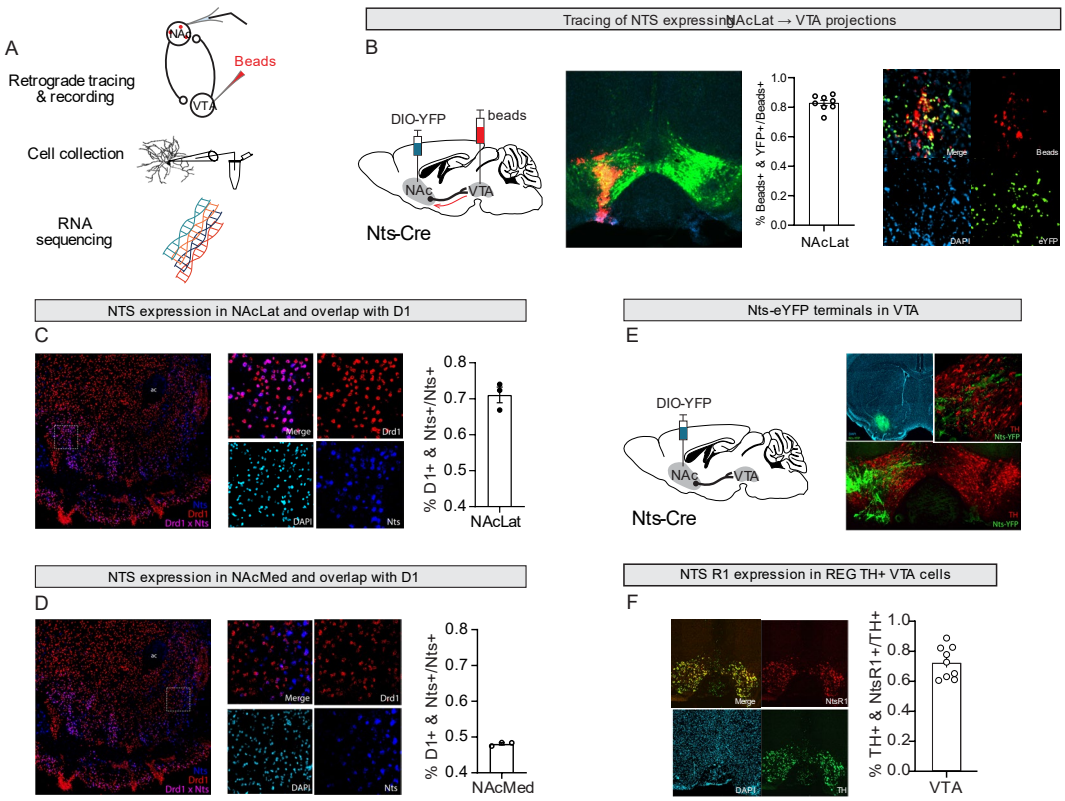

Supplementary Figure 5. Anatomical characterization of neurotensin in NAcLat→VTA, Related to Figure 2.

(A) Schematic of patch-sequencing protocol. Fluorescent retrobeads are injected into VTA and beads-labelled NAcLat cell activity is recorded using whole-cell patch clamp. After recording, cell cytosol is collected for RNA sequencing.

(B) Left: Virus driving expression of eYFP (AAV-DIO-eYFP) is injected into NAcLat of an Nts-Cre mouse and fluorescent red retrobeads are injected into the VTA. Middle: Beads (red) and NTS-eYFP (green) overlap in the VTA. Right: Of the beads-labelled cells found in NAcLat, 83% are eYFP+ (n= 7251 cells from 8 mice). Example fluorescent image showing beads (red), eYFP, DAPI, and merged channels.

(C) Fluorescent *in situ* hybridization reveals 71% of neurotensin positive cells in NAcLat are D1+ (n = 18,470 cells from 3 mice).

(D) Fluorescent *in situ* hybridization reveals 48% of neurotensin positive cells in NAcLat are D1+ (n = 2924 cells from 3 mice).

(E) Left: Schematic showing injection of virus expressing Cre-dependent eYFP (AAV-DIO-eYFP) into NAcLat of Nts-Cre mouse. Right: Example image showing eYFP at injection site in NAcLat. eYFP terminals are located among TH+ (red) cells in the VTA.

(F) Fluorescent *in situ* hybridization in the VTA reveals that 73% of TH+ cells co-express NtsR1.

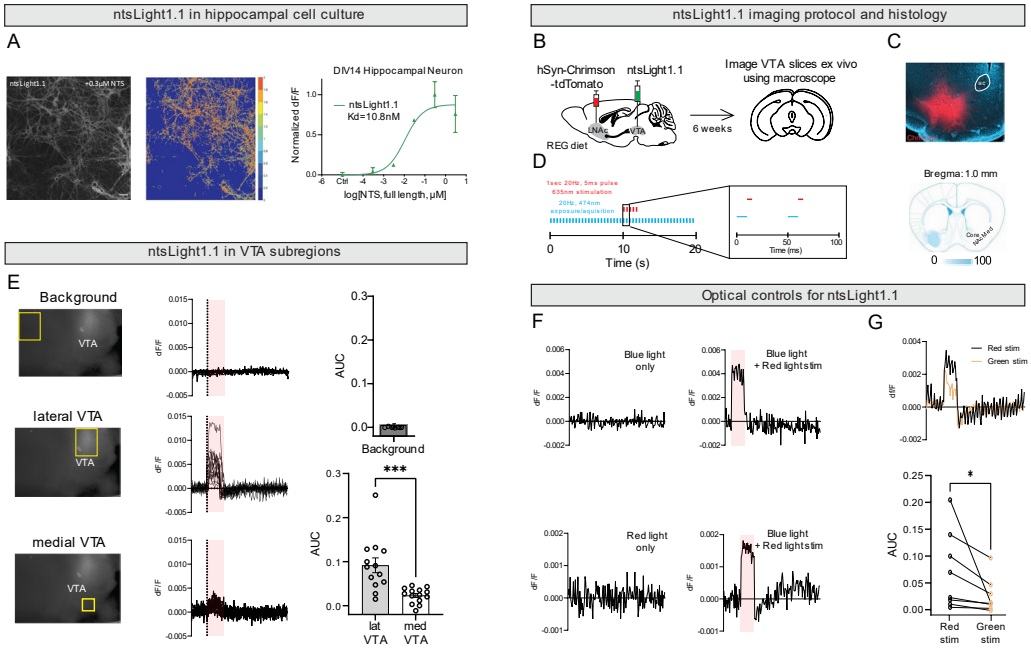

Supplementary Figure 6. Characterization of ntsLight1.1, Related to Figure 2.

(A) Left: Example image and background subtracted image of cultured mouse hippocampal neurons expressing ntsLight1.1. Scale bar, 50 μm. Right: Increasing neurotensin concentration increases ntsLight1.1 fluorescence in cultured hippocampal neurons.

(B) Red shifted ChR2 (AAV-hSyn-Chrimson) was injected into NAcLat and ntsLight1.1 was injected to VTA of REG mice. Following six weeks of expression, VTA slices were prepared for imaging under a custom macroscope.

(C) Top: Histological verification of Chrimson expression in NAcLat. Bottom: Group summary of Chrimson virus expression.

(D) Imaging paradigm for sensor experiment. Blue light was delivered constantly in 5ms at 20Hz at the same time as camera exposure. In the middle of recording, 1 second of 20Hz 5ms red light stimulation was delivered to activate chrimson. Zoom in of red and blue light pulse trains show separation of delivery of light pulses and that the camera was not exposing during red light stimulation.

(E) Example ntsLight1.1 recordings from coronal slices containing the VTA before, during, and after red light stimulation. Increase in fluorescence was not detected in a region dorsal to the VTA (top row; background), but was present during stimulation in the lateral VTA (middle row) compared to the medial VTA (bottom row). Area under the curve during light stimulation shows that there is more ntsLight1.1 fluorescence in lateral compared to medial VTA (right graphs).

(F) Blue light stimulation or red light stimulation only (left column) does not drive an increase in fluorescence, only the combination of blue and red light (right column) produces an increase in ntslight1.1 fluorescence.

(G) Top: Example trace from one slice that received either red light stimulation or green light stimulation. Green light, which activates Chrimson less, results in reduced area under the curve of fluorescence during light stimulation compared to red light.

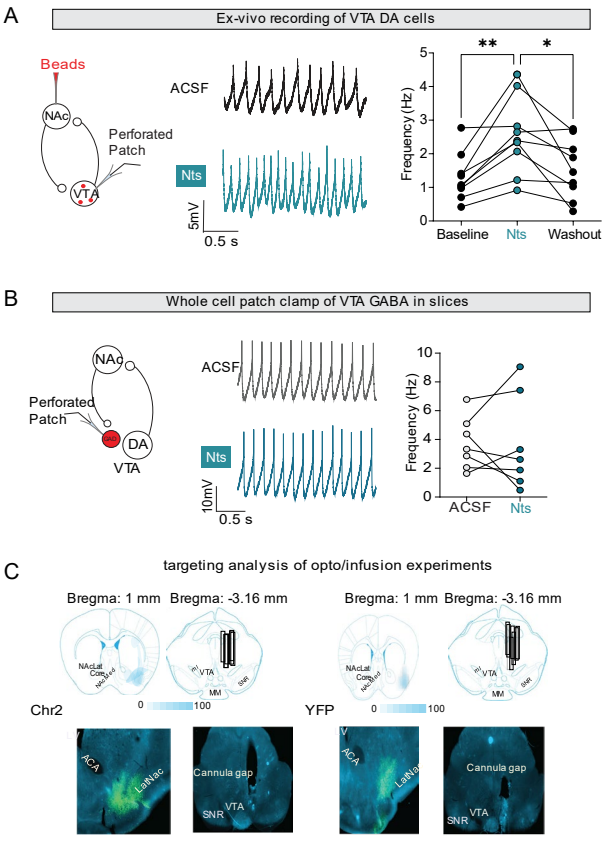

Supplementary Figure 7. Physiological effects of neurotensin on specific VTA subpopulations and histology, Related to Figure 2.

(A) Experimental design and sample traces of whole cell patch clamp recordings from retrobead-labeled VTA DA cells in ACSF (black) or during bath application of neurotensin (Nts:1µM, turquoise). Nts increased firing of NAcLat-projecting VTA DA neurons relative to baseline and washout. (n =7 cells, *p<0.05, ** P<0.01, 1-way ANOVA).

(B) Experimental design and sample traces of whole cell patch clamp recordings from VTA GABA cells in ACSF (black) or during bath application of neurotensin (Nts:1µM, turquoise). Bath application of NTS did not change the firing of VTA-GABA neurons compared to baseline. (n =10 cells, ns, paired t-test).

(C) Histological verification of virus expression and cannula implant location for combined optogenetic and pharmacology experiment in Fig. 2d. Top: Group summary of expression and implant locations for ChR2 (left) and eYFP (right) groups. Bottom: Example images of NAcLat virus expression and VTA cannula implant location for ChR2 (left) and eYFP (right) groups.

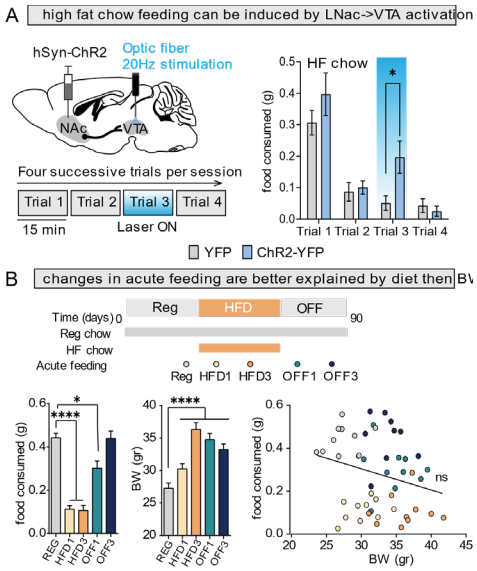

Supplementary Figure 8. Optogenetic stimulation of NAcLat→VTA drives consumption of high fat diet chow and free feeding of hedonic food does not correlate with body weight, Related to Figure 3.

(A) Left: Surgical schematic and feeding experiment design. Right: Optogenetic stimulation of NAcLat→VTA increases consumption of high fat chow compared to control mice (n_{ChR2}=9, n_{eYFP}=9 mice, 2-way ANOVA, * p<0.05).

(B) (Top) Experimental design for recording acute hedonic food consumption at time points during a series of diet changes. (Bottom left) Acute jelly consumed and body weight (BW) for each time point indicated in (A). Regular diet (REG), 1 week on HFD (HFD1), 3 weeks on HFD (HFD3), 1 week after returning to REG diet (OFF1), 3 weeks after returning to REG diet (OFF3) (n=10 mice ,1way ANOVA with multiple comparisons, *p<0.05, ****p<0.001). (Bottom right) Body weight (x) is plotted against jelly consumption (y) for all mice at all timepoints collected. There is no significant correlation between BW and acute jelly consumption. (n=10 mice, Pearson r=-0.24, p=0.08).

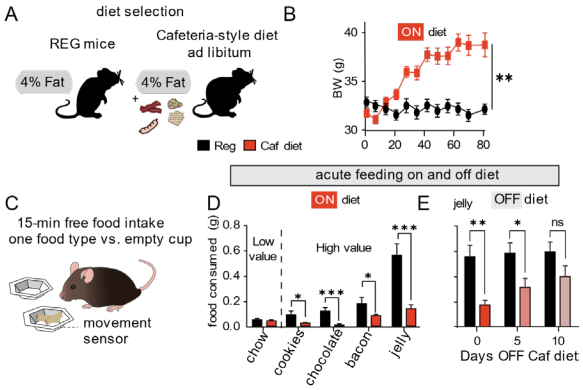

Supplementary Figure 9. Obesogenic cafeteria-style diet reduces acute hedonic feeding behavior, Related to Figure 3.

(A) REG mice were provided standard chow and cafeteria-style diet mice (CAF) were fed standard chow with additional foods in their homecage (Two different types of foods were provided each day, including: chocolate, cookies, waffles, butter, bacon, ham).
(B) Mice on CAF diet gained more weight compared to REG mice (n_{REG}=7, n_{CAF}=9, 2-way ANOVA).
(C) Acute feeding assay design: mice were provided 15 min free access to different food types.
(D) CAF diet mice consume less hedonic foods compared to REG mice during a 15 min acute feeding test with no difference in chow consumption between REG and CAF mice. (n_{REG}=7, n_{CAF} =9, unpaired t-test).
(E) CAF consumption of jelly in an acute feeding test remains less than REG mice at 5 days off CAF diet but does not differ 10 days after CAF diet (n_{REG}=7, n_{CAF} =8, 2-way ANOVA). *p<0.05,**p<0.1,***p<0.01.

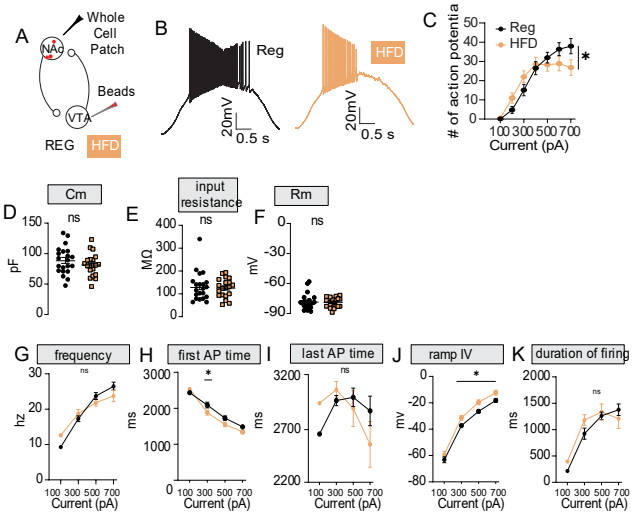

Supplementary Figure 10, Electrophysiological changes in NAcLat→VTA in HFD, Related to Figure 3.
(A) Experimental design for whole-cell patch clamp recordings.
(B) Example current ramp injections in beads-labelled NAcLat cells from REG and HFD mice.
(C) Fewer spikes are evoked in HFD beads-labelled NAcLat cells by current ramp injection compared to REG. (n_{REG}=23 cells n_{HFD}=20 cells, Mixed effects analysis with multiple comparisons test, *p<0.05).
(D) Membrane capacitance does not differ between REG and HFD beads-labelled NAcLat cells.
(E) Input resistance does not differ between REG and HFD beads-labelled NAcLat cells.
(F) Membrane resistance does not differ between REG and HFD beads-labelled NAcLat cells.
(G) No difference in frequency of action potential firing during current ramp injection between REG and HFD beads-labelled NAcLat cells.
(H) Time of first action potential during current ramp injection is earlier in HFD compared to REG beads-labelled NAcLat cells at 300pA.
(I) Time of last action potential during current ramp injection does not differ between REG and HFD beads-labelled NAcLat cells.
(J) Average membrane potential during current ramp injection is more depolarizied in HFD compared to REG beads-labelled cells.

(K) No difference in total duration of action potential spike train between REG and HFD beads-labelled NAcLat cells.

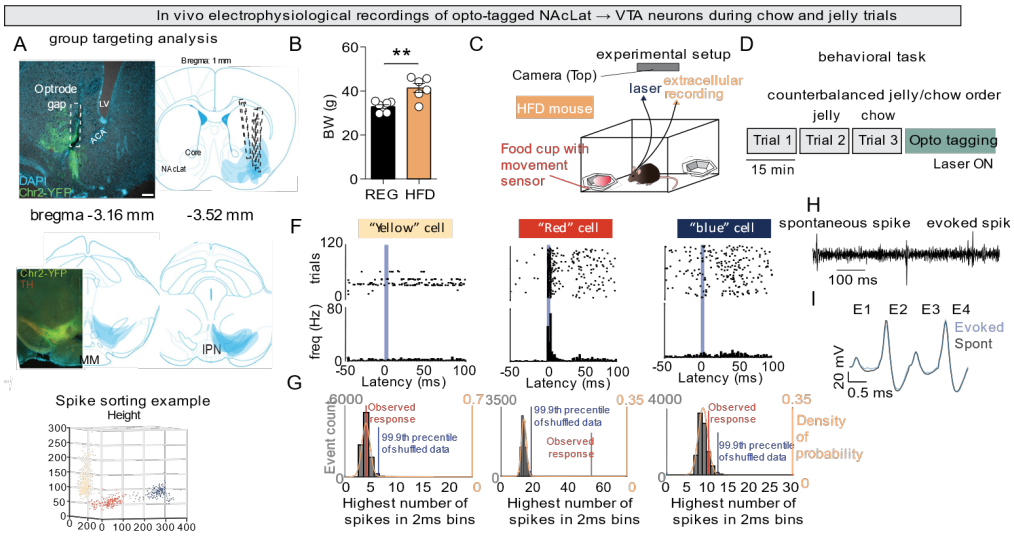

Supplementary Figure 11. Histology, spike sorting, and opto-tagging analysis for *in vivo* electrophysiology recordings during feeding behavior in HFD mice, Related to Figure 3.
(A) Histological verification of ChR2 expression and optrode location in NAcLat (above) and VTA (below) showing example images and group analysis summary.
(B) Body weight is greater in optrode-implanted mice on HFD compared to REG.
(C) HFD mice (>4 weeks on HFDwere placed in a chamber with two cups. One cup contained a single food type fitted with a touch sensor to record feeding times, which was confirmed by video recording.
(D) Schedule of consecutive 15 min trials of no food (Trial #1) followed by free access to different food types (Chow or Jelly) during recording of opto-tagged NAcLat→VTA units. Free access to jelly or chow was counterbalanced between Trials #2 and 3. At the end of Trial #3, laser stimulation (1-5 ms, 2Hz) was used to identify light responses in recorded units.
(E) Example of spike sorting. 3D plot of three simultaneously-recorded units according to action potential height. Colors indicate action potentials that belong to separate units.
(F) Raster plots showing example units from (E) firing 50 ms before and 100 ms after a 5 ms 488nm laser pulse. Each row represents a single trial containing one blue light pulse. Blue bar indicates time of blue laser stimulation. Cell labeling corresponds to the color scheme in panel A (data represent means ± SEM).
(G) Spike histograms corresponding to raster plot in (F).
(H) Example recording of "red" unit with light evoked and spontaneous spike.
(I) Example of the "red" unit's spontaneous (gray) and evoked (blue) spike waveform as recorded on the four separate channels (E1-E4) of the optrode.

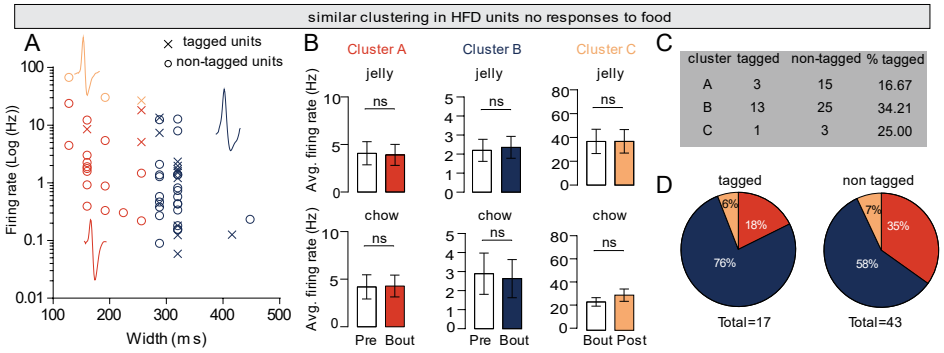

Supplementary Figure 12. Clustering of grouped optotagged and non-optotagged units during feeding behavior, Related to Figure 3..

(A) K-means clustering of all units recorded in NAcLat of HFD mice based on firing rate and action potential width (clustering of REG units was combined with HFD, see Fig. 1 and Supplementary Fig. 4). Separate clusters and corresponding example spike are indicated by color.

(B) (Top) Average firing rate of the units in each cluster before (Pre) and during feeding bout (Bout) for jelly. (Bottom) as above but for chow. Colors correspond to clusters plotted in (A). (n_A =28, n_B =57, n_C=5, unpaired t-test, *p<0.05, **p<0.01, ***p<0.001).

(C) Table summary of tagged and non-tagged HFD units in each cluster.

(D) Relative proportions of each cluster assigned to tagged (left) and non-tagged (right) HFD units.

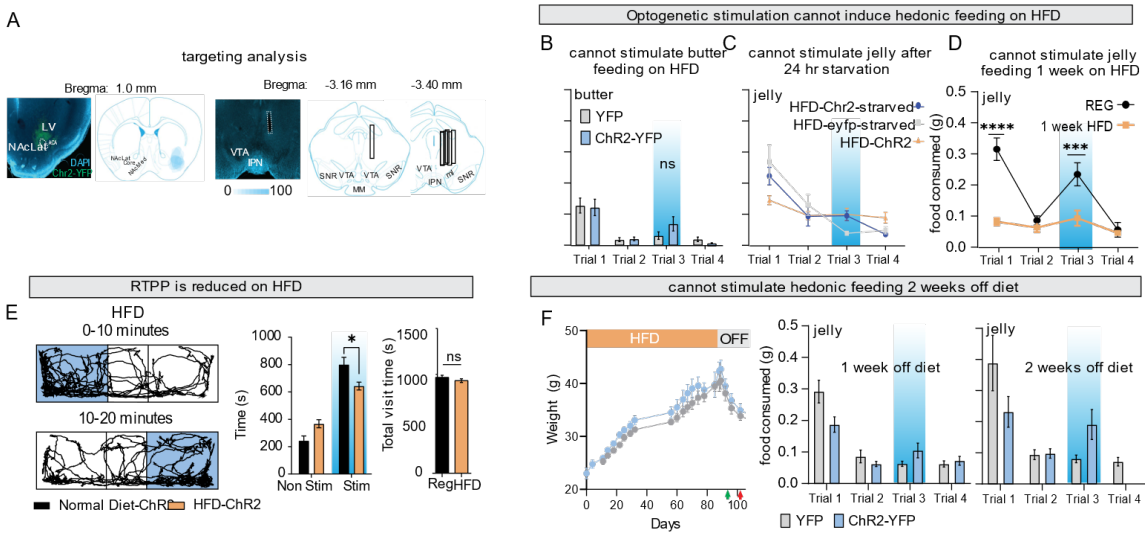

Supplementary Figure 13. Histology and additional optogenetic behavior experiments in HFD mice, Related to Figure 3.

(A) Histological verification of ChR2 injection site in NAcLat (left) and optic fiber implant above VTA (right) showing example image and group analysis summary for experiment in Fig. 3k.

(B) Light stimulation of NAcLat→VTA does not increase butter consumption in HFD compared to REG mice (n_{ChR2}=9, n_{eYFP}=9 mice, 2-way ANOVA, ns).

(C) HFD mice starved for 24 hr did not increase jelly feeding during Trial #3 NAcLat→VTA light stimulation. ($n_{HFD\text{-}ChR2\text{-}starved}$=6, $n_{HFD\text{-}eYFP\text{-}starved}$ =6 mice, $n_{HFD\text{-}ChR2}$ =8 mice 2-way ANOVA, ns).
(D) REG mice increased jelly consumption during NAcLat→VTA light stimulation, but the same group of mice after one week of HFD do not increase jelly consumption during NAcLat→VTA light stimulation (n_{HFD}=8, n_{REG}=8, 2-way ANOVA, ***p<0.01).
(E) Real-time place preference test. (Left) Example track of an HFD mouse in 0-10min and 10-20min during preference test. Blue shading indicates the side of chamber that drives stimulation of NAcLat→VTA when mice enter. (Middle) REG and HFD mice display preference for stimulated side of the chamber. HFD mice spent less time on the stimulated side than REG mice, but total visit time to chambers did not differ (n_{REG}=10, n_{HFD}=8 , 2-way ANOVA, *p<0.05).
(F) Weight change over time in eYFP and ChR2 mice on HFD and OFF HFD (n_{YFP}=7, n_{ChR2}=8).
(G) Light stimulation of NAcLat→VTA in Trial #3 does not increase jelly consumption in HFD mice that were OFF HFD for 1 and 2 weeks (n_{YFP}=7, n_{ChR2}=8, RM 2-way ANOVA, ns).

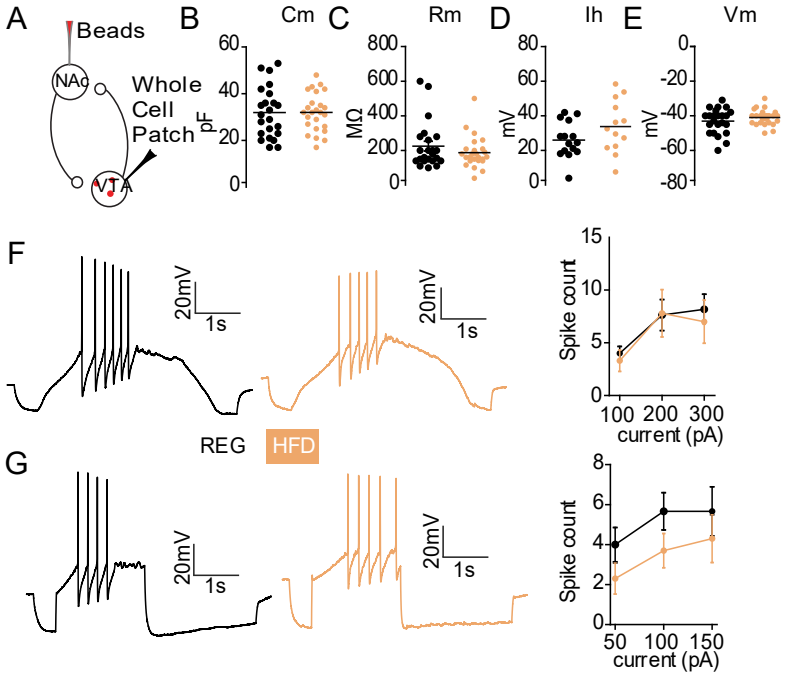

Supplementary Figure 14. Electrophysiology of VTA DA that project to NAcLat in REG and HFD, Related to Figure 3.
(A) Experimental design for whole-cell patch clamp recordings.
(B) Membrane capacitance in beads-labelled VTA DA cells that project to NAcLat does not differ between REG and HFD (Unpaired t-test, ns, n_{REG}=17, n_{HFD}=14 cells).
(C) Membrane resistance in beads-labelled VTA DA cells that project to NAcLat does not differ between REG and HFD (Unpaired t-test, ns, n_{REG}=17, n_{HFD}=14 cells).
(D) Hyperpolarization-activated cation current in beads-labelled VTA DA cells that project to NAcLat does not differ between REG and HFD (Unpaired t-test, ns, n_{REG}=17, n_{HFD}=14 cells).

(E) Resting membrane potential in beads-labelled VTA DA cells that project to NAcLat does not differ between REG and HFD (Unpaired t-test, ns, n_{REG}=17, n_{HFD}=14 cells).
(F) (Left) Example traces from REG and HFD beads-labelled VTA DA cells that project to NAcLat during current ramp injection. (Right) No difference in number of spikes evoked between REG and HFD cells (2-way RM ANOVA, ns n_{REG}=17, n_{HFD}=14 cells).
(G) (Left) Example traces from REG and HFD beads-labelled VTA DA cells that project to NAcLat during current step injection. (Right) No difference in number of spikes evoked between REG and HFD cells (2-way RM ANOVA, ns n_{REG}=17, n_{HFD}=14 cells).

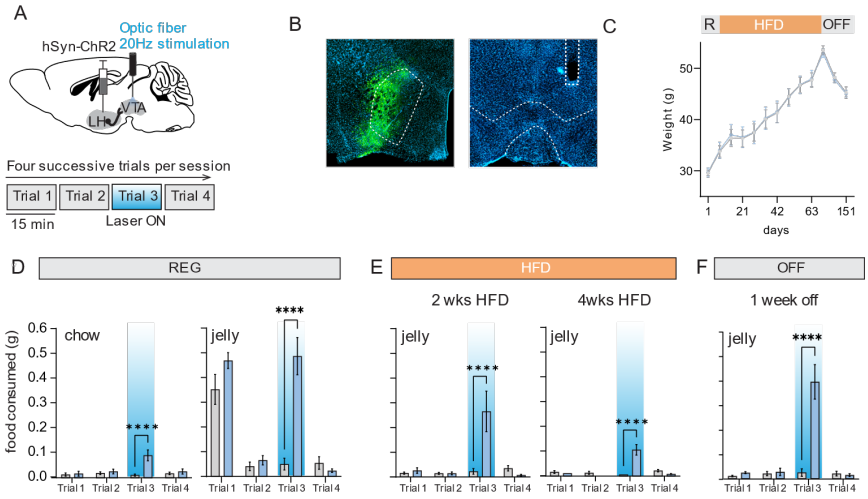

Supplementary Figure 15. Optogenetic feeding behavior in LH→VTA in REG and HFD, Related to Figure 3.
(A) Surgical schematic and feeding experiment design
(B) Example image of ChR2 virus expression in lateral hypothalamus (LH; left) and optic fiber implant above VTA (right).
(C) Body weight of ChR2 and eYFP mice during REG, HFD and OFF HFD (n_{eYFP}=7, n_{ChR2}=8).
(D) Optogenetic stimulation of LH→VTA promotes the consumption of chow (left) and jelly (right) during Trial #3 in REG mice (n_{eYFP}=7, n_{ChR2}=8, 2-way RM ANOVA, ****p<0.001).
(E) Optogenetic stimulation of LH→VTA promotes the consumption of jelly during Trial #3 in HFD mice on HFD for 2 and 4 weeks (n_{eYFP}=7, n_{ChR2}=8, 2-way RM ANOVA, ****p<0.001).
(F) Optogenetic stimulation of LH→VTA promotes the consumption of jelly in mice OFF HFD for one week (n_{eYFP}=7, n_{ChR2}=8, 2-way RM ANOVA, ****p<0.001).

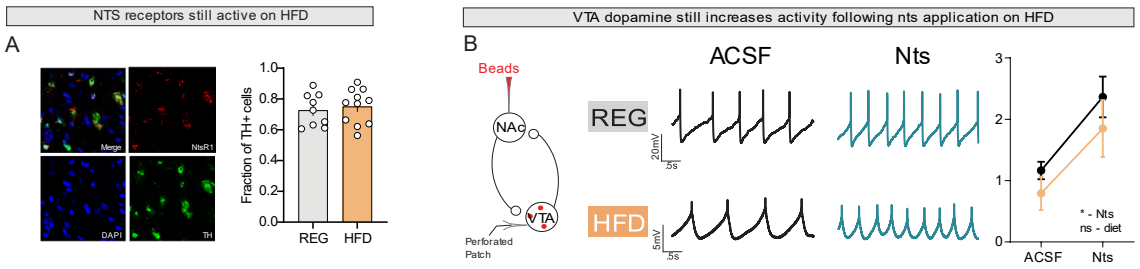

Supplementary Figure 16. Neurotensin receptor expression and function in VTA DA is not altered by HFD, Related to Figure 4.

(A) Left: Example image of fluorescent *in situ* hybridization of probes for DAPI (blue), NtsR1 (red), and TH (green). Right: Fraction of VTA TH+ cells that are also NtsR1+ does not differ between REG and HFD.
(B) Left: Experiment design for perforated patch experiment. Middle: Example recordings of VTA DA activity in REG (top) and HFD (bottom) in normal ACSF (left) or in the presence of 1µM ACSF. Right: Nts increases firing of VTA DA neurons and does not differ between REG and HFD. (2-way RM ANOVA **** effect of Nts, no significant multiple comparisons).

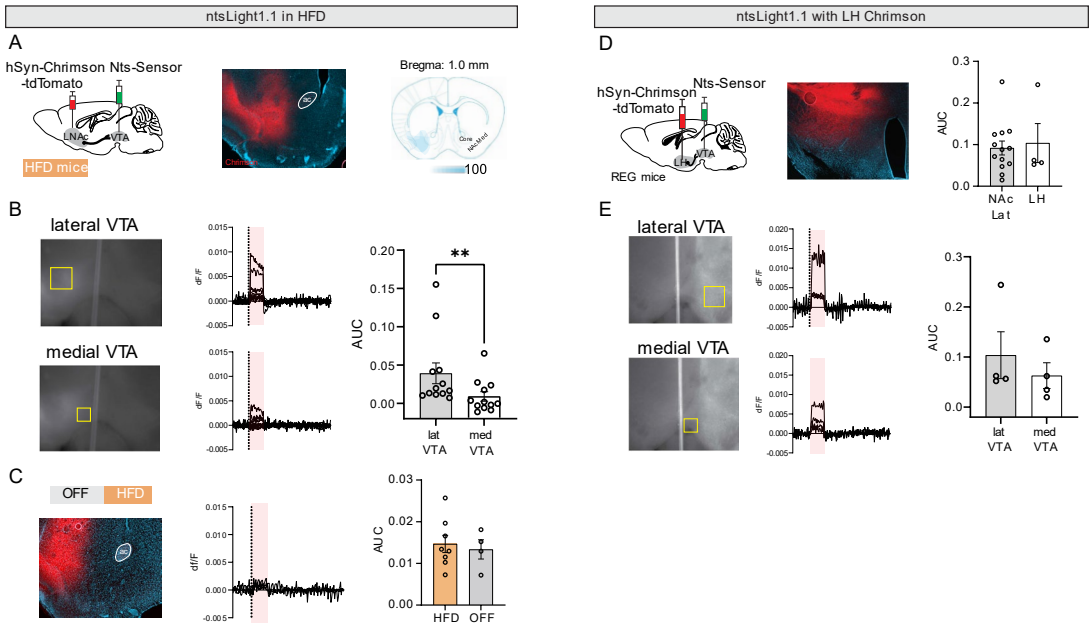

Supplementary Figure 17. Additional ntsLight1.1 recordings in HFD NAcLat→VTA and LH→VTA, Related to Figure 4.
(A) Left: Surgical schematic for ntsLight1.1 imaging in HFD mice. Middle: Example Chrimson virus expression in NAcLat. Right: Summary of group Chrimson virus expression.
(B) Left: Example ROIs from VTA subregions slice taken from HFD mouse. Middle: ntsLight1.1 imaging before, during, and after Chrimson light stimulation in lateral VTA (top) and medial VTA (bottom). Right: Area under the curve during Chrimson light stimulation reveals larger ntsLight1.1 fluorescence in lateral VTA compared to medial VTA. (n = 12 slices from 3 mice, paired t-test, **p<0.01)
(C) Left: Example image of Chrimson virus expression in an OFF HFD mouse. Middle: ntsLight1.1 imaging before, during, and after Chrimson light stimulation in lateral VTA. Right: Area under the curve during Chrimson light stimulation is not different in lateral VTA of HFD mice compared to OFF HFD mice. (n_{HFD}=8 slices from 2 mice, n_{OFF}=4 slices from 1 mouse).
(D) Left: Surgical schematic for ntsLight1.1 imaging in REG mice with Chrimson injected into lateral hypothalamus (LH). Middle: Example Chrimson virus expression in LH. Right: Area under the curve during Chrimson light stimulation in the lateral VTA is not different between mice with NAcLat Chrimson compared to mice with LH Chrimson. (n_{NAcLat}=14 slices from 5 mice, n_{LH}=4 slices from 1 mouse).
(E) Left: Example ROIs from VTA subregions slice taken from REG mouse with LH Chrimson. Middle: ntsLight1.1 imaging before, during, and after Chrimson light stimulation in lateral VTA

(top) and medial VTA (bottom). Right: Area under the curve during Chrimson light stimulation reveals no difference in ntsLight1.1 fluorescence in lateral VTA compared to medial VTA. (n = 4 slices from 1 mouse, paired t-test).

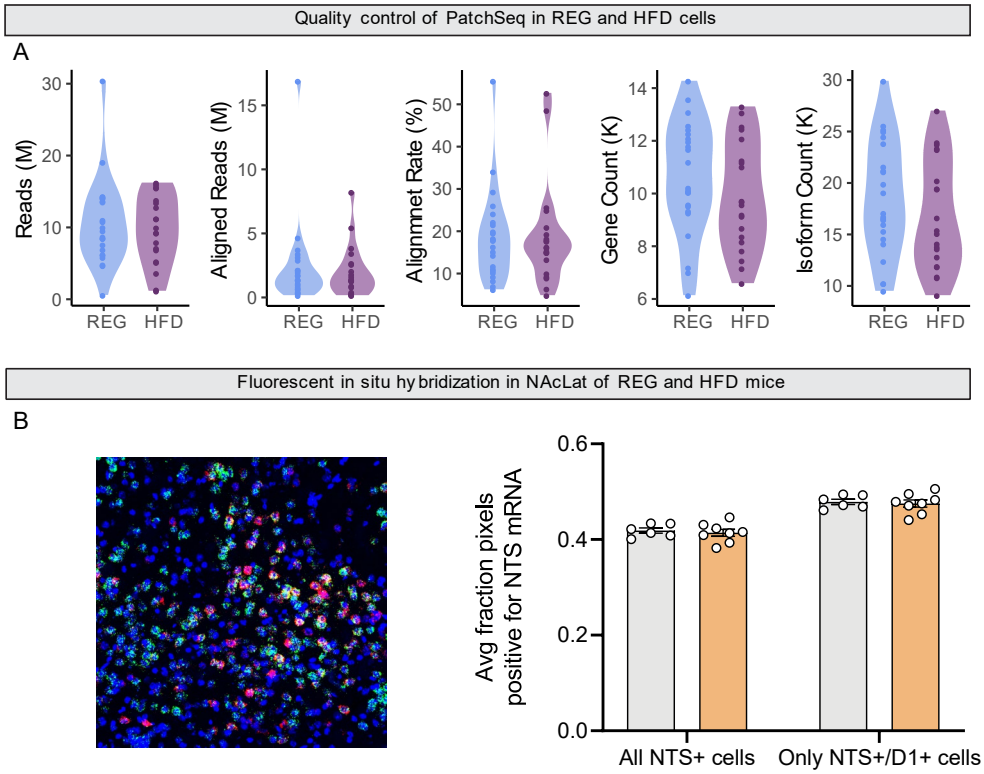

Supplementary Figure 18. Additional RNAseq metrics and fluorescent *in situ* hybridization in NAcLat of REG and HFD mice, Related to Figure 4.

(A) Violin plots of REG (blue) and HFD (purple) cells show no difference in metrics for quality of RNA sequencing between groups. From left to right, number of gene reads (M, million), number of aligned reads (million), alignment rate (%), gene count (K, thousand), isoform count (K, thousand). The violin plots show reads, aligned reads, alignment rate, gene count, and isoform count.

(B) Left: Example image of fluorescent *in situ* hybridization experiment in NAcLAt staining for DAPI (blue), Drd1 (green), and Nts (red). Right: Amount of Nts mRNA detected does not differ between REG (gray) and HFD (orange) NAcLat cells within all NTS+ cells as well as within NTS+ cells that also express D1+.

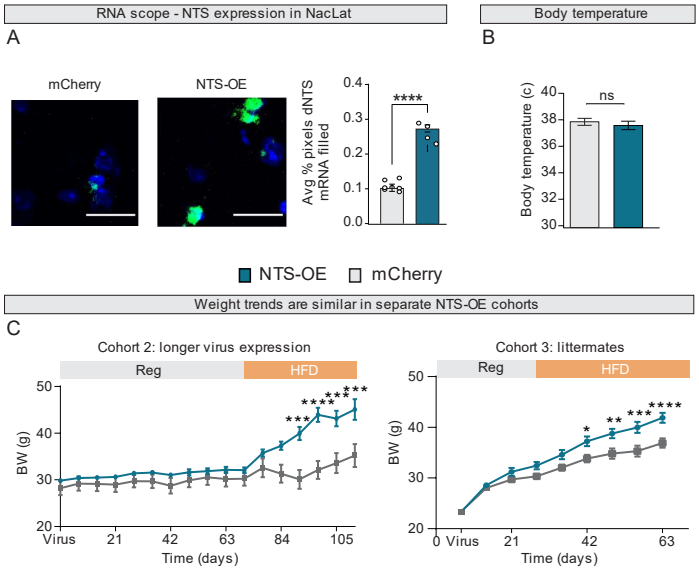

Supplementary Figure 19. Additional experiments in NTS-OE, Related to Figure 4.
(A) Left: Example images of fluorescent *in situ* hybridization in NAcLat of NTS-OE and mCherry control mice stained for DAPI (blue) and Nts (green) (scale bar: 20µm). Right: NTS-OE NTS+ NAcLat cells express more Nts than NTS+ cells in mCherry control mice. (cells quantified from $n_{mCherry}$=7,n_{NTSOE}= 4 images)
(B) Body temperature does not differ between HFD mice expressing NTS-OE or mCherry, corresponds to cohort in Fig. 4 (n_{eYFP} =10, n_{ChR2}=14, unpaired t-test, ns).
(C) Attenuated weight gain in HFD mice with NTS-OE compared to mCherry mice was observed in two additional cohorts of mice. Left: Mice expressed virus for longer on REG diet before switching to HFD ($n_{mCherry}$=4, n_{NTS-OE}=5, RM 2-way ANOVA, ***p<0.001, ****p<0.0001). Right: mCherry and NTS-OE mice were present in the same homecages ($n_{mCherry}$=9, n_{NTS-OE}=10, RM 2-way ANOVA, *p<0.05, **p<0.01,***p<0.001, ****p<0.0001).

SUPPLEMENTARY DATA TABLE

Table S1. TABLE OF STATISTICAL TEST OUTCOMES

Data	Mean ± SEM	Statistical Test	N	Outcome measure	p value
Fig 1d Chocolate	**eYFP:** 0.3179 ± 0.030 0.0041 ± 0.003 0.011 ± 0.007 0.023 ± 0.012 **ChR2:** 0.263 ± 0.041 0.051 ± 0.026 0.198 ± 0.066 0.020 ± 0.009	Two-way RM ANOVA with Holm-Šídák's multiple comparisons test	**eYFP:** n = 9 mice **ChR2:** n = 10 mice	Chocolate consumed	Effect of Trial: p <0.0001, F (3, 51) = 26.99 Effect of Virus type: p=0.0427, F (1, 17) = 4.801 Interaction: p=0.0060, F (3, 51) = 4.646 Multiple Comparisons: Trial 1: p=0.5589 Trial 2: p=0.5589 Trial 3: p=0.0006 Trial 4: p=0.9429
Fig 1d Butter	**eYFP:** 0.099 ± 0.012 0.043 ± 0.011 0.042 ± 0.014 0.035 ± 0.013 **ChR2:** 0.125 ± 0.020 0.034 ± 0.009 0.168 ± 0.069 0.024 ± 0.009	Two-way RM ANOVA with Holm-Šídák's multiple comparisons test	**eYFP:** n = 9 mice **ChR2:** n = 10 mice	Butter consumed	Effect of Trial: p=0.0086, F (3, 51) = 4.321 Effect of Virus type: p=0.0817, F (1, 17) = 3.424 Interaction: p=0.0844, F (3, 51) = 2.338 Multiple Comparisons: Trial 1: p=0.8906 Trial 2: p=0.9551 Trial 3: p=0.0109 Trial 4: p=0.9551
Fig 1d Peanut butter	**eYFP:** 0.094 ± 0.016 0.041 ± 0.010 0.025 ± 0.014 0.039 ± 0.013 **ChR2:** 0.137 ± 0.037 0.062 ± 0.009 0.146 ± 0.061 0.018 ± 0.009	Two-way RM ANOVA with Holm-Šídák's multiple comparisons test	**eYFP:** n = 9 mice **ChR2:** n = 10 mice	Peanut butter consumed	Effect of Trial: p=0.0170, F (3, 51) = 3.721 Effect of Virus type: p=0.0671, F (1, 17) = 3.825 Interaction: p=0.0955, F (3, 51) = 2.233 Multiple Comparisons: Trial 1: p=0.6321 Trial 2: p=0.8348 Trial 3: p=0.0151 Trial 4: p=0.8348
Fig 1d Jelly	**eYFP:** 0.308 ± 0.040 0.109 ± 0.017 0.111 ± 0.014 0.079 ± 0.007 **ChR2:** 0.329 ± 0.072 0.124 ± 0.015 0.290 ± 0.054 0.070 ± 0.013	Two-way RM ANOVA with Holm-Šídák's multiple comparisons test	**eYFP:** n = 9 mice **ChR2:** n = 10 mice	Jelly consumed	Effect of Trial: p<0.0001, F (3, 48) = 14.10 Effect of Virus type: p=0.0563, F (1, 16) = 4.233 Interaction: p=0.0942, F (3, 48) = 2.253 Multiple Comparisons: Trial 1: p=0.9730 Trial 2: p=0.9730 Trial 3: p=0.0081 Trial 4: p=0.9730
Fig 1e Chow	**eYFP:** 0.026 ± 0.007 0.027 ± 0.006 0.038 ± 0.009 0.040 ± 0.012 **ChR2:** 0.028 ± 0.013 0.030 ± 0.008 0.064 ± 0.020 0.019 ± 0.008	Two-way RM ANOVA with Holm-Šídák's multiple comparisons test	**eYFP:** n = 9 mice **ChR2:** n = 10 mice	Chow consumed	Effect of Trial: p=0.0721, F (3, 51) = 2.474 Effect of Virus type: p=0.8239, F (1, 17) = 0.05107 Interaction: p=0.1651, F (3, 51) = 1.767 Multiple Comparisons: No significant differences

Data	Mean ± SEM	Statistical Test	N	Outcome measure	p value
Fig 1e **Butter + Quinine**	**eYFP:** 0.070 ± 0.016 0.041 ± 0.016 0.033 ± 0.018 0.037 ± 0.019 **ChR2:** 0.074 ± 0.017 0.059 ± 0.017 0.053 ± 0.018 0.040 ± 0.018	Two-way RM ANOVA with Holm-Šídák's multiple comparisons test	**eYFP:** n= 7 mice **ChR2:** n = 7 mice	Bitter butter consumed	Effect of Trial: p<0.0001, F (3, 36) = 19.98 Effect of Virus type: p=0.6431, F (1, 12) = 0.2259 Interaction: p=0.1430, F (3, 36) = 1.925 Multiple Comparisons: No significant differences
Fig 1f **24hr starvation (Bottom)**	Trial 1: 0.072 ± 0.020 Trial 2: 0.046 ± 0.014 Trial 3: 0.037 ± 0.010 Trial 4: 0.048 ± 0.022	One-way RM ANOVA with Holm-Šídák's multiple comparisons test	n = 7 mice	Chow consumed	Effect of Trial: p= 0.3556, F (1.364, 8.186) = 1.076 Multiple Comparisons: No significant differences
Fig 1l **Firing pre and during bout (Chow)**	**Pre:** 4.037 ± 1.031 **Bout:** 4.632 ± 1.062	Paired t-test	n = 17 opto-tagged units	Average unit firing rate	p=0.1235, two-tailed, t=1.626, df=16
Fig 1l **Firing during bout and post (Chow)**	**Bout:** 5.012 ± 1.131 **Post:** 4.304 ± 1.075	Paired t-test	n = 17 opto-tagged units	Average unit firing rate	p= 0.2020, two-tailed, t=1.331, df=16
Fig 1l **Firing pre and during bout (Jelly)**	**Pre:** 4.209 ± 1.305 **Bout:** 6.524 ± 1.767	Paired t-test	n = 17 opto-tagged units	Average unit firing rate	p= 0.0037, two-tailed, t=3.399, df=16
Fig 1l **Firing during bout and post (Jelly)**	**Bout:** 5.881 ± 1.551 **Post:** 4.94 ± 1.479	Paired t-test	n = 17 opto-tagged units	Average unit firing rate	p= 0.0465, two-tailed, t=2.158, df=16
Fig 2a **Gene expression**	Hcrt: 0 ± 0 Ins1: 0 ± 0 Ins2: 0 ± 0 Pmch: 0 ± 0 Agrp: 0 ± 0 Lep: 0.0119 ± 0.0114 Trh: 0.0757 ± 0.0725 Crh: 0.143 ± 0.1 Igf1: 0.196 ± 0.0545 Cartpt: 0.291 ± 0.115 Pomc: 0.393 ± 0.127 Npy: 0.409 ± 0.183 Bdnf: 0.641 ± 0.0746 Oxt: 0.666 ± 0.14 Penk: 1.28 ± 0.153 Nts: 2.42 ± 0.209 Pdyn: 2.61 ± 0.0812	One-way RM ANOVA with Holm-Šídák's multiple comparisons test	n = 24 cells	Log transcripts per million	P<0.0001, F (5.139, 118.2) = 63.57 Multiple Comparisons: Nts vs. Hcrt: p<0.0001 Nts vs. Ins1: p<0.0001 Nts vs. Ins2: p <0.0001 Nts vs. Pmch: p <0.0001 Nts vs. Agrp: p <0.0001 Nts vs. Lep: p <0.0001 Nts vs. Trh: p <0.0001 Nts vs. Crh: p <0.0001 Nts vs. Igf1: p <0.0001 Nts vs. Cartpt: p <0.0001 Nts vs. Pomc: p <0.0001 Nts vs. Npy: p <0.0001 Nts vs. Bdnf: p <0.0001 Nts vs. Oxt: p <0.0001 Nts vs. Penk: p = 0.0013 Nts vs. Pdyn: p = 0.4015
Fig 2b **ntsLight1.1**	**REG:** 0.092 ± 0.017 **REG Sensor only:** 0.004 ± 0.004	Unpaired t-test with Welch's correction	**REG:** n= 13 slices from 5 mice **REG sensor only:** n = 3 slices from 1 mouse	Area under the curve during light stimulation	p=0.0002, two-tailed, t=5.107, df=13.05

Data	Mean ± SEM	Statistical Test	N	Outcome measure	p value
Fig 2c VTA DA whole cell patch	**ACSF:** 0.944 ± 0.487 2.527 ± 0.782 0.823 ± 0.415 **SR142948:** 0.905 ± 0.314 0.617 ± 0.255 0.904 ± 0.363	Two-way RM ANOVA with Holm-Šídák's multiple comparisons test	**ACSF**: n = 11 cells **SR142948:** n = 12 cells	Frequency of action potential firing (Hz)	Effect of Stimulation: p<0.0001, F (2, 42) = 18.58 Effect of Drug: p=0.3198, F (1, 21) = 1.038 Interaction: p<0.0001, F (2, 42) = 18.58 Multiple Comparisons: Off: p=0.9903 On: p=0.0132 Off: p=0.9903
Fig 2d Optogenetic feeding behavior + pharmacology (Saline)	**eYFP:** 0.261 ± 0.030 0.159 ± 0.022 0.139 ± 0.020 0.151 ± 0.016 **ChR2:** 0.405 ± 0.079 0.133 ± 0.014 0.321 ± 0.047 0.118 ± 0.013	Two-way RM ANOVA with Holm-Šídák's multiple comparisons test	**eYFP:** n = 10 mice **ChR2:** n = 7 mice	Jelly consumed	Effect of Trial: p<0.0001, F (3, 45) = 14.31 Effect of Virus type: p=0.0087, F (1, 15) = 9.081 Interaction: p=0.0031, F (3, 45) = 5.355 Multiple Comparisons: Trial 1: p=0.0104 Trial 2: p=0.7325 Trial 3: p=0.0013 Trial 4: p=0.7325
Fig 2d Optogenetic feeding behavior + pharmacology (SR142948)	**eYFP:** 0.287 ± 0.040 0.174 ± 0.032 0.135 ± 0.017 0.127 ± 0.016 **ChR2:** 0.266 ± 0.046 0.144 ± 0.015 0.180 ± 0.019 0.130 ± 0.026	Two-way RM ANOVA with Holm-Šídák's multiple comparisons test	**eYFP:** n = 10 mice **ChR2:** n = 7 mice	Jelly consumed	Effect of Trial: p<0.0001, F (3, 45) = 10.13 Effect of Virus type: p=0.9788, F (1, 15) = 0.0007277 Interaction: p=0.5918, F (3, 45) = 0.6423 Multiple Comparisons: Trial 1: p=0.8612 Trial 2: p=0.8588 Trial 3: p=0.7477 Trial 4: p=0.9370

Data	Mean ± SEM	Statistical Test	N	Outcome measure	p value
Fig 3b **Diet-induced weight gain**	**REG:** 21.211 ± 0.444 21.910 ± 0.436 22.332 ± 0.532 22.422 ± 0.538 22.943 ± 0.657 23.112 ± 0.664 23.860 ± 0.677 24.061 ± 0.728 24.464 ± 0.696 24.472 ± 0.729 25.086 ± 0.771 25.393 ± 0.872 25.328 ± 0.798 25.399 ± 0.858 25.837 ± 0.839 26.679 ± 0.928 26.867 ± 0.833 26.576 ± 0.820 26.584 ± 0.899 26.554 ± 0.888 27.039 ± 0.868 27.572 ± 0.747 27.892 ± 0.877 27.726 ± 0.942 27.917 ± 0.888 28.494 ± 0.828 28.430 ± 0.912 28.898 ± 0.940 28.941 ± 0.969 **HFD:** 21.515 ± 0.379 23.459 ± 0.450 24.775 ± 0.513 25.650 ± 0.603 26.644 ± 0.643 27.671 ± 0.678 29.078 ± 0.755 29.824 ± 0.813 31.356 ± 0.903 32.203 ± 0.961 33.409 ± 0.964 34.450 ± 1.065 35.814 ± 1.024 37.494 ± 1.102 39.263 ± 1.198 40.236 ± 1.183 41.354 ± 1.163 41.817 ± 1.138 43.412 ± 1.080 44.096 ± 1.090 45.082 ± 1.038 45.337 ± 1.017 45.275 ± 1.040 45.389 ± 1.058 45.362 ± 1.131 45.444 ± 1.113 45.574 ± 1.150 45.139 ± 1.149 45.432 ± 1.214	Two-way RM ANOVA	**REG:** n= 9 mice **HFD:** n = 19 mice	Body weight	Effect of Time: p<0.0001, F (28, 728) = 241.4 Effect of Diet: p<0.0001, F (1, 26) = 66.09 Interaction: p<0.0001, F (28, 728) = 80.68
Fig 3c **Acute food consumption by diet type (Standard chow)**	**REG:** 0.022 ± 0.002 **HFD:** 0.026 ± 0.001	Unpaired t-test	**REG:** n = 11 mice **HFD:** n = 19 mice	Standard chow consumed	p=0.0869, two-tailed, t=1.774, df=28

Data	Mean ± SEM	Statistical Test	N	Outcome measure	p value
Fig 3c Acute food consumption by diet type (High fat chow)	**REG:** 0.046 ± 0.012 **HFD:** 0.006 ± 0.003	Unpaired t-test	**REG:** n = 11 mice **HFD:** n = 19 mice	High fat chow consumed	p=0.0004, two-tailed, t=4.005, df=28
Fig 3c Acute food consumption by diet type (Chocolate)	**REG:** 0.069 ± 0.029 **HFD:** 0.003 ± 0.002	Unpaired t-test	**REG:** n = 11 mice **HFD:** n = 19 mice	Chocolate consumed	p=0.0052, two-tailed, t=3.034 df=28
Fig 3c Acute food consumption by diet type (Butter)	**REG:** 0.153 ± 0.041 **HFD:** 0.048 ± 0.011	Unpaired t-test	**REG:** n = 11 mice **HFD:** n = 19 mice	Butter consumed	p=0.0048, two-tailed, t=3.066 df=28
Fig 3c Acute food consumption by diet type (Jelly)	**REG:** 0.341 ± 0.061 **HFD:** 0.076 ± 0.010	Unpaired t-test	**REG:** n = 11 mice **HFD:** n = 19 mice	Jelly consumed	p<0.0001, two-tailed, t=5.611, df=28
Fig 3g HFD R^2 of regression	**Chow:** 0.098 ± 0.034 **Jelly:** 0.077 ± 0.039	Paired t-test	n = 12 opto-tagged units	R^2 of regression between food consumed and unit firing	p = 0.6616, two-tailed, t=0.4498, df=11
Fig 3h Diet effect on R^2 of regression	**REG:** 0.236 ± 0.042 **HFD:** 0.096 ± 0.036	Unpaired t-test	**REG:** n = 19 opto-tagged units **HFD:** n = 16 opto-tagged units	R^2 of regression between jelly consumed and unit firing	p=0.0196, two-tailed, t=2.454, df=33
Fig 3i Firing pre and during bout (Chow)	**Pre:** 7.342 ± 2.664 **Bout:** 8.632 ± 3.316	Paired t-test	n = 12 opto-tagged units	Average unit firing rate	p=0.2868, two-tailed, t=1.119, df=11
Fig 3i Firing during bout and post (Chow)	**Bout:** 7.607 ± 2.573 **Post:** 7.226 ± 2.409	Paired t-test	n = 12 opto-tagged units	Average unit firing rate	p=0.3940, two-tailed, t=0.8871, df=11
Fig 3i Firing pre and during bout (Jelly)	**Pre:** 5.994 ± 2.136 **Bout:** 6.079 ± 2.07	Paired t-test	n = 15 opto-tagged units	Average unit firing rate	p= 0.7680, two-tailed, t=0.3007, df=14
Fig 3i Firing during bout and post (Jelly)	**Pre:** 7.952 ± 2.259 **Bout:** 6.453 ± 2.101	Paired t-test	n = 15 opto-tagged units	Average unit firing rate	p= 0.2441, two-tailed, t=1.216, df=14
Fig 3j VTA DA whole cell patch	**REG:** 1.231 ± 0.221 1.675 ± 0.350 1.225 ± 0.206 **HFD:** 0.862 ± 0.157 0.857 ± 0.156 0.886 ± 0.149	Two-way RM ANOVA with Holm-Šídák's multiple comparisons test	**REG:** n = 16 cells **HFD:** n = 21 cells	Frequency of action potential firing (Hz)	Effect of Stimulation: p=0.0572, F (2, 70) = 2.981 Effect of Diet type: p=0.0651, F (1, 35) = 3.628 Interaction: p=0.0367, F (2, 70) = 3.467 Multiple Comparisons: Off: p=0.3735 On: p=0.0180 Off: p=0.3735

Data	Mean ± SEM	Statistical Test	N	Outcome measure	p value
Fig 3k Optogenetic feeding behavior (On HFD)	**eYFP:** 0.105 ± 0.028 0.104 ± 0.027 0.156 ± 0.032 0.097 ± 0.018 **ChR2:** 0.147 ± 0.014 0.098 ± 0.013 0.102 ± 0.020 0.091 ± 0.017	Two-way RM ANOVA with Holm-Šídák's multiple comparisons test	**eYFP:** n = 7 mice **ChR2:** n = 8 mice	Jelly consumed	Effect of Trial: p=0.3398, F (3, 39) = 1.153 Effect of Diet type: p=0.6187, F (1, 13) = 0.2600 Interaction: p=0.2443, F (3, 39) = 1.446 Multiple Comparisons: No significant differences
Fig 3k Optogenetic feeding behavior (Off HFD)	**eYFP:** 0.260 ± 0.036 0.122 ± 0.032 0.065 ± 0.015 0.056 ± 0.010 **ChR2:** 0.187 ± 0.020 0.072 ± 0.010 0.169 ± 0.035 0.039 ± 0.005	Two-way RM ANOVA with Holm-Šídák's multiple comparisons test	**eYFP:** n = 7 mice **ChR2:** n = 8 mice	Jelly consumed	Effect of Trial: p<0.0001, F (3, 39) = 22.15 Effect of Diet type: p=0.6402, F (1, 13) = 0.2291 Interaction: p=0.0014, F (3, 39) = 6.257 Multiple Comparisons: Trial 1: p=0.0903 Trial 2: p=0.2494 Trial 3: p=0.0102 Trial 4: p=0.6209
Fig 4d REG vs HFD Ntslight1.1	**REG:** 0.092 ± 0.017 **HFD:** 0.039 ± 0.014	Unpaired t-test	**REG:** n = 13 slices from 5 mice **HFD:** n = 12 slices from 4 mice	Area under the curve during light stimulation	p= 0.0244, two-tailed, t=2.409, df=23
Fig 4f Optogenetic feeding behavior in HFD NTS-OE and HFD mCherry	**mCherry:** 0.063 ± 0.015 0.058 ± 0.020 0.059 ± 0.008 0.036 ± 0.006 **NTS-OE:** 0.162 ± 0.037 0.083 ± 0.026 0.132 ± 0.035 0.053 ± 0.011	Two-way RM ANOVA with Holm-Šídák's multiple comparisons test	**mCherry:** n = 8 mice **NTS-OE:** n = 6 mice	Jelly consumed	Effect of Trial: p=0.0193, F (3, 36) = 3.749 Effect of Virus type: p=0.0016, F (1, 12) = 16.45 Interaction: p=0.1956, F (3, 36) = 1.648 Multiple Comparisons: Trial 1: p=0.0060 Trial 2: p=0.6212 Trial 3: p=0.0496 Trial 4: p=0.6212
Fig 4h Acute feeding during diet changes	**mCherry:** 0.395 ± 0.032 0.108 ± 0.017 0.107 ± 0.010 0.309 ± 0.035 0.439 ± 0.035 **NTS-OE:** 0.424 ± 0.027 0.231 ± 0.031 0.195 ± 0.025 0.471 ± 0.034 0.409 ± 0.030	Two-way RM ANOVA with Holm-Šídák's multiple comparisons test	**mCherry:** n = 10 mice **NTS-OE:** n = 14 mice	Jelly consumed	Effect of Diet: p<0.0001, F (4, 88) = 67.76 Effect of Virus type: p=0.0199, F (1, 22) = 6.299 Interaction: p=0.0008, F (4, 88) = 5.253 Multiple Comparisons: REG: p=0.7307 HFD1: p=0.0167 HFD2: p=0.1098 OFF1: p=0.0009 OFF2: p=0.7307

Data	Mean ± SEM	Statistical Test	N	Outcome measure	p value
Fig 4j Body weight during diet changes	**mCherry:** 0: 25.54 ± 0.90 7: 25.80 ± 0.88 14: 26.85 ± 0.83 21: 27.43 ± 0.77 28: 27.28 ± 0.78 35: 30.26 ± 0.79 42: 33.49 ± 0.98 49: 36.34 ± 1.03 56: 38.74 ± 1.11 61: 39.21 ± 1.03 63: 37.51 ± 1.03 70: 34.77 ± 0.95 77: 33.53 ± 0.83 84: 33.26 ± 0.82 **NTS-OE:** 0: 25.48 ± 0.74 7: 26.34 ± 0.56 14: 27.09 ± 0.48 21: 27.49 ± 0.46 28: 27.65 ± 0.56 35: 29.71 ± 0.50 42: 31.23 ± 0.50 49: 33.59 ± 0.56 56: 35.33 ± 0.73 61: 35.94 ± 0.77 63: 34.31 ± 0.73 70: 32.72 ± 0.53 77: 32.35 ± 0.48 84: 32.47 ± 0.54	Two-way RM ANOVA with Holm-Šídák's multiple comparisons test	**mCherry:** n = 10 mice **NTS-OE:** n = 14 mice	Body weight	Effect of Time: p<0.0001, F (13, 286) = 245.1 Effect of Virus type: p=0.1628, F (1, 22) = 2.086 Interaction: p<0.0001, F (13, 286) = 7.557 <u>Multiple Comparisons:</u> 0: p=0.9972 7: p=0.9960 14: p=0.9960 21: p=0.9972 28: p=0.9960 35: p=0.9960 42: p=0.2680 49: p=0.0929 56: p=0.0167 61: p=0.0243 63: p=0.0274 70: p=0.3715 77: p=0.9077 84: p=0.9844
Supp. Fig 2b Optogenetic frequency effect on feeding behavior	**1 Hz:** 0.104 ± 0.0244 **10 Hz:** 0.143 ± 0.0167 **20 Hz:** 0.29 ± 0.0542	One-way RM ANOVA with Holm-Šídák's multiple comparisons test	n = 10 mice	Jelly consumed	Effect of Frequency: p=0.0071, F (1.376, 12.38) = 8.925 <u>Multiple Comparisons:</u> 1 vs 10 Hz: p=0.1785 1 vs 20 Hz: p=0.0241 10 vs 20 Hz: p=0.0400
Supp. Fig 2c Optogenetic effect on Trial #1 feeding behavior	**eYFP:** Day 1: 0.332 ± 0.043 Day 2: 0.397 ± 0.023 **ChR2:** Day 1: 0.359 ± 0.047 Day 2: 0.655 ± 0.078	Two-way RM ANOVA with Holm-Šídák's multiple comparisons test	**eYFP:** n = 8 mice **ChR2:** n = 10 mice	Jelly consumed	Effect of Stimulation: p=0.0152, F (1, 16) = 7.380 Effect of Virus type: p=0.0038, F (1, 16) = 11.43 Interaction: p=0.1018, F (1, 16) = 3.014 <u>Multiple Comparisons:</u> Day 1: p=0.7325 Day 2: p=0.0051
Supp. Fig 2d ChR2 and eYFP body weight	**eYFP:** Before: 28.833 ± 0.666 After: 28.867 ± 0.663 **ChR2:** 29.110 ± 0.846 29.020 ± 0.730	Two-way RM ANOVA with Holm-Šídák's multiple comparisons test	**eYFP:** n = 9 mice **ChR2:** n = 10 mice	Body weight	Effect of Time: p=0.9359, F (1, 17) = 0.006670 Effect of Virus type: p=0.8301, F (1, 17) = 0.04750 Interaction: p=0.8610, F (1, 17) = 0.03159 <u>Multiple Comparisons:</u> No significant differences
Supp. Fig 2d Cell body optogenetic feeding behavior	0.223 ± 0.029 0.083 ± 0.012 0.086 ± 0.020 0.054 ± 0.018	One-way RM ANOVA with Holm-Šídák's multiple comparisons test	n = 8 mice	Jelly consumed	Effect of Stimulation: p= 0.0006, F (1.907, 13.35) = 13.99 <u>Multiple Comparisons:</u> Trial 1 vs 2: p =0.0209 Trial 1 vs 3: p =0.0116 Trial 1 vs 4: p =0.0149 Trial 2 vs 3: p =0.8540 Trial 2 vs 4: p =0.4378 Trial 3 vs 4: p =0.4378

Data	Mean ± SEM	Statistical Test	N	Outcome measure	p value
Supp. Fig 6a ntsLight lat vs med VTA AUC	**latVTA:** 0.092 ± 0.017 **medVTA:** 0.026 ± 0.004	Paired t-test	n = 13 slices from 5 mice	Area under the curve during light stimulation	p=0.0005, two-tailed, t=4.687, df=12
Supp. Fig 6a ntsLight Red vs Green stim AUC	**Red stim:** 0.07114 ± 0.02559 **Green stim:** 0.02594 ± 0.01145	Paired t-test	n = 8 slices from 3 mice	Area under the curve during light stimulation	p= 0.0394, one-tailed, t=2.056, df=7
Supp. Fig 7a Effect of Nts on VTA DA firing	**Baseline:** 1.300 ± 0.236 **Nts:** 2.530 ± 0.378 **Washout:** 1.542 ± 0.294	One-way RM ANOVA with Holm-Šídák's multiple comparisons test	n = 9 cells	Frequency of action potential firing (Hz)	Effect of Nts: p=0.0032, F (2, 16) = 8.430 Multiple Comparisons: Baseline vs. Nts: p=0.0040 Baseline vs. Washout: p=0.4829 Nts vs. Washout: p=0.0134
Supp. Fig 7a Effect of Nts on VTA GAD firing	**Baseline:** 3.796 ± 0.766 **Nts:** 2.872 ± 1.090	Paired t-test	n = 9 cells	Frequency of action potential firing (Hz)	p= 0.4191, two-tailed, t=0.8519, df=8
Supp. Fig 8a Optogenetic feeding behavior	**eYFP:** 0.306 ± 0.039 0.087 ± 0.030 0.051 ± 0.023 0.043 ± 0.022 **ChR2:** 0.397 ± 0.068 0.100 ± 0.021 0.197 ± 0.051 0.025 ± 0.016	Two-way RM ANOVA with Holm-Šídák's multiple comparisons test	**eYFP:** n = 9 mice **ChR2:** n = 9 mice	High fat diet consumed	Effect of Trial: p<0.0001, F (3, 48) = 22.30 Effect of Virus type: p=0.0016, F (1, 16) = 14.30 Interaction: p=0.2056, F (3, 48) = 1.584 Multiple Comparisons: Trial 1: p=0.2565 Trial 2: p=0.9336 Trial 3: p=0.0316 Trial 4: p=0.9336
Supp. Fig 8b Acute feeding by diet-type	**REG:** 0.442 ± 0.021 **HFD1:** 0.113 ± 0.016 **HFD3:** 0.107 ± 0.024 **OFF1:** 0.302 ± 0.033 **OFF3:** 0.439 ± 0.035	One-way RM ANOVA with Holm-Šídák's multiple comparisons test	n = 10 mice	Jelly consumed	Effect of Diet type: p<0.0001, F (2.694, 24.25) = 59.14 Multiple Comparisons: Reg vs. Hfd1: p<0.0001 Reg vs. Hfd3: p<0.0001 Reg vs. Off1: p=0.0111 Reg vs. Off3: p=0.9213
Supp. Fig 8b Body weight by diet-type	**REG:** 27.300 ± 0.783 **HFD1:** 30.300 ± 0.793 **HFD3:** 36.300 ± 1.030 **OFF1:** 34.800 ± 0.953 **OFF3:** 33.300 ± 0.824	One-way RM ANOVA with Holm-Šídák's multiple comparisons test	n = 10 mice	Body weight	Effect of Diet type: p<0.0001, F (2.404, 21.63) = 181.4 Multiple Comparisons: Reg vs. Hfd1: p<0.0001 Reg vs. Hfd3: p <0.0001 Reg vs. Off1: p <0.0001 Reg vs. Off3: p <0.0001
Supp. Fig 9d Food consumed on Cafeteria-diet (Chow)	**REG:** 0.051 ± 0.004 **CAF:** 0.043 ± 0.002	Unpaired t-test	**REG:** n = 7 mice **CAF:** n = 9 mice	Chow consumed	p=0.0589, two-tailed, t=2.056 df=14
Supp. Fig 9d Food consumed on Cafeteria-diet (Cookies)	**REG:** 0.089 ± 0.029 **CAF:** 0.025 ± 0.003	Unpaired t-test	**REG:** n = 7 mice **CAF:** n = 9 mice	Cookies consumed	p= 0.0230, two-tailed, t=2.553 df=14
Supp. Fig 9d Food consumed on Cafeteria-diet (Chocolate)	**REG:** 0.119 ± 0.024 **CAF:** 0.010 ± 0.005	Unpaired t-test	**REG:** n = 7 mice **CAF:** n = 8 mice	Chocolate consumed	p= 0.0003, two-tailed, t=4.833 df=13

Data	Mean ± SEM	Statistical Test	N	Outcome measure	p value
Supp. Fig 9d Food consumed on Cafeteria-diet (Bacon)	**REG:** 0.177 ± 0.046 **CAF:** 0.084 ± 0.007	Unpaired t-test	**REG:** n = 7 mice **CAF:** n = 8 mice	Bacon consumed	p= 0.0479, two-tailed, t=2.184, df=13
Supp. Fig 9d Food consumed on Cafeteria-diet (Jelly)	**REG:** 0.559 ± 0.090 **CAF:** 0.138 ± 0.031	Unpaired t-test	**REG:** n = 7 mice **CAF:** n = 8 mice	Jelly consumed	p=0.0004, two-tailed, t=4.665 df=13
Supp. Fig 9e Food consumed OFF Cafeteria-diet (Jelly)	**REG:** 0.559 ± 0.090 0.587 ± 0.083 0.597 ± 0.080 **CAF:** 0.173 ± 0.038 0.315 ± 0.072 0.401 ± 0.087	Two-way RM ANOVA with Holm-Šídák's multiple comparisons test	**REG:** n = 7 mice **CAF:** n = 8 mice	Jelly consumed	Effect of Day: p=0.1187, F (2, 26) = 2.316 Effect of Diet-type: p=0.0035, F (1, 13) = 12.63 Interaction: p=0.3270, F (2, 26) = 1.167 Multiple Comparisons: Day 0: p=0.0028 Day 5: p=0.0316 Day 10: p=0.0762
Supp. Fig 10c NAcLat *ex vivo* ephys (# ramp APs)	**REG:** 0.095 ± 0.095 12.238 ± 2.092 30.762 ± 2.620 37.952 ± 3.943 **HFD:** 0.294 ± 0.294 20.588 ± 3.324 29.059 ± 3.486 26.824 ± 4.025	Two-way RM ANOVA with Holm-Šídák's multiple comparisons test	**REG:** n = 21 cells **HFD:** n = 17 cells	Number of action potentials	Effect of Current: p<0.0001, F (3, 108) = 64.84 Effect of Diet type: p=0.6681, F (1, 36) = 0.1869 Interaction: p=0.0038, F (3, 108) = 4.739 Multiple Comparisons: 100pA: p=0.9607 300pA: p=0.1157 500pA: p=0.8933 700pA: p=0.0259
Supp. Fig 10d NAcLat *ex vivo* ephys (membrane capacitance)	**REG:** 88.80 ± 4.92 **HFD:** 81.70 ± 4.15	Unpaired t-test	**REG:** n = 21 cells **HFD:** n = 20 cells	Membrane capacitance	p= 0.2785, two-tailed, t=1.099, df=39
Supp. Fig 10e NAcLat *ex vivo* ephys (membrane resistance)	**REG:** 132 ± 13.8 **HFD:** 126 ± 9.28	Unpaired t-test	**REG:** n = 21 cells **HFD:** n = 20 cells	Membrane resistance	p=0.7047, two-tailed, t=0.3817, df=39
Supp. Fig 10f NAcLat *ex vivo* ephys (resting membrane potential)	**REG:** -78.5 ± 1.6 **HFD:** -78.9 ± 1.11	Unpaired t-test	**REG:** n = 23 cells **HFD:** n = 20 cells	Resting membrane potential	p= 0.8507, two-tailed, t=0.1894, df=41
Supp. Fig 10g NAcLat *ex vivo* ephys (ramp AP frequency)	**REG:** 9.276 ± 0.000 17.299 ± 0.798 23.722 ± 0.965 26.463 ± 1.176 **HFD:** 12.639 ± 0.000 18.734 ± 1.157 21.844 ± 0.961 23.749 ± 1.638	Mixed-effects model (REML) with Holm-Šídák's multiple comparisons test	**REG:** n = 21 cells **HFD:** n = 17 cells	Frequency of APs (Hz)	Effect of Current: p<0.0001, F (3, 65) = 23.30 Effect of Diet type: p=0.8266, F (1, 36) = 0.04868 Interaction: p=0.1945, F (3, 65) = 1.615 Multiple Comparisons: 100pA: p=0.7686 300pA: p=0.7459 500pA: p=0.5593 700pA: p=0.3142

Data	Mean ± SEM	Statistical Test	N	Outcome measure	p value
Supp. Fig 10h NAcLat *ex vivo* ephys (first ramp AP time)	**REG:** 2433.00 ± 0.00 2089.72 ± 78.60 1727.45 ± 59.19 1485.74 ± 44.02 **HFD:** 2539.00 ± 0.00 1878.52 ± 65.56 1550.53 ± 61.62 1344.11 ± 50.52	Mixed-effects model (REML) with Holm-Šídák's multiple comparisons test	**REG:** n = 21 cells **HFD:** n = 17 cells	Time of first AP in train (ms)	Effect of Current: p<0.0001, F (3, 66) = 368.5 Effect of Diet type: p=0.1050, F (1, 36) = 2.766 Interaction: p=0.1951, F (3, 66) = 1.611 <u>Multiple Comparisons:</u> 100pA: p=0.7409 300pA: p=0.0436 500pA: p=0.1270 700pA: p=0.2009
Supp. Fig 10i NAcLat *ex vivo* ephys (last ramp AP time)	**REG:** 2648.60 ± 0.00 2958.60 ± 46.81 2988.70 ± 85.80 2862.81 ± 136.67 **HFD:** 2934.60 ± 0.00 3060.56 ± 75.13 2884.66 ± 165.11 2552.22 ± 211.63	Mixed-effects model (REML) with Holm-Šídák's multiple comparisons test	**REG:** n = 21 cells **HFD:** n = 17 cells	Time of last AP in train (ms)	Effect of Current: p=0.0112, F (3, 66) = 3.996 Effect of Diet type: p=0.4272, F (1, 36) = 0.6451 Interaction: p=0.2250, F (3, 66) = 1.492 <u>Multiple Comparisons:</u> 100pA: p=0.9189 300pA: p=0.9189 500pA: p=0.9189 700pA: p=0.3227
Supp. Fig 10j NAcLat *ex vivo* ephys (ramp IV curve)	**REG:** -63.269 ± 2.201 -37.363 ± 1.103 -26.460 ± 1.189 -18.221 ± 1.433 **HFD:** -59.181 ± 2.249 -31.426 ± 1.699 -19.620 ± 1.866 -12.338 ± 1.844	Two-way RM ANOVA with Holm-Šídák's multiple comparisons test	**REG:** n = 21 cells **HFD:** n = 17 cells	Membrane potential (mV)	Effect of Current: p<0.0001, F (3, 108) = 786.9 Effect of Diet type: p=0.0102, F (1, 36) = 7.349 Interaction: p=0.5860. F (3, 108) = 0.6478 <u>Multiple Comparisons:</u> 100pA: p=0.0956 300pA: p=0.0474 500pA: p=0.0226 700pA: p=0.0474
Supp. Fig 10k NAcLat *ex vivo* ephys (ramp duration of AP firing)	**REG:** 215.60 ± 0.00 923.19 ± 104.63 1261.26 ± 72.00 1377.07 ± 109.36 **HFD:** 395.60 ± 0.00 1182.04 ± 101.30 1334.13 ± 153.89 1208.12 ± 186.49	Mixed-effects model (REML) with Holm-Šídák's multiple comparisons test	**REG:** n = 21 cells **HFD:** n = 17 cells	Duration of AP firing (ms)	Effect of Current: p=0.0030, F (3, 65) = 5.135 Effect of Diet type: p=0.9501, F (1, 36) = 0.003970 Interaction: p=0.2662, F (3, 65) = 1.349 <u>Multiple Comparisons:</u> 100pA: p=0.8917 300pA: p=0.4963 500pA: p=0.8917 700pA: p=0.6931
Supp. Fig 13b Optogenetic feeding on HFD (butter)	**eYFP:** 0.128 ± 0.024 0.018 ± 0.006 0.031 ± 0.012 0.019 ± 0.007 **ChR2:** 0.122 ± 0.027 0.020 ± 0.006 0.069 ± 0.023 0.009 ± 0.001	Two-way RM ANOVA with Holm-Šídák's multiple comparisons test	**eYFP:** n = 7 mice **ChR2:** n = 8 mice	Butter consumed	Effect of Trial: p<0.0001, F (3, 39) = 18.79 Effect of Virus type: p=0.5938, F (1, 13) = 0.2990 Interaction: p=0.4682, F (3, 39) = 0.8634 <u>Multiple Comparisons:</u> No significant differences

Data	Mean ± SEM	Statistical Test	N	Outcome measure	p value
Supp. Fig 13c Optogenetic feeding on HFD with starvation (Jelly)	**eYFP:** 0.271 ± 0.053 0.132 ± 0.033 0.041 ± 0.005 0.051 ± 0.011 **ChR2:** 0.225 ± 0.028 0.095 ± 0.031 0.098 ± 0.016 0.038 ± 0.007	Two-way RM ANOVA with Holm-Šídák's multiple comparisons test	**eYFP:** n = 6 mice **ChR2:** n = 6 mice	Jelly consumed	Effect of Trial: p<0.0001, F (3, 30) = 26.58 Effect of Virus type: p=0.7012, F (1, 10) = 0.1560 Interaction: p=0.1819, F (3, 30) = 1.731 <u>Multiple Comparisons:</u> No significant differences
Supp. Fig 13d Optogenetic feeding REG vs. HFD (Jelly)	**REG:** 0.308 ± 0.031 0.114 ± 0.013 0.240 ± 0.031 0.089 ± 0.020 **HFD:** 0.110 ± 0.010 0.095 ± 0.012 0.120 ± 0.021 0.080 ± 0.007	Two-way RM ANOVA with Holm-Šídák's multiple comparisons test	n = 8 mice	Jelly consumed	Effect of Trial: p<0.0001, F (3, 21) = 14.17 Effect of Virus type: p<0.0001, F (1, 7) = 72.22 Interaction: p<0.0001, F (3, 21) = 12.27 <u>Multiple Comparisons:</u> Trial 1: p<0.0001 Trial 2: p=0.7066 Trial 3: p=0.0004 Trial 4: p=0.7338
Supp. Fig 13e Body weight on HFD	**eYFP:** 25.29 ± 0.53 26.39 ± 0.43 27.34 ± 0.37 28.39 ± 0.43 29.79 ± 0.59 30.57 ± 0.58 31.29 ± 0.45 32.73 ± 0.50 33.53 ± 0.81 34.71 ± 1.00 35.54 ± 0.98 36.29 ± 1.13 37.30 ± 1.28 37.64 ± 1.12 40.14 ± 1.61 40.56 ± 1.65 38.14 ± 1.38 35.33 ± 1.10 33.87 ± 0.81 33.03 ± 0.68 **ChR2:** 25.91 ± 0.20 27.40 ± 0.42 28.66 ± 0.41 30.31 ± 0.55 31.20 ± 0.56 32.00 ± 0.80 33.06 ± 0.82 34.53 ± 1.04 35.49 ± 1.48 36.98 ± 1.73 38.18 ± 1.63 39.04 ± 1.79 39.59 ± 1.67 38.83 ± 1.3 42.31 ± 1.73 42.71 ± 1.65 39.50 ± 1.37 36.80 ± 1.32 34.93 ± 1.24 33.98 ± 0.96	Two-way RM ANOVA with Holm-Šídák's multiple comparisons test	**eYFP:** n = 7 mice **ChR2:** n = 8 mice	Body weight (g)	Effect of Day: p<0.0001, F (19, 247) = 103.6 Effect of Virus type: p=0.2322, F (1, 13) = 1.571 Interaction: p=0.9852, F (19, 247) = 0.4208 <u>Multiple Comparisons:</u> No significant differences

Data	Mean ± SEM	Statistical Test	N	Outcome measure	p value
Supp. Fig 13f Optogenetic feeding (1 week OFF)	**eYFP:** 0.292 ± 0.036 0.086 ± 0.020 0.063 ± 0.008 0.062 ± 0.010 **ChR2:** 0.187 ± 0.024 0.062 ± 0.008 0.105 ± 0.023 0.072 ± 0.014	Two-way RM ANOVA with Holm-Šídák's multiple comparisons test	**eYFP:** n = 7 mice **ChR2:** n = 8 mice	Jelly consumed	Effect of Trial: p<0.0001, F (3, 39) = 33.48 Effect of Virus type: p=0.1990, F (1, 13) = 1.832 Interaction: p=0.0054, F (3, 39) = 4.917 <u>Multiple Comparisons:</u> Trial 1: p=0.0022 Trial2: p=0.6449 Trial 3: p=0.3691 Trial 4: p=0.7166
Supp. Fig 13f Optogenetic feeding (2 weeks OFF)	**eYFP:** 0.388 ± 0.089 0.094 ± 0.016 0.081 ± 0.012 0.071 ± 0.014 **ChR2:** 0.232 ± 0.049 0.098 ± 0.015 0.191 ± 0.048 0.054 ± 0.006	Two-way RM ANOVA with Holm-Šídák's multiple comparisons test	**eYFP:** n = 7 mice **ChR2:** n = 8 mice	Jelly consumed	Effect of Trial: p<0.0001, F (3, 39) = 14.53 Effect of Virus type: p=0.6005, F (1, 13) = 0.2881 Interaction: p=0.0215, F (3, 39) = 3.611 <u>Multiple Comparisons:</u> Trial 1: p=0.0335 Trial 2: p=0.9503 Trial 3: p=0.1684 Trial 4: p=0.9456
Supp. Fig 14b VTA DA (membrane capacitance)	**REG:** 30.50 ± 2.66 **HFD:** 29.00 ± 2.35	Unpaired t-test	**REG:** n = 17 cells **HFD:** n = 14 cells	Membrane capacitance (pF)	p=0.6882, two-tailed, t=0.4054, df=29
Supp. Fig 14c VTA DA (membrane resistance)	**REG:** 173.0 ± 29.9 **HFD:** 187.0 ± 30.6	Unpaired t-test	**REG:** n = 17 cells **HFD:** n = 14 cells	Membrane resistance (MΩ)	p= 0.7523, two-tailed, t=0.3187, df=29
Supp. Fig 14d VTA DA (I_h current)	**REG:** 24.6 ± 3.85 **HFD:** 33.8 ± 4.18	Unpaired t-test	**REG:** n = 12 cells **HFD:** n = 13 cells	Current (pA)	p=0.1205, two-tailed, t=1.612, df=23
Supp. Fig 15c Weight gain on HFD	**eYFP:** 29.65 ± 0.59 34.14 ± 1.20 37.01 ± 1.73 37.01 ± 1.69 38.09 ± 1.74 40.73 ± 1.88 41.83 ± 2.02 44.95 ± 1.65 47.36 ± 1.54 48.27 ± 1.42 53.56 ± 0.99 48.30 ± 1.03 45.36 ± 1.26 **ChR2:** 29.62 ± 0.78 33.63 ± 1.43 36.35 ± 1.90 35.86 ± 1.91 36.86 ± 2.04 39.63 ± 2.02 40.97 ± 1.94 43.87 ± 1.56 46.14 ± 1.62 47.45 ± 1.52 53.03 ± 0.71 47.70 ± 0.50 44.96 ± 0.56	Mixed-effects model (REML) with Holm-Šídák's multiple comparisons test	**eYFP:** n = 9 mice **ChR2:** n = 9 mice	Body weight (g)	Effect of Time: p<0.0001, F (12, 189) = 214.6 Effect of Virus type: p=0.7942, F (1, 16) = 0.07038 Interaction: p=0.8569, F (12, 189) = 0.5797 <u>Multiple Comparisons:</u> No significant differences

Data	Mean ± SEM	Statistical Test	N	Outcome measure	p value
Supp. Fig 15d Optogenetic feeding behavior on REG (Chow)	**eYFP:** 0.013 ± 0.007 0.019 ± 0.006 0.011 ± 0.004 0.018 ± 0.005 **ChR2:** 0.017 ± 0.010 0.026 ± 0.010 0.091 ± 0.022 0.026 ± 0.010	Two-way RM ANOVA with Holm-Šídák's multiple comparisons test	**eYFP:** n = 9 mice **ChR2:** n = 9 mice	Chow consumed (g)	Effect of Trial: p=0.0132, F (3, 48) = 3.966 Effect of Virus type: p=0.0004, F (1, 16) = 20.14 Interaction: p=0.0032, F (3, 48) = 5.274 Multiple Comparisons: Trial 1: p=0.9389 Trial 2: p=0.9389 Trial 3: p<0.0001 Trial 4: p=0.9389
Supp. Fig 15d Optogenetic feeding behavior on REG (Jelly)	**eYFP:** 0.352 ± 0.061 0.041 ± 0.017 0.050 ± 0.024 0.054 ± 0.025 **ChR2:** 0.469 ± 0.032 0.066 ± 0.019 0.487 ± 0.075 0.023 ± 0.007	Two-way RM ANOVA with Holm-Šídák's multiple comparisons test	**eYFP:** n = 9 mice **ChR2:** n = 9 mice	Jelly consumed (g)	Effect of Trial: p<0.0001, F (3, 48) = 36.11 Effect of Virus type: p<0.0001, F (1, 16) = 47.09 Interaction: p<0.0001, F (3, 48) = 12.30 Multiple Comparisons: Trial 1: p=0.1123 Trial 2: p=0.8202 Trial 3: p<0.0001 Trial 4: p=0.8202
Supp. Fig 15e Optogenetic feeding behavior on 2wks HFD (Jelly)	**eYFP:** 0.016 ± 0.004 0.014 ± 0.004 0.022 ± 0.011 0.034 ± 0.011 **ChR2:** 0.026 ± 0.011 0.014 ± 0.006 0.261 ± 0.081 0.007 ± 0.004	Two-way RM ANOVA with Holm-Šídák's multiple comparisons test	**eYFP:** n = 9 mice **ChR2:** n = 7 mice	Jelly consumed (g)	Effect of Trial: p<0.0001, F (3, 42) = 12.46 Effect of Virus type: p=0.0205, F (1, 14) = 6.819 Interaction: p<0.0001, F (3, 42) = 12.48 Multiple Comparisons: Trial 1: p=0.9536 Trial 2: p=0.9966 Trial 3: p<0.0001 Trial 4: p=0.8456
Supp. Fig 15e Optogenetic feeding behavior on 4wks HFD (Jelly)	**eYFP:** 0.017 ± 0.006 0.013 ± 0.006 0.007 ± 0.005 0.022 ± 0.005 **ChR2:** 0.011 ± 0.010 0.001 ± 0.001 0.107 ± 0.021 0.009 ± 0.003	Two-way RM ANOVA with Holm-Šídák's multiple comparisons test	**eYFP:** n = 9 mice **ChR2:** n = 7 mice	Jelly consumed (g)	Effect of Trial: p<0.0001, F (3, 42) = 14.54 Effect of Virus type: p=0.0151, F (1, 14) = 7.653 Interaction: p<0.0001, F (3, 42) = 21.94 Multiple Comparisons: Trial 1: p=0.6652 Trial 2: p=0.5975 Trial 3: p<0.0001 Trial 4: p=0.5975
Supp. Fig 15f Optogenetic feeding behavior on Off HFD (Jelly)	**eYFP:** 0.011 ± 0.003 0.021 ± 0.008 0.026 ± 0.015 0.021 ± 0.009 **ChR2:** 0.025 ± 0.004 0.028 ± 0.015 0.395 ± 0.070 0.015 ± 0.006	Two-way RM ANOVA with Holm-Šídák's multiple comparisons test	**eYFP:** n = 9 mice **ChR2:** n = 6 mice	Jelly consumed (g)	Effect of Trial: p<0.0001, F (3, 39) = 36.56 Effect of Virus type: p<0.0001, F (1, 13) = 37.71 Interaction: p<0.0001, F (3, 39) = 33.67 Multiple Comparisons: Trial 1: p=0.9607 Trial 2: p=0.9672 Trial 3: p<0.0001 Trial 4: p=0.9672
Supp. Fig 16a VTA RNA expression	**REG:** 0.727 ± 0.035 **HFD:** 0.752 ± 0.034	Unpaired t-test	**REG:** n = 9 mice **HFD:** n = 12 mice	Percent of TH+ cells that are NtsR1+	p=0.6222, two-tailed, t=0.5013, df=18

Data	Mean ± SEM	Statistical Test	N	Outcome measure	p value
Supp. Fig 16b VTA DA perforated patch	**REG:** 1.17 ± 0.14 2.37 ± 0.33 **HFD:** 0.79 ± 0.27 1.85 ± 0.47	Two-way RM ANOVA with Holm-Šídák's multiple comparisons test	**REG:** n = 11 cells **HFD:** n = 8 cells	Frequency of action potential firing (Hz)	Effect of Nts: p<0.0001, F (1, 17) = 27.01 Effect of Diet type: p=0.2648, F (1, 17) = 1.330 Interaction: p=0.7460, F (1, 17) = 0.1084 Multiple Comparisons: No significant differences
Supp. Fig 17b med vs. lat VTA ntsLight (HFD)	**lat VTA:** 0.039 ± 0.014 **med VTA:** 0.009 ± 0.006	Paired t-test	n = 12 slices	Area under the curve during light stimulation	p=0.0037, two-tailed, t=3.661, df=11
Supp. Fig 17c VTA ntsLight HFD vs. OFF	**HFD:** 0.015 ± 0.002 **OFF:** 0.013 ± 0.002	Unpaired t-test	**HFD:** n = 8 slices **OFF:** n = 4 slices	Area under the curve during light stimulation	p=0.7064, two-tailed, t=0.3877, df=10
Supp. Fig 17d NAcLat vs. LH stim on VTA ntsLight	**NAcLat:** 0.092 ± 0.017 **LH:** 0.104 ± 0.047	Unpaired t-test	**NAcLat:** n = 13 slices **LH:** n = 4 slices	Area under the curve during light stimulation	p= 0.7659, two-tailed, t=0.3033, df=15
Supp. Fig 17e ntsLight in lat vs. med VTA (LH stim)	**latVTA:** 0.104 ± 0.047 **medVTA:** 0.063 ± 0.026	Paired t-test	n = 4 slices	Area under the curve during light stimulation	p=0.1811, two-tailed, t=1.735, df=3
Supp. Fig 18b NAcLat RNAscope REG vs. HFD (All Nts+)	**REG:** 0.419 ± 0.006 **HFD:** 0.414 ± 0.007	Unpaired t-test	**REG:** n = 6 mice **HFD:** n = 8 mice	Percent of NTS+ cells pixels containing NTS mRNA	p=0.657, two-tailed, t=0.4550, df=12
Supp. Fig 18b NAcLat RNAscope REG vs. HFD (All Nts+/D1+)	**REG:** 0.479 ± 0.006 **HFD:** 0.475 ± 0.007	Unpaired t-test	**REG:** n = 6 mice **HFD:** n = 8 mice	Percent of NTS+/D1+ cells pixels containing NTS mRNA	p=0.732, two-tailed, t=0.3506, df=12

REFERENCES

Chapter 1

Alsiö J, Olszewski PK, Norbäck AH, et al. Dopamine D1 receptor gene expression decreases in the nucleus accumbens upon long-term exposure to palatable food and differs depending on diet-induced obesity phenotype in rats. Neuroscience. 2010;171(3):779-787. doi:10.1016/j.neuroscience.2010.09.046

Altherr, E., Rainwater, A., Kaviani, D., Tang, Q., and Güler, A.D. (2021). Long-term high fat diet consumption reversibly alters feeding behavior via a dopamine-associated mechanism in mice. Behavioural Brain Research *414*, 113470. https://doi.org/10.1016/j.bbr.2021.113470.

Arcego, D.M., Krolow, R., Lampert, C., Toniazzo, A.P., Garcia, E. dos S., Lazzaretti, C., Costa, G., Scorza, C., and Dalmaz, C. (2020). Chronic high-fat diet affects food-motivated behavior and hedonic systems in the nucleus accumbens of male rats. Appetite *153*, 104739. https://doi.org/10.1016/j.appet.2020.104739.

Beier, K.T., Steinberg, E.E., DeLoach, K.E., Xie, S., Miyamichi, K., Schwarz, L., Gao, X.J., Kremer, E.J., Malenka, R.C., and Luo, L. (2015). Circuit Architecture of VTA Dopamine Neurons Revealed by Systematic Input-Output Mapping. Cell *162*, 622–634. https://doi.org/10.1016/j.cell.2015.07.015.

Beutler, L.R., Corpuz, T.V., Ahn, J.S., Kosar, S., Song, W., Chen, Y., and Knight, Z.A. (2020). Obesity causes selective and long-lasting desensitization of AgRP neurons to dietary fat. ELife *9*, e55909. https://doi.org/10.7554/eLife.55909.

Bond, C.W., Trinko, R., Foscue, E., Furman, K., Groman, S.M., Taylor, J.R., and DiLeone, R.J. (2020). Medial Nucleus Accumbens Projections to the Ventral Tegmental Area Control Food Consumption. J. Neurosci. *40*, 4727–4738. https://doi.org/10.1523/JNEUROSCI.3054-18.2020.

Brunzell, D.H., and McIntosh, J.M. (2012). Alpha7 Nicotinic Acetylcholine Receptors Modulate Motivation to Self-Administer Nicotine: Implications for Smoking and Schizophrenia. Neuropsychopharmacology *37*, 1134–1143. https://doi.org/10.1038/npp.2011.299.

Cador, M., Kelley, A.E., Le Moal, M., and Stinus, L. (1986). Ventral tegmental area infusion of substance P, neurotensin and enkephalin: Differential effects on feeding behavior. Neuroscience *18*, 659–669. https://doi.org/10.1016/0306-4522(86)90061-8.

Cagniard, B., Balsam, P.D., Brunner, D., and Zhuang, X. (2006). Mice with chronically elevated dopamine exhibit enhanced motivation, but not learning, for a food reward. Neuropsychopharmacology *31*, 1362–1370. .

Castro, D.C., and Bruchas, M.R. (2019). A Motivational and Neuropeptidergic Hub: Anatomical and Functional Diversity within the Nucleus Accumbens Shell. Neuron *102*, 529–552. https://doi.org/10.1016/j.neuron.2019.03.003.

Christoffel DJ, Walsh JJ, Heifets BD, et al. Input-specific modulation of murine nucleus accumbens differentially regulates hedonic feeding. Nat Commun. 2021;12(1):2135. Published 2021 Apr 9. doi:10.1038/s41467-021-22430-7

Cooke, J.H., Patterson, M., Patel, S.R., Smith, K.L., Ghatei, M.A., Bloom, S.R., and Murphy, K.G. (2009). Peripheral and Central Administration of Xenin and Neurotensin Suppress Food Intake in Rodents. Obesity *17*, 1135–1143. https://doi.org/10.1038/oby.2008.652.

Cunningham, C.L., and Henderson, C.M. (2000). Ethanol-induced conditioned place aversion in mice. Behavioural Pharmacology *11*, 591–602. .

Donofry, S.D., Stillman, C.M., and Erickson, K.I. (2020). A review of the relationship between eating behavior, obesity and functional brain network organization. Social Cognitive and Affective Neuroscience *15*, 1157–1181. https://doi.org/10.1093/scan/nsz085.

Espinosa-Carrasco, J., Burokas, A., Fructuoso, M., Erb, I., Martín-García, E., Gutiérrez-Martos, M., Notredame, C., Maldonado, R., and Dierssen, M. (2018). Time-course and dynamics of obesity-related behavioral changes induced by energy-dense foods in mice. Addict Biol *23*, 531–543. https://doi.org/10.1111/adb.12595.

Ettenberg, A., Raven, M.A., Danluck, D.A., and Necessary, B.D. (1999). Evidence for Opponent-Process Actions of Intravenous Cocaine. Pharmacology Biochemistry and Behavior *64*, 507–512. https://doi.org/10.1016/S0091-3057(99)00109-4.

Ferrario, C.R., Labouèbe, G., Liu, S., Nieh, E.H., Routh, V.H., Xu, S., and O'Connor, E.C. (2016). Homeostasis Meets Motivation in the Battle to Control Food Intake. J. Neurosci. *36*, 11469–11481. https://doi.org/10.1523/JNEUROSCI.2338-16.2016.

Fudala, P.J., and Iwamoto, E.T. (1987). Conditioned aversion after delay place conditioning with nicotine. Psychopharmacology *92*, 376–381. https://doi.org/10.1007/BF00210847.

Fudala, P.J., and Iwamoto, E.T. (1990). Conditioned aversion after delay place conditioning with amphetamine. Pharmacology Biochemistry and Behavior *35*, 89–92. https://doi.org/10.1016/0091-3057(90)90209-Z.

Fulton, S., Pissios, P., Manchon, R.P., Stiles, L., Frank, L., Pothos, E.N., Maratos-Flier, E., and Flier, J.S. (2006). Leptin regulation of the mesoaccumbens dopamine pathway. Neuron *51*, 811–822. https://doi.org/10.1016/j.neuron.2006.09.006.

Geisler S, Derst C, Veh RW, Zahm DS. Glutamatergic afferents of the ventral tegmental area in the rat. J Neurosci. 2007;27(21):5730-5743. doi:10.1523/JNEUROSCI.0012-07.2007

Goldstein, N., Carty, J.R.E., and Betley, J.N. (2022). Specificity of Varenicline in Blocking Mesolimbic Circuit Activation to Natural and Drug Rewards. Neuroscience *483*, 40–51. https://doi.org/10.1016/j.neuroscience.2021.12.016.

Hanlon, E.C., Baldo, B.A., Sadeghian, K., and Kelley, A.E. (2004). Increases in food intake or food-seeking behavior induced by GABAergic, opioid, or dopaminergic stimulation of the nucleus accumbens: is it hunger? Psychopharmacology *172*, 241–247. .

Harenza, J.L., Muldoon, P.P., De Biasi, M., Damaj, M.I., and Miles, M.F. (2014). Genetic variation within the Chrna7 gene modulates nicotine reward-like phenotypes in mice. Genes Brain Behav *13*, 213–225. https://doi.org/10.1111/gbb.12113.

Hariri, N., and Thibault, L. (2010). High-fat diet-induced obesity in animal models. Nutrition Research Reviews *23*, 270–299. .

Hawkins, M.F. (1986). Aphagia in the rat following microinjection of neurotensin into the ventral tegmental area. Life Sciences *38*, 2383–2388. https://doi.org/10.1016/0024-3205(86)90606-5.

Jennings, J.H., Ung, R.L., Resendez, S.L., Stamatakis, A.M., Taylor, J.G., Huang, J., Veleta, K., Kantak, P.A., Aita, M., Shilling-Scrivo, K., et al. (2015). Visualizing Hypothalamic Network Dynamics for Appetitive and Consummatory Behaviors. Cell *160*, 516–527. https://doi.org/10.1016/j.cell.2014.12.026.

Johnson, P.M., and Kenny, P.J. (2010). Dopamine D2 receptors in addiction-like reward dysfunction and compulsive eating in obese rats. Nat Neurosci *13*, 635–641. https://doi.org/10.1038/nn.2519.

Lam, T.K.T., Schwartz, G.J., and Rossetti, L. (2005). Hypothalamic sensing of fatty acids. Nat Neurosci *8*, 579–584. https://doi.org/10.1038/nn1456.

Lammel S, Lim BK, Ran C, et al. Input-specific control of reward and aversion in the ventral tegmental area. Nature. 2012;491(7423):212-217. doi:10.1038/nature11527

Lammel S, Lim BK, Malenka RC. Reward and aversion in a heterogeneous midbrain dopamine system. Neuropharmacology. 2014;76 Pt B(0 0):351-359. doi:10.1016/j.neuropharm.2013.03.019

Morton, G.J., Cummings, D.E., Baskin, D.G., Barsh, G.S., and Schwartz, M.W. (2006). Central nervous system control of food intake and body weight. Nature *443*, 289–295. https://doi.org/10.1038/nature05026.

Nieh, E.H., Matthews, G.A., Allsop, S.A., Presbrey, K.N., Leppla, C.A., Wichmann, R., Neve, R., Wildes, C.P., and Tye, K.M. (2015). Decoding Neural Circuits that Control Compulsive Sucrose-Seeking. Cell *160*, 528–541. https://doi.org/10.1016/j.cell.2015.01.003.

Nieh, E.H., Vander Weele, C.M., Matthews, G.A., Presbrey, K.N., Wichmann, R., Leppla, C.A., Izadmehr, E.M., and Tye, K.M. (2016). Inhibitory Input from the Lateral Hypothalamus to the Ventral Tegmental Area Disinhibits Dopamine Neurons and Promotes Behavioral Activation. Neuron *90*, 1286–1298. https://doi.org/10.1016/j.neuron.2016.04.035.

Nurrish S. (2014). Dense core vesicle release: controlling the where as well as the when. Genetics, 196(3), 601–604. https://doi.org/10.1534/genetics.113.159905

Nusbaum MP, Blitz DM, Marder E. Functional consequences of neuropeptide and small-molecule co-transmission. Nat Rev Neurosci. 2017;18(7):389-403. doi:10.1038/nrn.2017.56

O'Connor, E.C., Kremer, Y., Lefort, S., Harada, M., Pascoli, V., Rohner, C., and Lüscher, C. (2015). Accumbal D1R Neurons Projecting to Lateral Hypothalamus Authorize Feeding. Neuron *88*, 553–564. https://doi.org/10.1016/j.neuron.2015.09.038.

Opland, D., Sutton, A., Woodworth, H., Brown, J., Bugescu, R., Garcia, A., Christensen, L., Rhodes, C., Myers, M., and Leinninger, G. (2013). Loss of neurotensin receptor-1 disrupts the control of the mesolimbic dopamine system by leptin and promotes hedonic feeding and obesity. Molecular Metabolism *2*, 423–434. https://doi.org/10.1016/j.molmet.2013.07.008.

Patterson, C.M., Wong, J.-M.T., Leinninger, G.M., Allison, M.B., Mabrouk, O.S., Kasper, C.L., Gonzalez, I.E., Mackenzie, A., Jones, J.C., Kennedy, R.T., et al. (2015). Ventral Tegmental Area Neurotensin Signaling Links the Lateral Hypothalamus to Locomotor Activity and Striatal Dopamine Efflux in Male Mice. Endocrinology *156*, 1692–1700. https://doi.org/10.1210/en.2014-1986.

Salamone, J.D., Correa, M., Farrar, A.M., Nunes, E.J., and Pardo, M. (2009). Dopamine, behavioral economics, and effort. Frontiers in Behavioral Neuroscience *3*, 13. .

Sampey, B.P., Vanhoose, A.M., Winfield, H.M., Freemerman, A.J., Muehlbauer, M.J., Fueger, P.T., Newgard, C.B., and Makowski, L. (2011). Cafeteria diet is a robust model of human metabolic syndrome with liver and adipose inflammation: comparison to high-fat diet. Obesity *19*, 1109–1117. .

Schwartz, M.W., Woods, S.C., Porte, D., Seeley, R.J., and Baskin, D.G. (2000). Central nervous system control of food intake. Nature *404*, 661–671. https://doi.org/10.1038/35007534.

Sharma, S., Zhuang, Y., and Gomez-Pinilla, F. (2012). High-fat diet transition reduces brain DHA levels associated with altered brain plasticity and behaviour. Scientific Reports *2*, 1–8. .

Taylor, J.R., and Robbins, T.W. (1986). 6-Hydroxydopamine lesions of the nucleus accumbens, but not of the caudate nucleus, attenuate enhanced responding with reward-related stimuli produced by intra-accumbens d-amphetamine. Psychopharmacology *90*, 390–397. .

Tschumi, C.W., and Beckstead, M.J. (2019). Diverse actions of the modulatory peptide neurotensin on central synaptic transmission. Eur J Neurosci *49*, 784–793. https://doi.org/10.1111/ejn.13858.

Watabe-Uchida, M., Zhu, L., Ogawa, S.K., Vamanrao, A., and Uchida, N. (2012). Whole-Brain Mapping of Direct Inputs to Midbrain Dopamine Neurons. Neuron *74*, 858–873. https://doi.org/10.1016/j.neuron.2012.03.017.

Wise, R.A., Spindler, J., DeWit, H., and Gerberg, G.J. (1978). Neuroleptic-induced" anhedonia" in rats: pimozide blocks reward quality of food. Science *201*, 262–264. .

Watabe-Uchida, M., Zhu, L., Ogawa, S.K., Vamanrao, A., and Uchida, N. (2012). Whole-Brain Mapping of Direct Inputs to Midbrain Dopamine Neurons. Neuron *74*, 858–873. https://doi.org/10.1016/j.neuron.2012.03.017.

Woodworth, H.L., Batchelor, H.M., Beekly, B.G., Bugescu, R., Brown, J.A., Kurt, G., Fuller, P.M., and Leinninger, G.M. (2017a). Neurotensin Receptor-1 Identifies a Subset of Ventral Tegmental Dopamine Neurons that Coordinates Energy Balance. Cell Rep *20*, 1881–1892. https://doi.org/10.1016/j.celrep.2017.08.001.
Woodworth, H.L., Beekly, B.G., Batchelor, H.M., Bugescu, R., Perez-Bonilla, P., Schroeder, L.E., and Leinninger, G.M. (2017b). Lateral hypothalamic neurotensin neurons orchestrate dual weight loss behaviors via distinct mechanisms. Cell Reports *21*, 3116–3128. .

Woodworth, H.L., Batchelor, H.M., Beekly, B.G., Bugescu, R., Brown, J.A., Kurt, G., Fuller, P.M., and Leinninger, G.M. (2017c). Neurotensin Receptor-1 Identifies a Subset of Ventral Tegmental Dopamine Neurons that Coordinates Energy Balance. Cell Reports *20*, 1881–1892. https://doi.org/10.1016/j.celrep.2017.08.001.

Woodworth, H.L., Brown, J.A., Batchelor, H.M., Bugescu, R., and Leinninger, G.M. (2018). Determination of neurotensin projections to the ventral tegmental area in mice. Neuropeptides *68*, 57–74. https://doi.org/10.1016/j.npep.2018.02.003.

Yang, H., de Jong, J.W., Tak, Y., Peck, J., Bateup, H.S., and Lammel, S. (2018). Nucleus Accumbens Subnuclei Regulate Motivated Behavior via Direct Inhibition and Disinhibition of VTA Dopamine Subpopulations. Neuron *97*, 434-449.e4. https://doi.org/10.1016/j.neuron.2017.12.022.

Chapter 2

Akerboom, J., Chen, T.-W., Wardill, T.J., Tian, L., Marvin, J.S., Mutlu, S., Calderón, N.C., Esposti, F., Borghuis, B.G., Sun, X.R., et al. (2012). Optimization of a GCaMP calcium indicator for neural activity imaging. J. Neurosci. *32*, 13819–13840. https://doi.org/10.1523/JNEUROSCI.2601-12.2012.

Antolin-Fontes, B., Ables, J.L., Görlich, A., and Ibañez-Tallon, I. (2015). The habenulo-interpeduncular pathway in nicotine aversion and withdrawal. Neuropharmacology *96*, 213–222. https://doi.org/10.1016/j.neuropharm.2014.11.019.

Ashton, H., Stepney, R., and Thompson, J.W. (1979). Self-titration by cigarette smokers. Br. Med. J. *2*, 357–360.

Berridge, M.S., Apana, S.M., Nagano, K.K., Berridge, C.E., Leisure, G.P., and Boswell, M.V. (2010). Smoking produces rapid rise of [11C]nicotine in human brain. Psychopharmacology (Berl.) *209*, 383–394. https://doi.org/10.1007/s00213-010-1809-8.

Besson, M., David, V., Baudonnat, M., Cazala, P., Guilloux, J.-P., Reperant, C., Cloez-Tayarani, I., Changeux, J.-P., Gardier, A.M., and Granon, S. (2012). Alpha7-nicotinic receptors modulate nicotine-induced reinforcement and extracellular dopamine outflow in the mesolimbic system in mice. Psychopharmacology (Berl.) *220*, 1–14. https://doi.org/10.1007/s00213-011-2422-1.

Brischoux, F., Chakraborty, S., Brierley, D.I., and Ungless, M.A. (2009). Phasic excitation of dopamine neurons in ventral VTA by noxious stimuli. Proc. Natl. Acad. Sci. *106*, 4894–4899. .

Bromberg-Martin, E.S., Matsumoto, M., and Hikosaka, O. (2010). Dopamine in Motivational Control: Rewarding, Aversive, and Alerting. Neuron *68*, 815–834. https://doi.org/10.1016/j.neuron.2010.11.022.

Brunzell, D.H., and McIntosh, J.M. (2012). Alpha7 Nicotinic Acetylcholine Receptors Modulate Motivation to Self-Administer Nicotine: Implications for Smoking and Schizophrenia. Neuropsychopharmacology *37*, 1134–1143. https://doi.org/10.1038/npp.2011.299.

Brunzell, D.H., McIntosh, J.M., and Papke, R.L. (2014). Diverse strategies targeting alpha7 homomeric and alpha6beta2* heteromeric nicotinic acetylcholine receptors for smoking cessation. Ann. N. Y. Acad. Sci. *1327*, 27–45. https://doi.org/10.1111/nyas.12421.

Cachope, R., Mateo, Y., Mathur, B.N., Irving, J., Wang, H.-L., Morales, M., Lovinger, D.M., and Cheer, J.F. (2012). Selective activation of cholinergic interneurons enhances accumbal phasic dopamine release: setting the tone for reward processing. Cell Rep. *2*, 33–41. https://doi.org/10.1016/j.celrep.2012.05.011.

Coe, J.W., Brooks, P.R., Vetelino, M.G., Wirtz, M.C., Arnold, E.P., Huang, J., Sands, S.B., Davis, T.I., Lebel, L.A., Fox, C.B., et al. (2005). Varenicline: An α4β2 Nicotinic Receptor Partial Agonist for Smoking Cessation. J. Med. Chem. *48*, 3474–3477. https://doi.org/10.1021/jm050069n.

Coimbra, B., Soares-Cunha, C., Vasconcelos, N.A.P., Domingues, A.V., Borges, S., Sousa, N., and Rodrigues, A.J. (2019). Role of laterodorsal tegmentum projections to nucleus accumbens in reward-related behaviors. Nat. Commun. *10*, 4138. https://doi.org/10.1038/s41467-019-11557-3.

Damaj, M.I., Glassco, W., Dukat, M., and Martin, B.R. (1999). Pharmacological Characterization of Nicotine-Induced Seizures in Mice. J. Pharmacol. Exp. Ther. *291*, 1284–1291. .

Dani, J.A., and Harris, R.A. (2005). Nicotine addiction and comorbidity with alcohol abuse and mental illness. Nat Neurosci *8*, 1465–1470. https://doi.org/10.1038/nn1580.

Dautan, D., Souza, A.S., Huerta-Ocampo, I., Valencia, M., Assous, M., Witten, I.B., Deisseroth, K., Tepper, J.M., Bolam, J.P., Gerdjikov, T.V., et al. (2016). Segregated cholinergic transmission modulates dopamine neurons integrated in distinct functional circuits. Nat. Neurosci. *19*, 1025–1033. https://doi.org/10.1038/nn.4335.

Di Chiara, G., and Imperato, A. (1988). Drugs abused by humans preferentially increase synaptic dopamine concentrations in the mesolimbic system of freely moving rats. Proc. Natl. Acad. Sci. U. S. A. *85*, 5274–5278. https://doi.org/10.1073/pnas.85.14.5274.

Engle, S.E., McIntosh, J.M., and Drenan, R.M. (2015). Nicotine and Ethanol Cooperate to Enhance Ventral Tegmental Area AMPA Receptor Function via α6-Containing Nicotinic Receptors. Neuropharmacology *0*, 13–22. https://doi.org/10.1016/j.neuropharm.2014.11.014.

Erhardt, S., Schwieler, L., and Engberg, G. (2002). Excitatory and inhibitory responses of dopamine neurons in the ventral tegmental area to nicotine. Synapse *43*, 227–237. https://doi.org/10.1002/syn.10044.

Fenster, C.P., Rains, M.F., Noerager, B., Quick, M.W., and Lester, R.A.J. (1997). Influence of Subunit Composition on Desensitization of Neuronal Acetylcholine Receptors at Low Concentrations of Nicotine. J. Neurosci. *17*, 5747–5759. https://doi.org/10.1523/JNEUROSCI.17-15-05747.1997.

Fowler, C.D., and Kenny, P.J. (2011). Intravenous nicotine self-administration and cue-induced reinstatement in mice: Effects of nicotine dose, rate of drug infusion and prior instrumental training. Neuropharmacology *61*, 687–698. https://doi.org/10.1016/j.neuropharm.2011.05.012.

Fowler, C.D., and Kenny, P.J. (2014). Nicotine aversion: Neurobiological mechanisms and relevance to tobacco dependence vulnerability. Neuropharmacology *76*, 533–544. https://doi.org/10.1016/j.neuropharm.2013.09.008.

Fowler, C.D., Lu, Q., Johnson, P.M., Marks, M.J., and Kenny, P.J. (2011). Habenular α5 nicotinic receptor subunit signalling controls nicotine intake. Nature *471*, 597–601. https://doi.org/10.1038/nature09797.

Fowler, C.D., Tuesta, L., and Kenny, P.J. (2013). Role of α5* nicotinic acetylcholine receptors in the effects of acute and chronic nicotine treatment on brain reward function in mice. Psychopharmacology (Berl.) https://doi.org/10.1007/s00213-013-3235-1.

Frahm, S., Ślimak, M.A., Ferrarese, L., Santos-Torres, J., Antolin-Fontes, B., Auer, S., Filkin, S., Pons, S., Fontaine, J.-F., Tsetlin, V., et al. (2011). Aversion to Nicotine Is Regulated by the Balanced Activity of β4 and α5 Nicotinic Receptor Subunits in the Medial Habenula. Neuron *70*, 522–535. https://doi.org/10.1016/j.neuron.2011.04.013.

Franklin, K.B.J., and Paxinos, G. (2013). Paxinos and Franklin's The mouse brain in stereotaxic coordinates (Amsterdam: Academic Press, an imprint of Elsevier).

Fudala, P.J., and Iwamoto, E.T. (1987). Conditioned aversion after delay place conditioning with nicotine. Psychopharmacology (Berl.) *92*, 376–381. https://doi.org/10.1007/BF00210847.

Fudala, P.J., Teoh, K.W., and Iwamoto, E.T. (1985). Pharmacologic characterization of nicotine-induced conditioned place preference. Pharmacol. Biochem. Behav. *22*, 237–241. https://doi.org/10.1016/0091-3057(85)90384-3.

Gao, M., Jin, Y., Yang, K., Zhang, D., Lukas, R.J., and Wu, J. (2010). Mechanisms involved in systemic nicotine-induced glutamatergic synaptic plasticity on dopamine neurons in the ventral tegmental area. J. Neurosci. Off. J. Soc. Neurosci. *30*, 13814–13825. https://doi.org/10.1523/JNEUROSCI.1943-10.2010.

Goldberg, S.R., Spealman, R.D., Risner, M.E., and Henningfield, J.E. (1983). Control of behavior by intravenous nicotine injections in laboratory animals. Pharmacol. Biochem. Behav. *19*, 1011–1020. https://doi.org/10.1016/0091-3057(83)90408-2.

Goldstein, N., Carty, J.R.E., and Betley, J.N. (2022). Specificity of Varenicline in Blocking Mesolimbic Circuit Activation to Natural and Drug Rewards. Neuroscience *483*, 40–51. https://doi.org/10.1016/j.neuroscience.2021.12.016.

Graupner, M., Maex, R., and Gutkin, B. (2013). Endogenous Cholinergic Inputs and Local Circuit Mechanisms Govern the Phasic Mesolimbic Dopamine Response to Nicotine. PLoS Comput. Biol. *9*, e1003183. https://doi.org/10.1371/journal.pcbi.1003183.

Grieder, T.E., Besson, M., Maal-Bared, G., Pons, S., Maskos, U., and van der Kooy, D. (2019). β2* nAChRs on VTA dopamine and GABA neurons separately mediate nicotine aversion and reward. Proc. Natl. Acad. Sci. *116*, 25968–25973. https://doi.org/10.1073/pnas.1908724116.

Grottick, A.J., Trube, G., Corrigall, W.A., Huwyler, J., Malherbe, P., Wyler, R., and Higgins, G.A. (2000). Evidence that nicotinic alpha(7) receptors are not involved in the hyperlocomotor and rewarding effects of nicotine. J. Pharmacol. Exp. Ther. *294*, 1112–1119. .

Hajek, P., and Stead, L.F. (2001). Aversive smoking for smoking cessation. Cochrane Database Syst. Rev. *2001*, CD000546. https://doi.org/10.1002/14651858.CD000546.pub2.

Harenza, J. L., Muldoon, P. P., De Biasi, M., Damaj, M. I., & Miles, M. F. (2014). Genetic variation within the Chrna7 gene modulates nicotine reward-like phenotypes in mice. Genes, brain, and behavior, *13*(2), 213–225. https://doi.org/10.1111/gbb.12113

Heishman, S.J., and Henningfield, J.E. (2000). Tolerance to repeated nicotine administration on performance, subjective, and physiological responses in nonsmokers. Psychopharmacology (Berl.) *152*, 321–333. https://doi.org/10.1007/s002130000541.

Hnasko, T.S., Sotak, B.N., and Palmiter, R.D. (2007). Cocaine-Conditioned Place Preference by Dopamine-Deficient Mice Is Mediated by Serotonin. J. Neurosci. *27*, 12484–12488. https://doi.org/10.1523/JNEUROSCI.3133-07.2007.

Hsu, Y.-W.A., Tempest, L., Quina, L.A., Wei, A.D., Zeng, H., and Turner, E.E. (2013). Medial Habenula Output Circuit Mediated by 5 Nicotinic Receptor-Expressing GABAergic Neurons in the Interpeduncular Nucleus. J. Neurosci. *33*, 18022–18035. https://doi.org/10.1523/JNEUROSCI.2927-13.2013.

Hu, M.-C., Davies, M., and Kandel, D.B. (2006). Epidemiology and Correlates of Daily Smoking and Nicotine Dependence Among Young Adults in the United States. Am. J. Public Health *96*, 299–308. https://doi.org/10.2105/AJPH.2004.057232.

Imperato, A., Mulas, A., and Di Chiara, G. (1986). Nicotine preferentially stimulates dopamine release in the limbic system of freely moving rats. Eur. J. Pharmacol. *132*, 337–338. https://doi.org/10.1016/0014-2999(86)90629-1.

Jin, Y., Yang, K., Wang, H., and Wu, J. (2011). Exposure of nicotine to ventral tegmental area slices induces glutamatergic synaptic plasticity on dopamine neurons. Synap. N. Y. N *65*, 332–338. https://doi.org/10.1002/syn.20850.

de Jong, J.W., Afjei, S.A., Pollak Dorocic, I., Peck, J.R., Liu, C., Kim, C.K., Tian, L., Deisseroth, K., and Lammel, S. (2019). A Neural Circuit Mechanism for Encoding Aversive Stimuli in the Mesolimbic Dopamine System. Neuron *101*, 133-151.e7. https://doi.org/10.1016/j.neuron.2018.11.005.

Klink, R., d'Exaerde, A. de K., Zoli, M., and Changeux, J.-P. (2001). Molecular and Physiological Diversity of Nicotinic Acetylcholine Receptors in the Midbrain Dopaminergic Nuclei. J. Neurosci. *21*, 1452–1463. https://doi.org/10.1523/JNEUROSCI.21-05-01452.2001.

Kmiotek, E.K., Baimel, C., and Gill, K.J. (2012). Methods for intravenous self administration in a mouse model. J. Vis. Exp. JoVE e3739. https://doi.org/10.3791/3739.

Kohlmeier, K.A. (2013). Off the Beaten Path: Drug Addiction and the Pontine Laterodorsal Tegmentum. ISRN Neurosci. *2013*, 1–24. https://doi.org/10.1155/2013/604847.

Lachenmeier, D.W., and Rehm, J. (2015). Comparative risk assessment of alcohol, tobacco, cannabis and other illicit drugs using the margin of exposure approach. Sci. Rep. *5*, 8126. https://doi.org/10.1038/srep08126.

Lammel, S., Lim, B.K., Ran, C., Huang, K.W., Betley, M.J., Tye, K.M., Deisseroth, K., and Malenka, R.C. (2012). Input-specific control of reward and aversion in the ventral tegmental area. Nature *491*, 212–217. https://doi.org/10.1038/nature11527.

Laviolette, S.R., van der Kooy, D. (2003). The motivational valence of nicotine in the rat ventral tegmental area is switched from rewarding to aversive following blockade of the alpha7-subunit-containing nicotinic acetylcholine receptor. Psychopharmacology (Berl). *166*, 306-313. https://doi: 10.1007/s00213-002-1317-6.

Laviolette, S.R., and van der Kooy, D. (2004). The neurobiology of nicotine addiction: bridging the gap from molecules to behaviour. Nat. Rev. Neurosci. *5*, 55–65. https://doi.org/10.1038/nrn1298.

Laviolette, S.R., Lauzon, N.M., Bishop, S.F., Sun, N., and Tan, H. (2008). Dopamine Signaling through D1-Like versus D2-Like Receptors in the Nucleus Accumbens Core versus Shell

Differentially Modulates Nicotine Reward Sensitivity. J. Neurosci. *28*, 8025–8033. https://doi.org/10.1523/JNEUROSCI.1371-08.2008.

Loney, G.C., King, C.P., and Meyer, P.J. (2021). Systemic nicotine enhances opioid self-administration and modulates the formation of opioid-associated memories partly through actions within the insular cortex. Sci. Rep. *11*, 3321. https://doi.org/10.1038/s41598-021-81955-5.

Lowes, D.C., Chamberlin, L.A., Kretsge, L.N., Holt, E.S., Abbas, A.I., Park, A.J., Yusufova, L., Bretton, Z.H., Firdous, A., Enikolopov, A.G., et al. (2021). Ventral tegmental area GABA neurons mediate stress-induced blunted reward-seeking in mice. Nat. Commun. *12*, 3539. https://doi.org/10.1038/s41467-021-23906-2.

Luscher, C., and Malenka, R.C. (2011). Drug-evoked synaptic plasticity in addiction: from molecular changes to circuit remodeling. Neuron *69*, 650–663. https://doi.org/10.1016/j.neuron.2011.01.017.

Mameli-Engvall, M., Evrard, A., Pons, S., Maskos, U., Svensson, T.H., Changeux, J.-P., and Faure, P. (2006). Hierarchical Control of Dopamine Neuron-Firing Patterns by Nicotinic Receptors. Neuron *50*, 911–921. https://doi.org/10.1016/j.neuron.2006.05.007.

Mansvelder, H.D., and McGehee, D.S. (2000). Long-term potentiation of excitatory inputs to brain reward areas by nicotine. Neuron *27*, 349–357. https://doi.org/10.1016/s0896-6273(00)00042-8.

Mansvelder, H.D., Keath, J.R., and McGehee, D.S. (2002). Synaptic Mechanisms Underlie Nicotine-Induced Excitability of Brain Reward Areas. Neuron *33*, 905–919. https://doi.org/10.1016/S0896-6273(02)00625-6.

Mao, D., Gallagher, K., and McGehee, D.S. (2011). Nicotine Potentiation of Excitatory Inputs to Ventral Tegmental Area Dopamine Neurons. J. Neurosci. *31*, 6710–6720. https://doi.org/10.1523/JNEUROSCI.5671-10.2011.

Markou, A., and Paterson, N.E. (2001). The nicotinic antagonist methyllycaconitine has differential effects on nicotine self-administration and nicotine withdrawal in the rat. Nicotine Tob. Res. Off. J. Soc. Res. Nicotine Tob. *3*, 361–373. https://doi.org/10.1080/14622200110073380.

Matta, S.G., Balfour, D.J., Benowitz, N.L., Boyd, R.T., Buccafusco, J.J., Caggiula, A.R., Craig, C.R., Collins, A.C., Damaj, M.I., Donny, E.C., et al. (2007). Guidelines on nicotine dose selection for in vivo research. Psychopharmacology (Berl.) *190*, 269–319. https://doi.org/10.1007/s00213-006-0441-0.

McCaul, M.E., Wand, G.S., Kuwabara, H., Dannals, R.F., Wong, D., and Xu, X. (2019). The Relationship of Varenicline Agonism of α4β2 Nicotinic Acetylcholine Receptors and Nicotine-Induced Dopamine Release in Nicotine-Dependent Humans. Nicotine Tob. Res. *22*, 892–899. https://doi.org/10.1093/ntr/ntz080.

Mihalak, K.B., Carroll, F.I., and Luetje, C.W. (2006). Varenicline is a partial agonist at alpha4beta2 and a full agonist at alpha7 neuronal nicotinic receptors. Mol. Pharmacol. *70*, 801–805. https://doi.org/10.1124/mol.106.025130.

Natarajan, R., Wright, J.W., and Harding, J. (2011). Nicotine-induced conditioned place preference in adolescent rats. Pharmacol. Biochem. Behav. https://doi.org/10.1016/j.pbb.2011.05.004.

Nguyen, C., Mondoloni, S., Le Borgne, T., Centeno, I., Come, M., Jehl, J., Solié, C., Reynolds, L.M., Durand-de Cuttoli, R., Tolu, S., et al. (2021). Nicotine inhibits the VTA-to-amygdala dopamine pathway to promote anxiety. Neuron *109*, 2604-2615.e9. https://doi.org/10.1016/j.neuron.2021.06.013.

Omelchenko, N., and Sesack, S.R. (2005). Laterodorsal tegmental projections to identified cell populations in the rat ventral tegmental area. J. Comp. Neurol. *483*, 217–235. https://doi.org/10.1002/cne.20417.

Peng, C., Engle, S.E., Yan, Y., Weera, M.M., Berry, J.N., Arvin, M.C., Zhao, G., McIntosh, J.M., Chester, J.A., and Drenan, R.M. (2017). Altered nicotine reward-associated behavior following α4 nAChR subunit deletion in ventral midbrain. PloS One *12*, e0182142. https://doi.org/10.1371/journal.pone.0182142.

Petersen, D.R., Norris, K.J., and Thompson, J.A. (1984). A comparative study of the disposition of nicotine and its metabolites in three inbred strains of mice. Drug Metab. Dispos. Biol. Fate Chem. *12*, 725–731. .

Picciotto, M.R., and Kenny, P.J. (2021). Mechanisms of Nicotine Addiction. Cold Spring Harb. Perspect. Med. *11*, a039610. https://doi.org/10.1101/cshperspect.a039610.

Picciotto, M.R., Zoli, M., Rimondini, R., Léna, C., Marubio, L.M., Pich, E.M., Fuxe, K., and Changeux, J.-P. (1998). Acetylcholine receptors containing the β2 subunit are involved in the reinforcing properties of nicotine. Nature *391*, 173–177. https://doi.org/10.1038/34413.

Picciotto, M.R., Addy, N.A., Mineur, Y.S., and Brunzell, D.H. (2008). It's not "either/or": activation and desensitization of nicotinic acetylcholine receptors both contribute to behaviors related to nicotine addiction and mood. Prog. Neurobiol. *84*, 329–342. https://doi.org/10.1016/j.pneurobio.2007.12.005.

Rice, M.E., and Cragg, S.J. (2004). Nicotine amplifies reward-related dopamine signals in striatum. Nat. Neurosci. *7*, 583–584. https://doi.org/10.1038/nn1244.

Risinger, F.O., and Oakes, R.A. (1995). Nicotine-induced conditioned place preference and conditioned place aversion in mice. Pharmacol. Biochem. Behav. *51*, 457–461. https://doi.org/10.1016/0091-3057(95)00007-J.

Saal, D., Dong, Y., Bonci, A., and Malenka, R.C. (2003). Drugs of abuse and stress trigger a common synaptic adaptation in dopamine neurons. Neuron *37*, 577–582. https://doi.org/10.1016/s0896-6273(03)00021-7.

Sambo, D.O., Lin, M., Owens, A., Lebowitz, J.J., Richardson, B., Jagnarine, D.A., Shetty, M., Rodriquez, M., Alonge, T., Ali, M., et al. (2017). The sigma-1 receptor modulates methamphetamine dysregulation of dopamine neurotransmission. Nat. Commun. *8*, 2228. https://doi.org/10.1038/s41467-017-02087-x.

Sartor, C.E., Lessov-Schlaggar, C.N., Scherrer, J.F., Bucholz, K.K., Madden, P.A.F., Pergadia, M.L., Grant, J.D., Jacob, T., and Xian, H. (2010). Initial response to cigarettes predicts rate of progression to regular smoking: Findings from an offspring-of-twins design. Addict. Behav. *35*, 771–778. https://doi.org/10.1016/j.addbeh.2010.03.004.

Schilström, B., Rawal, N., Mameli-Engvall, M., Nomikos, G.G., and Svensson, T.H. (2003). Dual effects of nicotine on dopamine neurons mediated by different nicotinic receptor subtypes. Int. J. Neuropsychopharmacol. *6*, 1–11. https://doi.org/10.1017/S1461145702003188.

Schultz, W. (1997). Dopamine neurons and their role in reward mechanisms. Curr Opin Neurobiol *7*, 191–197. .

Scuppa, G., Cippitelli, A., Toll, L., Ciccocioppo, R., and Ubaldi, M. (2015). Varenicline decreases nicotine but not alcohol self-administration in genetically selected Marchigian Sardinian alcohol-preferring (msP) rats. Drug Alcohol Depend. *156*, 126–132. https://doi.org/10.1016/j.drugalcdep.2015.09.002.

Sellings, L.H.L., Baharnouri, G., McQuade, L.E., and Clarke, P.B.S. (2008). Rewarding and aversive effects of nicotine are segregated within the nucleus accumbens. Eur. J. Neurosci. *28*, 342–352. https://doi.org/10.1111/j.1460-9568.2008.06341.x.

Siu, E.C.K., and Tyndale, R.F. (2007). Characterization and comparison of nicotine and cotinine metabolism in vitro and in vivo in DBA/2 and C57BL/6 mice. Mol. Pharmacol. *71*, 826–834. https://doi.org/10.1124/mol.106.032086.

Soden, M.E., Chung, A.S., Cuevas, B., Resnick, J.M., Awatramani, R., and Zweifel, L.S. (2020). Anatomic resolution of neurotransmitter-specific projections to the VTA reveals diversity of GABAergic inputs. Nat. Neurosci. *23*, 968–980. https://doi.org/10.1038/s41593-020-0657-z.

St Helen, G., Ross, K.C., Dempsey, D.A., Havel, C.M., Jacob, P., and Benowitz, N.L. (2016). Nicotine Delivery and Vaping Behavior During ad Libitum E-cigarette Access. Tob. Regul. Sci. *2*, 363–376. https://doi.org/10.18001/TRS.2.4.8.

Steidl, S., Wang, H., Ordonez, M., Zhang, S., and Morales, M. (2017). Optogenetic excitation in the ventral tegmental area of glutamatergic or cholinergic inputs from the laterodorsal tegmental area drives reward. Eur. J. Neurosci. *45*, 559–571. https://doi.org/10.1111/ejn.13436.

Tan, K.R., Yvon, C., Turiault, M., Mirzabekov, J.J., Doehner, J., Labouèbe, G., Deisseroth, K., Tye, K.M., and Lüscher, C. (2012). GABA Neurons of the VTA Drive Conditioned Place Aversion. Neuron *73*, 1173–1183. https://doi.org/10.1016/j.neuron.2012.02.015.

Tang, J., and Dani, J.A. (2009). Dopamine Enables In Vivo Synaptic Plasticity Associated with the Addictive Drug Nicotine. Neuron *63*, 673–682. https://doi.org/10.1016/j.neuron.2009.07.025.

Tapper, A.R., McKinney, S.L., Nashmi, R., Schwarz, J., Deshpande, P., Labarca, C., Whiteaker, P., Marks, M.J., Collins, A.C., and Lester, H.A. (2004). Nicotine Activation of α4* Receptors: Sufficient for Reward, Tolerance, and Sensitization. Science *306*, 1029–1032. https://doi.org/10.1126/science.1099420.

Taylor, D.H., Burman, P.N., Hansen, M., Wilcox, R.S., Larsen, B.R., Blanchard, J.K., Merrill, C., Edwards, J., Sudweeks, S., wu, J., et al. (2013). Nicotine Enhances the Excitability of Gaba Neurons in the Ventral TegmentalArea via Activation of Alpha 7 Nicotinic Receptors on Glutamate Terminals. Biochem. Pharmacol. 1–9. https://doi.org/10.4172/2167-0501.S1-002.

Threlfell, S., Lalic, T., Platt, N.J., Jennings, K.A., Deisseroth, K., and Cragg, S.J. (2012). Striatal dopamine release is triggered by synchronized activity in cholinergic interneurons. Neuron *75*, 58–64. https://doi.org/10.1016/j.neuron.2012.04.038.

Tolu, S., Eddine, R., Marti, F., David, V., Graupner, M., Pons, S., Baudonnat, M., Husson, M., Besson, M., Reperant, C., et al. (2013). Co-activation of VTA DA and GABA neurons mediates nicotine reinforcement. Mol. Psychiatry *18*, 382–393. https://doi.org/10.1038/mp.2012.83.

Tsai, H.-C., Zhang, F., Adamantidis, A., Stuber, G.D., Bonci, A., de Lecea, L., and Deisseroth, K. (2009). Phasic firing in dopaminergic neurons is sufficient for behavioral conditioning. Science *324*, 1080–1084. https://doi.org/10.1126/science.1168878.

Tuesta, L.M., Chen, Z., Duncan, A., Fowler, C.D., Ishikawa, M., Lee, B.R., Liu, X.-A., Lu, Q., Cameron, M., Hayes, M.R., et al. (2017). GLP-1 acts on habenular avoidance circuits to control nicotine intake. Nat. Neurosci. *20*, 708–716. https://doi.org/10.1038/nn.4540.

Verharen, J.P.H., Zhu, Y., and Lammel, S. (2020). Aversion hot spots in the dopamine system. Curr. Opin. Neurobiol. *64*, 46–52. https://doi.org/10.1016/j.conb.2020.02.002.

Walters, C.L., Brown, S., Changeux, JP., et al. (2006). The β2 but not α7 subunit of the nicotinic acetylcholine receptor is required for nicotine-conditioned place preference in mice. Psychopharmacology. *184***,** 339–344. https://doi.org/10.1007/s00213-005-0295-x.

Wang, H.-L., and Morales, M. (2009). Pedunculopontine and laterodorsal tegmental nuclei contain distinct populations of cholinergic, glutamatergic and GABAergic neurons in the rat. Eur. J. Neurosci. *29*, 340–358. https://doi.org/10.1111/j.1460-9568.2008.06576.x.

Weissbourd, B., Ren, J., DeLoach, K.E., Guenthner, C.J., Miyamichi, K., and Luo, L. (2014). Presynaptic partners of dorsal raphe serotonergic and GABAergic neurons. Neuron *83*, 645–662. https://doi.org/10.1016/j.neuron.2014.06.024.

Whiteaker, P., Christensen, S., Yoshikami, D., Dowell, C., Watkins, M., Gulyas, J., Rivier, J., Olivera, B.M., and McIntosh, J.M. (2007). Discovery, Synthesis, and Structure Activity of a Highly Selective α7 Nicotinic Acetylcholine Receptor Antagonist. Biochemistry *46*, 6628–6638. https://doi.org/10.1021/bi7004202.

Wilson, R.C., and Collins, A.G. (2019). Ten simple rules for the computational modeling of behavioral data. ELife *8*, e49547. https://doi.org/10.7554/eLife.49547.

Wolfman, S.L., Gill, D.F., Bogdanic, F., Long, K., Al-Hasani, R., McCall, J.G., Bruchas, M.R., and McGehee, D.S. (2018). Nicotine aversion is mediated by GABAergic interpeduncular nucleus inputs to laterodorsal tegmentum. Nat. Commun. *9*, 2710. https://doi.org/10.1038/s41467-018-04654-2.

Wooltorton, J.R.A., Pidoplichko, V.I., Broide, R.S., and Dani, J.A. (2003). Differential Desensitization and Distribution of Nicotinic Acetylcholine Receptor Subtypes in Midbrain Dopamine Areas. J. Neurosci. *23*, 3176–3185. https://doi.org/10.1523/JNEUROSCI.23-08-03176.2003.

Yang, C.F., Chiang, M.C., Gray, D.C., Prabhakaran, M., Alvarado, M., Juntti, S.A., Unger, E.K., Wells, J.A., and Shah, N.M. (2013). Sexually dimorphic neurons in the ventromedial hypothalamus govern mating in both sexes and aggression in males. Cell *153*, 896–909. https://doi.org/10.1016/j.cell.2013.04.017.

Yang, H., Yang, J., Xi, W., Hao, S., Luo, B., He, X., Zhu, L., Lou, H., Yu, Y., Xu, F., et al. (2016). Laterodorsal tegmentum interneuron subtypes oppositely regulate olfactory cue-induced innate fear. Nat. Neurosci. *19*, 283–289. https://doi.org/10.1038/nn.4208.

Zhao-Shea, R., Liu, L., Pang, X., Gardner, P.D., and Tapper, A.R. (2013). Activation of GABAergic Neurons in the Interpeduncular Nucleus Triggers Physical Nicotine Withdrawal Symptoms. Curr. Biol. *23*, 2327–2335. https://doi.org/10.1016/j.cub.2013.09.

Chapter 3

Beier, K.T., Steinberg, E.E., DeLoach, K.E., Xie, S., Miyamichi, K., Schwarz, L., Gao, X.J., Kremer, E.J., Malenka, R.C., and Luo, L. (2015). Circuit Architecture of VTA Dopamine Neurons Revealed by Systematic Input-Output Mapping. Cell *162*, 622–634. https://doi.org/10.1016/j.cell.2015.07.015.

Bond, C.W., Trinko, R., Foscue, E., Furman, K., Groman, S.M., Taylor, J.R., and DiLeone, R.J. (2020). Medial Nucleus Accumbens Projections to the Ventral Tegmental Area Control Food Consumption. J. Neurosci. 40, 4727–4738. https://doi.org/10.1523/JNEUROSCI.3054-18.2020.

Cador, M., A. E. Kelley, M. Le Moal, and L. Stinus. “Ventral Tegmental Area Infusion of Substance P, Neurotensin and Enkephalin: Differential Effects on Feeding Behavior.” Neuroscience 18, no. 3 (July 1, 1986): 659–69. https://doi.org/10.1016/0306-4522(86)90061-8.

Cooke, J.H., Patterson, M., Patel, S.R., Smith, K.L., Ghatei, M.A., Bloom, S.R., and Murphy, K.G. (2009). Peripheral and Central Administration of Xenin and Neurotensin Suppress Food Intake in Rodents. Obesity 17, 1135–1143. https://doi.org/10.1038/oby.2008.652.

Davis, J. F., Tracy, A. L., Schurdak, J. D., Tschöp, M. H., Lipton, J. W., Clegg, D. J., & Benoit, S. C. (2008). Exposure to elevated levels of dietary fat attenuates psychostimulant reward and mesolimbic dopamine turnover in the rat. Behavioral Neuroscience, 122(6), 1257–1263. https://doi.org/10.1037/a0013111

Donofry, S.D., Stillman, C.M., and Erickson, K.I. (2020). A review of the relationship between eating behavior, obesity and functional brain network organization. Social Cognitive and Affective Neuroscience 15, 1157–1181. https://doi.org/10.1093/scan/nsz085.

Ferrario, C.R., Labouèbe, G., Liu, S., Nieh, E.H., Routh, V.H., Xu, S., and O'Connor, E.C. (2016). Homeostasis Meets Motivation in the Battle to Control Food Intake. J. Neurosci. *36*, 11469–11481. https://doi.org/10.1523/JNEUROSCI.2338-16.2016.

Finger, B. C., Dinan, T. G., & Cryan, J. F. (2012). Diet-induced obesity blunts the behavioural effects of ghrelin: Studies in a mouse-progressive ratio task. Psychopharmacology, 220(1), 173–181. https://doi.org/10.1007/s00213-011-2468-0

Harb, M. R., & Almeida, O. F. X. (2014). Altered motivation masks appetitive learning potential of obese mice. Frontiers in Behavioral Neuroscience, 8. https://www.frontiersin.org/article/10.3389/fnbeh.2014.00377

Hawkins, M.F. (1986). Aphagia in the rat following microinjection of neurotensin into the ventral tegmental area. Life Sciences 38, 2383–2388. https://doi.org/10.1016/0024-3205(86)90606-5.

la Fleur, S. E., Vanderschuren, L. J. M. J., Luijendijk, M. C., Kloeze, B. M., Tiesjema, B., & Adan, R. A. H. (2007). A reciprocal interaction between food-motivated behavior and diet-induced obesity. International Journal of Obesity, 31(8), 1286–1294. https://doi.org/10.1038/sj.ijo.0803570

O'Connor, E.C., Kremer, Y., Lefort, S., Harada, M., Pascoli, V., Rohner, C., and Lüscher, C. (2015). Accumbal D1R Neurons Projecting to Lateral Hypothalamus Authorize Feeding. Neuron 88, 553–564. https://doi.org/10.1016/j.neuron.2015.09.038.

Patterson, C.M., Wong, J.-M.T., Leinninger, G.M., Allison, M.B., Mabrouk, O.S., Kasper, C.L., Gonzalez, I.E., Mackenzie, A., Jones, J.C., Kennedy, R.T., et al. (2015). Ventral Tegmental Area Neurotensin Signaling Links the Lateral Hypothalamus to Locomotor Activity and Striatal Dopamine Efflux in Male Mice. Endocrinology 156, 1692–1700. https://doi.org/10.1210/en.2014-1986.

Tschumi, C.W., and Beckstead, M.J. (2019). Diverse actions of the modulatory peptide neurotensin on central synaptic transmission. Eur J Neurosci *49*, 784–793. https://doi.org/10.1111/ejn.13858.

Watabe-Uchida, M., Zhu, L., Ogawa, S.K., Vamanrao, A., and Uchida, N. (2012). Whole-Brain Mapping of Direct Inputs to Midbrain Dopamine Neurons. Neuron *74*, 858–873. https://doi.org/10.1016/j.neuron.2012.03.017.

Woodworth, H.L., Batchelor, H.M., Beekly, B.G., Bugescu, R., Brown, J.A., Kurt, G., Fuller, P.M., and Leinninger, G.M. (2017a). Neurotensin Receptor-1 Identifies a Subset of Ventral Tegmental Dopamine Neurons that Coordinates Energy Balance. Cell Rep *20*, 1881–1892. https://doi.org/10.1016/j.celrep.2017.08.001.

Woodworth, H.L., Beekly, B.G., Batchelor, H.M., Bugescu, R., Perez-Bonilla, P., Schroeder, L.E., and Leinninger, G.M. (2017b). Lateral Hypothalamic Neurotensin Neurons Orchestrate Dual Weight Loss Behaviors via Distinct Mechanisms. Cell Reports 21, 3116–3128. https://doi.org/10.1016/j.celrep.2017.11.068.

Woodworth, H.L., Brown, J.A., Batchelor, H.M., Bugescu, R., and Leinninger, G.M. (2018). Determination of neurotensin projections to the ventral tegmental area in mice. Neuropeptides 68, 57–74. https://doi.org/10.1016/j.npep.2018.02.003.

Wise, R.A. (2004). Dopamine, learning and motivation. Nat Rev Neurosci *5*, 483–494. https://doi.org/10.1038/nrn1406

Yang, H., de Jong, J.W., Tak, Y., Peck, J., Bateup, H.S., and Lammel, S. (2018). Nucleus Accumbens Subnuclei Regulate Motivated Behavior via Direct Inhibition and Disinhibition of VTA Dopamine Subpopulations. Neuron *97*, 434-449.e4. https://doi.org/10.1016/j.neuron.2017.12.022.